Sedimentology and Geochemistry of the Mesoproterozoic Pass Lake and Rossport Formations, Sibley Group

By

Riku T. Metsaranta

Submitted in partial fulfillment of the requirements for the degree of

Master of Science

Nov 2006

Supervisor: Dr. P. Fralick

Department of Geology
Lakehead University
Thunder Bay, ON P7B5E1

Your file Votre référence
ISBN: 978-0-494-31199-8
Our file Notre référence
ISBN: 978-0-494-31199-8

Abstract

The Sibley Group is an essentially unmetamorphosed, Mesoproterozoic sedimentary succession consisting of a mixture of siliciclastic and chemical sedimentary rocks. This study examined the sedimentology and geochemistry of the Pass Lake and Rossport Formations, the lowermost lithostratigraphic units of the Sibley Group.

Lithofacies analysis subdivided the sections studied into sixteen lithofacies associations corresponding to distinct depositional environments. These were divided into four informally defined allostratigraphic units, roughly equivalent to previous lithostratigraphic subdivisions. A lower clastic unit is comprised of the following lithofacies associations: boulder conglomerate-sandstone-dolocrete (proximal ephemeral braided stream), pebble to cobble conglomerate (ephemeral braided stream), massive cobble conglomerate (transgressive lag, reworking of braided stream deposits during transgression), trough cross-stratified sandstone (braided stream), green sandstone-siltstone (wave and storm influenced fluvial dominated delta), planar cross-stratified sandstone (nearshore migration of large sandwaves), and thinning-upward sandstone (beach and storm remobilized nearshore sandstone sheets). The lower clastic unit is disconformably to confomably, depending on geographic location, overlain by a mixed siliciclastic-carbonate unit. The mixed siliciclastic-carbonate unit is comprised of the red siltstone (non-saline lake), red siltstone-dolostone (perennial saline lake, distal from clastic source) and red siltstone-dolomitic sandstone (perennial saline lake, proximal to clastic source) lithofacies associations and is sharply overlain by an upper clastic unit. The upper clastic unit consists of the sheet sandstone (ephemeral playa lake (?) or perennial lake with increased sand supply with respect to underlying units) and black chert-carbonate (microbial mats forming at restricted, shallow, subaqeuous shoreline) lithofacies associations. Subaerial exposure features are present at the top of the black-chert-carbonate lithofacies association and include the intraformational conglomerate lithofacies association (subaerial debris flows, intrusive and/or extrusive sedimentary breccias, terra rossa style soils, dissolution collapse breccias). Subaerial exposure features at the top of the upper clastic unit are overlain by the massive dolostone (saline lake), red siltstone-sulfate (wet evaporite-rich mudflats around lake margins) and fine-

grained sandstone (dry, evaporite-poor mud and sand flats around lake margins) lithofacies associations of the mixed siliciclastic-carbonate-evaporite unit.

During deposition of the lower clastic unit paleocurrents and detrital zircon geochronology suggest a south- to southeast-down paleoslope. A lack of major thickness changes in stratigraphic units or laterally extensive coarse-grained clastic deposits is consistent with a broad intracratonic sag architecture during initial basin subsidence. Paleocurrents from the upper clastic unit suggest a change to northward oriented paleoslope during its deposition. This corresponds with an apparent thickening of the upper two units towards the north and Black Sturgeon Fault, consistent with the development of a half-graben structure and increased evidence of tectonic activity (e.g. intrusive sedimentary breccias, synsedimentary faulting and debris flows).

Carbon, oxygen and sulfur stable isotope analyses, Sr isotope analyses and trace element analyses (in some cases analyses include rare earth elements) were preformed on a variety of distinct carbonate and sulfate lithologies. Sulfur isotope compositions, strontium isotope compositions and rare earth element/yttrium ratios support a non-marine depositional setting. Low $\delta^{18}O$ values appear to be a good indicator of diagenetically altered samples. $\delta^{13}C$ values have typical marine values consistent with lacustrine carbonate precipitated in equilibrium with atmospheric CO_2. Stratigraphic changes in C and O isotope compositions in the red siltstone-dolostone lithofacies association were likely driven by evaporation and residence time effects. Stratigraphic variations in sulfur isotope compositions may reflect changes in the composition of sulfides weathering to supply sulfate to the basin. Overall, both the interpretation of physical sedimentologic and various types of geochemical data strongly support a non-marine lacustrine setting for the deposition of the Pass Lake and Rossport Formations.

Acknowledgements

This study was funded by the Ontario Prospectors Association (OPA) Lake Nipigon Region Geoscience Initiative and Natural Sciences and Engineering Research Council of Canada grants to Dr. Fralick. Without funding from the OPA numerous aspects of this thesis would not have been possible.

I would like to acknowledge and thank numerous people for their assistance through the course of this study. First, I should thank Dr. Fralick for his enthusiasm and patience. I should also thank Allan Mackenzie for assistance and training on the SEM; Ain Raitsakas for ICP AES analyses; Anne Hammond for preparing numerous thin sections; Dr. Conly for use of his lab facilities and discussions on isotope geochemistry; Dr. Hollings for use of the petrographic microscope and camera; Dr. Brian Cousens at Carleton University for assistance with Sr isotopic analyses; the Queens University Isotope Lab for stable isotopic analyses; Ontario Geoscience Laboratories for trace element analyses by ICP MS and Dr. Noel James for a constructive external review. Thank you also to Malcolm Alexander and Robert Scott for their assistance with fieldwork during 2003 and 2004.

Finally I should thank my family and Dawn-Ann for their love and support.

Table of Contents

List of Figures

Chapter 1

Chapter 2

Chapter 3

Chapter 4

Chapter 5

List of Tables

Chapter 1. Introduction.

1.1 General Introduction

The Sibley Group is a relatively thin (maximum observed thickness 950 m; Rogala, 2003), flat lying succession of Mesoproterozoic mixed chemical and siliciclastic sedimentary rocks exposed to the northwest of Lake Superior in the area immediately to the south and west of Lake Nipigon. These rocks are very well preserved, being generally unmetamorphosed, with the exception of local contact metamorphic effects. This excellent preservation of depositional and early diagenetic features, combined with the diversity of genetically distinct chemical sedimentary rocks present, allows them to be studied from both physical and chemical sedimentological standpoints. Using a multidisciplinary approach allows for a more powerful characterization of the paleoenvironmental evolution of the Sibley Group than has previously been invoked by traditional stratigraphic studies (Franklin et al. 1980; Cheadle, 1986 a and b; Rogala 2003). The purpose of this thesis was to conduct a detailed lithofacies analysis of the Pass Lake and Rossport Formations of the Sibley Group and to combine this with information gained from a variety of geochemical methods, in order to understand the depositional setting of the Sibley Group, the nature of paleohydrologic systems operating during Sibley Group deposition and to place the Sibley Group into a context of global Mesoproterozoic atmospheric and oceanic evolution.

1.2 Study Area

The Sibley Group crops out over an area of approximately 15 000 km^2 (Figs. 1.1, 1.2). To the east, outcrops of Sibley Group strata are found as far as Copper Island near

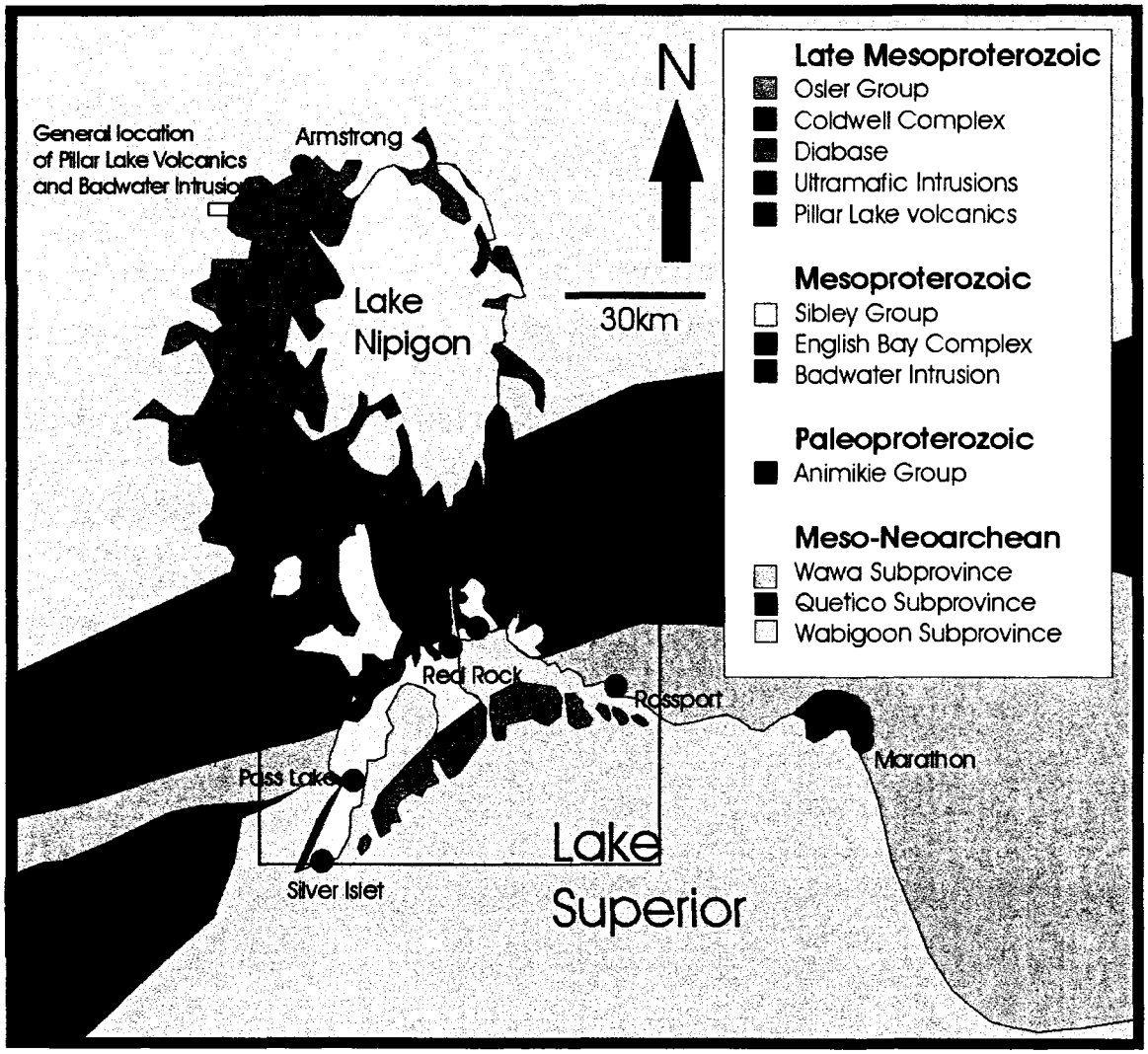

Figure 1.1. Generalized geology of the study region. The majority of sections examined in this study are located in the area outlined by the rectangle. The Sibley Group is present underlying the area covered by diabase and probably also underlies a portion of the area covered by the Osler Group. The original spatial extent of the Sibley Basin is not known and it is difficult to recognize where original basin margins may have been. The possible trace of the Black Sturgeon Fault, an important structure controlling the outcrop pattern of the Sibley Group is shown by a thick red line (Modified from Cheadle, 1986a; MacDonald, 2004).

the town of Rossport. The Pass Lake area marks the westernmost extent of Sibley Group outcrops. North to south the Sibley Group stretches from northern Lake Nipigon to Silver Islet at the tip of the Sibley Peninsula. This study focuses on drill core and outcrop data in the area south of Lake Nipigon. To the north of this, outcrops are scarce and the

intrusion of thick diabase complexes has metamophosed Sibley Group strata to a larger extent than in the south making it difficult to recognize and correlate lithologies.

1.3 Regional Geological Setting

The geology of northwestern Ontario is dominated by Meso to Neoarchean aged rocks and these underlie the majority of the Sibley Basin. Exceptions to the dominantly Archean basement occur in the area rimming Lake Superior where Paleoproterozoic rocks of the Gunflint (about 1878 Ma; Fralick et al., 2002) and Rove (1835-1780 Ma; Addison et al., 2005; Heaman and Easton, 2005) Formations underlie the Sibley Group. Mesoproterozoic igneous rocks of the English Bay Complex (1546.5 +/- 3.9 Ma, Heaman and Easton, 2006) and Badwater Intrusion (Syenite phase 1590 +/- 0.8 Ma; Gabbro phase 1598 +/- 1.1 Ma; Heaman and Easton, 2006) also appear to underlie a portion of the Sibley Basin near the northwestern shore of Lake Nipigon. Hollings et al. (2004) reported that sandstones lithologically correlative with the Sibley Group overlie the English Bay complex. Similarly, Davis and Sutcliffe (1985) suggested that the same sandstone units are intercalated with rhyolites associated with the English Bay Complex.

Archean rocks underlying the Sibley Group belong to the Quetico,Wabigoon and Wawa subprovinces of the Superior Province. The Superior Province, in a simplified sense, consists of roughly east-west trending sub-parallel, lithologically and structurally defined subprovinces that contain rocks ranging in age from Mesoarchean (roughly 3.0 Ga) to Neoarchean (roughly 2.6 Ga) (e.g., Card, 1990). To the northwest, rocks of the Superior Province are truncated by rocks of the Paleoproterozoic Trans-Hudson Orogen and to the south and east they are truncated by rocks associated with the Penokean, New Quebec and Grenville orogens (Card, 1990). The Wabigoon Subprovince underlies the

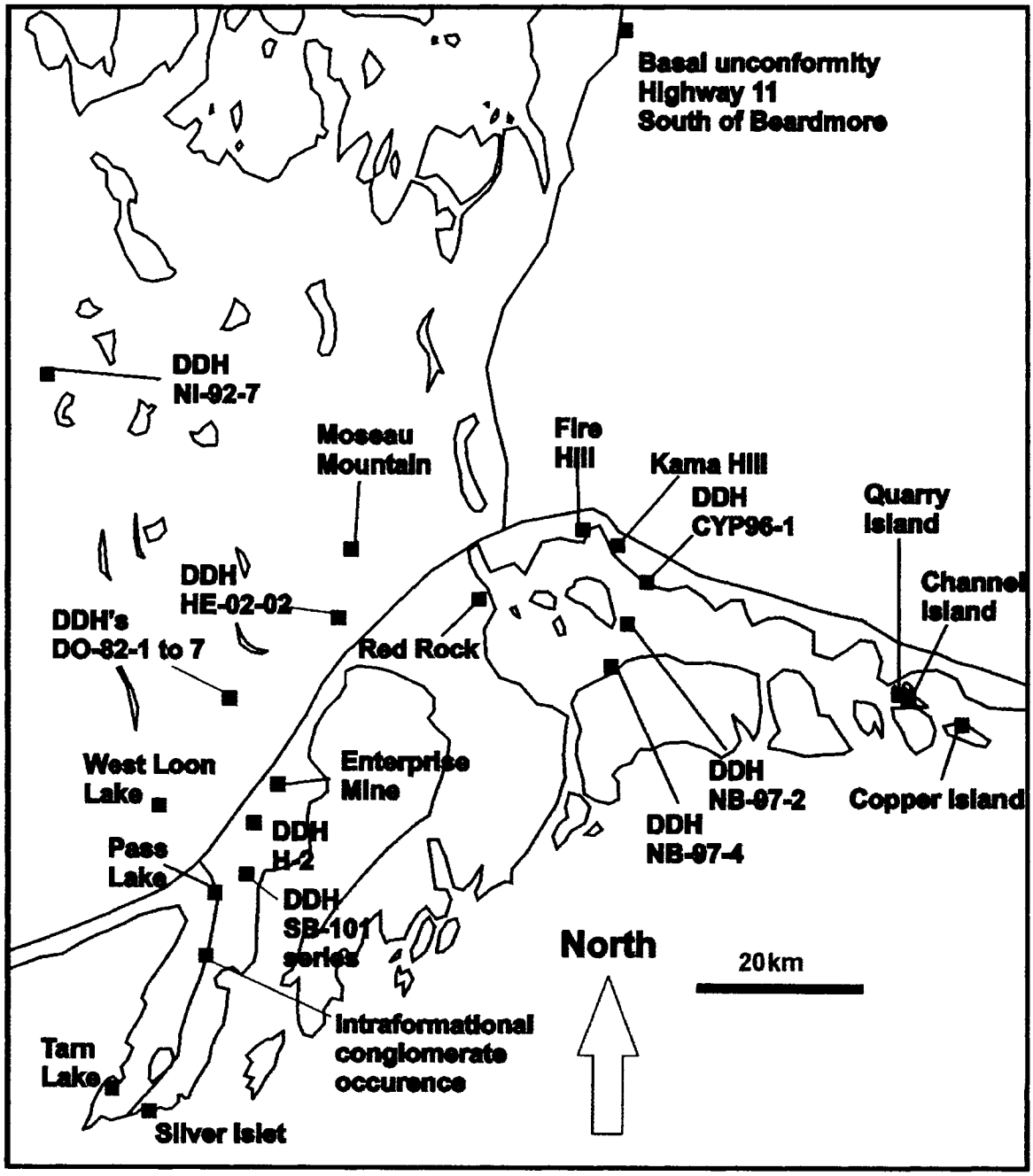

Figure 1.2. Location map showing positions of important drill core and outcrop locations.

northern portions of the Sibley Group and consists primarily of felsic plutonic rocks and supracrustal volcanic dominated greenstone belts (e.g., Blackburn et al., 1991). Minor sedimentary rocks are present and consist of siliciclastic metasedimentary rocks and iron formation. The Quetico Subprovince underlies the central portions of the Sibley Group

and consists primarily of homogeneous, turbiditic metasedimentary lithologies, felsic intrusive rocks, rare metavolcanic rocks and mafic and ultramafic intrusive rocks (e.g., Williams, 1991).

The southern portions of the Sibley Basin lie on Paleoproterozoic rocks of the Animikie Group, both the Gunflint and overlying Rove Formations. The Animikie Basin developed on the southern margin of the Superior Province and forms a southward thickening wedge deposited on a shelf during trangressive-regressive-transgressive cycles (Fralick and Barrett, 1995; Pufahl, 1996; Pufahl and Fralick, 2004). Lithologically, the Gunflint Formation consists of conglomerate, black shales/slates, iron-rich carbonate, chert, jasper and hematite-magnetite grainstones (e.g., Pufahl, 1996). The Rove Formation is a thick clastic dominated succession composed of black shale, sandstone and siltstone (Maric, 2006). The Animikie Basin likely developed in a back-arc setting associated with northward oriented subduction beneath the Superior Province prior to the collision that caused the Penokean Orogeny (e.g., Fralick et al., 2002). Alternatively, it has been interpreted to represent a northward migrating foreland basin (e.g., Ojakangas et al., 2001).

The Sibley Group is intruded by mafic sills that range in age from 1119 +/- 2.4 Ma (Inspiration diabase sills, Heaman and Easton, 2006) to 1110-1114 Ma (Nipigon diabase sills, Heaman and Easton, 2005) and is overlain by mafic volcanic rocks and associated coarse-grained clastic sedimentary rocks of the circa 1107 Ma Osler Group (Davis and Sutcliffe, 1985). Newly recognized volcanic rocks and intercalated sandstones at Pillar Lake, near Armstrong, the Pillar Lake Volcanics (MacDonald, 2004), appear to be younger than the Sibley Group based on paleomagnetic data of Borradaile and Middleton

(2006) which yielded an apparent polar wander path age of 1000-1040 Ma. However, this age is problematic as the Pillar LakeVolcanics are overlain (intruded) by the Inspiration diabase sills (ca. 1120 Ma, Heaman and Easton, 2006). Detrital zircons from a sandstone unit in the Pillar Lake Volcanics suggest an age of less than 1514 Ma (Heaman and Easton, 2005). The age of the Pillar Lake Volcanics and associated clastic sedimentary rocks, as well as their relationship to the Badwater Intrusion, Sibley Group and the Mid-continent rift is poorly understood and should be the focus of further study.

1.4 Previous work

Historical accounts of the previous geologic work on the Sibley Group are given in Franklin et al. (1980) and Cheadle (1986a and b). These outline the various contributions to Sibley Group geology from the middle to late 1800's onwards. Relatively modern work on the Sibley Group began in the late 1960's and 1970's with the work of Hofmann (1969) and regional mapping by McIlwaine (1971a, 1971b and 1975), Coates (1972) and Giguere (1975). The most relevant studies of the Sibley Group are the works of Franklin et al. (1980), Cheadle (1986a and 1986b) and Rogala (2003). Lakehead University bachelors theses concerning the Sibley Group were written by Campling (1973), Battrum (1975), Cheadle (1981), Mailman (1999) and Rogala (2000). Campling (1973) examined the petrography and geochemistry of possible weathering profiles developed on Sibley Group basement. Battrum (1975) investigated the mineralogy and sedimentology of the Kama Hill Formation. Cheadle (1981) described the type-section of the Rossport Formation on Channel Island and suggested possible depositional environments. Mailman (1999) examined controls on the development of red siltstone-dolostone cycles in the Channel Island Member of the Rossport Formation. Rogala (2001) examined

contact metamorphic effects of diabase intrusion on lithologies in the Channel Island Member. Franklin and Mitchell (1977) provided an account of lead-zinc barite mineralization within the Sibley Group. Recently Hanly (2005) completed a Ph.D. thesis concerning the potential for uranium mineralization in the Sibley Group. Data from Hanly's work showed that the Sibley Group experienced only low temperature diagentic alteration (max ca. 150 °C) in the presence of only meteoric fluids. Robertson (1973) conducted paleomagentic work on Sibley Group rocks. Recent geophysical surveys, geologic mapping, geochemical and stratigraphic studies were carried out during the Lake Nipigon Region Geoscience Initiative 2003-2005 (for a summary see Hart, 2005).

1.5 Lithostratigraphy

The basic lithostratigraphic subdivisions of the Sibley Group were outlined by Franklin et al. (1980); the original subdivisions were subsequently improved by Cheadle (1986a) and recent additions of two Formations were proposed by Rogala (2003) and Rogala et al. (2005). Figure 1.3 shows the generalized lithostratigraphy of the Sibley Group from Rogala (2003). According to Rogala (2003) the Sibley Group contains five Formations with a total observed thickness of up to 950m. From base to top these are the Pass Lake, Rossport, Kama Hill, Outan Island and Nipigon Bay Formations.

The Pass Lake Formation is subdivided into the Loon Member and the Fork Bay Member (Cheadle, 1986a). The Loon Member, at its formal type section, is approximately 12 m thick and comprised of polymicitic conglomerates with minor sandstone and siltstone lenses (Cheadle, 1986a). The Fork Bay Member is comprised dominantly of sandstones that vary from well-sorted quartz arenites to grey feldspathic wackes, with minor red carbonate-rich siltstones and very rarely dark green to black

shales (Cheadle, 1986b). At the stratotype, defined by Cheadle (1986a), the thickness of the Pass Lake Formation is 37 m, although Rogala (2003) noted that the thickness is typically 5-25 m and occasionally up to 100 m.

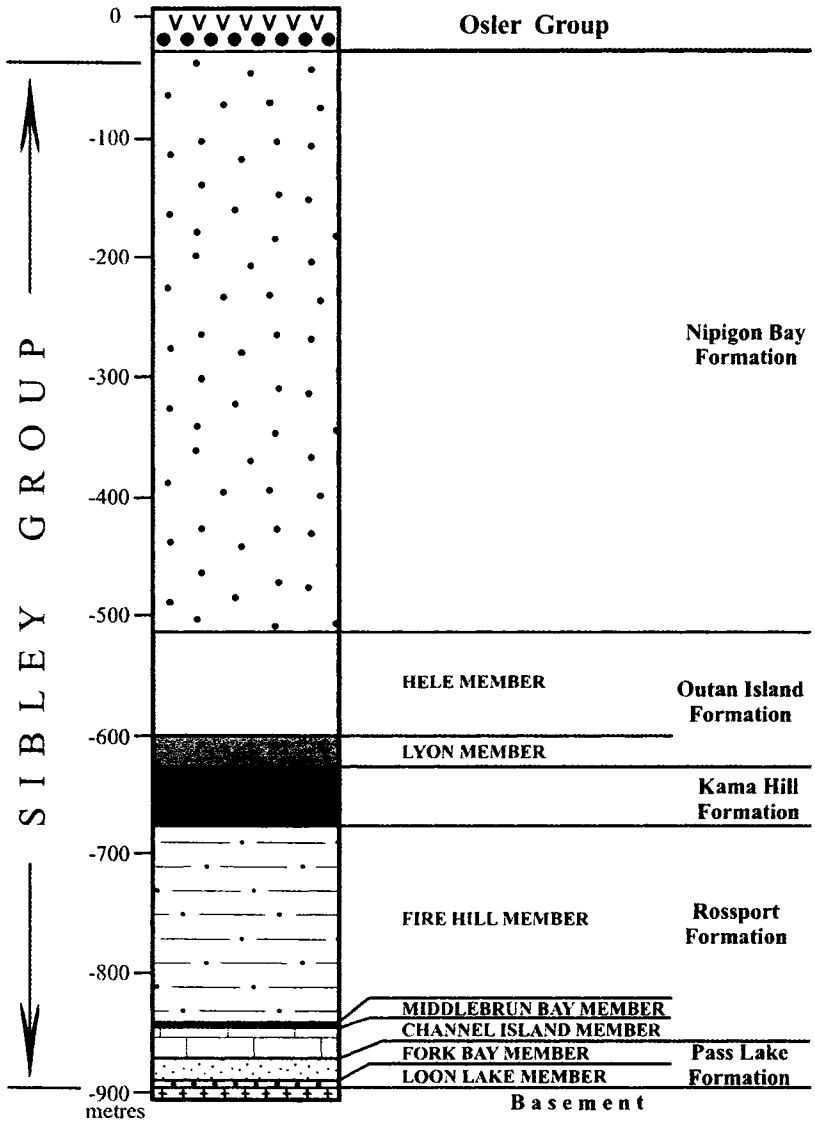

Figure 1.3. Generalized stratigraphy of the Sibley Group showing the relative thicknesses and stratigraphic positions of various units, modified from Rogala (2003) and Rogala et al. (submitted).

The Rossport Formation disconformably overlies the Pass Lake Formation and is subdivided into Channel Island, Middlebrun Bay and Fire Hill Members (Cheadle,

1986a). The Channel Island Member consists of a mixture of clastic and carbonate lithologies including: red siltstones, buff and red dolomicritic mudstones, dolomitic sandstones and discrete arenitic sandstone beds (Cheadle 1986a; Rogala 2003). On Channel Island, at its stratotype, the Channel Island Member is about 50m thick (Cheadle, 1986a). The Channel Island Member is conformably overlain by the Middlebrun Bay Member, a thin (generally 1 m or less), distinctive stromatolitic chert-carbonate unit comprised of finely laminated to thinnly bedded chert and fine-grained carbonate with penecontemponareous breccias and hemispherical stromatololitic domes (Cheadle, 1986a). The Fire Hill Member disconformably overlies the Middlebrun Bay Member. According to Cheadle (1986a) and Franklin et al. (1980), the Fire Hill Member is comprised of a basal intraformational conglomerate, red-orange to buff dolomicritic mudstone and purple mudstone with chert nodules. The type section, at Fire Hill, is just under 9m in thickness. Based on new drill core data, Rogala (2003) showed that the Fire Hill Member is in places much thicker, up to 80 m, and more lithologically complex than earlier workers believed.

The Kama Hill Formation disconformably overlies the Fire Hill Member (Cheadle, 1986a and b). It is comprised primarily of fine-grained sandstones and purple mudstones with fine horizontal and ripple cross-laminae. Stromatolitic carbonate layers are present near its base (Franklin et al., 1980; Cheadle, 1986a and b; Hofmann, 1969). Rogala (2003) found the Kama Hill Formation to range from 10 to 50 m in thickness.

Rogala (2003) modified the threefold stratigraphic subdivision of Franklin et al. (1980) and Cheadle (1986a) by the addition of the Outan Island Formation and the Nipigon Bay Formation. The Outan Island Formation consists of up to 250 m of

predominantly clastic sedimentary rocks. Rogala (2003) identified five distinct lithofacies associations in this Formation. These were termed: mudstone, laminated sandstone/mudstone, siltstone, sandstone and conglomerate lithofacies associations respectively. A general coarsening upwards of lithofacies was noted with finer-grained lithofacies associations, with coarsening upwards sandstone packages, forming the base of the Formation and associations with fining upward sandstone packages forming the top. The finer-grained lower portion is termed the Lyon Member and the coarser-grained upper portion the Hele Member. During the course of this study (e.g., Metsaranta and Fralick, 2004), widespread intraformational conglomerates comprised of lithofacies similar to those described by Rogala (2003) were observed in outcrops in various areas of the southern portion of the Sibley Basin, particularly south of the town of Red Rock along the eastern coast of the Black Bay Peninsula.

The Nipigon Bay Formation is approximately 450-500 m thick and disconformably overlies the Outan Island Formation (Rogala, 2003). It is lithologically very homogeneous and consists primarily of medium-grained sandstones with large-scale planar cross-stratification. It is present in a few drill cores from Nipigon Bay and on the northern shores of Simpson Island in Nipigon Bay. It is unconformably overlain by conglomerates of the basal Osler Group (Hollings et al., in press).

1.7 Depositional Environments

As the purpose of this study is to understand the depositional environments of the Sibley Group a brief review of previous interpretations of depositional environments is given below.

Franklin et al. (1980) interpreted sandstones of the Pass Lake Formation to represent deposition in a quiet, shallow lacustrine environment with the basal conglomeratic unit representing minor fluvial fillings of local depressions in the basement surface and overlying sandstones representing first beach then shallow offshore environments during a transgression. The Rossport Formation was interpreted to represent deposition in a saline lacustrine setting with major fluctuations in lake size. Finally the Kama Hill Formation was interpreted to represent a periodically dry mudflat based on the presence of mudcracks, possible evaporite casts and mud-chip conglomerates.

Cheadle (1986a and 1986b) refined the interpretations of the depositional environments of the Sibley Group based on a much more thorough examination of Sibley Group exposures and drill core. Cheadle (1986a) interpreted the Pass Lake Formation to represent small-scale alluvial fans (basal conglomerate) and sandy alluvial outwash flats (sandstones). Similar to Franklin et al. (1980), Cheadle interpreted the Rossport Formation to represent a playa lake with largely climatic controls on the variations in carbonate and clastic deposition. Cheadle (1986a) suggested that Kama Hill Formation was deposited through sheet flow processes on a distal alluvial floodplain.

Rogala (2003) again interpreted the Pass Lake Formation as a fluvial-lacustrine system. The Rossport Formation was interpreted as representing playa lake, sahbka and mudflat environments. The sahbka interpretation was added with the recognition of extensive nodular sulfate deposits in the Fire Hill Member. Similar to the interpretation of Cheadle (1986a) the Kama Hill Formation was interpreted by Rogala (2003) to represent a subaerial mudflat environment. The Outan Island Formation was interpreted to represent deltaic deposits (Lyon Member) and meandering fluvial deposits (Hele

Member). The deposition of the Nipigon Bay Formation was ascribed to largely aeolian processes.

1.8 Age

The age of the Sibley Group is somewhat poorly constrained. A minimum age of 1339 +/- 33 Ma has often been cited as the depositional age of the Sibley Group (e.g. Franklin et al., 1980; Cheadle, 1986a and b). This age was based on a Rb-Sr isochron derived from fine-grained Sibley Group samples from both the Rossport and Kama Hill Formations (Franklin, 1978). Rb-Sr isochron age determinations in sedimentary rocks have numerous sources of potential error, especially where whole-rock samples are used (e.g. Clauer, 1981). However, this age does provide a reasonable bracket for the youngest depositional age of the lower units in the Sibley Group. The maximum age of the Sibley Group is constrained by possible stratigraphic relationships with the English Bay Complex and by detrital zircon geochronology. If the sandstone units overlying the English Bay complex are correlative with the lowermost Sibley Group, then the maximum age of the Sibley Group is bracketed between 1547 +/- 4 Ma, the U-Pb zircon age of the English Bay intrusion (Heaman and Easton, 2005) and 1339 Ma. As it is difficult to correlate this sandstone unit with certainty, it may be more prudent to use the detrital zircon data (Heaman and Easton, 2005; Rogala et al, submitted). Figure 1.4 shows detrital zircons age distributions for sandstone samples from the Pass Lake, Outan Island and Nipigon Bay Formations (Rogala et al, submitted). The youngest zircon found in a sample of Pass Lake Formation sandstones from near the town of Pass Lake is about 1634 Ma. The youngest zircon from a sample of sandstone from the Outan Island

Formation (Heaman and Easton, 2005) has a much younger age of about 1450 Ma though it is much higher in the stratigraphy.

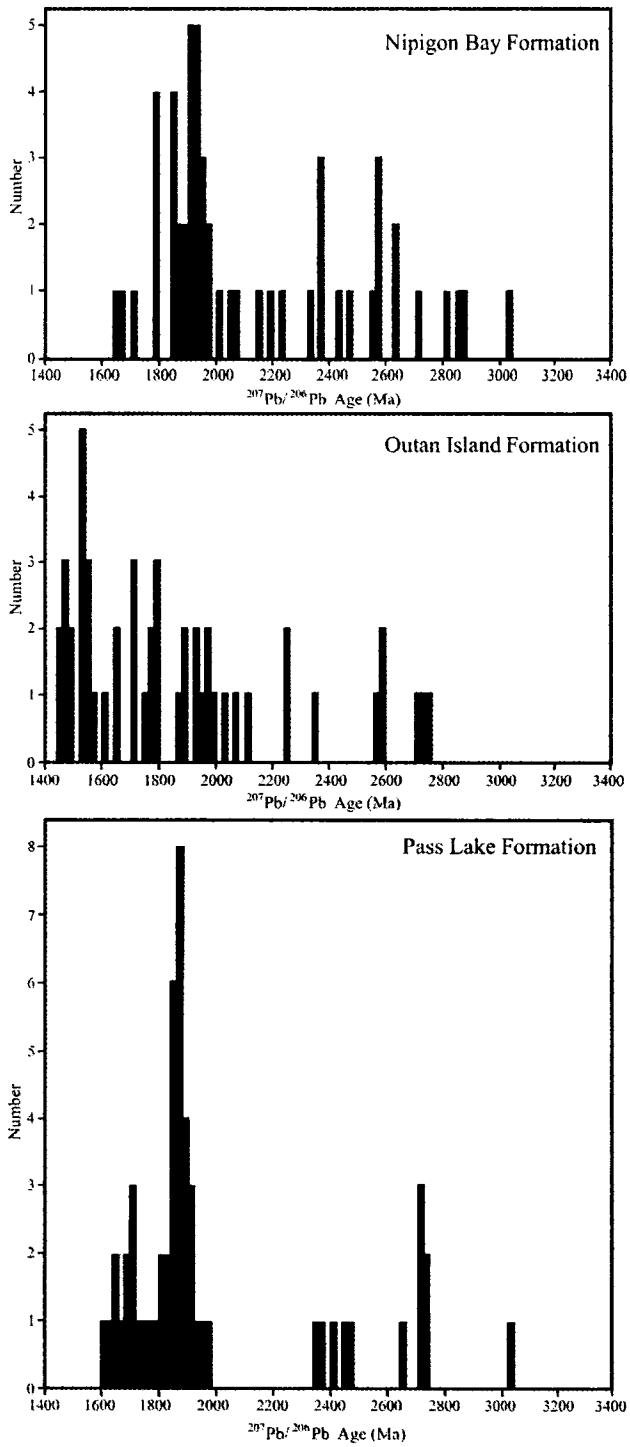

Figure 1.4. Detrital zircon $^{207}Pb/^{206}Pb$ age distributions for Sibley Group sandstone samples from the Nipigon Bay (top), Outan Island (middle) and Pass Lake (bottom) Formations (from Rogala et al. submitted)

Based on the above data, the basal portions of the Sibley Group are constrained between about 1634 and 1339 Ma, though the maximum age is likely younger, around the age of the English Bay intrusion. The Sibley Group from the Outan Island Formation and above can be constrained between 1450 Ma and about 1100 Ma (approximate age of Nipigon Diabase intrusions). A paleopole determined for the Kama Hill and Outan Island Formations by Rogala (2003) suggests an age of 1450 to 1500 Ma and supports a post English Bay intrusion maximum age for at least the middle Sibley Group. Hanly (2005) suggested that the mininimum age of the Sibley Group is constrained at about 1700 Ma based on Pb-Pb geochronology of galena veins that cross-cut the Pass Lake Formation and Ar-Ar ages for diagenetic illites in the Pass Lake Formation. This age constraint is invalid based on the detrital zircon results discussed above.

1.9 Tectonic and Paleogeographic setting of the Sibley Basin

The tectonic setting in which the Sibley Basin developed in has received relatively little attention. Franklin et al. (1980) noted that the Sibley Group occupies an elongate area extending away from the region of major flexure in the late Mesoproterozoic Mid-continent rift system and associated the Sibley Group with a failed arm of the rift system. They also proposed that filling of the Sibley Basin was controlled by a southerly fault scarp based on an observation of increased clastic material in the southern portions of the basin. However, subsequent studies (Cheadle, 1986 a and b; Rogala, 2003) have not noted a thickening of siliciclastic material in southern parts of the basin. Franklin et al. (1980) linked the timing of Sibley Group deposition either to pre-Grenvillian spreading proposed by Baer (1974) or to the first stages of rifting associated with the Mid-continent rift system. Linkage to the rift event was made based on correlation with a Sibley-like

paleomagnetic age for the South Range volcanic rocks near Ironwood Michigan (Books, 1969, 1972). Cheadle (1986a, b) proposed that the Sibley group was deposited in a broadly subsiding intracratonic basin with little evidence for fault control and graben formation. This interpretation was based on a lack of major changes in Formation thicknesses towards possible bounding faults and the lack of development of coarse-grained clastic material near basin margins. Cheadle (1986a) cited that the age of the onset of igneous activity associated with the Mid-continent rift of 1200-1225 Ma, reported by Van Schmus et al. (1982), was too much younger than the 1339 Ma age of the Sibley Group for the two events to be related. Cheadle (1986a), however, did not totally discount a possible relation to the rift system and noted that broad subsidence was often found to precede major rift related igneous activity (Mohr, 1982, McKenzie, 1978). Cheadle (1986b) and Davis and Sutcliffe (1985) first noted a possible link between the English Bay Complex and the development of the Sibley Group. Cheadle (1986b) suggested a possible relationship between widespread Mesoproterozoic anorogenic granite suites across North America and the English Bay Complex/Sibley Group. Rogala (2003), Hollings et al. (2004) and Rogala et al. (2005) have supported a genetic link between the English Bay Complex and the Sibley Group. Rogala et al. (2005) proposed that the basin-fill pattern of the Sibley Group began with an intial broad sag during the deposition of the Pass Lake Formation and lower Rossport Formation, followed by a change to a half-graben architecture during the deposition of the upper Rossport Formation. Rivers and Corrigan (2002) have proposed that the now eastern portions of North America from roughly Labrador to Texas were the site of a major convergent margin from about 1500 to 1230 Ma, prior to collision and development of the Grenville

Orogen. Intraplate stresses associated with this convergent margin may have played a role in Sibley Basin initiation and development.

Robertson's (1973) paleomagnetic work has suggested that the Sibley Group was deposited within 10 degrees south of the paleo-equator. Rogala (2003) supported this finding with a paleo-latitude of 20 degrees south for the Kama Hill Formation. These suggest that the Sibley Group was deposited in a warm low latitude setting. Oxidative weathering of pre-Sibley Basement (Campling, 1973; Franklin et al., 1980; Cheadle, 1986b) indicates that the area was subaerially exposed prior to the onset of deposition. The presence of the older Archean craton to the north, west and east and rocks of the Penokean Orogen and Baraboo interval quartzites (Medaris et al., 2003) to the south places the Sibley Group in the continental interior, at least a few hundred kilometres away from continental margins, during its deposition.

1.10 Methods

Data collection for this thesis began with detailed logging of diamond drill core and outcrop sections. In some cases data was compiled from logs found in Cheadle (1986b) and Rogala (2003). In most cases outcrops and diamond drill core sections compiled from other authors were examined in order to maintain continuity with the logging style used during the course of this study. Sedimentologic data was plotted as 1:100 scale stratigraphic sections and subdivison into lithofacies association was made by inspection. During logging representative samples of various carbonate and sulfate lithofacies were collected. Trace elemental compositions, including rare earth elements (REE's); sulfur stable isotopic compositions; carbon and oxygen stable isotopic compositions and Sr isotopic compositions were determined for selected carbonate and sulfate lithologies.

Trace element analyses for a variety of whole rock and partially leached sulfate and carbonate lithologies were carried out by ICP-AES (Inductively coupled plasma atomic emission spectrometry) and ICP-MS (inductively coupled plasma mass spectrometry) at Lakehead University (ICP-AES) and Ontario Geoscience Laboratories in Sudbury ON (ICP-MS). Stable isotopic compositions of sulfur (for sulfate samples) and carbon and oxygen (for carbonate samples) were measured at Queens University. Sr isotopic compositions for some carbonate and sulfate samples were determined at Carleton University. Detailed geochemical methodologies are described in chapter 5.

1.11 Scope of thesis

This thesis is organized into two broad sections. The first section develops a depositional model for the lower Sibley Group based on lithofacies analysis and stratigraphic data. The second section uses the stratigraphic framework and understanding of depositional environments from the first section to identify samples and interprets geochemical data in a sedimentologic context. The second section serves to elaborate the physical and chemical environments of deposition and examines in greater detail the paleohydrology of the basin.

Chapter 2. Lithofacies Associations.

2.1 Introduction

This chapter outlines the lithofacies associations that have been identified in the lower portions of the Sibley Group. Subdivision into lithofacies associations was done after examination of detailed sedimentologic data collected from outcrop and drillcore sections during this study as well as published data from Cheadle (1986a and b) and Rogala (2003). Descriptions of lithofacies associations are given below. Section 2.2 describes the lithofacies associations present in the Pass Lake Formation and section 2.3 describes the Rossport Formation.

2.2 Pass Lake Formation

The lowest portion of the Sibley Group is dominated by clastic sedimentary rocks termed the Pass Lake Formation (Franklin et al., 1980). The Pass Lake Formation is subdivided into the Loon Lake and Fork Bay Members (Cheadle, 1986a). The Loon Lake Member is comprised of conglomerates, coarse sandstones, occasional thin carbonate-rich siltstones, and sporadically developed dolocretes. The Fork Bay Member consists primarily of sandstone. The thickness of the Pass Lake Formation ranges from 0 to about 100m.

The distribution of the Loon Lake Member is sporadic, and probably controlled by proximity to areas of high local relief in basement topography, or the development of local fault scarps (Cheadle, 1986a; Franklin et al., 1980). Accumulations of this member range from 0 to about 15 m in thickness. Scattered exposures of this Member are present in the southern portions of the basin. Drillcore occurences of this Member are generally

absent or very thin and sandstones of the Fork Bay Member usually lie in contact with basement. Three lithofacies associations have been identified in the basal conglomerate. These are termed: the boulder conglomerate/sandstone/dolocrete, the massive cobble conglomerate, and the pebble-cobble conglomerate sandstone lithofacies associations respectively.

The Fork Bay Member is a clastic dominated unit that is present over most of the Sibley Basin. In the south, notable absences of the Pass Lake Formation include the section at Kama Hill and these may relate to features in the basin floor topography (Cheadle, 1986a and b). In this study, the Fork Bay Member is divided into four lithofacies associations. These are termed: the green sandstone/siltstone association, the planar cross-stratified sandstone association, the thinning upwards sandstone association, and the trough cross-stratified sandstone association.

2.2.1 Boulder conglomerate/sandstone/dolocrete lithofacies association

The Boulder conglomerate/sandstone/dolocrete lithofacies association is rarely exposed but crops out in a few localities in the southern portion of the Sibley Basin. A number of lithofacies comprise the Boulder conglomerate/sandstone/dolocrete lithofacies association. The most volumetrically significant are massive, clast-supported, polymictic cobble to boulder conglomerates. The conglomerates show little evidence for internal stratification and tend to be massive, although vague 40-50 cm scale cross-stratification is present in places. The average size of clasts in the conglomerate facies is about 15-20 cm though very large 60-70 cm clasts are present. Clast compositions in the conglomerate are variable and appear to be controlled by the nature of local basement (Cheadle, 1986 a

and b), with various Archean lithologies dominating some conglomerate units and Animikie Group clasts dominating others. The conglomerates typically have matrix compositions dominated by poorly sorted sandstone, with abundant hematite. Carbonate cement is also present in places. Occasional massive coarse-sandstone lenses on the order of 30-50 cm thick are present in the conglomerates. The conglomerates fill large scours that cross-cut coarse-grained sandstones, polymictic pebble conglomerates, dolocretes and rare thin carbonate-rich pink siltstone lithofacies which together comprise the remainder of the association. The coarse-grained sandstones are sometimes laterally continuous at outcrop scale, but more commonly form lensoid bodies that cross-cut one another. Sandstone beds are generally less than 1 m thick and are usually massive textured, though upper flow regime parallel laminations are present in some cases. Thin, polymictic pebbly conglomerates are interbedded with the coarse-grained sandstones and have massive matrix-supported fabrics. Siltstones found within sandstone beds form decimetre-scale lenses that are traceable only for about 10m. The dolocrete lithofacies is present as relatively thick (30-50cm) massive or vaguely laminated silicified carbonate and as cements in the conglomerate lithofacies.

Petrographically, the dolocrete layers consist primarily of finely crystalline carbonate. However, more coarsely crystalline areas are present and these form thin irregular pods and veins. Oxidized clasts of various basement lithologies are common. Coatings of carbonate are present around clasts. Sporadic rhombs of dolomite are distributed within the dominantly microcrystalline matrix as are occasional seams of hematitic clay.

The best example of the boulder conglomerate/sandstone/dolocrete lithofacies association is present near Loon Lake. Figure 2.1 shows photographs of some of the lithofacies present at this exposure.

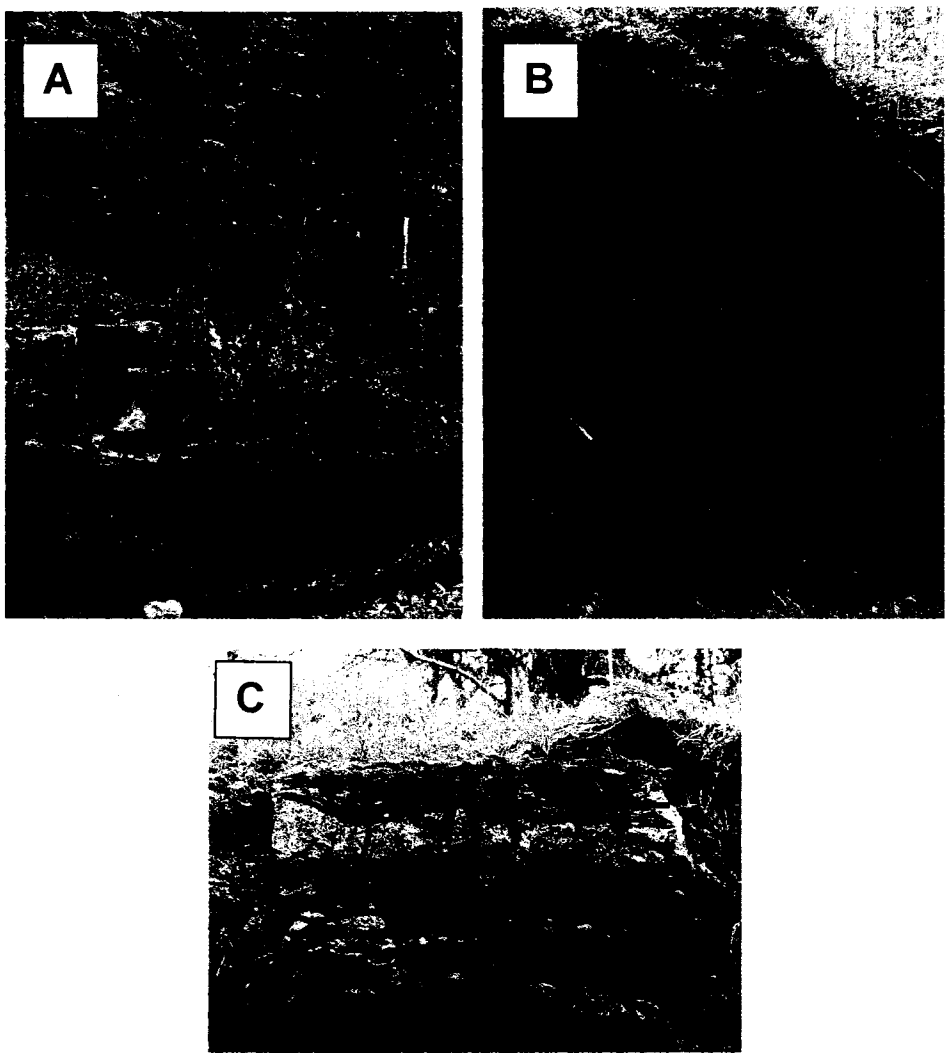

Figure 2.1. Typical lithofacies of the boulder conglomerate/sandstone/dolocrete lithofacies association. A) A thick channel filled with clast-supported coarse conglomerates cutting across horizontal beds of coarse-grained sandstone and siltstone. Hammer handle is 30cm long. B) An exposure of the coarse-grained sandstone and siltstone lithofacies illustrating the tabular geometry of the sandstone beds as well as the thin lensoid nature of the interbedded siltstones (Locations of siltstone units are indicated by arrows). Hammer handle is 30cm long. C) A well developed, approximately 50cm thick dolocrete horizon developed over top of a conglomerate bed showing a lower portion where the carbonate contains matrix- supported cobble-sized clasts, a middle portion that is massive textured and an upper portion with poorly developed irregular laminations.

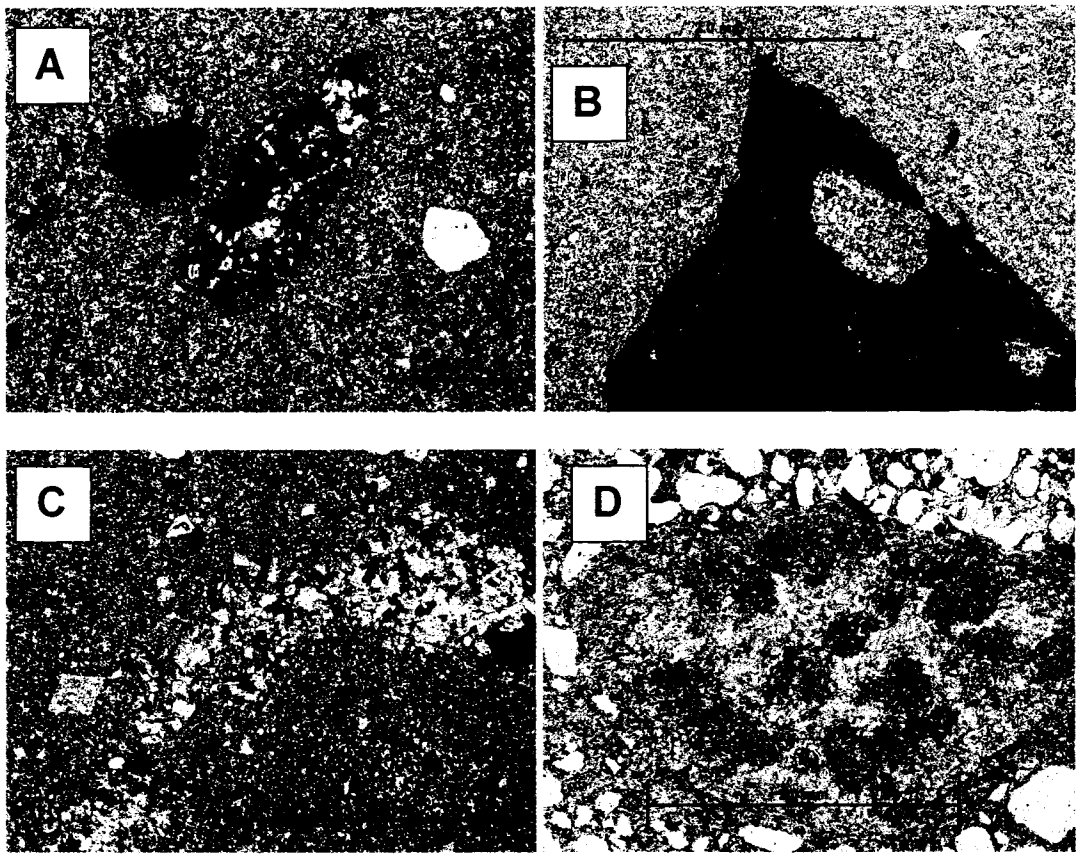

Figure 2.2. Petrographic characteristics of dolocrete lithofacies (all in cross-polarized light). A) Finely crystalline dolomite matrix with "floating" grains of quartz and what appears to be a clast of oolitic hematite-rich chert, probably from the Gunflint Formation. B) A hematite-rich etched clast in very fine dolomite. C) A thin vein of slightly coarser dolomite and examples of euhedral dolomite rhombs. D) A reworked carbonate grain in quartz sandstone.

2.2.2 Massive cobble conglomerate lithofacies association

The massive cobble conglomerate lithofacies association is present underlying the Fork Bay Member near the town of Pass Lake. It is generally very thin forming tabular exposures less than two metres in thickness that overlie red oxidized shales of the Rove Formation (Fig 2.2). A horizon of clast-supported polymictic cobble conglomerate with sandy hematite-rich matrix typically comprises this association. Weak imbrication may be present, but it is poorly developed at best. Clast compositions are variable. However, clasts from the Gunflint Formation and Rove Formation predominate. The conglomerate is sharply overlain by Fork Bay Member sandstones, though occasional pebble-sized

clasts are present in some of the sandstone beds. Laterally, the single conglomerate horizon is in places interbedded with a sandstone bed. Figure 2.3 shows an example of this association at the Pass Lake exposure and illustrates the massive or weakly imbricated texture as well as the sharp contact with overlying sandstones.

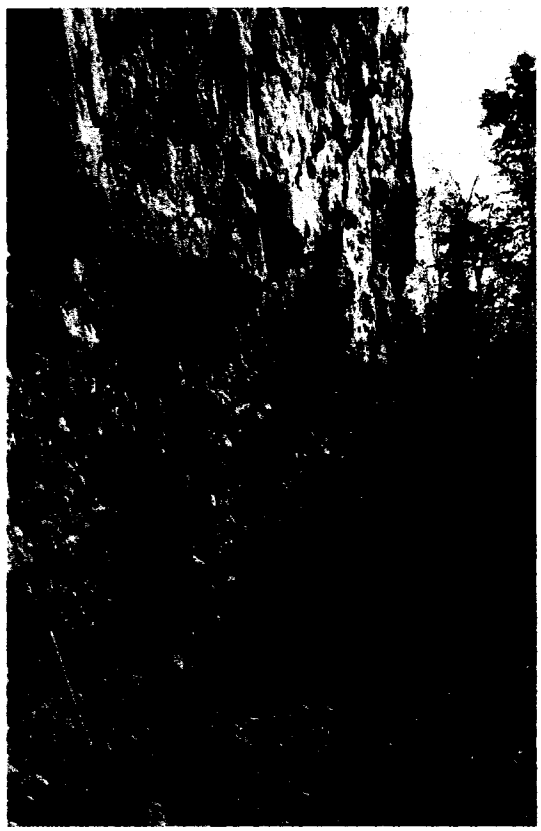

Figure 2.3. An exposure of the massive cobble conglomerate lithofacies near the town of Pass Lake (hammer handle is 40cm long)

2.2.3 Pebble-cobble conglomerate/sandstone lithofacies association

The pebble-cobble conglomerate/sandstone lithofacies association forms thin lenses of a few metres thickness and crops out sporadically throughout the southern portion of the Sibley Basin. It is comprised of matrix and clast supported polymictic pebble to cobble conglomerate with a hematite-rich, poorly sorted sandstone matrix and medium- to very coarse-grained, massive, or vaguely cross-stratified sandstone (Fig 2.4).

Clasts within the conglomerate are generally less than 10 cm in diameter and often show an oxidized weathering rind up to 0.5 cm in thickness. Though exposure is not complete, the conglomerates appear to fill small-scale topographic features in the underlying basement (Cheadle, 1986a and b). In some outcrops a crude stratigraphy is present with lower portions dominated by matrix and clast supported conglomerates and an upper portion dominated by sandstone with lenses of clast supported conglomerate. A good example of this lithofacies association is present near the town of Silver Islet (Fig 2.4).

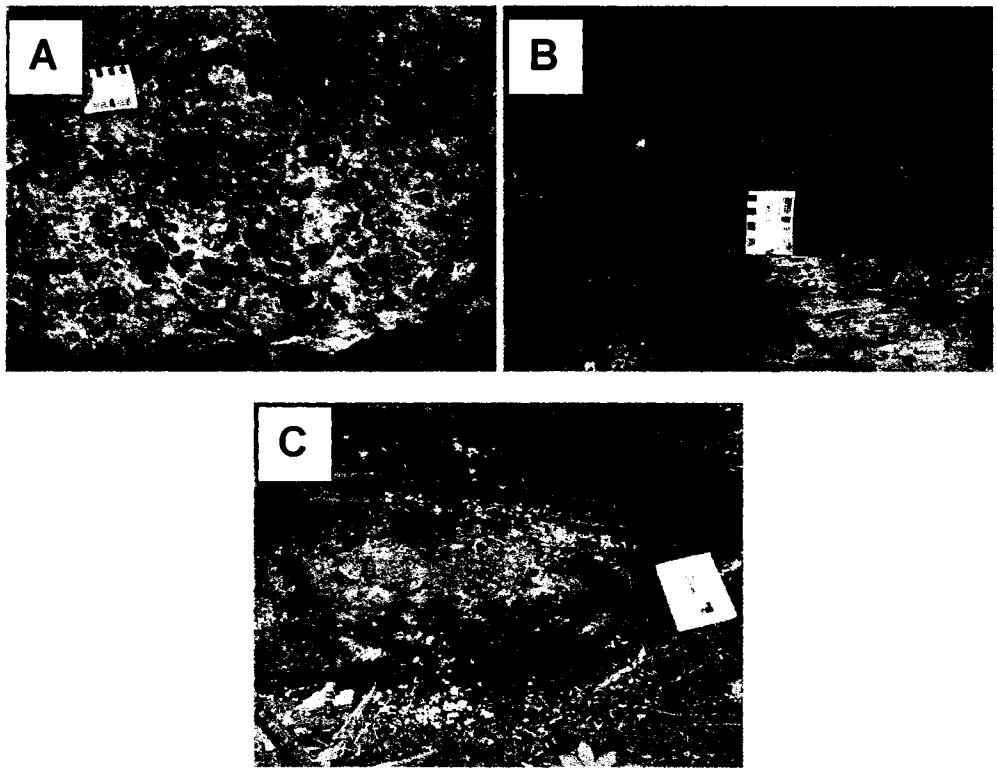

Figure 2.4. Lithofacies present at the Silver Islet exposure of the Loon Lake Member. A) An example of the pebble/cobble conglomerate lithofacies with massive, clast supported texture. Gradations on scale card are in centimetres. B) Oxidized Rove Formation shales overlain by matrix supported conglomerate. Scale card with cm divisions is situated on the unconformity. C) The edge of a conglomerate lense that fills a scour cut into poorly sorted, thin-bedded, cross-stratified medium-grained sandstone. Clipboard shown for scale is 25cm wide.

2.2.4 Green sandstone/siltstone association

The green sandstone/siltstone association appears to occur in a geographically restricted area along the southeastern margin of the exposed Sibley Basin. The only exposures have been noted on Copper and Channel Islands off Rossport. Where present it appears to form the base of the Sibley Group. It is distinct from other portions of the Sibley Group in that rather than having a red oxidized appearance, sandstones and siltstones in this association are pale-green coloured and unoxidized. Coarsening- and thickening-upwards cycles occur within this association at Copper Island (Fig. 2.6). Siltstone lithofacies generally occur as thin, wavy, green coloured layers between sandstone beds and can occasionally contain lenticular bedded sandstone (Fig. 2.5a). They also occur as thicker massive or thinly laminated units of a few metres thickness. In many examples thin siltstone partings between sandstone beds display striking synerisis crack features (Fig. 2.5f). The sandstone lithofacies is generally a pale-green colour with individual beds commonly graded and containing a variety of sedimentary structures including: parallel lamination, wave ripples, lenticular bedding, and medium-scale trough cross-stratification (Fig. 2.5). Parallel laminations are in places transitional to hummocky cross-stratification. Irregular loading features are common at the bases of most sandstone beds as are thin siltstone chip conglomerates (Fig. 2.5 e and f). Sandstone bed geometries vary from lenses that scour one another to tabular laterally continuous units. The thickness of sandstone beds varies from about 5cm to 3m with an average of about 50-60cm. The coarsening and thickening upwards cycle on Copper Island begins with lensoid, decimetre-scale thickness, medium-grained sandstone beds

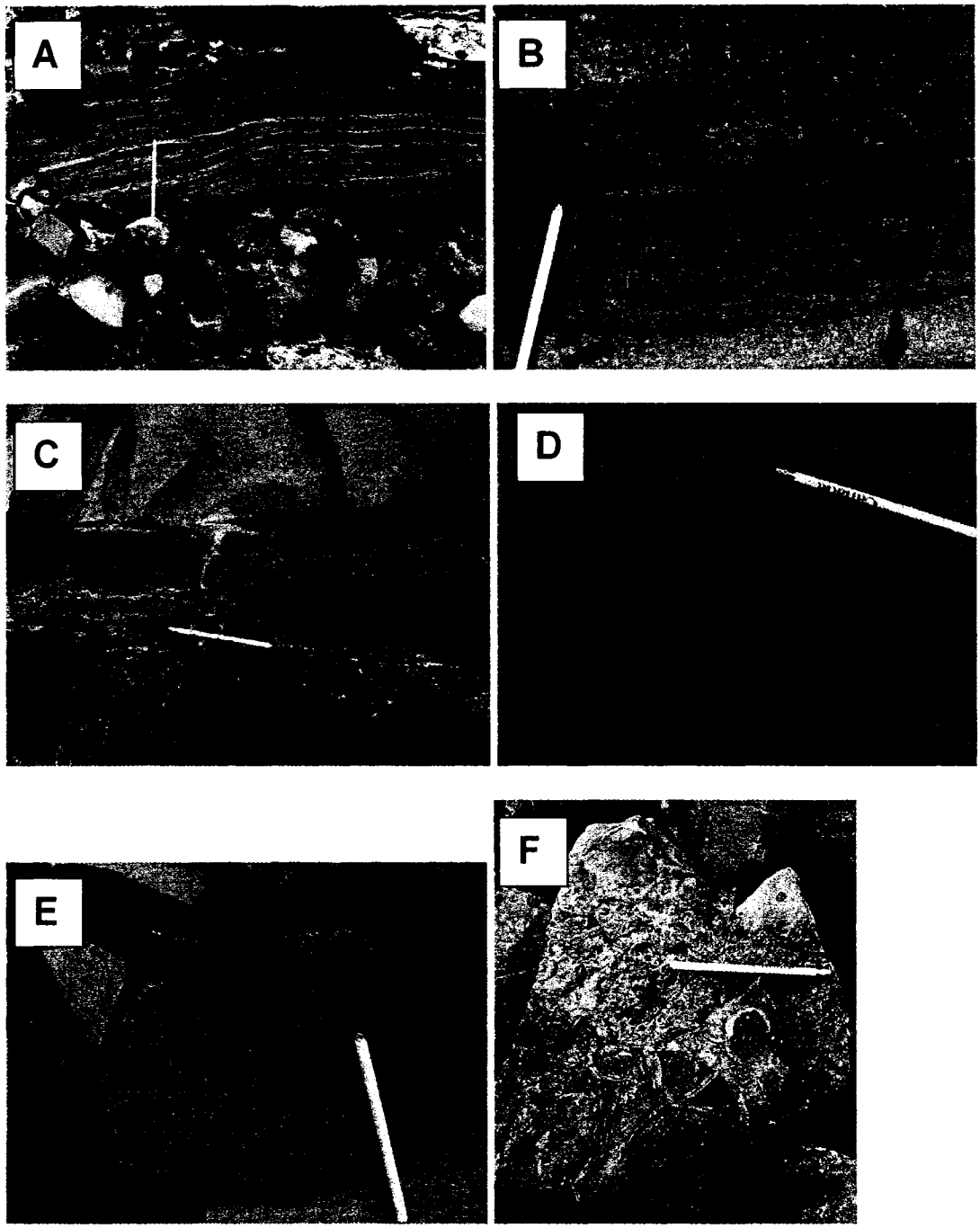

Figure 2.5. Lithofacies present in the green sandstone/siltstone association. Pencil used for scale is approximately 15cm long. A) Thinnly laminated/bedded green silstones near the base of a coarsening and thickening-upwards cycle on Copper Island. B) Lenticular bedding in a siltstone/sandstone unit between two sandstone lenses near the base of the section at Copper Island. C) Lensoid sandstone beds with wave rippled silt-rich tops that occur near the base to middle of the thickening-upwards cycle on Copper Island. D) Trough cross-stratified sandstone typical of sandstone beds near the top of the Copper Island section. E) green siltstone chip conglomerate at the base of a sandstone bed typical of sandstone beds throughout the Copper Island section. F) Irregular load features on the base of a sandstone boulder from Copper Island. The load features occur along synerisis cracks developed in the thin siltstones that commonly cap sandstone beds.

with intervals of thinly laminated siltstone which are succeeded upwards by progressively thicker and more tabular, coarser-grained, sandstone beds. Higher in the cycle trough-cross-stratification becomes more common. Bed thicknesses at the top of the coarsening upwards cycle are commonly on the order of 1-2 m.

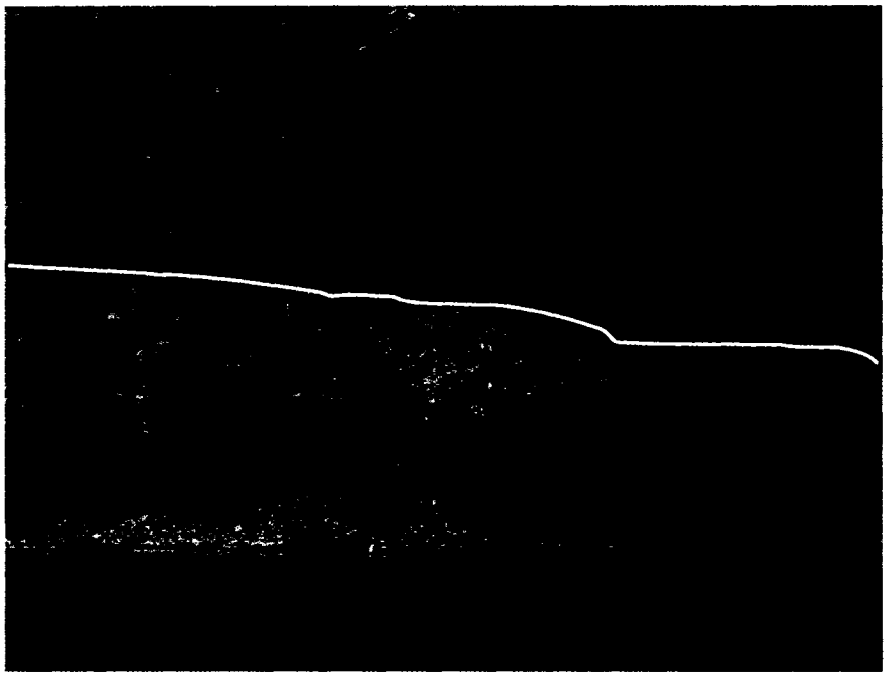

Figure 2.6. A view of the Copper Island section that shows the trend of increasing bed thickness in the Pass Lake Formation and a slight discontinuity in bedding orientation with overlying strata of the Rossport Formation. The arrow represents approximately 20m of section.

2.2.5 Planar cross-stratified lithofacies association

The planar cross-stratified lithofacies association occurs in spatial and stratigraphic proximity to the green sandstone/siltstone association. Outcrops of this association have been noted only on Quarry Island near Rossport. A single large-scale planar cross-stratified, medium-grained sandstone lithofacies comprises the majority of this association (Fig. 2.7). However, the basal portions of the section on Quarry Island are comprised of massive, poorly bedded, possibly wave rippled, greenish sandstones similar to some sandstone units in the green sandstone-siltstone lithofacies association.

These sandstones are interpreted to be a part of the green sandstone-siltstone lithofacies association and lie in contact with shales of the Rove Formation. Within the planar cross-stratified lithofacies, individual co-set packages are typically 1-3 m in thickness, though Cheadle (1986b) described individual co-set packages of up to 10m in thickness. Chemically, the sandstones are very mature and homogeneous. Pebble and cobble sized clasts are present but exceedingly rare.

Figure 2.7. Large-scale cross-stratification in medium grained sandstone at Quarry Island near Rossport. Hammer shown for scale is 25 cm long.

2.2.6 Thinning upwards sandstone lithofacies association

The thinning upwards sandstone lithofacies association consists primarily of mature medium-grained sandstones (Fig. 2.8). The best example of this association occurs at Pass Lake and the spatial distribution of this association appears to be restricted to the area between Pass Lake and Nipigon. Grading, low-angle planar to wavy cross-stratification, parallel lamination and wave ripples are present throughout the association

but appear to decrease in frequency upwards replaced by more massive beds. The top of the association becomes dominated by red siltstones interbedded with occasional massive or parallel laminated sandstone beds, with wave rippled tops. The bases of sandstone beds often have downward oriented sandstone dikes intruding into underlying siltstones.

Figure 2.8. Thinning upwards cycle in sandstone beds at Pass Lake. Photgraph shows approxiamtely 15 metres of section.

2.2.7 Trough cross-stratified sandstone/red siltstone association

This lithofacies association is comprised of a relatively diverse range of lithologies that are somewhat broadly categorized as belonging to a single lithofacies association. The most common lithofacies is a medium- to coarse-grained sandstone that

is either massive or trough cross-stratified (Fig. 2.9). Bed thickness varies considerably from decimetre-scale to metre-scale. In places, thin layers of red or purple mudstone cap sandstone beds and in places the mudstone fragments form thin intraformational mudchip conglomerates at various positions within the sandstones. In many cases sandstone beds

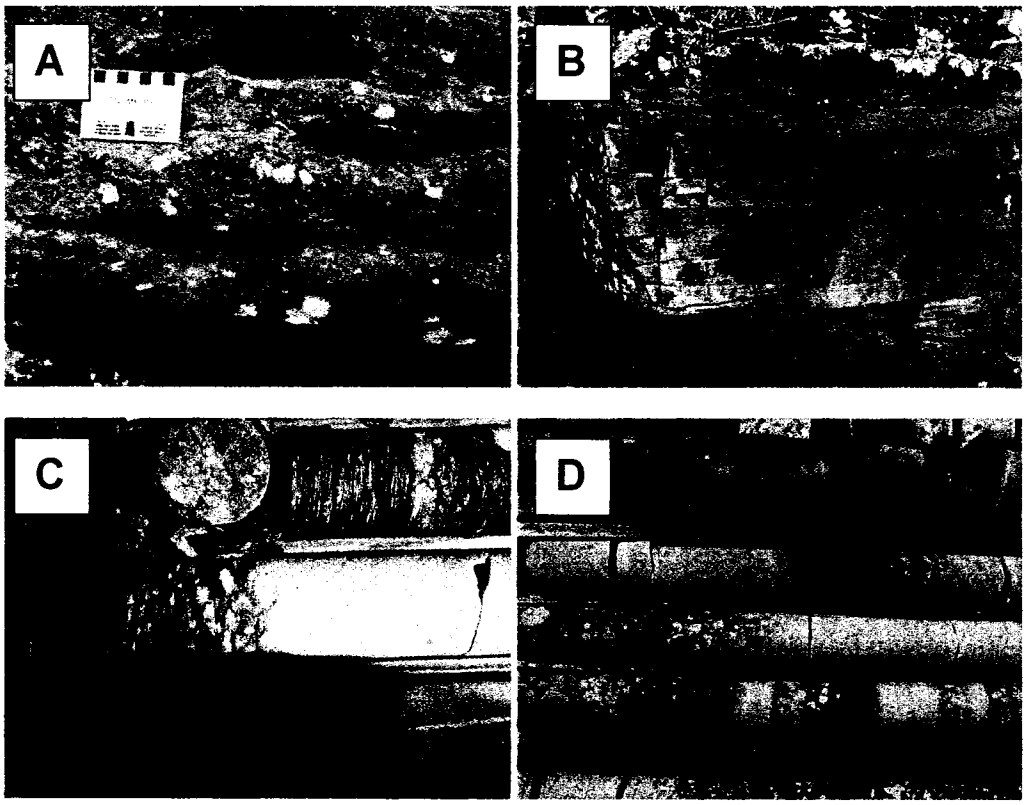

Figure 2.9. Examples of the trough cross-stratified sandstone lithofacies association. A) Discontinuous lenses filled with trough cross-stratified sandstone near Silver Islet. Gradations on scale card are in centimetres. B) Medium-scale trough cross-stratified sandstone near the Enterprise mine. Green pocket knife shown for scale is 10cm long. C) Pedogenically (?) modified top of a massive sandstone bed near the Sibley-Archean contact in drill core NB-97-2. (d) Massive sandstone beds from drill core NI-92-7, occasional vague cross-stratification is present.

have graded matrix compositions with a higher silt concentration towards the top of individual beds. Some sandstone bed tops display distrupted textures consisting of irregular balls of sandstone surrounded by "skins" of clay- or silt-rich material (Fig. 2.9c). Sulfate veins or nodules are present in some sections, but are relatively rare. Intervals up to several metres thick that consist of centimeter-scale interbedded red

siltstone and sandstone are present within this association. In some drill-holes (e.g. the DO-82 series) this association contains decimetre-scale layers of clast-supported conglomerates and pebbly sandstones, particularly near the basal contact. At the Silver Islet locality zones of metre-scale thickness, composed of stacked, decimetre thick lenses of trough cross-stratified, medium-grained, sandstone are interbedded with zones composed of tabular, thinnly-bedded medium-grained, silty sandstone that contain laterally discontinuous lenses of better sorted medium-grained sandstone (Fig. 2.10).

Figure 2.10. The trough cross-stratifed sandstone lithofacies association west of Silver Islet, showing a lower zone of thinnly interbedded red, silty sandstone and lensoid buff-coloured better sorted sandstone and an upper zone of buff-coloured stacked lenses of trough cross-stratified sandstone. Trough cross-stratification is not visible in the photo. Packsack shown for scale is about 30cm wide.

2.3 Rossport Formation

The Rossport Formation consists of the Channel Island, Middlebrun Bay and Fire Hill Members (Franklin et al., 1980; Cheadle, 1986a and b). In a general sense, the Channel Island Member is comprised of a mixture of fine-grained red siliciclastic rocks, muddy dolostones, dolomitic sandstones and occasional sheet-like sandstone beds. The Middlebrun Bay Member is a thin spatially discontinuous layer of laminated black chert and carbonate. The Fire Hill Member consists of red mudstones and siltstones with variable dolomite content, occasional sandstone beds, nodular carbonates and evaporite minerals (gypsum/anhydrite).

The Rossport Formation overlies the Pass Lake Formation through a number of different contact styles. At the sections on Copper Island and Channel Island, the Rossport and Pass Lake Formations are separated by a thin (less than 1 m thick) conglomerate unit with both extra and intraformational clast types (Fig. 2.11). At Copper Island elongate, angular, up to cobble-sized clasts of Pass Lake Formation sandstone form a thin (10-20 cm) matrix-supported layer. On Channel Island the conglomerate at the lithostratigraphic contact is a thicker (up to 1 m) matrix-supported, polymictic horizon. Green shale clasts are abundant in the conglomerate on Channel Island and these may be derived either from underlying Pass Lake Formation shales or the Rove Formation. On Copper Island the contact is also a slight angular disconfomity (Fig. 2.6). However, a gradational contact is the most common style with the transition marked by a decrease in the frequency of sandstone beds and an increase in the frequency of red siltstone beds.

Nine distinct lithofacies associations have been identified in the Rossport Formation. These are termed: the red siltstone lithofacies association, the red siltstone-dolostone lithofacies association, the red siltstone-dolomitic sandstone lithofacies association, the sheet sandstone lithofacies association, the black chert-carbonate lithofacies association, the intraformational conglomerate/breccia lithofacies association, the massive dolostone lithofacies association, the red siltstone-sulfate lithofacies association, and the red siltstone-fine-grained sandstone lithofacies association.

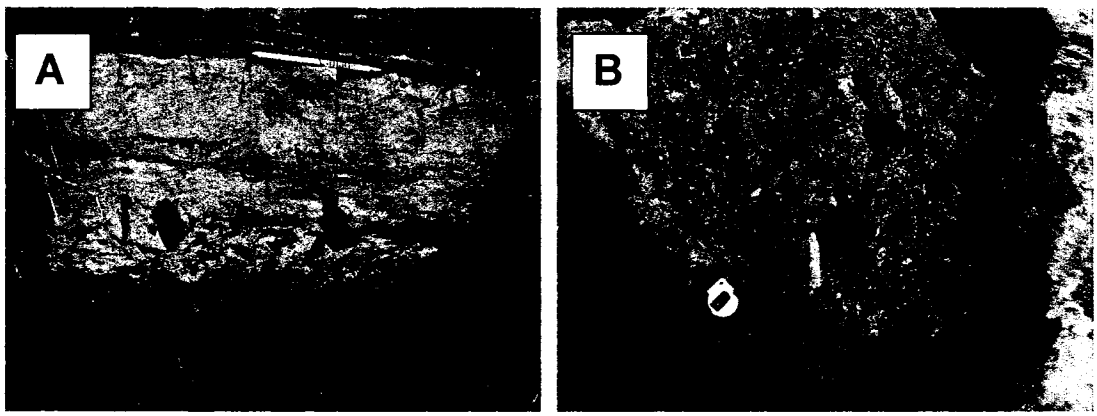

Figure 2.11. A) Angular clasts of Pass Lake Formation sandstone at the contact between sandstones of the green sandstone/siltstone lithofacies association (Pass Lake Formation) and contact metamorphosed pale green dolomitic siltstone of the red siltstone lithofacies association (Rossport Formation), Copper Island. Pencil shown for scale is about 15cm long. B) Conglomerate at the Pass Lake Formation-Rossport Formation contact with a variety of intra- and extrabasinal clasts, Channel Island. Tape measure is shown for scale is about 10cm wide.

2.3.1 Red siltstone lithofacies association

This generally ten to twenty metres thick lithofacies association is dominated by massive red siltstones (Fig. 2.12) and commonly occurs at the base of the Rossport Formation. The siltstones range from pale red to brick red probably reflecting differences in dolomite versus siliciclastic content (Mailman, 1999). Medium- to coarse-grained sandstones are also present and form thin beds a few centimetres to 40 centimetres in thickness (Fig. 2.12b). In outcrops on Channel Island sandstone beds are generally

laterally continuous but in a few cases the beds, especially thicker sandstone beds, are lensoid and have lateral continuities of 5-10 m (Fig. 2.12b). The sandstones are generally massive, and are normally graded in many cases. In a number of sections individual horizons that coarsen-upward, from red siltstone to coarse sandstone over a few decimetres to metres, are present (Fig. 2.12c). Matrix supported grains of sand are commonly found throughout siltstone beds (Fig. 2.12d).

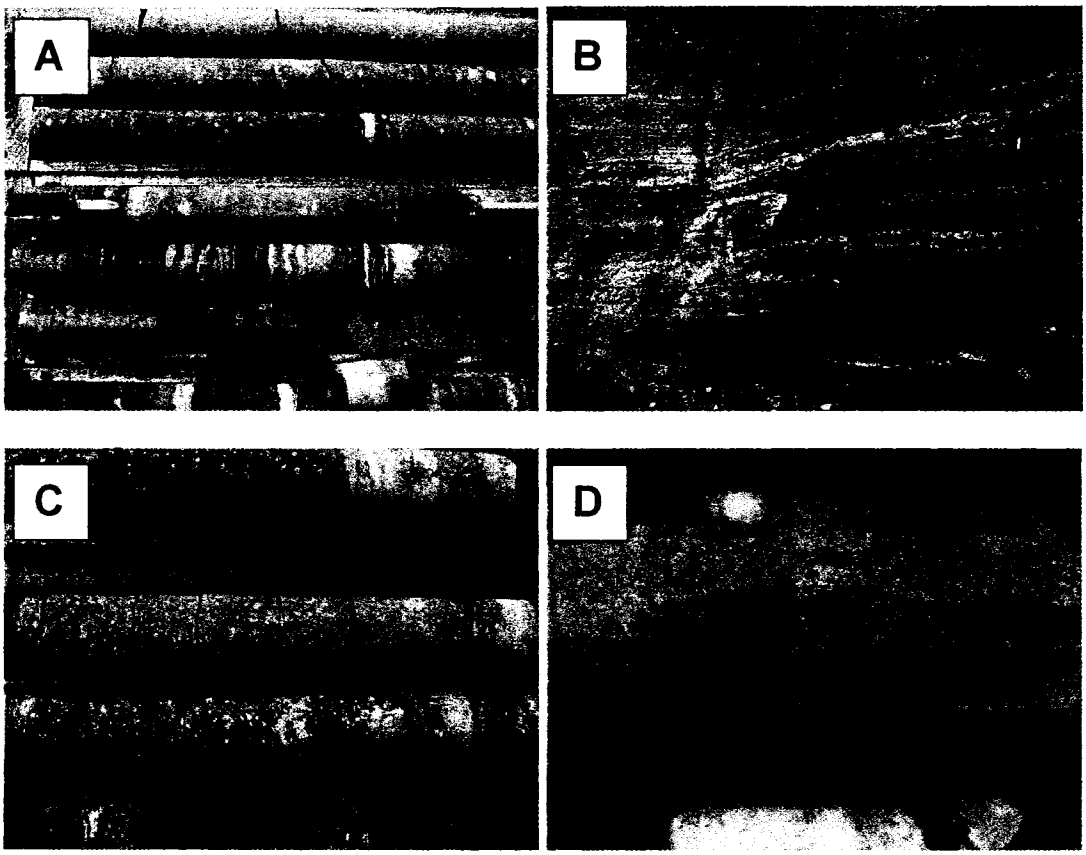

Figure 2.12. Lithofacies that are common in the red siltstone lithofacies association. A) A coarsening upwards unit approximately 40 cm thick that illustrates a change from massive red siltstones at the base (marked by yellow pen) to a coarse-grained sandstone top marked by pen knife blade. B) The red siltstone facies at Channel Island showing a sandstone lense about 40 cm thick near the base of the photo and thin beds of red siltstone interbedded thin graded sandstone beds above it. C) Red to pale red siltstones from DDH NB-97-2 that are the dominant lithofacies in this association. D) An irregular zone of coarse-grained sandstone. Similar sandstone layers are common throughout thick zones dominated by siltstone.

The red siltstone-dolomite or red siltstone-dolomitic sandstone lithofacies associations overlie this unit. A gradational contact is common, with a change to a more distinct periodic/cyclic bedding style characteristic of the red siltstone-dolomite or red siltstone-dolomitic sandstone lithofacies associations occurring over a few metres.

2.3.2 Red siltstone-dolostone lithofacies association (cyclic facies)

The red siltstone-dolomite association consists of two basic facies: pale pink to grey dolomitic mudstone (dolostone) and pale red to red dolomitic mudstone-siltstone (red siltstone) (Figs. 2.13, 2.14, 2.15). Both lithofacies are present as pure "end members" but also as variable mixtures that are interbedded complexly at various scales with individual layer thickness ranging from millimetre-scale to decimetre-scale. On occasion, metre-scale intervals that are dominated by the red siltstone lithofacies are present. Thin (<10cm) massive clast or matrix supported coarse to very coarse-grained sandstone beds are found sporadically throughout the association. Thin layers of fine-grained sandstone are also found within some dolostone beds. Petrographically, both the red siltstone lithofacies and the dolostone lithofacies are comprised mostly of very finely-crystalline dolomite (Fig. 2.14). The primary difference between the two lithofacies is the presence of abundant very fine-grained hematite in the red siltstone lithofacies along with slightly coarser grain-size and slightly lower dolomite content (Mailman, 1999).

Ca-sulfate minerals occur in three primary forms within this lithofacies association. The most common form is as nodules within dolostone or, less commonly, red siltstone beds. Nodules range from millimetre-scale to 2 cm in diameter. Irregular rosette-like forms are the most common. Inclusions of dolomite are present in many

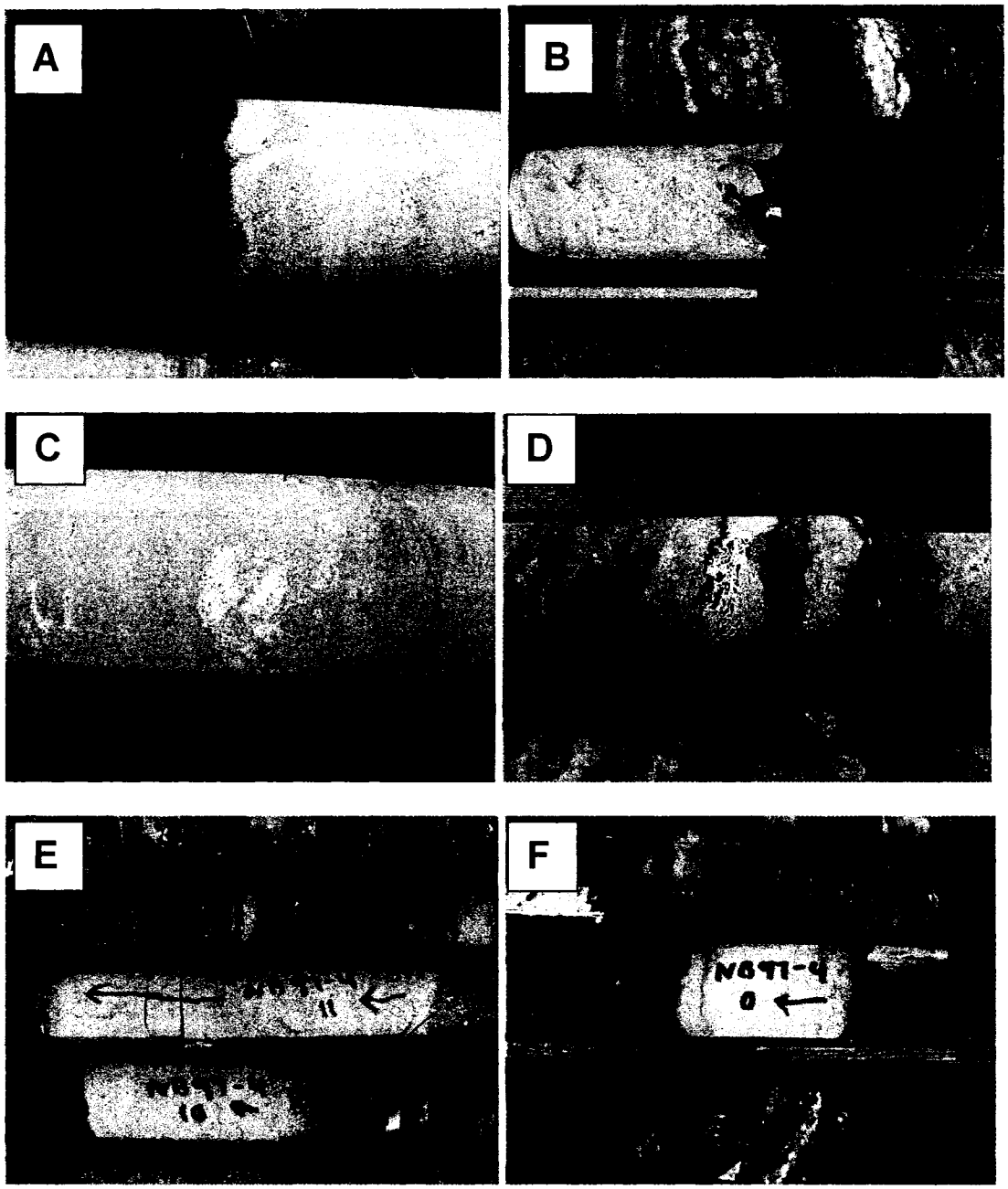

Figure 2.13. Examples of lithofacies and contact styles in the the red siltstone-dolostone association. A) A mudcrack on the surface of a dolostone bed, the younging direction is towards the left of the photograph. B) An irregular brecciated top of a dolostone bed, the younging direction is to the right. C) Sulfate nodule near the centre of a relatively thick dolostone bed from DDH NB-97-4. D) A thin dolostone bed with fine-grained bladed sulfate nodules E) Two distinct contact styles between plae dolomite beds and red siltstone. The middle section of core labeled NB97-4 11 shows a symmetrical dolomite bed with gradational contacts at both the base and the top. The lower section of core, labeled NB97-4 10, shows an asymmetrical dolomite bed with gradational basal contact and a sharp upper contact. F) A symmetrical dolomite bed with sharp upper and lower contacts.

examples. Another mode of occurrence of Ca-sulfate minerals is as thin infills of mudcracks at the tops of some dolomite beds. The cracks are wedge shaped and typically less than 2 cm long (max 5cm) and are 1-5 mm wide at their tops. Bladed sulfate

crystals are also present as sand sized particles within some dolomite beds. Small anhedral barite nodules are also present, and one example of a subhedral (10 um) celestite crystal was noted.

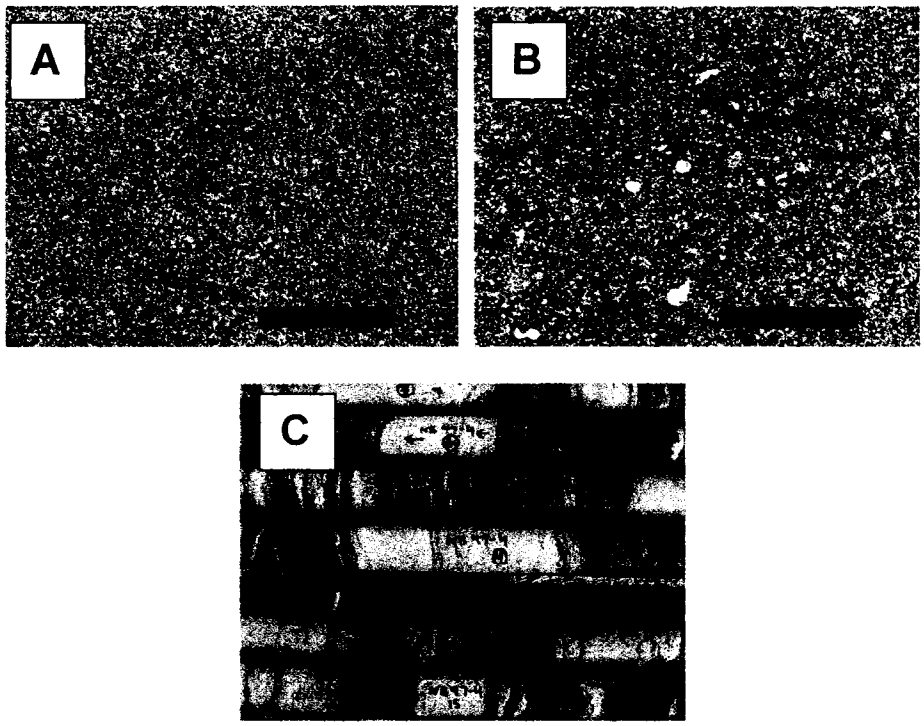

Figure 2.14. Petrographic comparison between typical red siltstone and dolostone lithofacies. Scale bars in A and B are 500 um in length. A) dolostone displaying uniform micritic crystal size. B) red siltstone composed of similar micriitc dolomite with abundant hematite and higher abundance of coarser silt-sized material. C) Variable scales of interbedding between red siltstone and dolostone lithofacies.

Contact styles between red siltstone and dolostone beds are variable. Dolostone beds can be classified into 3 basic types (Figs. 2.13 e and f): symmetrical beds with relatively sharp upper and lower contacts, symmetrical beds with gradational upper and lower contacts, and asymmetrical beds with a gradational lower contact and a sharp upper contact. A typical bedding cycle consists of a sharp lower contact, a basal portion consisting of red siltstone, an upwards gradual change to paler coloured dolomitic mudstone followed by another sharp contact with red siltstone. In some examples, the tops of dolomitic mudstones display mudcracks that are filled with sulfate minerals or

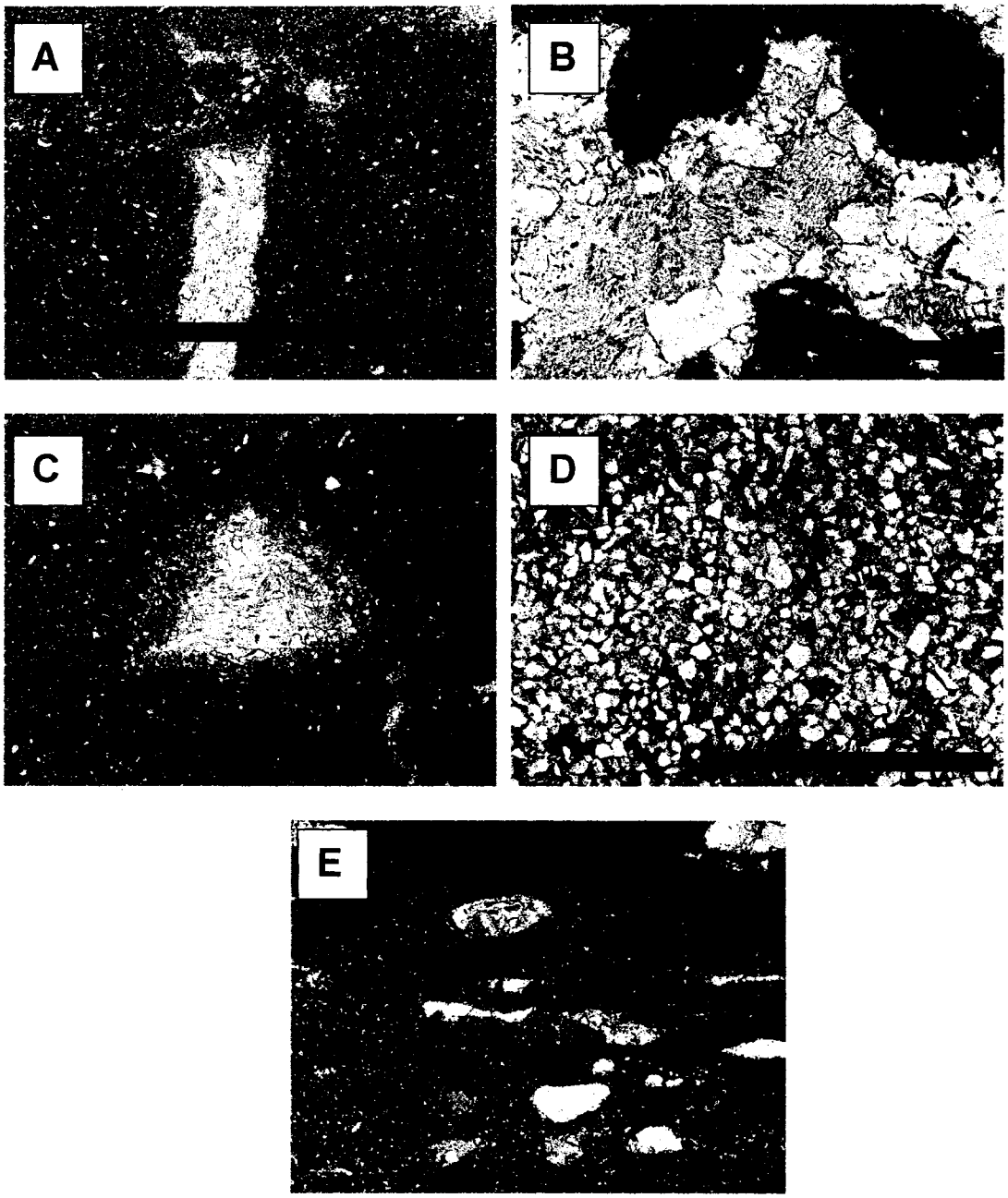

Figure 2.15. Photomicrographs showing petrographic characteristics of the red siltstone-dolomite lithofacies association. Scale bars are all 2mm except B which is 500 um. A) A dolomite layer top marked by fine sulfate-filled mudcrack. B) An irregular sulfate nodule with inclusions of dolomite and some replacement by coarser dolomite crystals. C) discrete subhedral gypsum/anhydrite nodule in dolomite. D) Fine-grained siliciclastic-rich layer within a dolomite bed. E) dolostone layer with rounded sulfate grains.

coarser dolomite replacement of sulfate minerals. Sulfate-filled mud cracks are present within some individual dolostone horizons. In other cases the tops of dolostone beds are

very irregular and in places a few matrix-supported clasts of dolostone mark remnants of originally tabular beds.

2.3.3 Red siltstone-dolomitic sandstone association

Superficially this association resembles the red siltstone dolomite association with the dolomite lithofacies replaced by medium- to coarse-grained dolomitic sandstone. Sandstones in this association have both siliciclastic and carbonate grains but are cemented by dolomite. The best exposure of this association occurs on Channel Island. The sandstone lithofacies is medium to coarse-grained and massive and in some examples graded. Trough cross-stratification is preserved in some sandstone beds, but this is rare. Sandstone bed thickness is variable and ranges from 1-40cm with an average thickness of about 10-15cm (Fig. 2.15). Red siltstone interbeds have similar thicknesses. The red siltstone facies is red to pale red and massive to crudely layered. Thin discontinuous sandstone lenses are present and individual matrix-supported sand grains are common within red siltstone layers. Load features are common along the basal contacts of sandstone beds (Fig. 2.15a). On Channel Island coarse- to very coarse-grained sand-sized black siltstone clasts are common at the bases of graded sandstone beds. The grain-size of the sandstone beds varies stratigraphically and there appear to be zones with much coarser- grained sandstone intercalated with zones of much finer-grained dolomitic sandstone or even the red silstone-dolomite lithofacies association. Where present the thickness of this unit ranges from 10 to 20 m. The lower contact of this unit with the red siltstone lithofacies association appears to occur over a few metres and is marked by a change to a distinct periodic/cyclic bedding style. The upper contact

of this unit is abrupt and is marked by the appearance of thick medium- to coarse-grained sandstone beds of the sheet sandstone association.

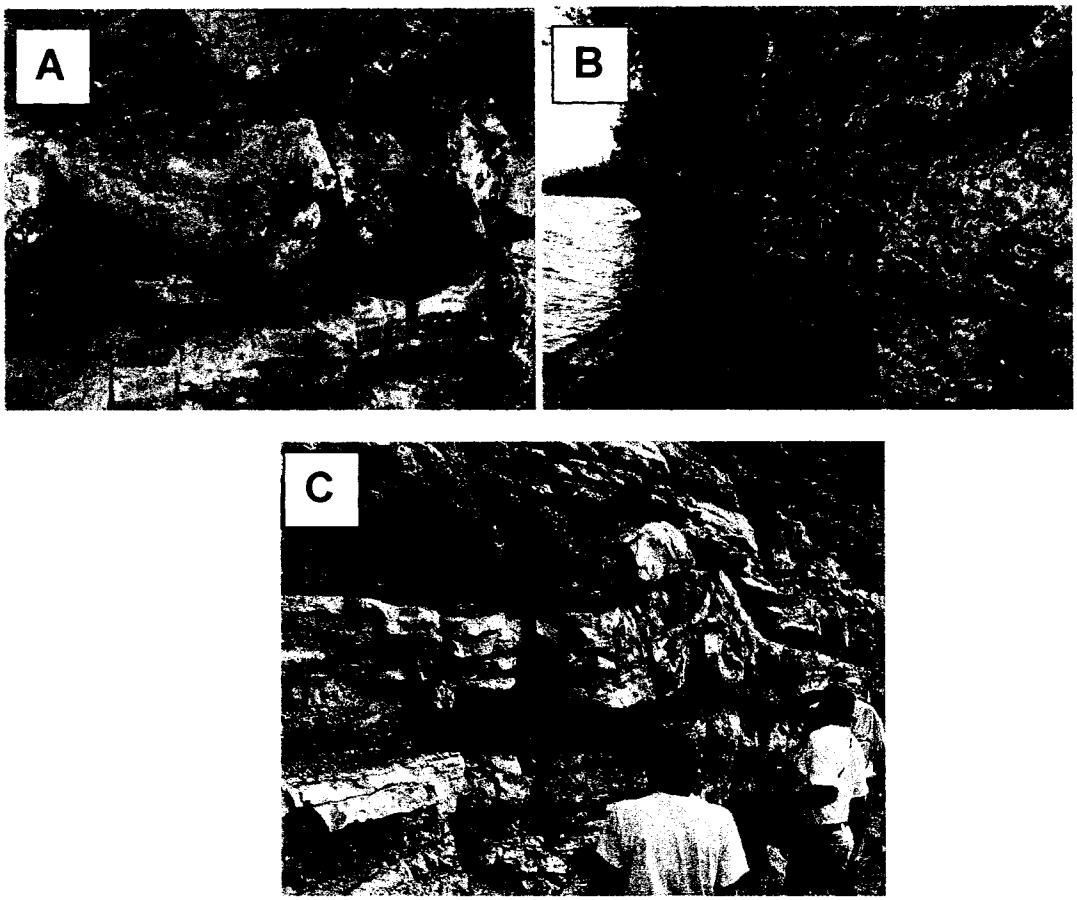

Figure 2.15. Red siltstone-dolomitic sandstone association. A) distinct load features at the base of a coarse-grained dolomitic sandstone, Channel Island. Pen knife shown for scale is 12cm long. B) "Cyclic facies" at Channel Island with pale red beds of siltstone and pale white resistant layers of dolomitic sandstone, note the similarity to the appearance of the red siltstone-dolostone association. Photograph shows approximately 5m of vertical section. C) "Cyclic facies" in red siltstone-dolostone lithofacies association at Kama Hill, pale beds are micritic dolostone rather than the dolomite cemented sandstones in A and B.

2.3.4 Sheet sandstone lithofacies association

This association occurs in nearly all of the sections studied. It usually separates the cyclic red siltstone/dolomite association from the black chert/carbonate association or other associations higher in the stratigraphy when the black chert-carbonate lithofacies

association is absent. The thickness of this unit varies from 5 to 30 m. The sheet sandstone lithofacies association consists of two basic lithofacies. The first is a red siltstone lithofacies common to most of the associations in the Rossport Formation (Fig. 2.16b). The red siltstone lithofacies in predominantly massive but fine horizontal

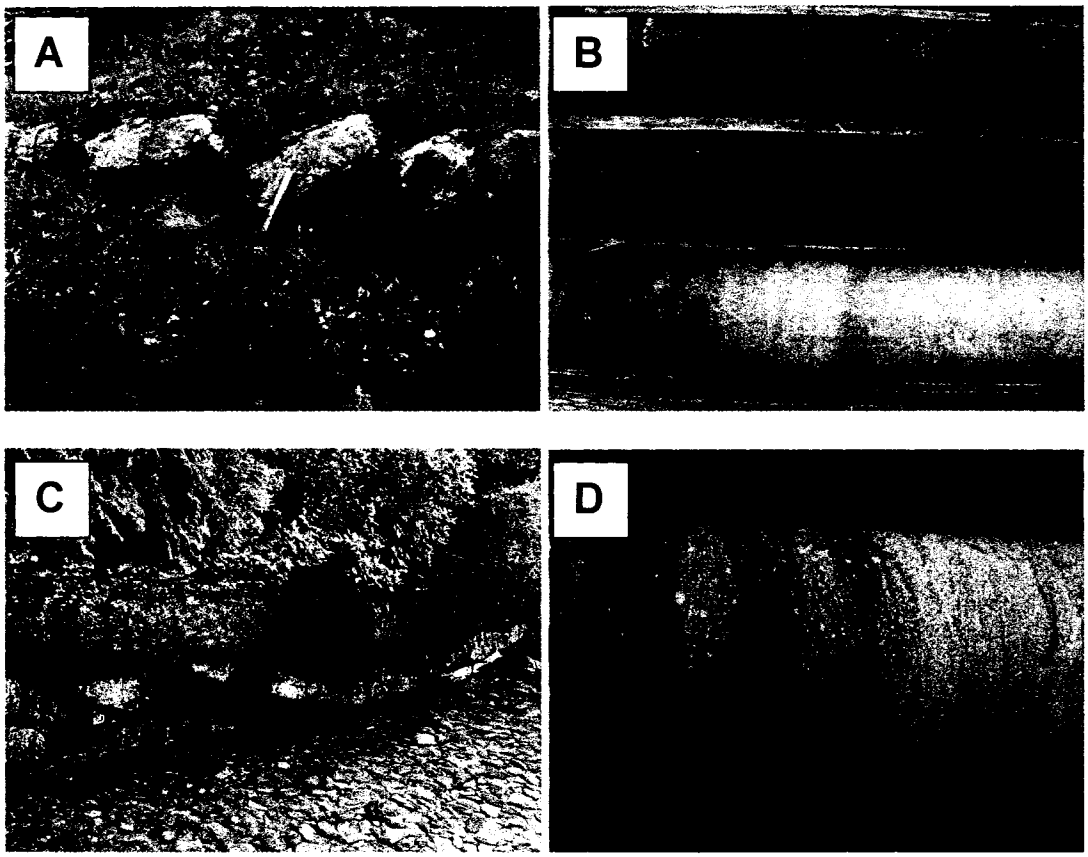

Figure 2.16. A) Synsedimentary listric faults with southward (basinward) dipping fault planes in a well sorted medium-grained sandstone bed at the Kama Hill locality. Hammer shown for scale is about 30cm long. B) A typical example of the red siltstone lithofacies in the sheet sandstone lithofacies association from drill core NB-97-4. C) A typical thick sandstone bed with medium to large scale trough cross-stratification, Channel Island. Photograph shows about 1m of section. D) Rippled, siltier, top of a sheet sandstone bed DDH NB-97-4.

laminations and current or wave ripple laminations occur at some horizons. At Channel Island the top of this association contains rippled fine-grained sandstone immediately underlying the black-chert carbonate lithofacies association. Sulfate nodules are rare but present within the siltstone lithofacies. The second, more distinctive, lithofacies consists of tabular to lensoid, medium- to coarse-grained, well-sorted quartz-rich sandstone (Fig.

2.16). The sandstone lithofacies is generally massive, although parallel lamination and trough cross-stratification (Fig. 2.16c) are present in some cases. Sandstone beds range from 5 to 250cm in thickness, red siltstone beds are commonly a similar thickness but may also be much thicker, on the scale of several metres. Sandstone intrusions are common, and they are present as wedge shaped cracks (Fig. 2.17) that cut downwards from sandstone beds, tabular dikes that average about 10 cm in thickness and diapirs with diameters of several metres that disrupt overlying beds. Synsedimentary listric faults are present in some exposures (Fig. 2.16a), particularly in sections with thinner sandstone beds and a higher proportion of red siltstone. The tops of many sheet sandstone beds are siltier and show ripple lamination (Fig. 2.16d).

Figure 2.17. Clastic dike emanating from the base of a massive sandstone bed intruding downward into a mottled red siltstone. Author's hand for scale. Lake Superior shoreline northeast of the town of Silver Islet.

2.3.5 Black chert-carbonate association

The black chert-carbonate association is equivalent to the Middlebrun Bay Member in the lithostratigraphic subdivision of the Sibley Group. This association consists of layers of massive micritic carbonate (mainly dolomite) interbedded with layers of chert. Layering varies from thin millimetre- to centimetre-scale laminations of chert and carbonate to several centimetre thick layers of micritic carbonate. Contacts between chert and carbonate laminae are sharp. Individual beds or laminae are commonly laterally continuous at outcrop scale, though chert sometimes occurs as irregular pod-like features. Laterally linked hemispherical structures (stromatolites) are present in most outcrops of this facies and have amplitudes of up to 10 cm. Cone-shaped structures are also present and these are generally 5 to 10cm in height with basal diameters of 8-10 cm. Gypsum nodules are commonly present but are in many cases replaced by carbonate or silicified. Cheadle (1986a and b) and Rogala (2003) both noted the presence of halite in this association. A number of carbonate-replaced cubes were noted in thin section but could not be firmly identified as halite. Very rarely small clusters of framboidal or cubic pyrite grains were noted in thin sections of finely laminated black chert and carbonate. Organic carbon is also present, often as micron-scale spheres that form nuclei for round chert nodules. Synsedimentary breccias cross-cut layering in a number of exposures of this association.

A fairly consistent vertical organization of lithological elements is present in exposures of this lithofacies association. The base is commonly comprised of 20-30 cm of "crinkly", mm-scale laminations of grey to black chert and carbonate. The laminations are generally very flat features with the amplitude of "crinkles" typically being 0-2 cm.

Occasional asymmetrical domes with basal diameters of about 5cm and heights of 3-4cm are developed. Inheritance of laminae shape is common from one layer to the next. Thicker layers of white carbonate, however, do not usually conform to the shape of the previous depositional layers. The basal portion is overlain by 10-20 cm of massive white micritic dolomite. This portion often contains brecciated zones as well as irregular pods of chert. Chert pods vary from white/pale grey in colour to deep black. The second unit is overlain by 20-30 cm of flat mm-scale laminated chert and carbonate and distinct stromatolitic domes comprised of similar laminated chert and carbonate. In the third unit, Cheadle (1986b) recognized two stromatolite form types, mainly from the outcrops of this lithofacies association at Kama Hill. The relatively flat laminated chert and carbonate Cheadle (1986b) termed crypt-algal laminites consistent with the form genus and species stratifera metula in the stromatolite classification of Komar (1966). Cheadle (1986b) classified laterally linked hemispherical domes as columnar stromatolites belonging to the form genus and species conophyton metula (Komar et al., 1965). The third unit is in turn overlain by more flat finely laminated carbonate and chert lacking distinct domal features. Cheadle (1986a and b) reported dolomite pseudomorphs after skeletal halite just above the horizon containing abundant stromatolitic domes. This four-fold stratigraphic organization is generalized and all four units are not always present at all exposures.

The top of this association commonly has a chalky, poorly consolidated, weathered appearance (Fig. 2.20). The altered zone is approximately 10-20 cm thick and contains distrupted original carbonate layering, abundant purple and red oxide-rich clay/silt sized material and silica 1mm to 2 cm in diameter. Purple and red oxide rich

mudstone and siltstone often form thin coatings around fragments of original carbonate layers and also around silica nodules. In thin section irregular laminae of hematite-rich

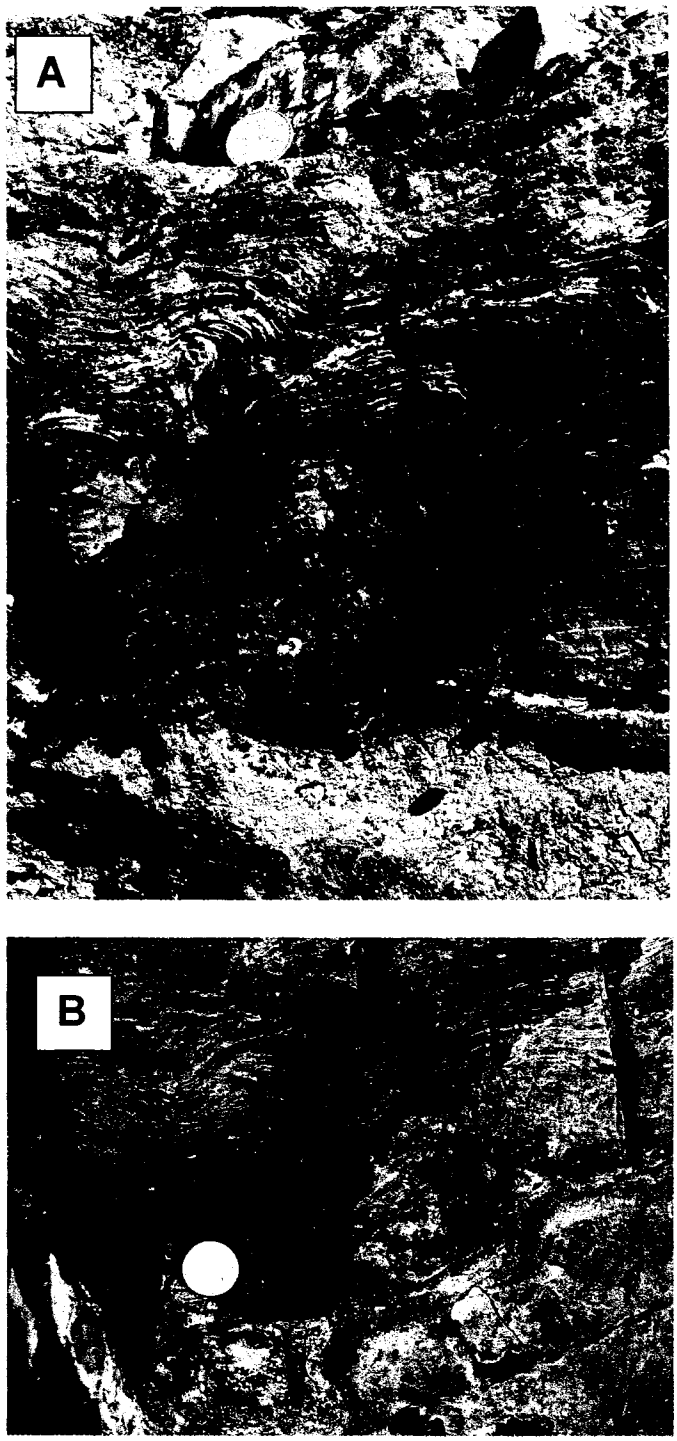

Figure 2.18. Stromatolitic domes in the black chert-carbonate association. A) (left) asymmetrical domes comprised of thin carbonate and chert laminae. Note that domes are skewed to the right of

the photograph. 5 cent coin shows scale. B) (right) Symmetrical low relief domes comprised of carbonate and chert laminae. 5 cent coin shows scale.

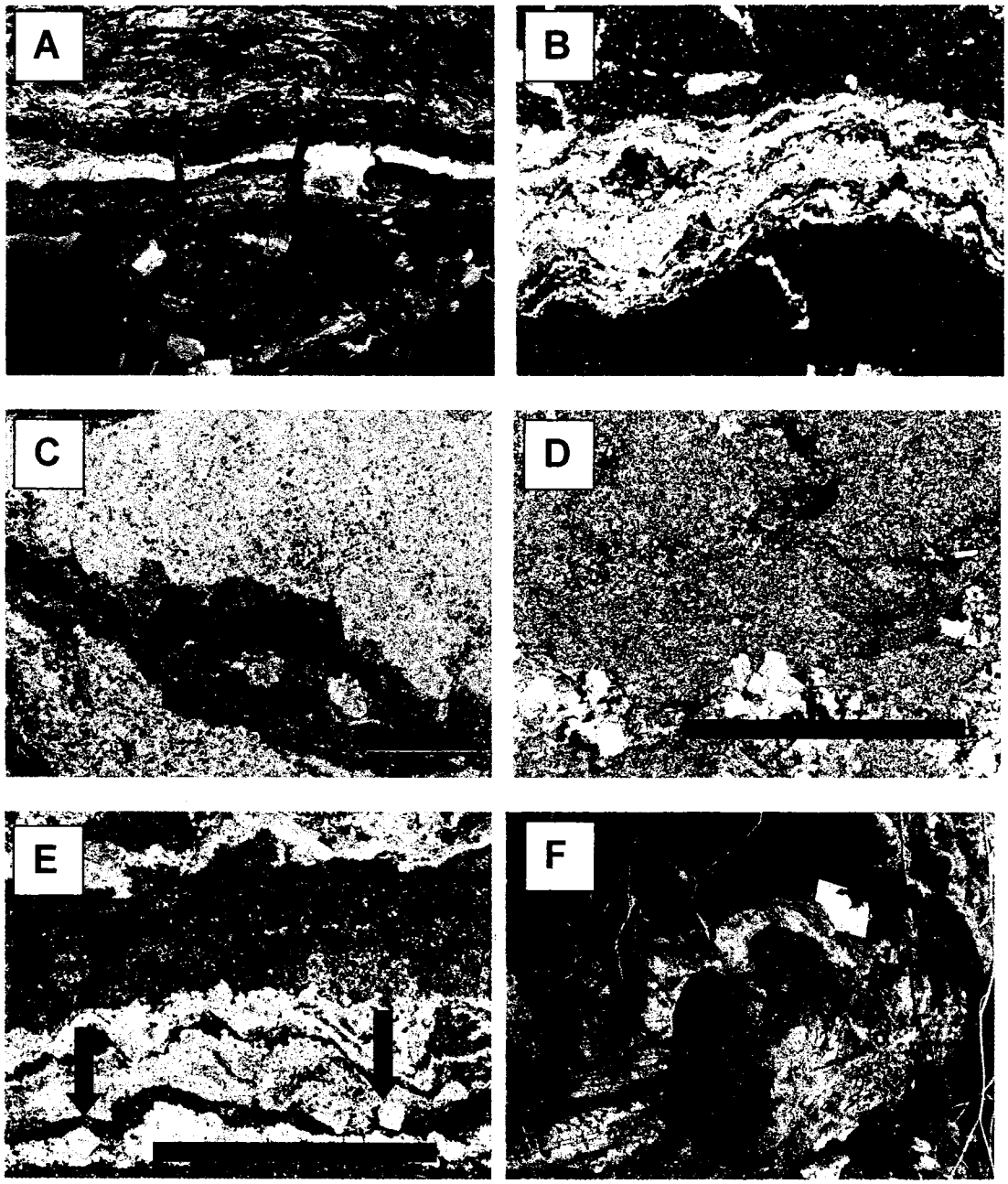

Figure 2.19. Photographs and photomicrographs showing important features of the black chert-carbonate lithofacies association. A) outcrop photograph showing a lower section of massive white micritic carbonate with diagenetic chert nodules overlain by a zone of flat crinkly chert-carbonate laminae, Channel Island. Pen knife shown for scale is 12cm long. B) Photomicrograph showing typical chert (light) and carbonate (dark) laminae. Scale bar is 2mm. C) irregular zone of pyrite in a carbonate rich layer. Scale bar is 200um. D) altered top of the black-chert carbonate lithofacies association at Kama Hill outcrop showing round chert nodules and irregular wisps of hematite rich mudstone. Scale bar is 2mm. E) Possible halite cubes along lower margin of a chert layer (shown with arrows). Scale bar is 2mm. F) irregular pod of black chert in massive white micrite, near Red Rock. Scale card near top right of photo is 10cm wide.

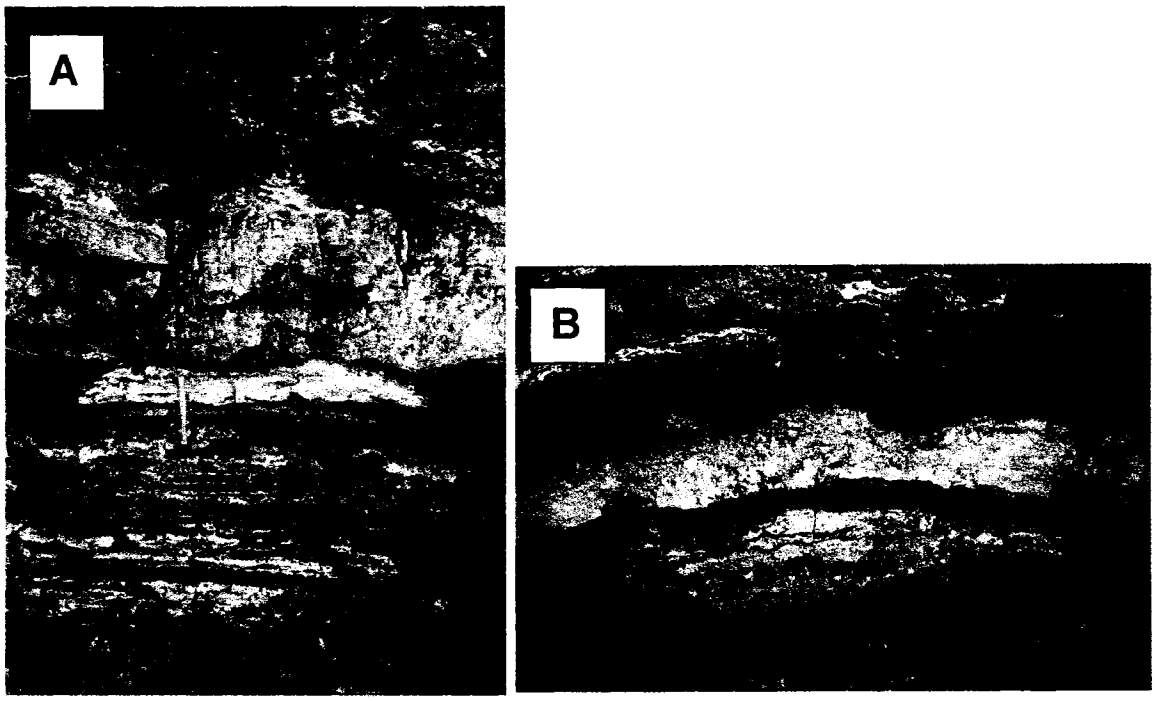

Figure 2.20. Typical stratigraphy of the transition between sheet sandstone, black chert-carbonate and intraformational conglomerate lithofacies associations, Channel Island. A) The lower portion of the top photo consists of red siltstones and rippled fine-grained sandstones. The middle section of the photo, comprised of the black chert-carbonate lithofacies association, sharply overlies the lower section. The top portion consists of intraformational conglomerate which sharply overlies the weathered top of black chert carbonate association. Hammer shown for scale is about 30cm long. B) Detail of internal stratigraphy within the black chert-carbonate lithofacies association showing a lower portion of massive muddy to silty carbonate with chert nodules, and an upper portion of krinkly laminated stromatolite. Field of view is about 60 cm high.

siltstone/mudstone are found in variably oriented thin seams within micritic carbonate fragments (Fig. 2.19d). Red hematitic mudstone is also found in cm-scale fractures on the tops of bedding plane exposures. The top of this altered zone, and the top of this lithofacies association, is in sharp contact with overlying intraformational conglomerate (Fig. 2.20).

2.3.6 Intraformational conglomerate/breccia lithofacies association

Several types of intraformational conglomerate/breccia have been identified in the Rossport Formation. One type occurs as clearly secondary cross-cutting zones usually involving the red siltstone-dolomite association (Fig. 2.22). These cross-cutting breccias form diapir shaped bodies several metres high and wide and consist of local lithologic types. A second type, already mentioned in the description of the sheet sandstone association, occurs in association with clastic dikes and intrusions associated with sheet sandstone beds. Two further types of intraformational conglomerate have also been identified and are described in detail below. One type occurs above the black chert-carbonate association, another type occurs in one example near the town of Pass Lake at a similar stratigraphic position.

Figure 2.22. Cross-cutting intraformational breccia in the red siltstone/dolomitic sandstone lithofacies association, Channel Island. Hammers shown for scale are both about 30cm long.

The black chert-carbonate association is commonly sharply overlain by 0.5-2 metres of intraformational conglomerate. The conglomerate is generally clast supported and consists of angular to slightly rounded intrabasinal clasts. Clast types are dominated by red siltstone and dolostone, but black chert and sandstone clasts are also present. The matrix composition of the conglomerate is hematitic and carbonate-rich. Occurrences of this association appear to be restricted to sections where it directly overlies the black chert-carbonate lithofacies association, but the black chert-carbonate association is not always overlain by intraformational conglomerate. In one instance on the southwest side of Channel Island two units of intraformational conglomerate are present with a lower layer dominated by chert and carbonate clasts (i.e., comprised entirely of clasts from the black chert carbonate association) and an upper layer comprised of primarily red siltstone and medium-grained sandstone clasts. The geometry of the intraformational conglomerate layers is generally tabular although lateral changes in clast types, grainsize and matrix compositions are common. The contact with the overlying massive dolostone lithofacies association is sharp.

A second style of intraformational conglomerate is present in one exposure in a road cut south of the town of Pass Lake. The stratigraphic position of this exposure is unknown though it is interpreted to be roughly equivalent lithologies overlying the black chert-carbonate lithofacies association. A crude vertical organization of lithofacies is present within the exposure. The base consists of an irregular contact with a sandy dolostone bed. The contact is very sharp and varies from horizontal to nearly vertical in orientation. A concentration of red to purple mudstone to siltstone is present draping the lower contact. The sandy dolostone at the contact also contains concentric nodules of

dolomite in some places. Tapered cracks up to 10 cm wide at the top and 30-40cm long filled with hematite rich siltstone and mudstone are present at the tops of the dolomitic sandstone. Above the sharp basal contact there is 1-2 m of intraformational conglomerate. The intraformational conglomerate is comprised of angular to somewhat rounded clasts of dolomite, red siltstone and, more rarely, purple mudstone and medium-grained red or buff coloured sandstone. Clast sizes range from a few centimetres to 75 cm in diameter.

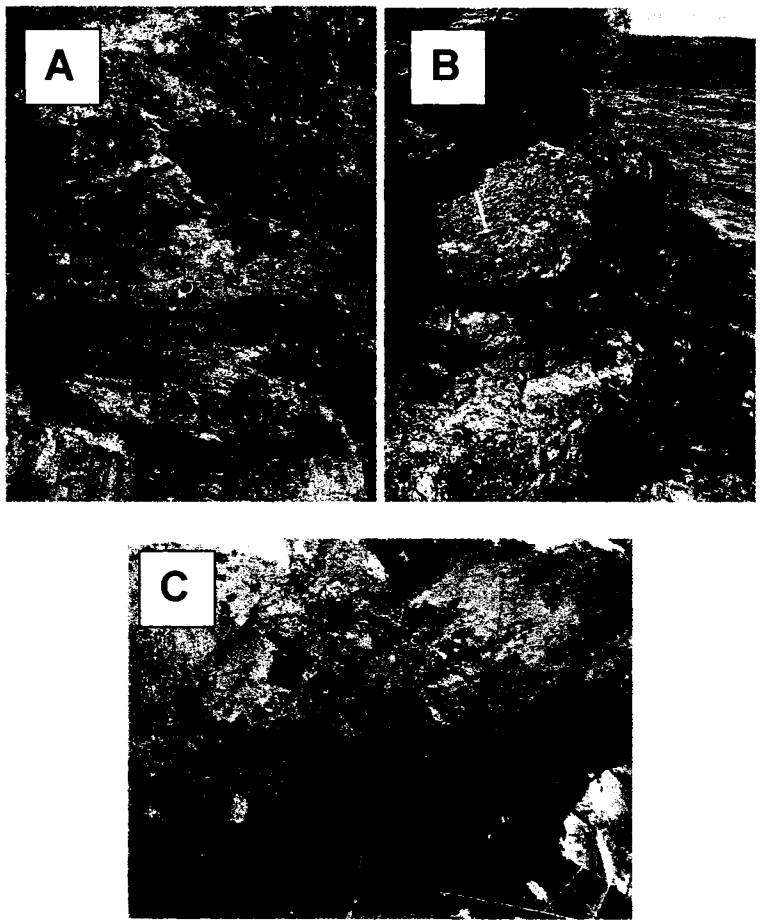

Figure 2.23. Intraformational conglomerates overlying the black-chert carbonate lithofacies association. A) Matrix supported angular clasts of fine-grained dolomitic sandstone and red siltstone overlying a sharp contact with the black-chert carbonate association, Channel Island. Tape measure shown for scale is 10cm wide. B) Two distinct horizons of intraformational conglomerate on the northeast side of Channel Island, a lower horizon consisting of cherty carbonate lithologies and and upper horizon consisting of red siltstone, dolomite and fine-grained sandstone clasts. Hammer shown for scale is 30cm long. C) Clasts of black chert in a carbonate-rich matrix. Pencil shown for scale is about 12cm long.

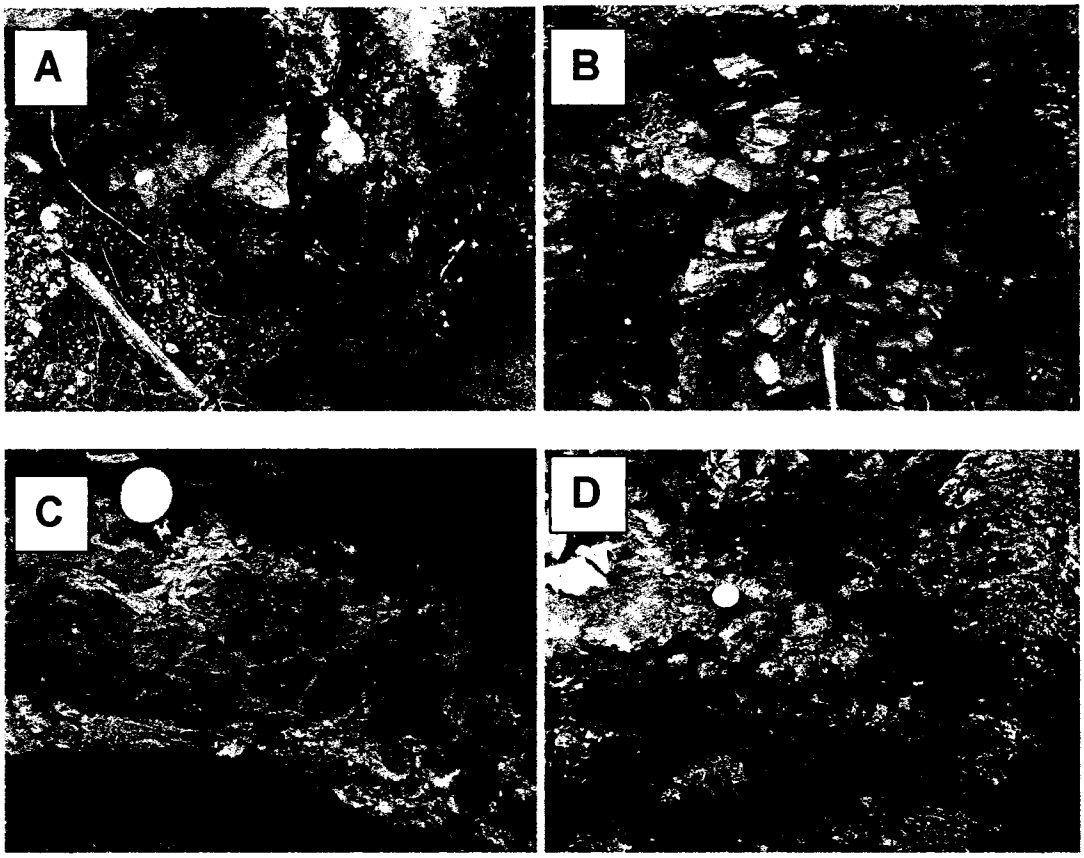

Figure 2.24. Features of intraformational conglomerate near the contact between red siltstone-dolomite/red siltstone dolomitic sandstone lithofacies associations and the sheet sandstone lithofacies association, south of Pass Lake. A) Large crack filled with hematite-rich rubble in the top of dolomitic fine-grained sandstone bed. Canadian penny shown for scale. B) Large rounded block, or possibly relief in fine-grained dolomitic sandstone bed draped with red to purple oxide rich clay and siltstone overlain by intraformational conglomerate. Portion of hammer handle shown for scale is about 20cm long. C) round nodular carbonates at the contact between dolomitic sandstone and overlying conglomerate. Canadian penny shown for scale. D) intraformational conglomerate with purple oxide-rich matrix. Canadian penny shown for scale.

Matrix composition in the conglomerate is typically a red dolomitic siltstone, though in places it is sand rich. The intraformational conglomerate is overlain by lenses of medium-grained sandstone. Sandstone lenses are laterally continuous for a few metres and range from 20-50 cm in thickness.

Figure 2.25. Crude stratigraphy in intraformation conglomerate lithofacies association south of Pass Lake showing, intraformational conglomerate horizon and overlying lenses of medium-grained massive sandstone. The basal contact with dolomitic sandstone is obscured by grass. Hammer shown for scale is 30cm long.

2.3.7 Massive dolostone lithofacies association

Dolostones similar in appearance to dolostones in the red-siltstone/dolostone association are present overlying the black chert-carbonate and intraformational conglomerate lithofacies associations in the southern portions of the basin. The thickness

of this association is approximately 10-20 m. Lithofacies present in this association are mottled dolostones that vary from a pale brown to red colour and thin lenses of red to purple more siliciclastic-rich siltstone to mudstone. Bedding is difficult to distinguish in the dolomitic mudstone, but it has a crudely banded appearance defined by colour variations. Interbeds of siltstone/mudstone are generally less than 20 cm thick and pinch out laterally at outcrop scales. Horizons rich in small (<1cm diameter) chert nodules are common in outcrop. Rosettes of calcite pseudomorphs after sulfate nodules are also present. Wave rippled and possibly hummocky cross-stratified fine sandstones and massive dark purple to green siltstones/mudstones of the Kama Hill Formation appear to abruptly overlie this association in the sections where it is present.

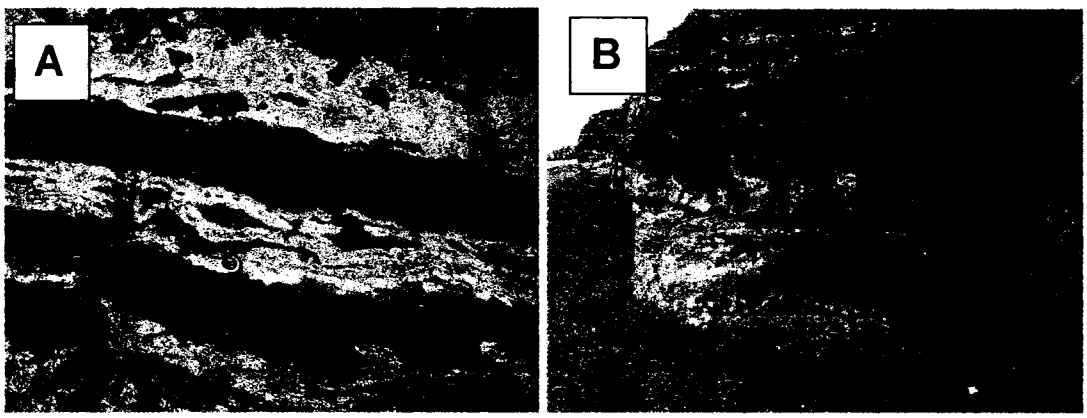

Figure 2.26. The massive dolostone lithofacies association. A) Massive mottled dolostone with two purple mudstone/siltstone horizons, Channel Island. Tape measure shown for scale is 10cm wide. B) Massive mottled dolomitc mudstone at Kama Hill exposure. Field of view is about 4m high.

2.3.8 Red siltstone-sulfate lithofacies association

The red siltstone-sulfate lithofacies association is dominated by red siltstone or very fine-grained sandstone with occasional massive medium grained sandstone beds as well as rare, thin dolostone beds similar to the cyclic facies and dolomitic mudstone association. A thick (2-3 m) carbonate horizon with stromatolitic domes or teepee

structures also occur in this association. The most striking feature in this association is the abundance of diagenetic sulfate and carbonate minerals. Sulfate minerals occur as discrete or coalesced round shaped nodules a few centimetres in diameter, fine-grained angular nodules similar to those in the red siltstone-dolomite association, veins a few centimeters in thickness, detrital grains, pervasive fine-grained zones and cements in thin intraformational breccias. In diamond drill core NI-92-7 this association is approximately 75 metres thick.

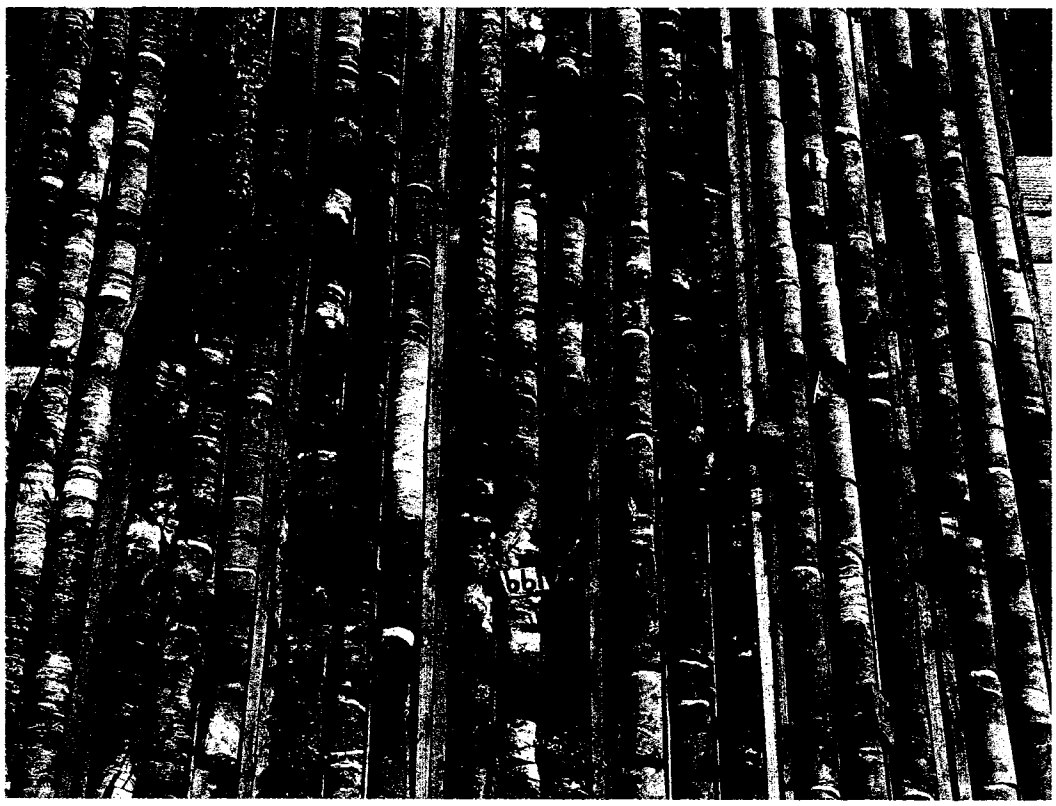

Figure 2.27. Red siltstone sulfate association in drill core NI-92-7. Up is towards the right and top of the photograph. White coloured zones represent sulfate-rich horizons.

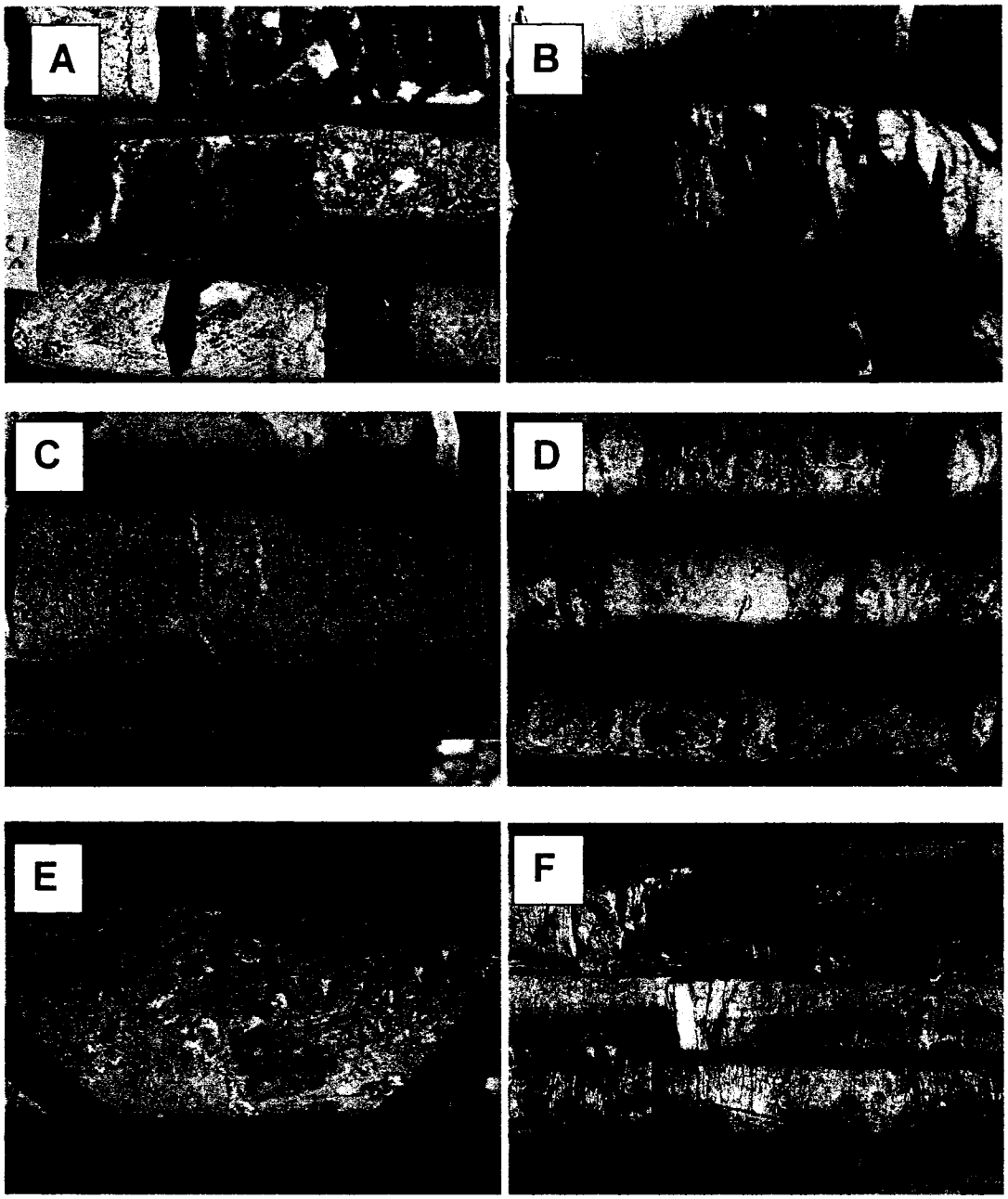

Figure 2.28. The red silstone-sulfate association. A) White carbonate horizon with abundant nodular gypsum. B) Coalesced gypsum nodules in red siltstone. C) An occurrence of detrital gypsum. D) Fine-grained gypsum nodule in a dolomite bed surrounded by red siltstone that contains pervasive fine-grained carbonate minerals (replacements after sulfates?) E) thin intrafromational breccia with sulfate cement. F) Massive red siltstone cut be remobilzed gypsum vein and green reduced patches.

2.3.9 Red siltstone-fine-grained sandstone lithofacies association

This association occupies a similar stratigraphic position to the red silstone-sulfate association. Lithologically it is similar to the red siltstone-sulfate association but it lacks

the extensive diagenetic sulfate mineralization. Fine-grained red sandstone is the most common lithofacies in this association. The sandstone lithofacies is typically massive with very indistinct bed contacts. It contains disseminated fine-grained (less than 1cm diametre) nodules of sulfate minerals (usually carbonate replaced). A complex variety of alteration/diagenetic features are present within the fine-sandstone lithofacies. These include: irregular horizons, 1-5 cm thick, of purple mudstone and associated thin irregular zones of silicified carbonate, isolated irregular nodules of carbonate less than 1cm to 3 cm in diameter, zones of up to 1m in thickness characterised by irregularly oriented wisps of red and purple mudstone (clay rich cutans), small nodular fine-grained sandstone (soil peds) and silicified carbonate layers/nodules. Isolated thicker layers (50 to 150 cm in thickness) of more intense alteration are also present. These layers consist primarily of very friable, blocky textured red to purple mudstone or siltstone with layers of massive (sometimes laminated) white, carbonate-rich mudstone, intraformational breccia, and round carbonate nodules. Silicification is present in portions these thicker altered horizons.

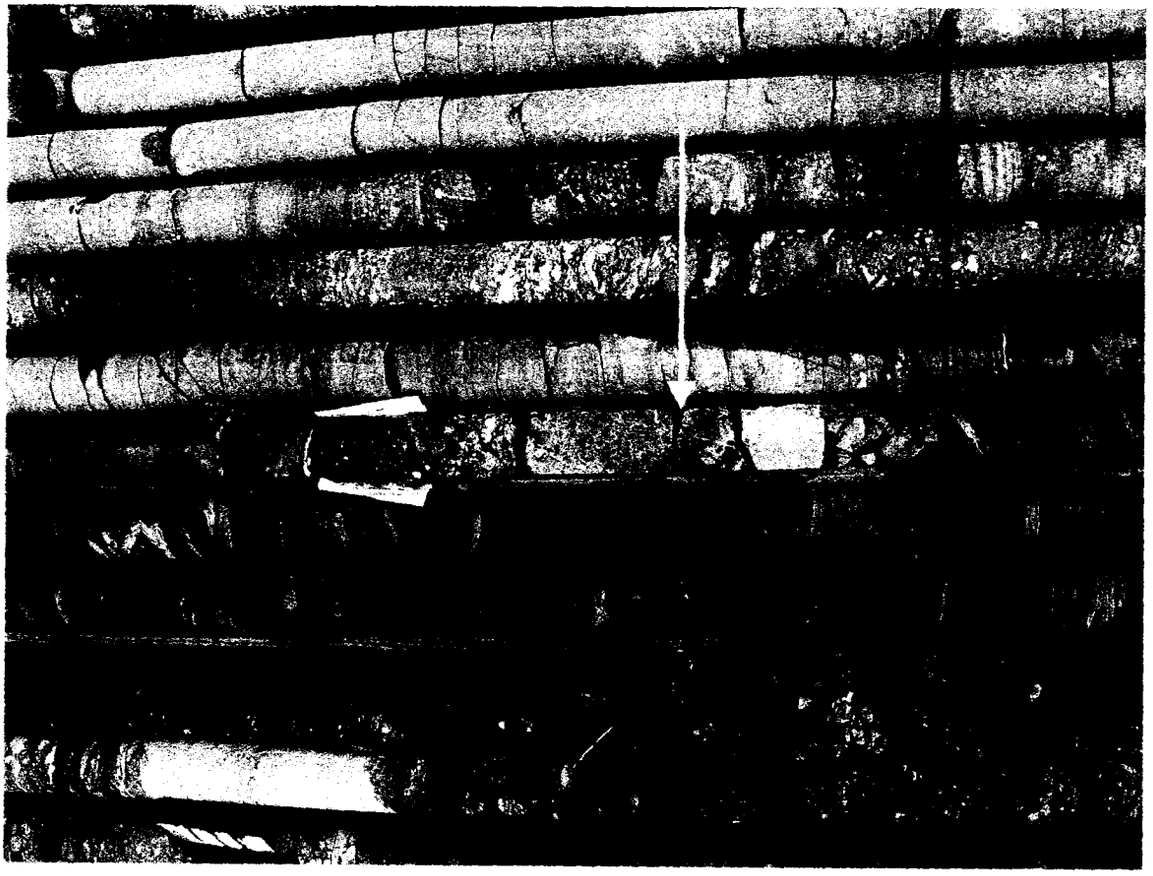

Figure 2.29. Contact between sheet sandstone lithofacies association (sections of core overlain by downward black arrow) and red siltstone-fine-grained sandstone lithofacies association (sections of core overlain upward black arrow). White arrow shows intraformational conglomerate consisting of clasts of black chert-carbonate lithofacies association. The black chert-carbonate lithofacies association is not present in this drill core. Up is towards the top of the photograph and to the left. Drill core NB-97-4.

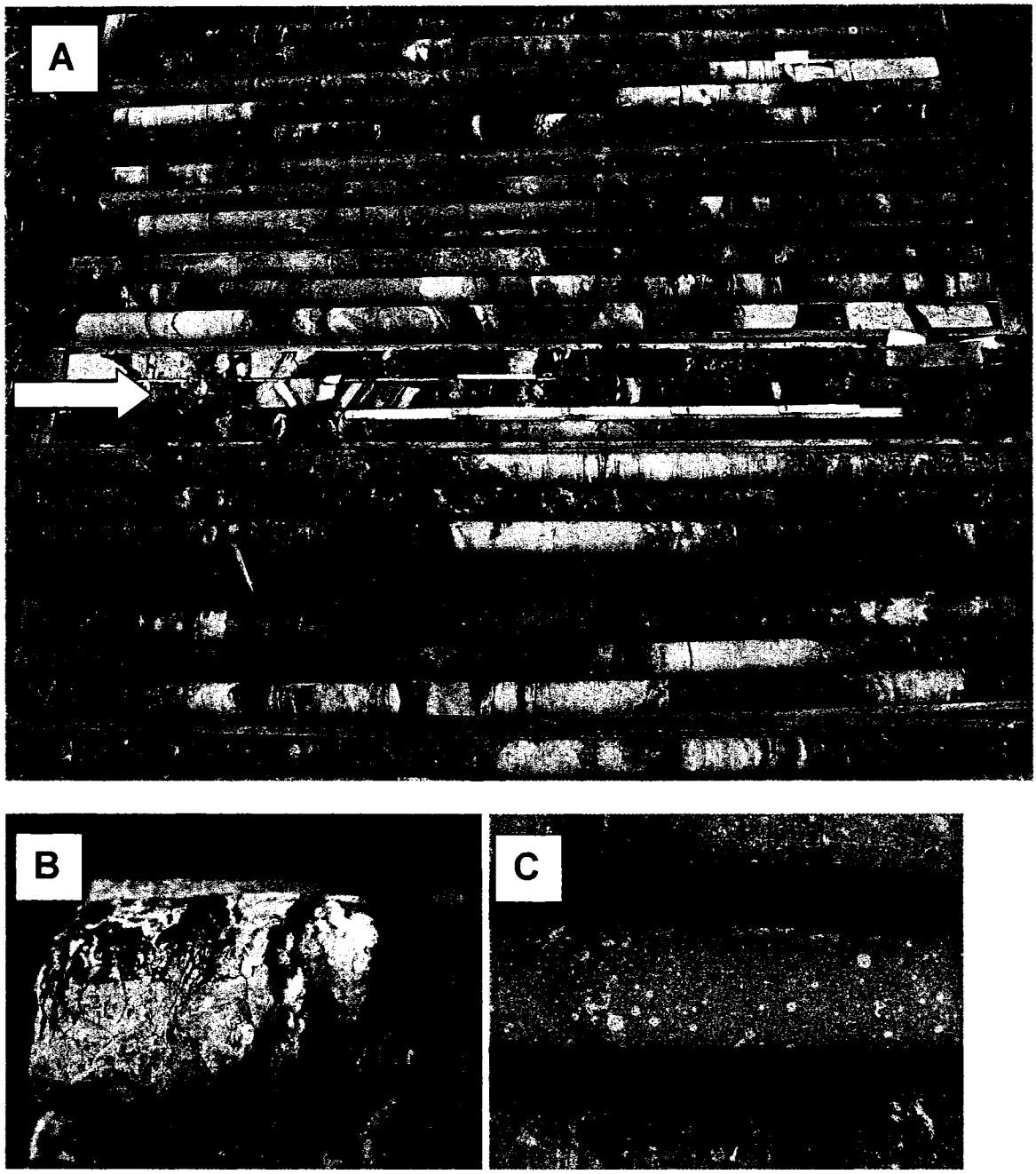

Figure 2.30. Red siltstone-fine-grained sandstone lithofacies association. A) Contact between sheet sandstone lithofacies association (Lower 3 core boxes) and red siltstone-fine-grained sandstone lithofacies association (top 4 core boxes) in drill core NB-97-2. The friable section at the center of the photograph (arrow) likely represents subaerial exposure with soil profile development and is correlative with subaerial exposure features at the top of the black-chert carbonate lithofacies association. Contact at left tip of ruler. B) Pedogenic? carbonate nodule from NB-97-4. C) Fine-grained unaltered sandstone that comprises the majority of this lithofacies association.

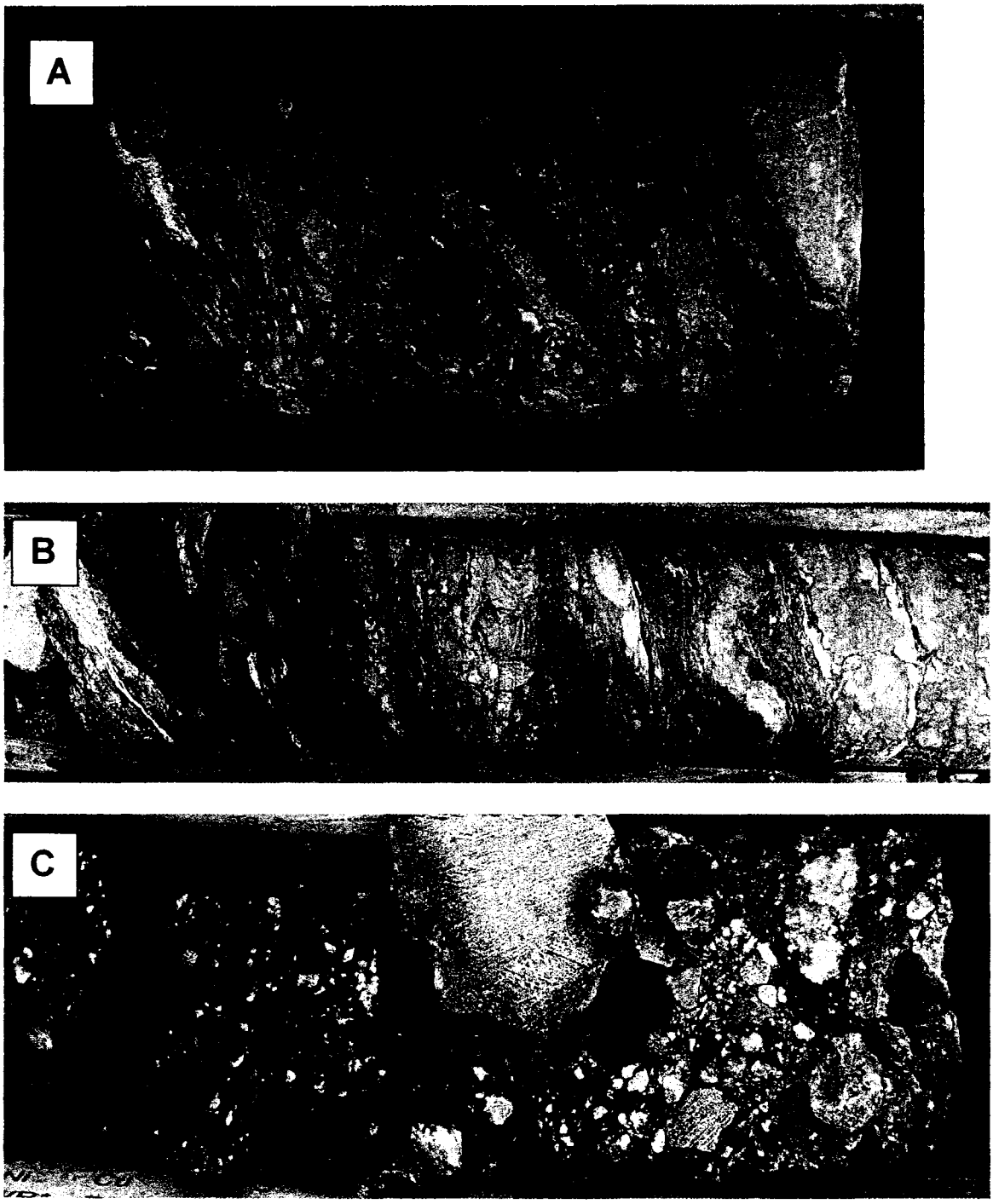

Figure 2.31. Pedogenic (?) features in the red siltstone-fine-grained sandstone lithofacies association. A) and B) nodular fine grained sandstone (soil peds?) in red hematite rich-matrix (hematitic cutans?). C) Pedogenic (?) carbonate nodule-rich horizon. Photos from drill core NB-97-4, younging direction is to the left.

Chapter 3. Stratigraphy

3.1 Introduction

The purpose of this chapter is to outline the stratigraphic organization of lithofacies associations across the Sibley Basin. Previous stratigraphic work in the Sibley Group has focused on developing a model for its lithostratigraphic organization (Franklin et al., 1980; Cheadle, 1986a and b; Rogala, 2003). The approach taken here is to correlate based on the units bounded by unconformable surfaces (allostratigraphy). As much as possible the correlation in this section attempts to be non-genetic. However, there is some degree of interpretation involved in the recognition of unconformities and features of subaerial exposure. Detailed stratigraphic correlation of lithofacies associations serves as an important framework for the interpretation of geochemical data in later chapters.

3.2 Allostratigraphic Correlations

Basin-wide correlations in the Sibley Group are hampered by a lack of distinct chronostratigraphic marker horizons. This poses a problem for understanding the temporal relationships between lithofacies associations. In some instances disconformable surfaces or distinct lithological changes can be identified and used for correlation. One example, the top of the Pass Lake Formation, appears to be unconformable on the islands south of Rossport. However, this datum is problematic, as the lithostratigrahic contact elsewhere is gradational and difficult to define. Another possible datum for correlation is the intraformational conglomerate/black chert carbonate lithofacies association pair that is present near the central portion of the Rossport

Formation. The top of the black chert/carbonate appears to represent subaerial exposure and as such could be a distinctive surface on which to base stratigraphic correlations. The occurrence of the black chert-carbonate association is relatively restricted, however, and it appears to be present only in the more southerly sections in the study area. A third possible horizon is the first appearance of a sandstone bed in the sheet sandstone association. The sheet sandstone beds are laterally widespread, distinctive and their interpreted depositional setting and process suggests that they may have been deposited quite rapidly. Basal contacts between the Sibley Group and basement are inappropriate as a datum for correlation as topographic relief of the basement surface appears to have been extensive, on the order of 200m (Cheadle, 1986a), which is a greater thickness than the portion of the Sibley Group being studied. Inferences about the topographic relief of pre-Sibley basement is based on modern observations of the vertical distances between the tops of hills of Archean granites and outcrops of the Sibley Group-basement contact, onlap of Pass Lake Formation sandstones onto basement, and the lack of a basal clastic unit in some sections.

The correlation of lithofacies associations across a few transects (Fig 3.1) of the Sibley Basin is shown in Figures 3.2, 3.3 and 3.4. The figures use the first appearance of a sandstone bed in the sheet sandstone association as a datum for correlation. Figure 3.2 shows a roughly east to west section line that extends from diamond drill core NI-92-7 in the northwest to Copper Island in the east (Fig. 3.1). Figure 3.3 shows a north to south line across Nipigon Bay from Kama Hill to diamond drill core NB-97-2 (Fig. 3.1). Figure 3.4 shows an idealized, roughly north to south section line that extends from near

Disreali Lake in the north to Silver Islet in the south (Fig. 3.1). Vertical exaggeration and scale varies as the diagrams are fitted for display on a single page.

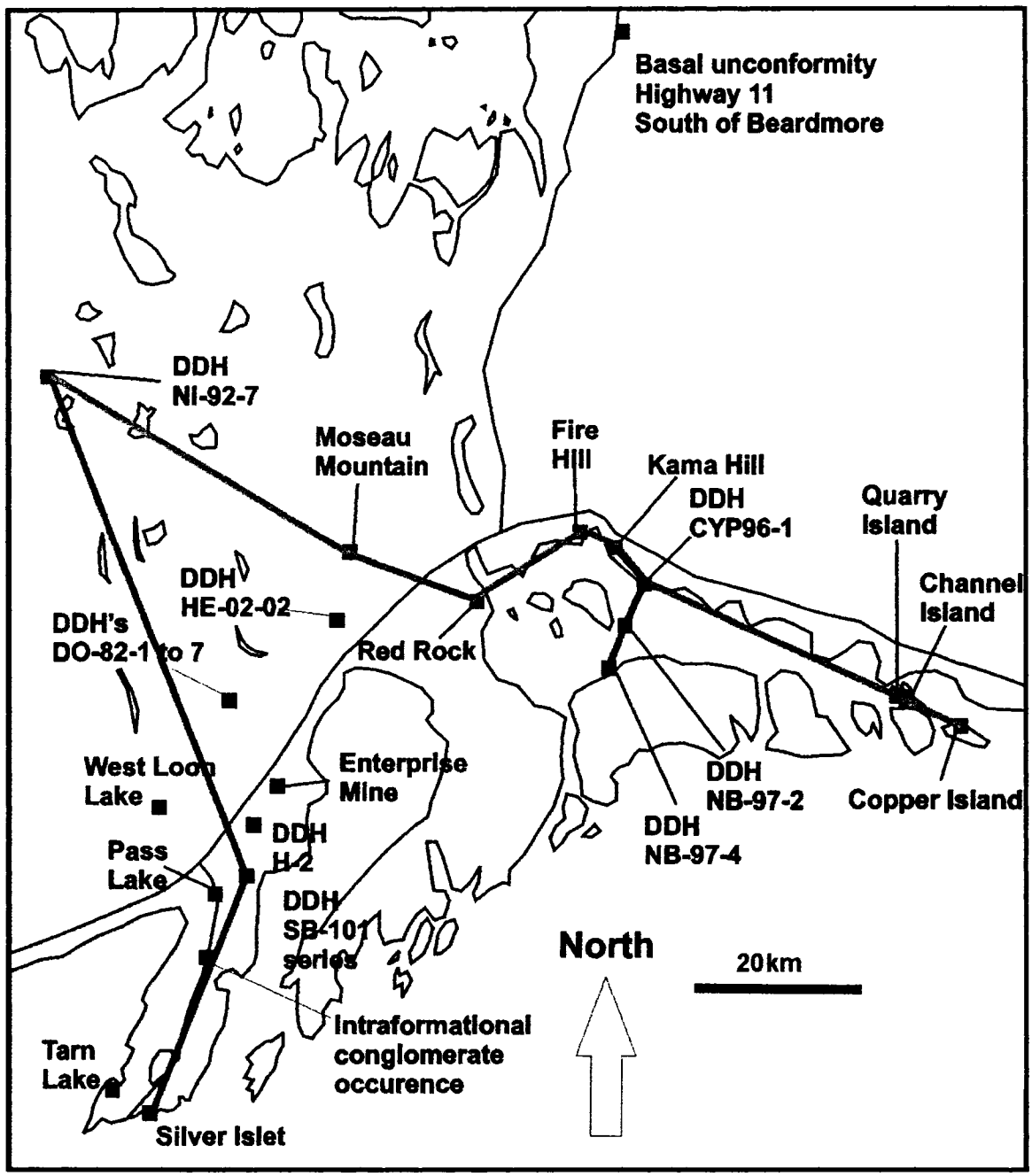

Figure 3.1. Location map for sections shown in Figures 3.2 (green line), 3.3 (blue line) and 3.4 (red line).

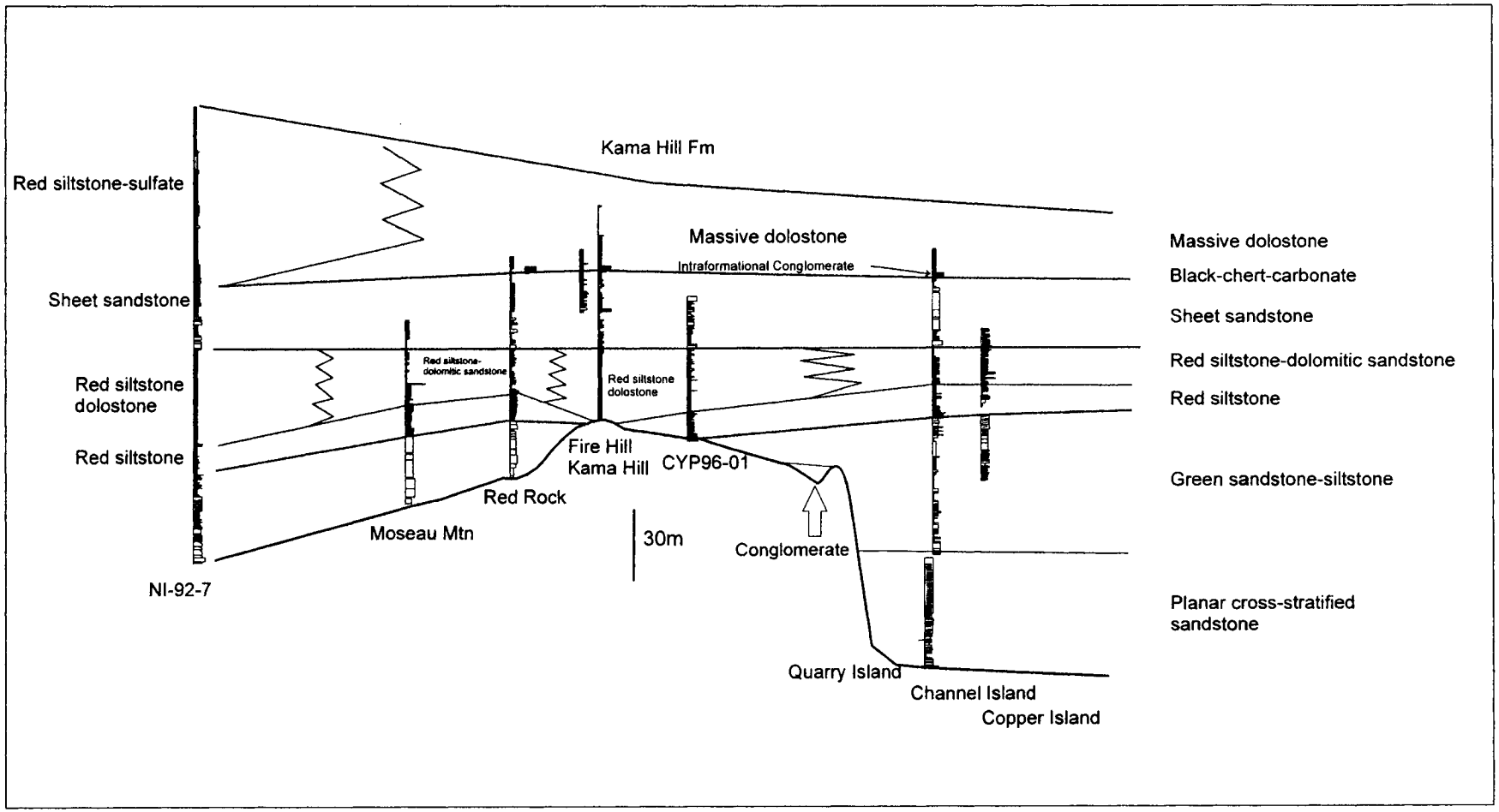

Figure 3.2. Idealized west to east cross-section from DDH NI-92-7 to Copper Island showing correlation of lithofacies associations and allostratigraphic units (separated by red lines). Data for some sections modified from Cheadle (1986b and Rogala 2003)

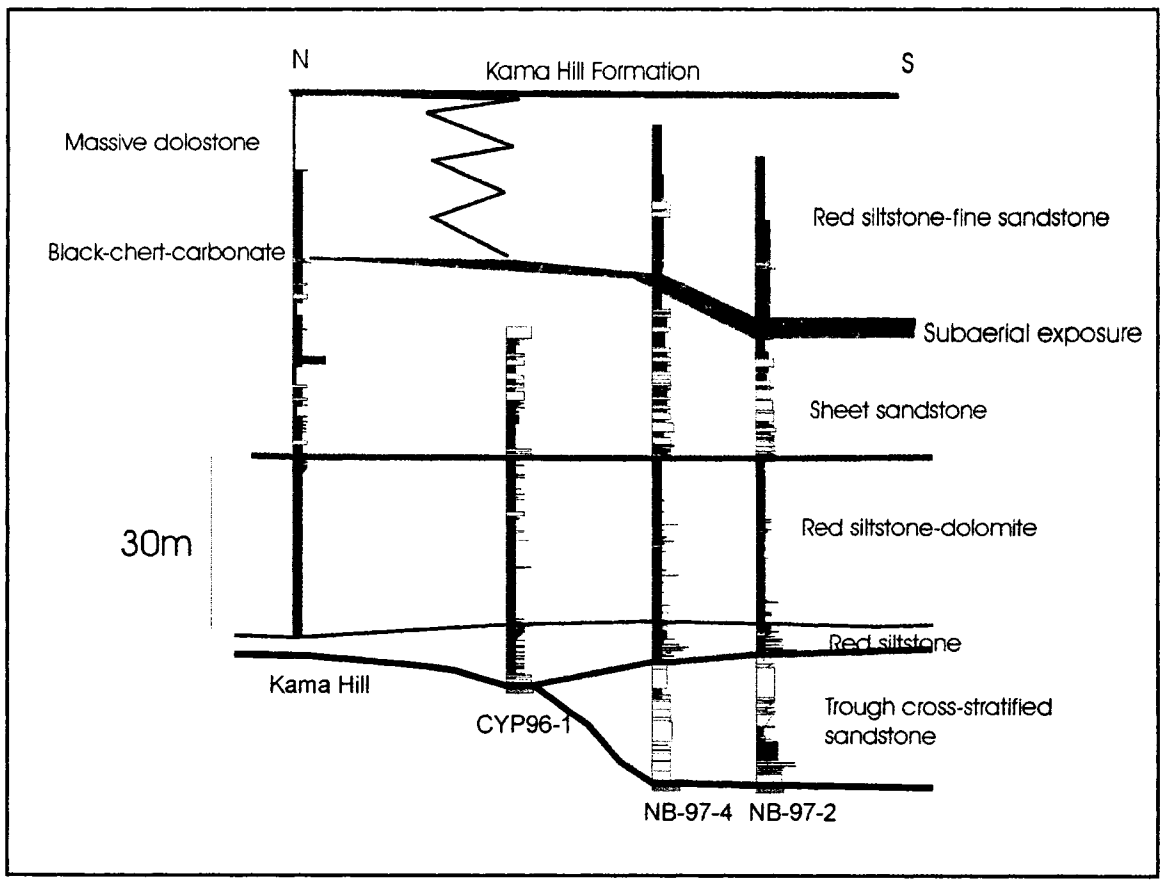

Figure 3.3. North to south cross-section across Nipigon Bay from the section at Kama Hill to diamond drill core NB-97-2 showing allostratigraphic units (divided by red lines) and correlation of lithofacies associations. Note inferred topographic relief of the basement surface which is composed of Archean granite and metasedimentary lithologies (Data for CYP96-1 is from Rogala, 2003).

From Figures 3.2 to 3.4 the Sibley Group can be divided into 4 informal allostratigraphic units based on lithology and also possible disconformable surfaces. The first unit consists primarily of siliciclastic rocks and is comprised of the various lithofacies associations of the Pass Lake Formation. The base of this unit is defined as the unconformable contact between underlying Archean and Paleoproterozoic rocks and the conglomerates and sandstones that are present at the base of the Sibley Group. The top of the basal siliciclastic unit is defined as either the unconformable contact between the basal siliciclastic unit and the mixed carbonate-siliciclastic unit as present on the

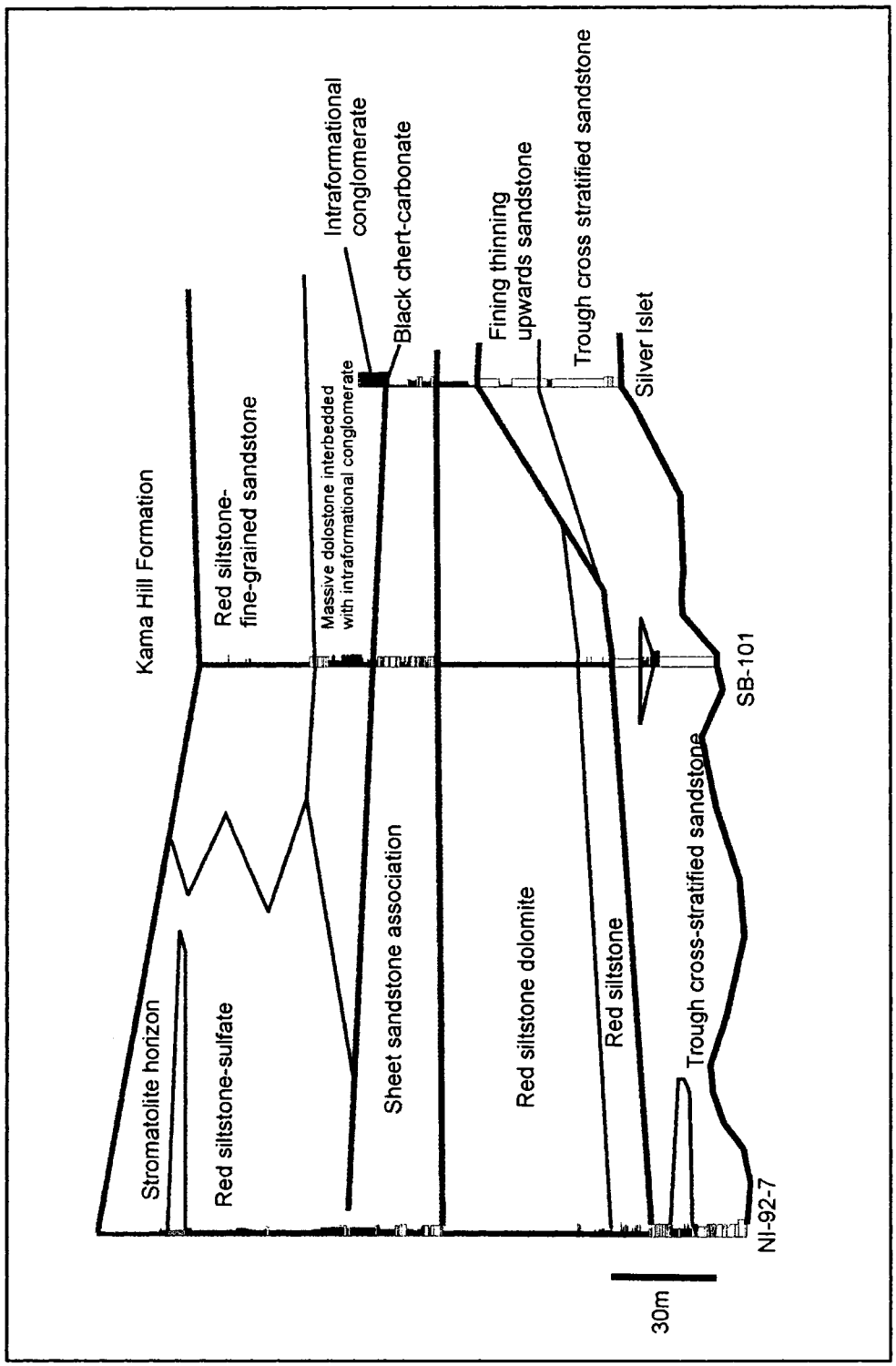

Figure 3.4. Idealized north to south section from DDH NI-92-7 to Silver Islet section showing allostratigraphic units and correlation of lithofacies associations. Sections for SB-101 and Silver Islet are modified from Cheadle (1986a) and Rogala (2003)

islands off Rossport or the gradational contact as exposed elsewhere. The second unit consists of mixed siliciclastic and carbonate rocks and includes the red siltstone lithofacies association, the red siltstone-dolostone lithofacies association, and the red

siltstone-dolomitic sandstone lithofacies association. At its base the mixed siliciclastic carbonate unit is in gradational contact with the basal siliciclastic portion or sharply overlies a disconformity in the Rossport area. The second unit consists of equivalent lithologies to the cyclic facies of the Channel Island Member in the lithostratigraphic nomenclature of Cheadle (1986a). The third unit consists of the sheet sandstone lithofacies association and the black chert-carbonate lithofacies association. The basal contact of this unit is abrupt and the top of the unit is marked by interpreted subaerial exposure of the black-chert carbonate lithofacies association. The upper unit is comprised of a mixture of clastic, carbonate and evaporite rocks including the intraformational conglomerate lithofacies association, the massive dolostone lithofacies association, the red siltstone-sulfate lithofacies association and the red siltstone-fine-grained sandstone lithfacies association. The basal contact of this unit is sharp and the upper contact is gradational with the Kama Hill Formation. The characteristics of each of the four stratigraphic units, including (where possible) paleocurrent patterns for individual lithofacies associations are discussed individually in the next section.

3.2.1 Basal siliciclastic unit

Examining the lithofacies associations in Figure 3.2, shows that the thickest accumulations of clastic material at the base of the Sibley Group occur in the east in the islands offshore from Rossport. The area of thick accumulation is filled by up to 100 m of the green sandstone-siltstone lithofacies association and the planar cross-stratified lithofacies association. Towards the west the thickness of the Pass Lake Formation decreases and in the area of the Kama Hill section the red siltstone and red siltstone-dolomite lithofacies associations rest on Archean basement. Further west approximately

30 metres of the trough cross-stratified and fining thinning upwards sandstone lithofacies associations form the basal portions of the Sibley Group. In Figure 3.3 the Pass Lake Formation is again dominated by about 20-40 m of the trough cross-stratified lithofacies association but it rapidly thins and onlaps an Archean granite at the Kama Hill section.

The distribution of paleocurrents in the basal clastic unit is shown in Figure 3.5. Taken together the majority of paleocurrent indicators suggest a trend towards the southeast for the basal clastic unit. The southeastward trend is present in the trough cross-stratified and fining thinning upwards associations and also in the planar cross-stratified association. The green sandstone-siltstone association shows a southwesterly trend about perpendicular to the general trend shown by the other lithofacies associations. The paleocurrent patterns in the basal clastic unit suggests a southward paleoslope during its deposition. Detrital zircon ages for samples from the fining- and thinning-upwards sandstone lithofacies association at Pass Lake are shown in Figure 1.4. The Pass Lake Formation has a zircon population extending in age from the Mesoarchean to approximately 1600 Ma with the greatest concentration in the age bracket between 1840 Ma and 1900 Ma (Fig 1.4). This corresponds to the age of igneous rocks associated with the Trans-Hudson Orogenic zone to the northwest and the Penokean Orogenic zone to the south. There is also a grouping of zircons at approximately 2.4 Ga, the age of Huronian volcanism. The grouping of zircons at 2.7 Ga corresponds to the main igneous phase of the Kenoran Orogeny. Igneous, zircon-bearing rocks in the age bracket 1.6 to 1.8 Ga are not present in Superior Province directly north of the Sibley Group. The closest occurrences of source rocks of this age are to the south and northwest adjacent to Superior Province.

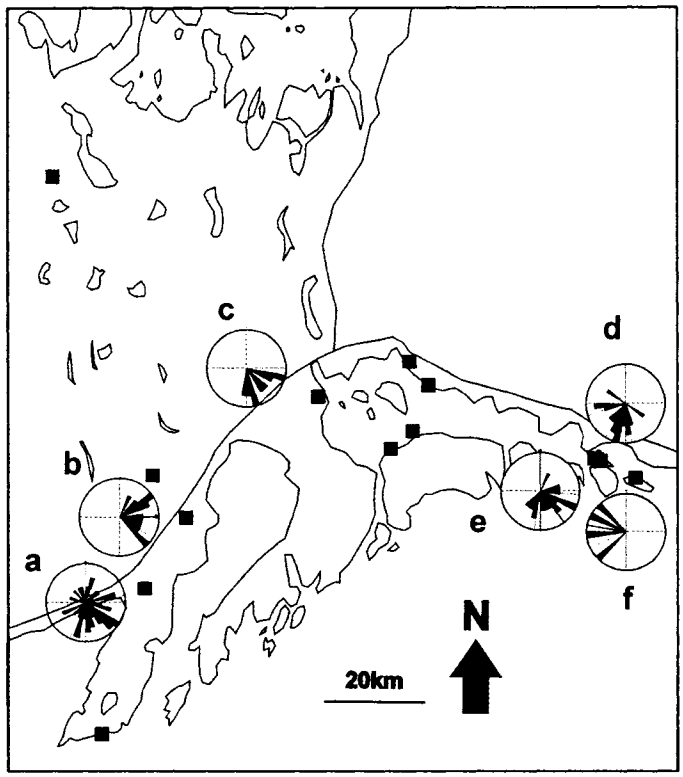

Figure 3.5. Paleocurrent data for the basal siliciclastic unit. The three current roses on the eastern margin of the diagram show data for the green sandstone-siltstone lithofacies association (d, f) and the planar cross-stratified sandstone lithofacies association (e). The current roses in the western portion show data for the trough cross-stratified sandstone lithofacies association (b, c) and the fining thinning upwards sandstone lithofacies association (a). Paleocurrent data are from this study as well as Cheadle (1986b).

3.2.2 Mixed siliciclastic-carbonate unit

Figures 3.2 to 3.4 show that the mixed siliciclastic-carbonate unit is 20-70 m thick and laterally continuous across most of the basin. The thickest noted accumulation of this unit is in the north where diamond drill core NI-92-7 was drilled. Basal portions of this unit are almost always comprised of about 10 to 20 m of the red siltstone lithofacies association. The red siltstone lithofacies association is succeeded upwards by 20-50 m of either the red siltstone-dolomite association or the red siltstone-dolomitic sandstone association. Laterally, the red siltstone-dolomite and the red siltstone-dolomitic

sandstone associations appear to interfinger. The red siltstone-dolomitic sandstone association occurs primarily in the Red Rock and Rossport areas.

3.2.3 Upper siliciclastic unit

The upper siliciclastic unit sharply overlies the mixed siliciclastic unit. The majority of the unit is comprised of the sheet sandstone association. The black chert-carbonate association, where present, forms the top. The thickness of this unit ranges from 0-45m. In general, the thickness is rather uniform basin wide. However, in rare instances it is absent. An example of a section where it is absent is at Tarn Lake, north-west of Silver Islet. At Tarn Lake the black chert-carbonate lithofacies association lies directly above the dolostone-red siltstone lithofacies association. The definition of the upper boundary of this association is somewhat arbitrary especially with regard to the inclusion of the intraformational conglomerate association in the upper unit as it may also be related to subaerial exposure at the top of the black-chert carbonate association. Paleocurrents for the sheet sandstone association are shown in Figure 3.6. Where a significant number of measurements were made the paleocurrent roses for the sheet sandstone association show considerable scatter. The three unidirectional roses contain only a few data points and are from single beds or stratigraphically restricted areas.

3.2.4 Mixed siliciclastic-carbonate-evaporite unit

The upper mixed siliciclastic-carbonate-evaporite unit ranges from about 20 to 75 m in thickness. The thickest accumulations of this unit are again in the north around DDH NI-92-7 (Fig. 3.2), but a similar thickness is also present in drill holes from Nipigon Bay in the southeastern corner of the basin (Fig. 3.3). In Sibley Group lithostratigraphy this unit is the equivalent of the Fire Hill Member. In sections where the

black-chert carbonate association is present this unit is usually comprised of the intraformational conglomerate

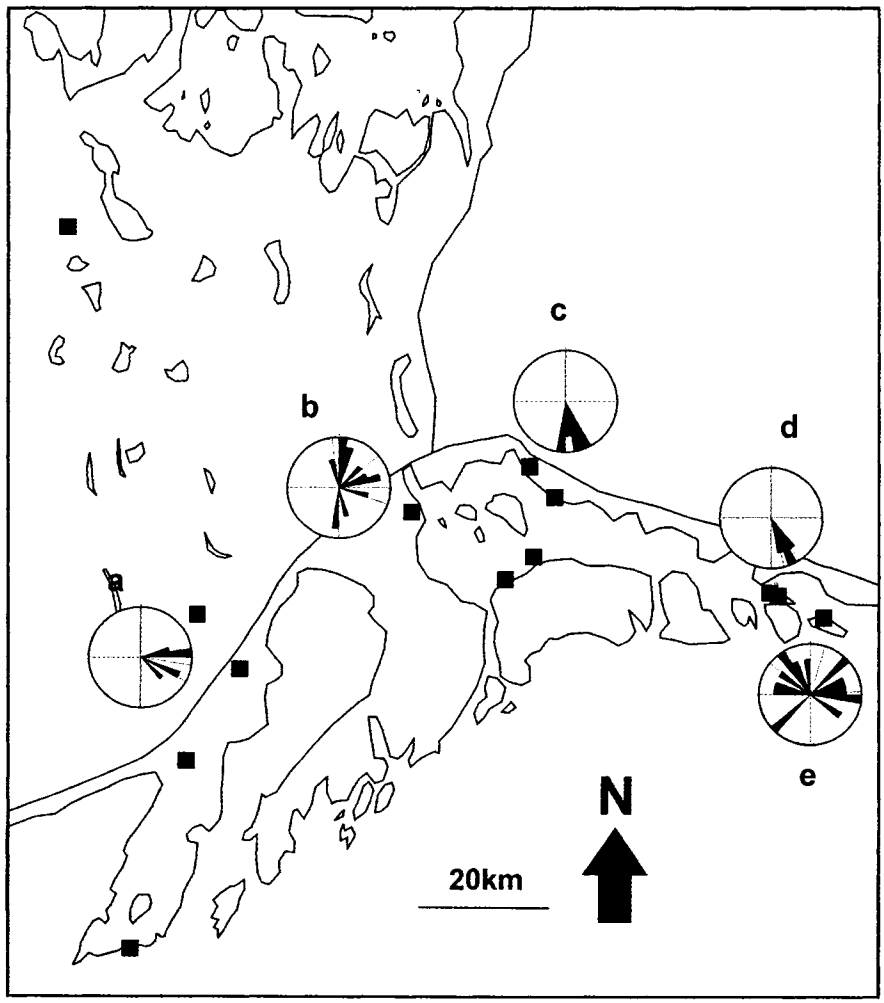

Figure 3.6. Paleocurrent data for the sheet sandstone lithofacies association. Data are from this study and Cheadle (1986b). Localities are as follows: (a) Moseau Mtn, (b) Red Rock, (c) Kama Hill, (d) Channel Island, (e) Copper Island. Although data at individual locations appears to be unidirectional, there is a scarcity of good paleocurrent inicators at these locations and consequently few data points.

lithofacies association overlain by the massive dolostone lithofacies association. Other sections are comprised of a mixture of the red siltstone-sulfate association and the red siltstone-fine sandstone association. More northernly sections, such as NI-92-7, contain the red siltstone-sulfate association whereas the southernly sections, such as NB-97-2 and NB-97–4 are characterized by the red siltstone-fine sandstone association. Laterally, the

massive dolostone association appears to intercalate with the other associations. No paleocurrent data was collected from the associations in this unit as no suitable sedimentary structures were found in outcrop. The upper contact of this unit with the Kama Hill Formation is variable. In sections containing the massive dolostone lithofacies association the contact is rather abrupt. In other sections the contact is gradational. During the course of this study, logging of sections was stopped where sections became dominated by lithologies ascribed to the Kama Hill Formation by other authors. However, in many cases it is difficult to define the boundary between red siltstones associated with the Fire Hill Member (i.e. the upper mixed siliciclastic-carbonate evaporite unit) and red to purple siltstones of the Kama Hill Formation.

3.3 Summary

The stratigraphic units described above differ slightly from the formal lithostratigraphic subdivisions of the Sibley Group (e.g. Cheadle, 1986a). The main difference is the grouping of the sheet sandstone lithofacies association, which is equivalent to the mudstone facies in the Channel Island Member, and the black chert-carbonate association, which is the equivalent of the Middlebrun Bay Member, into the upper clastic unit, whereas previously these were portions of two different lithostratigraphic members.

Lateral changes in thickness of both lithofacies associations and allostratigraphic units are minimal, important exceptions are apparent, however, in the two lowest units. In the basal clastic unit, a thickening to the southeast and southeastward oriented paleocurrent pattern suggest a southerly depocenter. Conversely, the mixed carbonate-siliciclastic unit thickens towards the northwest suggesting that subsidence increased in

the area of DDH NI-92-7 during the deposition of this unit. An overall change in paleoslope cannot be supported by paleocurrent data as few paleocurrent indicators are present in the mixed carbonate-clastic unit. The upper clastic unit shows relatively homogeneous thickness across the basin and a scattered paleocurrent pattern. The presence of some northward oriented paleocurrent measurements may be significant in suggesting a change in regional paleodrainage pattern. The upper mixed carbonate-siliciclastic-evaporite unit is thickest in the northwest in drill core NI-92-7.

Rogala et al. (2005) have suggested that the Fire Hill Member, which is basically equivalent to the upper mixed siliclastic-carbonate-evaporite unit, thickens as the result of half-graben formation that resulted from movement along the Black Sturgeon fault during deposition of this unit. However, the timing of half-graben formation is unclear and thickening of Sibley Group units towards the Black Sturgeon Fault (general location shown in Figure 1.1) may have also resulted from subsidence along the fault during the later Mesoproterozoic Mid-continent rift event with subsequent erosive removal of more Sibley Group material from areas further removed from the fault.

Chapter 4 Depositional Environments

4.1 Deposltional environments of individual lithofacies associations

The purpose of this chapter is to discuss the depositional environments represented by the lithofacies associations introduced in chapter 2. Although the depositional environments of the Sibley Group have been defined by other authors (Franklin et al., 1980; Cheadle, 1986a and b and Rogala, 2003) finer details concerning depositional subenvironments and processes, particularly in the Fire Hill Member, can be added. Below, the depositional environment of each lithofacies association is discussed in turn, followed by a summary of the depositional history of the study sections in light of stratigraphic and paleocurrent data from chapter 3.

4.1.1 Boulder conglomerate-sandstone-dolocrete lithofacies association

Cheadle (1986a and b) interpreted lithofacies equivalent to the boulder conglomerate/sandstone/dolocrete lithofacies association to represent the development of small-scale alluvial fans deposited primarily through debris-flow processes. The limited lateral and vertical extent of this association suggests that if this association represents an alluvial fan environment, the scale at which alluvial fans developed was quite small. The lack of well developed bedding and cross-stratification, and the poorly sorted mud-rich matrix of many conglomerates supports a debris flow origin for the boulder conglomerate lithofacies (e.g., Rust, 1978; Miall, 1996; Blair, 1999a). Stream-flow deposited conglomerates generally have better sorted matrix compositions and cross-strata that represent the development of in channel bar complexes, dunes, or standing wave produced antidunes (Steel and Thompson, 1983; Miall, 1996; Blair, 1999b). However,

debris flow deposits are generally considered to be matrix supported, an observation that Cheadle (1986a) used to suggest that the conglomerates may have been water-lain. Lenses of massive sandstone interbedded with the conglomerate lithofacies may represent deposition from intermittent lower energy stream-flows (Nemec and Steel, 1984). The incising nature of the boulder conglomerate lithofacies is similar to channel deposits in modern arid alluvial fan systems (Blair, 1999a). In modern arid fan systems, incised channels may be filled with either stream deposited stratified conglomerates or poorly sorted, massive, debris-flow conglomerates similar to those observed in channel fills in this lithofacies association. Coarse-grained sandstone and pebbly sandstone lithofacies probably represent sheet-flow deposits. They may have formed in overbank areas adjacent to major fan channels or represent variation in depositional style between a sheet-flow or channel dominated fan through time. Parallel lamination in coarse-grained sandstone units suggests deposition from high-energy upper flow regime conditions (e.g., Stear, 1985). Rapid deposition is also supported by the presence of dewatering features. Thin lenses of fine-grained, pink, carbonate-rich siltstone may represent ephemeral pond deposits left after major rainfall/flood events.

The dolocrete lithofacies may be of either pedogenic or groundwater origin (e.g., Wright and Tucker, 1991; Spotl and Wright, 1992; Alonzo-Zarza, 2003). Pedogenic calcretes/dolocretes form above the local groudwater table, whereas groundwater calcretes/dolocretes form near the groundwater table in the vadose or phreatic zones (Esteban and Clappa, 1983). Both pedogenic and groundwater calcretes/dolocretes provide important paleoenvironmental information, as both pedogenic and groundwater calcretes/dolocretes form primarily in semi-arid to arid climates (Alonzo-Zarza, 2003),

with pedogenic carbonate horizons in modern settings forming where annual precipitation is less than 760 mm (Royer, 1999). A distinction between the groundwater and pedogenic calcretes/dolocretes is important as pedogenic calcretes/dolocretes form mainly from waters that infiltrate down from surface whereas the groundwater variety forms from groundwater. Sources of carbonate in pedogenic calcretes/dolocretes are varied and include rainfall, seaspray, surface runoff, groundwater, dust, bioclasts, vegetation litter, and rock, whereas groundwater calcretes/dolocretes are sourced primarily by groundwater (Wright and Tucker, 1991).

Wright (1990) proposed two broad micromorphological classes of calcrete/dolocrete termed beta fabrics and alpha fabrics. Beta microfabrics are of biologic origin, whereas alpha microfabrics are abiotic. Beta microfabrics, including alveolar septal structures and rhizoliths, commonly cited as evidence of pedogenic origin, are primarily caused by plants and fungi and would not be expected in a Mesoproterozoic calcrete/dolocrete. Grains coated by micritic envelopes are possible beta microfabrics in a Mesoproterozoic calcrete/dolocrete as they are formed through fungal or cyanobacterial processes (Alonzo-Zarza, 2003). Alpha microfabrics common in calcretes/dolocretes include: crystalline carbonate groundmass, crystic plasmic fabric (Brewer, 1964), voids or fractures filled with carbonate cement, carbonate rhombs, nodules, and floating etched clastic grains (Alonzo-Zarza, 2003).

Petrographically, the massive dolocrete layers in this lithofacies association are composed of primarily micritic dolomite with occasional coarser-grained euhedral dolomite rhombs, voids/cracks filled with coarser-grained cement, and oxidized silicate and carbonate clasts and, as such, conform more to typical characteristics of alpha-type

calcretes. Groundwater calcretes/dolocretes are typically dominated by alpha type microfabrics (Wright and Tucker, 1991; Spotl and Wright, 1992). In the absence of plant roots and fungi, it is reasonable to assume that a pedogenic calcrete/dolocrete of Mesoproterozoic age would also be dominated by alpha type microfabric making a distinction between pedogenic and groundwater calcretes/dolocretes based on micromorphology inappropriate for the dolocrete lithofacies. The origins of carbonate cements in conglomerate units were not studied in any petrographic detail, however, they are interpreted to be an early feature, nearly contemporaneous with deposition, based on the presence of carbonate cemented sandstone intraclasts in some conglomerate beds. Thick pedogenic carbonate horizons require long periods of time to form (Gile et al., 1966; Machette, 1985; Alonzo-Zarza 2003) and their presence suggests that sedimentation was episodic or that the position of major channel features was fairly stable.

Overall, it appears that the boulder conglomerate/sandstone/dolocrete lithofacies association was deposited in a coarse-sediment dominated braided fluvial system. Both sediment-gravity processes and fluvial processes appear to be have been active during deposition. The sporadic distribution of this lithofacies association suggests that, rather than forming along distinct linear features such as basin bounding faults, coarse conglomeratic material was likely concentrated around isolated basement topographic features. Evidence of rapid deposition, dolocrete horizons, carbonate filled "ponds" and the presence of pervaisive carbonate cements suggest a semi-arid climatic setting (e.g. Miall, 1996).

4.1.2 Pebble-cobble conglomerate-sandstone lithofacies association

Cheadle (1986a) considered thicker deposits of the boulder conglomerate/sandstone/dolocrete lithofacies association to represent proximal alluvial fan deposits which thinned basinward into finer-grained distal alluvial fan deposits represented by lithofacies equivalent to the pebble-cobble conglomerate/sandstone lithofacies association. The mixture of matrix- and clast-supported conglomerates in this association suggest that both debris-flow and stream-flow processes were active during its deposition. Similar distal alluvial fan facies are described in the late Precambrian Van Horne sandstone (McGowen and Groat, 1971). Overall, this interpretation is difficult to support as, perhaps due to lack of exposure, intermediate fan facies are not present and correlation of an individual laterally thinning alluvial fan complex is not possible. Interpretation of both the boulder conglomerate/sandstone/calcrete lithofacies association and the pebble-cobble conglomerate/sandstone lithofacies association as the products of ephemeral braided streams on an alluvial plain rather than a distinct laterally thinning alluvial fan is more appropriate. Lithofacies in this association are comparable to the shallow gravel-bed braided and gravel-bed braided with sediment gravity flow fluvial styles proposed by Miall (1996). A gradual fining upwards transition into overlying sandstones of the trough cross-stratified sandstone association may represent gradual fluvial filling of confining channels or valleys in the pre-Sibley Group surface.

4.1.3 Massive cobble conglomerate lithofacies association

The massive cobble conglomerate lithofacies association is lithologically similar to the other two basal conglomerate lithofacies associations. However, it lacks any well-defined lateral channel forms and has few interbedded sandstone and no associated finer-

grained lithofacies. Franklin et al. (1980) and Rogala (2003) interpreted these conglomerates to be the result of wave reworking of previously deposited conglomeratic units (i.e. the fluvial/alluvial fan conglomerates) by transgressive lake waters that deposited overlying well-sorted quartz sandstones sheets. Franklin et al. (1980) interpreted the lower portions of the fining-thinning upward sandstone association to represent a beach system. The tabular nature of the conglomerate in this association, along with weak imbrication, supports a possible beach origin for the conglomerate. However, the poorly sorted matrix composition of the conglomerate is problematic for this interpretation as beach deposits are commonly well sorted as compared to fluvial conglomerates (Reading and Collinson, 1996). This association may indeed simply represent coarse-grained lag that was spread over a local ravinement surface during transgression, similar to coarse-grained conglomeratic deposits ascribed to a comparable process of reworking of fluvial and deltaic gravels described by Ulicny (2001) from the Cretaceous Bohemian basin of the Czech Republic.

4.1.4 Green sandstone/siltstone association

The significance of green sandstones and siltstones comprising this lithofacies association seems to have been over-looked by previous authors (Franklin et al., 1980 and Rogala, 2003). Cheadle (1986b) termed lithologies equivalent to this association the heterolithic facies and considered them to be a locally developed anoxic lacustrine facies. Cheadle (1986b) interpreted sandstones of this association to represent turbidity currents that originated from the entry points of flows from adjacent alluvial fans. Siltstone and shale lithofacies were interpreted as the result of settling of both flow-related and ambient

lacustrine suspended load. Cheadle (1986b) also postulated that the heterolithic facies was deposited in a stratified lake with an anoxic hypolimnion.

New stratigraphic data from Copper Island shows a clear coarsening and thickening upward trend in this association. The progradation of deltaic facies is often cited as producing coarsening and thickening upwards sandstone-siltstone units (e.g., Elliot, 1974; Pulham, 1989; Reading and Collinson, 1996). The coarsening- and thickening-upwards unit on Copper Island has characteristics of a vertical succession produced by the progradation of a distributary mouth bar in a wave influenced fluvial dominated delta (Pulham, 1989). Thin interbedded siltstones and fine-grained sandstones near the base of the coarsening- and thickening-upwards unit likely represent a prodelta. The upward increase in sandstone bed thickness, lateral continuity and occurrence of current generated structures likely represent progradation of delta front to distributary mouth bar or braided distributary channel lithofacies. Wave influence is suggested by the ubiquitous presence of wave rippled sandstone bed tops. The sharp disconformable top contact of this unit may record delta lobe abandonment, although the occurrence of a thin conglomeratic horizon and slight angular nature of this contact may suggest a more significant unconformable boundary. The section on Channel Island does not show a clear coarsening- and thickening-upward trend. On Channel Island, trough cross-stratified sandstones directly overlie green shales. This may represent partial erosion of distal bar and prodelta facies by prograding proximal delta lithofacies.

4.1.5 Planar cross-stratified lithofacies association

Interpretation of the depositional environment of the planar cross-stratified sandstones in this association depends to some degree on whether the stratigraphic

position of this unit is interpreted to underlie the green sandstone-siltstone association or if it is interpreted to be positioned lateral to it. Cheadle (1986b) interpreted these sandstones to be positioned lateral to his heterolithic facies, and suggested that they represent either the migration of continuous crested subaqueous or aeolian dunes. Cheadle (1986b) favoured an aeolian origin for the large-scale planar cross-strata on Quarry Island. However, given the deeper, offshore/deltaic interpretation of the green sandstone-siltstone association and the stratigraphic interpretation in chapter 3, a different origin for this lithofacies association is probable.

Arnaud (2004) described giant planar cross-strata from the Neoproterozoic Port Askaig Formation and provided a review of possible depositional environments of similar successions. Typically, large-scale planar cross-stratification is interpreted as aeolian, however, they may also be formed in deep fluvial systems with large scale bedforms, tidally influenced coastal embayments and on shelves with strong tidal or geostrophic currents (Arnaud, 2004). A fluvial origin is unlikely as formation of such large bedforms would require deep stable channels, whereas Precambrian fluvial systems are typically braided and characterised by broad, unstable, shallow channels (Eriksson et al., 1998). A tide influenced setting is unlikely, as there is scant evidence for tidal influence such as bidirectional paleocurrent pattern, herringbone cross-stratification or tidal bundles. As aforementioned, an aeolian origin is unlikely because of stratigraphic association and also because of the presence of sporadic pebble to cobble sized clasts. Stratigraphic association with green shales, deltaic deposits and the presence of underlying wave rippled sandstone and shale suggests a subaqeuous orgin for the planar cross-stratified sandstones. Migration of large continuous crested dunes in a shallow subaqeuous setting

is a possible depositional process for this unit. However, interpretation of this unit is problematic.

4.1.6 Cross-stratified sandstone/red siltstone association

The cross-stratified sandstone/red siltstone association was probably deposited in a fluvial environment. In Precambrian successions, distinction between fluvial, shallow marine and aeolian deposits is difficult mainly because of a lack of fossil evidence (e.g. Rainbird, 1992; McCormick and Grotzinger, 1993; Eriksson et al., 1998). However, the association of clast supported conglomerates/pebbly sandstones, with trough cross-stratified sandstones, illuviation features (clay skins and sand peds) and mudchip conglomerates strongly suggests a fluvial setting rather than a shallow marine or aeolian setting. An aeolian origin is difficult to support because of the presence of relatively coarse-grained units. A roughly unimodal paleocurrent pattern in individual sections favours a fluvial rather than marine origin as does the presence of subaerial exposure features such as mudcracks and soil structures. Many of the sedimentologic features of this lithofacies association are consistent with ephemeral bradied fluvial systems described in the literature. Possible recent or ancient analogs include fluvial strata of the Carboniferous Karoo Supergroup (Bordy and Catuneau, 2001), Quaternary ephemeral rivers of the largely vegetation-free Skeleton Coast of Namibia (Svendsen et al., 2003), the Triassic Bunter sandstone (Olsen, 1987) or Quarternary braided rivers of the Lake Eyre basin of Australia (Croke et al., 1998). In the classification of fluvial styles outlined by Miall (1996) lithofacies in this association best match either the Bijou-creek or South Saskatchewan types.

4.1.7 Thining-upwards sandstone lithofacies association

An overall upwards decrease in bedding thickness suggests that this lithofacies association records a transgressive event. Franklin et al. (1980) interpreted the lower portions of this association to represent a beach environment based on the very mature nature of these sandstones and the association of wave ripples, low angle planar cross-stratification and parallel laminations and intrepreted beds higher in the succession to be the result of subaqueous deposition in a shallow lacustrine or marine environment during northward migration of a strand-line. The association of wave generated structures, and thinning-upwards in bed thickness definitely supports deposition in a transgressive, wave-dominated near shore environment. Low angle, possibly hummocky, cross-stratification suggests that storm waves may have been important depositional processes. Sand stored in beach systems may have been remobilized during storm events and deposited as offshore sheets in a progressively expanding system.

4.1.8 Red siltstone lithofacies association

The red siltstone lithofacies association probably represents a continuation of the transgressive succession represented by the fining- and thinning-upwards sandstone association. The red siltstone lithofacies likely represents deposition from suspension in a quiet offshore setting. Thin, tabular, graded sandstone units and massive sandstone units were probably deposited by storm processes like those depositing sandstone beds in the underlying fining- and thinning-upwards lithofacies association. Alternatively, they may represent waning of alluvial sheet-like or channelized flows as they entered the expanding lacustrine system. Sporadic sand grains found within siltstone units may represent wind blown materials supplied relatively continuously to the basin. The

gradual upward change to the distinct periodic bedding style of the overlying red siltstone-dolostone lithofacies association or red siltstone-dolomitic sandstone association may represent a gradual change in climatic conditions towards a dryer climate characterized by evaporitic carbonate deposition.

4.1.9 Red siltstone-dolostone lithofacies association and the red siltstone-dolomitic sandstone lithofacies association

The red siltstone dolostone lithofacies association and the red siltstone-dolomitic sandstone lithofacies association are best discussed together. Cheadle (1986a) collectively termed these associations the cyclic facies and they have been interpreted to represent lacustrine deposition in a semi-arid setting (Cheadle, 1986a; Mailman, 1999; Rogala, 2003). Cheadle (1986a) considered the cyclic facies to represent marginal lacustrine deposits that precipitated dolomite and accumulated clay and silt from suspension. Both autocyclic and allocyclic controls likely played a role in the deposition of these two lithofacies associations.

In Cheadle's (1986a) model, proximity to the mouths of incised alluvial channels or the toes of alluvial fans was suggested as a primary control on lithofacies distribution. At areas far from sources of clastic input relatively pure dolostone beds would have been deposited, whereas proximal to sources of clastic input dolomitic sandstone lithofacies would have developed. Intermediate areas would have accumulated red dolomitic siltstone. Cheadle (1986a) noted that both the red siltstone-dolomite and red-siltstone-dolomitic sandstone cycles could have been produced contemporaneously through this model. This simple autocyclic model provides a reasonable explanation for the distribution of the dolomitic sandstone-siltstone association in relating them to points of

major clastic input, it does not, however, provide adequate explanation for the observed contact styles and diagenetic sulfate minerals present.

Climatic controls were also critical in controlling the deposition of these lithofacies associations. Cheadle (1986a) suggested that clastic supply was probably sporadic leading to their cyclic nature. Cheadle (1986a) felt that carbonate production was probably constant while clastic input fluctuated with variations in rainfall, thus during periods of increased rainfall, clastic deposition, represented by red dolomitic siltstones, would have dominated, while during periods of drier climate dolomite deposition would have continued on its own. The presence of dolomite clasts in dolomitic sandstone beds lead Cheadle (1986a) to suggest that at least portions of the lake dried up during low lake levels and were subsequently reworked.

Differences in dolomite bedding styles reflect variations in clastic input (wet-dry cycles), shoreline proximity and redox conditions (likely a function of water depth and organic carbon loading). Symmetrical dolomite beds with gradational upper and lower contacts probably represent periods of perennial subaqueous conditions in a relatively deep setting far from the water bodies margins. The gradational lower contact of such a bed may represent a gradual decrease in clastic input reflecting a change to more arid conditions. The gradual upper contact may reflect gradual reintroduction of clastic material from a suspended sediment plume introduced with a return to wetter climatic conditions or gradual increase in clastic input because of a change in river mouth positioning and subsequent progradation. Alternatively, the gradational contacts may represent redox boundaries reflecting changes between oxidizing, red dolostone, and slightly reducing, pale beige dolostone, conditions. This interpretation is not supported

by the work of Mailman (1999) who found redder colouration also tends to indicate a higher proportion of siliciclastic material relative to dolomite content. Symmetrical, sharp-sided dolostone beds may have had sharp lower contacts produced by changes in river mouth position (abrupt decrease in clastic supply and change to carbonate dominated sedimentation) and sharp upper contacts produced through subaerial exposure. Asymmetrical beds, characterised by gradational lower contacts and sharp, mud-cracked or brecciated top contacts reflect conditions near lake margins. The return of a wet climatic period would have brought fine-grained clastic material in suspension creating the gradual basal contact. As clastic sedimentation waned dolomite precipitation would have become dominant producing a dolostone bed that continued to develop during the evaporitive drying of the lake. The sharp upper contact represents subareal exposure during low water, more arid, intervals as is indicated by the presence of mudcracks and brecciation on the tops of this style of dolostone bed.

Evaporation was an important control on the deposition of the red siltstone-dolostone association. Ca-sulfate nodules and dessication cracks on dolomite beds tops attest to the periodic drying of the depositional system along with evaporitic concentration of lake or shallow ground waters. Ca-sulfate minerals formed syndepostionally as is indicated by their preservation in mudcracks on bed tops. Exposure features may not represent complete drying of the entire lake system and could be equally well explained through fluctuation of shoreline positions resulting from partial drying during evaporative intervals. This style of sulfate occurrence may be analogous to efflorescent crusts formed on playa or sahbka surfaces in modern arid environments. Nodular Ca-sulfates are also interpreted to have formed in the very shallow subsurface

during periods of subaerial exposure and evaporitic concentration of shallow subsurface waters.

The occurrence of coarse-grained sandstone horizons could have been produced by a number of processes. One possibility is an exceptional rainfall/storm event. These may have delivered coarser than normal clastic material to more distal portions of the lake system. A second possibilty could be debris flows triggered by minor shoreline slope failures. Evidence of slope instability is also present in the form of syndepositional folding of red siltstone-dolomite couplets at the Kama Hill exposure.

Numerous analogs to these lithofacies associations are present in the literature on saline lake and arid shallow marine systems. Reinhardt and Ricken (2000) described a very similar succession from the Middle Upper Triassic Steinmergel Keuper in Southern Germany. These deposits contain micritic dolomite horizons interbedded with mudstone in patterns almost identical to those found in the red siltstone-dolomite lithofacies association. These were interpreted to have formed in a playa lake environment that was influenced by climatic changes controlled by variations in monsoon cycles. The primary difference between the red siltstone-dolomite association and the deposits described by Reinhardt and Ricken (2000) is the almost complete lack of carbonate in their clastic dominated horizons and the presence of unoxidized clastic horizons. Quaternary occurences of lacustrine dolomite have been summarized by Last (1990) and many of these are likely analogs for the climatic and hydrologic conditions that led to the deposition of the dolostone-red siltstone occurrences in the Sibley Group. Rogala (2003) noted similarities between the cyclic facies and playa lakes of the Ebro Basin of Spain (Salvany et al., 1994) and the Office Basin of Australia (White and Youngs, 1980).

4.1.10 Sheet sandstone lithofacies association

The development of the sheet sandstone association records a major change in depositional conditions from the underlying cyclic facies. Cheadle (1986a) termed lithologies equivalent to this association the mudstone facies of the Rossport Formation's Channel Island Member. The two basic lithofacies present are red mudstone to siltstone and relatively thick, sheet-like sandstone beds. Cheadle (1986a) noted that the red siltstone lithofacies was nearly identical to the red siltstone and dolomicritic beds of the cyclic facies. In outcrop exposures this is apparent, however, in better preserved drill core examples it is evident that the red siltstone lithofacies in this association lacks the purer dolostone beds found in the underlying association. Cheadle (1986a) interpreted this association to represent an ephemeral playa system. Red fine-grained lithologies were thought to represent settling of fine clastic material after flash flooding of the basin, while sandstone beds were interpreted to be the result of infrequent, major sheet-flow events.

The red siltstone lithofacies lacks diagnostic features making it difficult to draw conclusions about its origin. Load features at the bases of sandstone beds suggest that the deposition of the sand-sheets may have been subaqeuous or at least the underlying surface of the red siltstones they were deposited on was water saturated. Current ripple and wave ripple laminae in fine sandstones and siltstones in this association immediately underlying the black chert-carbonate lithofacies on Channel Island definitely represent subaqeuous conditions, however, their occurrence is isolated to one observed example. Cheadle (1986a) noted the presence of adhesion structures (e.g., Kocurek and Fielder, 1982) and dessication cracks which, although not noted during this study, suggest that

aeolian adhesion to a wet mud-rich surface may have been an accumulation mechanism for the red siltstones.

Similar featureless red mudstones have been described from the Late Triassic Mercia Mudstone Group in England (Talbot et al., 1994). Red mudstones and siltstones from this group may have been deposited in a variety of environments including: entirely subaqueous accumulation in lakes, subaerial aeolian accumulation on playa-like flats or in low angle alluvial fans (Talbot et al., 1994 and references therein). A lack of carbonate beds in this association may argue against a lacustrine origin given the abundance of dolomite beds in the underlying lacustrine unit. The lack of lamination or primary sedimentary structures also argues against a lacustrine environment where fine lamination, organic rich layers or carbonate laminae would be expected (e.g. Hardie et al., 1978). Secondary processes such as pedogenesis or diagenesis, however, may have destroyed these primary features. Further, increased siliciclastic influx may have overwhelmed carbonate sedimentation leading to the dearth of the pure dolostone beds that characterize the underlying unit. A non-saline lacustrine setting similar to the red siltstone lithofacies association is possible for this association.

An aeolian origin for the red siltstone lithofacies is also possible. Thick blankets of silty clay of aeolian origin (Butler, 1956; McTanish, 1989) cover large areas near the arid interior of Australia. McTanish (1989) noted that in the presence of a sufficient source of material, accumulation rates of up to 10 cm/yr are possible for these fine-grained aeolian deposits. A low angle alluvial fan environment seems unlikely, although deposition in mud dominated floodplains of braided fluvial channels is possible. Marriott and Wright (2004) described similar deposits from the lowermost Old Red sandstone in

Wales and attributed them as the products of deposition on braidplains dominated by low sinuosity, mud dominated, ephemeral braided channels with occasional infrequent high-magnitude flood events that produced sheet-like sandstone beds or intraformational conglomerates. However, the lack of stratification in mudstone and siltstone units in this lithofacies association and also the lack of associated channel deposits argues against a fluvial origin.

Although a subaerial aeolian origin is possible for the massive siltstone lithofacies, well-laminated fine-grained sandstones and siltstones near the top of this association on Channel Island have clearly subaqeuous origins. Wave-ripple lamination suggests depositional conditions above wave base. The occurrence of the stromatolitic black-chert carbonate association, probably a shoreline (Rogala, 2003), overlying the well-laminated lithofacies suggests that subaqeuous lacustrine conditions were present during the deposition of at least the top of the sheet sandstone lithofacies association.

Sandstone beds were deposited very rapidly through broad unconfined, sheetflow processes. Evidence of rapid deposition comes from the presence of clastic dykes and synsedimentary breccias that probably resulted from penecontemporaneous liquefaction. Parallel lamination and rare primary current lineation also attest to high-energy rapid deposition. Wave rippled tops of some sandstone beds indicate the uppermost portions of sandstone beds were reworked subaqeuously. This may represent reworking in a shallow lacustrine environment, or may represent reworking in ephemeral flood lakes (e.g., Hardie et al., 1978).

4.1.11 Black chert-carbonate lithofacies association

Cheadle (1986a) interpreted this lithofacies association to represent development of a broad, shallow, spring fed and alkaline lacustrine system characterised by precipitated components. Modern spring fed playa lakes in California (e.g., Hardie, 1968) were offered as a possible analog. Extreme aridity was suggested as a climatic control that led to a cessation of surface run off and hence clastic supply to the basin (Cheadle, 1986a). Fluctuations in alkalinity were offered as an explanation for variations between carbonate and chert laminae. Rogala (2003) noted that the occurrence of this stromatolitic carbonate horizon was not as widespread as suggested by Cheadle (1986a and b) and felt that the stromatolites were deposited in shallow restricted bays and near shorelines rather than in a widespread closed lake system.

Mudcracked surfaces and pseudomorphed gypsum nodules indicate periodic wetting and drying and support a shoreline interpretation. Halite and gypsum pseudomorphs indicate strongly evaporitic conditions. Limited amplitudes of stromatolitic domes may suggest that wave action and shallow water restricted the height of growth forms. Conical stromatolites described in this unit by Cheadle (1986b) also have an apparent association with hypersaline evaporitic conditions (e.g. Grotzinger and Knoll, 1999). Silicification that produced the chert laminae occurred early as is suggested by the presence of angular black chert clasts in overlying intraformational conglomerates and fine-grained dolomite filled mudcracks on the upper surfaces of some chert laminae.

Grotzinger and Knoll (1999) and Riding (2000) have provided reviews of stromatolites and other microbial carbonate deposits. Stromatolites are "attached,

lithified sedimentary growth structures, accretionary away from a point or limited surface of initiation" (Grotzinger and Knoll, 1999). Lamination in the black-chert carbonate association fits this non-genetic definition. Commonly, microbial mats are considered to be involved in the trapping and binding of sediment or precipitation of sediments forming the accretionary layers. However, strong evidence for this is commonly absent from the preserved rock record (Grotzinger and Knoll, 1999). Cursory examination of thin-sections of black chert cut for the purpose of finding microfossils revealed the presence of sporadic spheres of organic carbon that may be microfossil remains. However, these could not be texturally linked with mat building or sediment accretion. The organic-rich nature of this unit, coupled with stromatolitic lamination suggest that microbial activity was involved in carbonate precipitation. The presence of pyrite grains likely reflects the occurrence of post-depositional sulfate reduction. Both photosynthetic removal of CO_2 by cyanobacteria and sulfate reduction by other bacteria can increase alkalinity and may have promoted carbonate precipitation (Riding, 2000).

Microbially laminated carbonate deposits in general can occur in a variety of depositional settings. These include shallow marine and lacustrine environments, but also fluvial, spring, cave and soil environments (Riding, 2000). In modern marine environments stromatolites are generally restricted to intertidal and supratidal zones, though they are also present in subtidal areas (Hofmann, 1973; Browne et al., 2000). Flat stromatolite lamination is cited as having origins in shallow intertidal or supratidal zones, whereas, large amplitude domes are typically considered to have formed in deeper, subtidal environments (e.g. Sumner and Grotzinger, 2004). The flat nature of the laminations in this lithofacies association along with dessication features both support a

shallow depositional setting. In many ways, the black chert-carbonate lithofacies association resembles modern supratidal algal mat deposits from arid carbonate environments such as the Arabian Gulf (Alsharhan and Kendall, 2003). The main similarities are the flat lamination style, the presence of evaporite pseudomorphs and evidence for desiccation. The flat lamination in this lithofacies association is also very similar to travertines and stromatolites forming in some modern lake marginal settings (Valero-Garcés et al., 2001).

4.1.12 Intraformational conglomerate lithofacies association

Cheadle (1986a) invoked two possible origins for intraformational conglomerates in the Fire Hill Member. He proposed, based an offshore lacustrine interpretation of the massive dolostone lithofacies association (equivalent to the chalcedonic mudstone facies; Cheadle 1986a), that the conglomerates represented resedimentation of dolostones and red siltstones on a lacustrine slope. Alternatively, Cheadle (1986a) suggested that the intraformational conglomerate might represent extrusive equivalents of cross-cutting intraformational breccias that intrude underlying units. Rogala (2003) proposed that intraformational conglomerates were the result of debris flows and intrusive sedimentary breccias that formed in response to increased tectonic activity related to subsidence in the northern portions of the basin. Given evidence for subaerial exposure of the top of the black chert-carbonate lithofacies association, which intraformational conglomerates directly overlie, a subaerial origin is likely. At localities where the intraformational conglomerate is dominated by bright red, oxide-rich matrix material, such as is found overlying the black chert-carbonate lithofacies association east of Red Rock, the intraformational conglomerate may represent the development of a terra rosa-style soil

horizon (for example, Bronger and Bruhn-Lobin, 1997). A detailed petrographic study would be required to fully support such a classification. At the locality south of Pass Lake, nodular carbonate concretions, clay and silt filled v-shaped cracks and concentrations of clay and silt draping underlying carbonate-rich sandstones probably formed in a setting where karstic processes were acting (e.g., Esteban and Klappa, 1983).

4.1.13 Massive dolostone lithofacies association

The massive dolostone lithofacies association, red siltstone sulfate and fine grained sandstone lithofacies associations appear to intercalate laterally and are interpreted to have formed contemporaneously based on this stratigraphic relationship (Figs. 3.2 and 3.3). The massive dolostone lithofacies association corresponds to the Fire Hill Member as described by Cheadle (1986a) and Franklin et al. (1980). Cheadle (1986a) proposed an offshore relatively deep lacustrine setting for these rocks based on a lack of both coarse clastic material and evidence for subaerial exposure. Franklin et al. (1980) proposed a similar origin. The massive dolostones in this association are very similar to the fine-grained dolomite beds in the red-silstone-dolomite lithofacies association but they lack distinct interbedded clastic-rich units. A lacustrine interpretation suggests reflooding of portions of the basin after subaerial exposure of the black chert-carbonate unit. Similar thick beds of massive fine-grained lacustrine dolomite have been described from Pliocene deposits from Spain and were interpreted to have formed in a shallow, hydrologically closed, perennial lake system (Angeles Garcia Del Cura et al. 2001). The presence of chert pseudomorphs after sulfate nodules may reflect periodic drying and exposure of the lake system.

4.1.14 Red siltstone-sulfate lithofacies association

The red siltstone-sulfate lithofacies association appears to represent a clastic-dominated, sabkha-like environment. Fine-grained clastic sediments that dominate this lithofacies association were probably deposited by alluvial and/or aeolian and/or lacustrine processes similar to proposed depositional mechanisms for the red siltstone lithofacies in the sheet sandstone lithofacies association. Sulfates were deposited within the fine-clastic host rocks thourgh evaporitic processes. The source of water for the precipitation of these evaporites may be represented by the lacustrine massive dolostone lithofacies association. Evaporation at the subaerially exposed sabkha surface likely set up a gradient by which lake waters were pumped through lake marginal sediments towards the sabkha surface. Carbonate horizons with teepee structures and abundant nodular sulfates may represent areas of seepage inflow similar to carbonate horizons described by Hanford et al. (1984). Alternatively, they may represent lagoonal or minor lake/pond environments where microbial mats flourished and induced carbonate production. Modern analogues to this lithofacies association include siliciclastic dominated sabkha environments such as Salina Ometepec in Baja California. Possible ancient analogs include the Permian Shattuck Sandstone of Texas and New Mexico (Mazzulo et al., 1991) or the Permian Yates Formation of Texas (Andreason, 1992).

4.1.15 Red siltstone-fine-grained sandstone lithofacies association

Like the red siltstone-sulfate association and the sheet sandstone association, the fine-grained siliciclastic material that composes the majority of this lithofacies association was probably deposited by alluvial and aeolian processes. Though the environment of deposition of the clastic sedimentary rocks of this association was likely

similar to the red siltstone-sulfate lithofacies association, there is little evidence of early diagenetic sulfate mineralization. This suggests that saline shallow groundwaters were not present to provide a source for the precipitation of evaporites. The distinction between these two very similar lithofacies associations, therefore, is likely the result of a local difference in hydrology. The red siltstone-fine-grained sandstone lithofacies association may represent an area of active water recharge and consequently did not accumulate major intrasediment evaporite minerals (e.g., Rosen, 1994). Conversely, the red siltstone-sulfate lithofacies association may represent an area of local evaporitic, groundwater discharge and as such accumulated extensive sulfate minerals. Iron-rich clay cutans and blocky peds, along with nodular carbonate horizons sporadically present in this association attest to subaerial conditions and soil formation. Homogeneous fine-grained sandstones may be of aeolian origin.

4.2 Depositional History

The above discussion provided details concerning the depositional settings of individual lithofacies associations. The following sections examine the stratigraphic relationships between depositional environments in the informally defined allostratigraphic units outlined in chapter 3. Cheadle (1986a and b) considered the deposition of the Sibley Group to be the product of three distinct phases: an early alluvial phase (the Pass Lake Formation), a middle lacustrine phase (the Rossport Formation), and a final alluvial phase (the Kama Hill Formation). The first two phases correspond to the section of the Sibley Group that were examined during this study.

Cheadle (1986 a and b) suggested that the early alluvial phase consisted of the development of small alluvial fans and extensive alluvial outwash flats. Interpretation of

the green sandstone-siltstone, planar cross-stratified sandstones and thinning upward sandstone units as fluvial dominated deltas, products of subaqueous sandwave migration in a nearshore clastic dominated environment, and beach/storm remobilized near shore sandstone sheets respectively, requires modification of the alluvial fan/ alluvial outwash flat model. Cheadle (1986 a and b) subdivided the middle lacustrine phase into four separate depositional episodes: an early high stand represented by his cyclic facies (red siltstone-dolostone, red siltstone-dolomitic sandstone lithofacies associations), a low stand that deposited his mudstone lithofacies (sheet sandstone lithofacies association), a period dominated by groundwater influx when the Middlebrun Bay Member (black chert-carbonate lithofacies association) was deposited and a subsequent transgression where the dolomitic muds of the Fire Hill Member (massive dolostone lithofacies association) were deposited. This model also requires modification based on the interpretation of non-saline lacustrine deposits at the base of the mixed siliciclastic carbonate unit, interpretation of the sheet sandstone lithofacies association as largely subaqeuous rather than as a dry playa system and interpretation of the black-chert carbonate lithofacies association as a shoreline environment rather than a spring-fed, restricted, shallow lacustrine system. Further, the recognition of wet and dry mudflat (sabkha) deposits requires a more complex depositional model.

Idealized block diagrams illustrating the changes in depositional environments through the deposition of the four stratigraphic units are shown in Figures 4.4 to 4.9. The diagrams are generalized to show broad changes in climate and deposition environment through the deposition of the portion of the Sibley Group studied. The diagrams do not show exact changes in geographic positions of lithofacies association and their

thicknesses, but are meant to serve as conceptual models for the broad spatial distribution of environments in space and time.

4.2.1 Basal siliciclastic unit

The basal siliciclastic dominated portion of the Sibley Group can be modeled as the product of two distinct depositional episodes and two conceptual models can be invoked to explain the distribution of lithofacies association in this unit. In the first proposed model (Fig. 4.1), alluvial sediments deposited by small debris flow dominated alluvial fan systems and braided fluvial systems, initially filled paleotopographic lows, valleys, in the pre-Sibley Group surface. A major transgression followed the deposition of fluvial units partially reworking them in the process. Two styles of vertical clastic dominated successions may have developed in response to the transgressive episode. The green sandstone-siltstone lithofacies association may represent areas that were near the primary source of sediment delivery to the basin where high sediment delivery produced progradational, wave-dominated deltaic deposits. The thinning upwards sandstone lithofacies association represents areas away from major sources of sediment delivery (greater accomodation space) where progressively drowning strand-line deposits formed. In the second proposed model (Fig. 4.2), braided fluvial systems feeding from the northwest again filled paleotopographic valleys in the pre-Sibley surface but may have debouched into a waterbody located in the southeastern portion of the basin where deltaic sediments accumulated. Following the fluvial/deltaic deposits, trangressive shoreline deposits of the fining thinning upwards lithofacies association were deposited in a similar fashion to the first model. With the available stratigraphic data, it is difficult to discern which of these two models best fits the observed stratigraphic data. Figure 4.3 shows a

schematic representation of the distribution of depositional environments in the basal clastic unit with braided streams feeding delta outbuilding in the south. Figure 4.4 depicts the transgressive episode that deposited the upper portions of the basal siliciclastic unit and lower portions of the mixed siliciclastic carbonate unit.

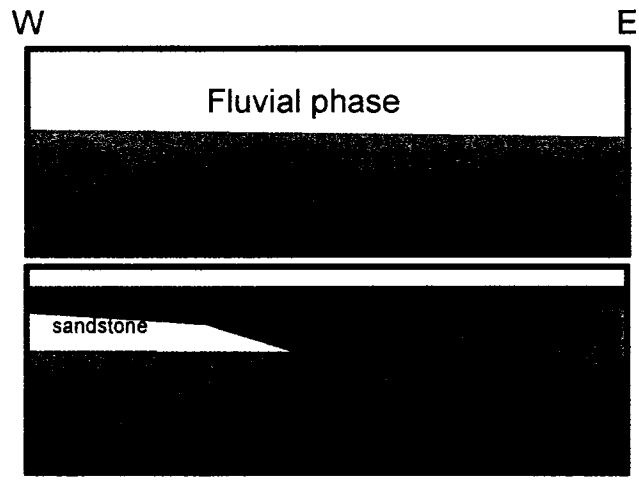

Figure 4.1. A conceptual model for the deposition of the basal clastic unit (Only very general spatial relationships are implied by the diagram). The upper box depicts initial fluvial infilling of topographic lows in the pre-Sibley Group surface. The lower box depicts trangression of waters over the basin with fining-thinning upwards sandstone successions developing in some areas, and progradation of deltaic deposits where high sediment supply created forced regressions.

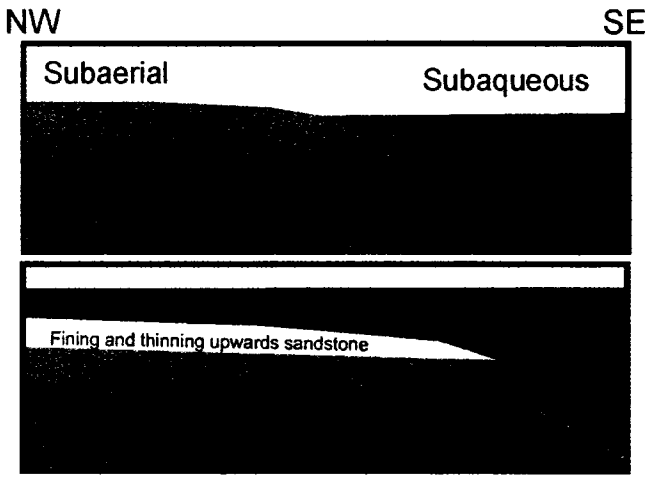

Figure 4.2. A second conceptual model for the deposition of the lower clastic unit. The upper box depicts initial fluvial deposits in the northern portion of the study area feeding deltaic deposits in the southeast. The lower box depicts the trangressive event that may have followed depositing the thinning-upward sandstone association. The primary difference between the two models is the relative age of the deltaic deposits. The first model has deltaic deposits forming during the transgressive episode responsible for the deposition of the thinning upward sandstone lithofacies association. In the second model, deltaic deposits are forming prior to the transgressive episode, and are related temporally to the braided fluvial deposits.

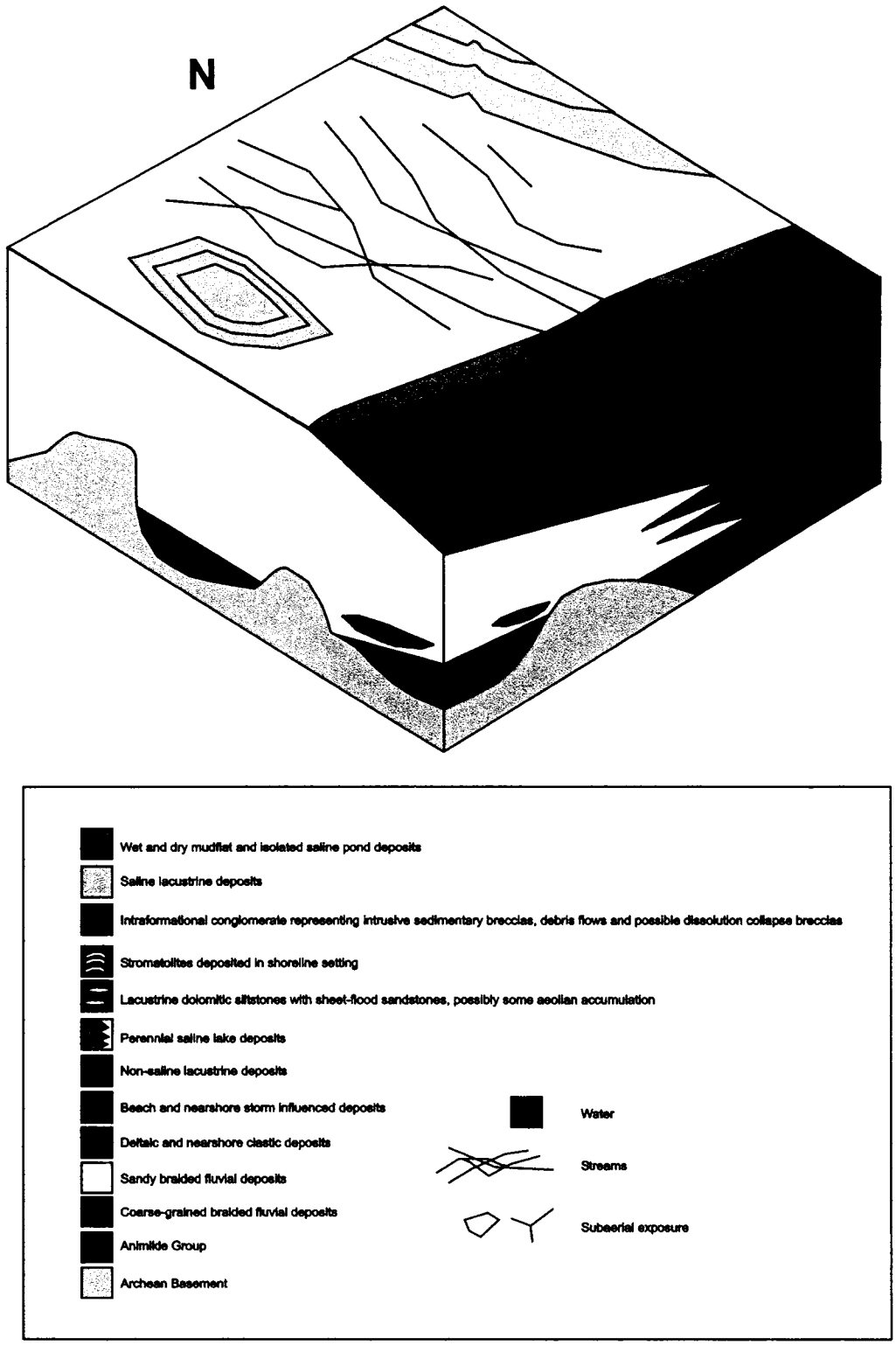

Figure 4.3. Schematic representation of a depositional model for the fluvial and deltaic portions of the basal clastic unit. The northern portion of the area is interpreted to have been filled by topographically controlled braided fluvial depositional systems which fed delta deposition in a water body to the south and south-east.

Figure 4.4. Schematic block model showing the development of a non-saline lacustrine system following trangression and deposition of fining- and thinning-upward sandstone units, and during the deposition of the red siltstone lithofacies association. The legend for this diagram is the same as Figure 4.4.

4.2.2 Mixed siliciclastic-carbonate unit

The mixed siliciclastic-carbonate unit records lacustrine deposition that appears to have changed from non-saline to saline through time. The non-saline lacustrine deposits of the red siltstone lithofacies association are gradational from the underlying thinning-upwards sandstone lithofacies association and are likely related to the same transgressive

event, with red siltstones representing progressively further offshore deposits. The stratigraphic distribution of cyclic deposits of the red siltstone-dolostone and red siltstone-dolomitic sandstone lithofacies associations attest to the presence of a widespread, shallow, perennial, saline lake system. Lateral variations in the distribution of red siltstone-dolostone versus red silstone-dolomitic sandstone reflect relative proximity to sources of clastic input. Relatively short-term variation between wet (clastic rich layers) and dry (dolomite/sulfate rich layers) climates is recorded in the red siltstone-dolostone lithofacies association (Fig. 4.5). Periodic subaerial exposure, indicated by mudcracked or brecciated dolostone layers, displacive sulfate nodules, and sulfate filled mudcracks, relate to periods of exceptionally dry climate and subaerial exposure in more shore proximal regions. Distal lake deposits are represented by successions with little evidence for exposure. Further constraints of the paleoenvironmental and chemical evolution of lithologies in this unit is provided by geochemical data discussed in chapter 5. Overall, this unit appears to record a fairly stable period where a large lacustrine system covered the majority of the study area (Fig. 4.6). The climate was probably quite dry as shown by the presence of evaporitic dolomite and sulfate, however, a significant source of inflow must have been present to maintain perennial lake conditions.

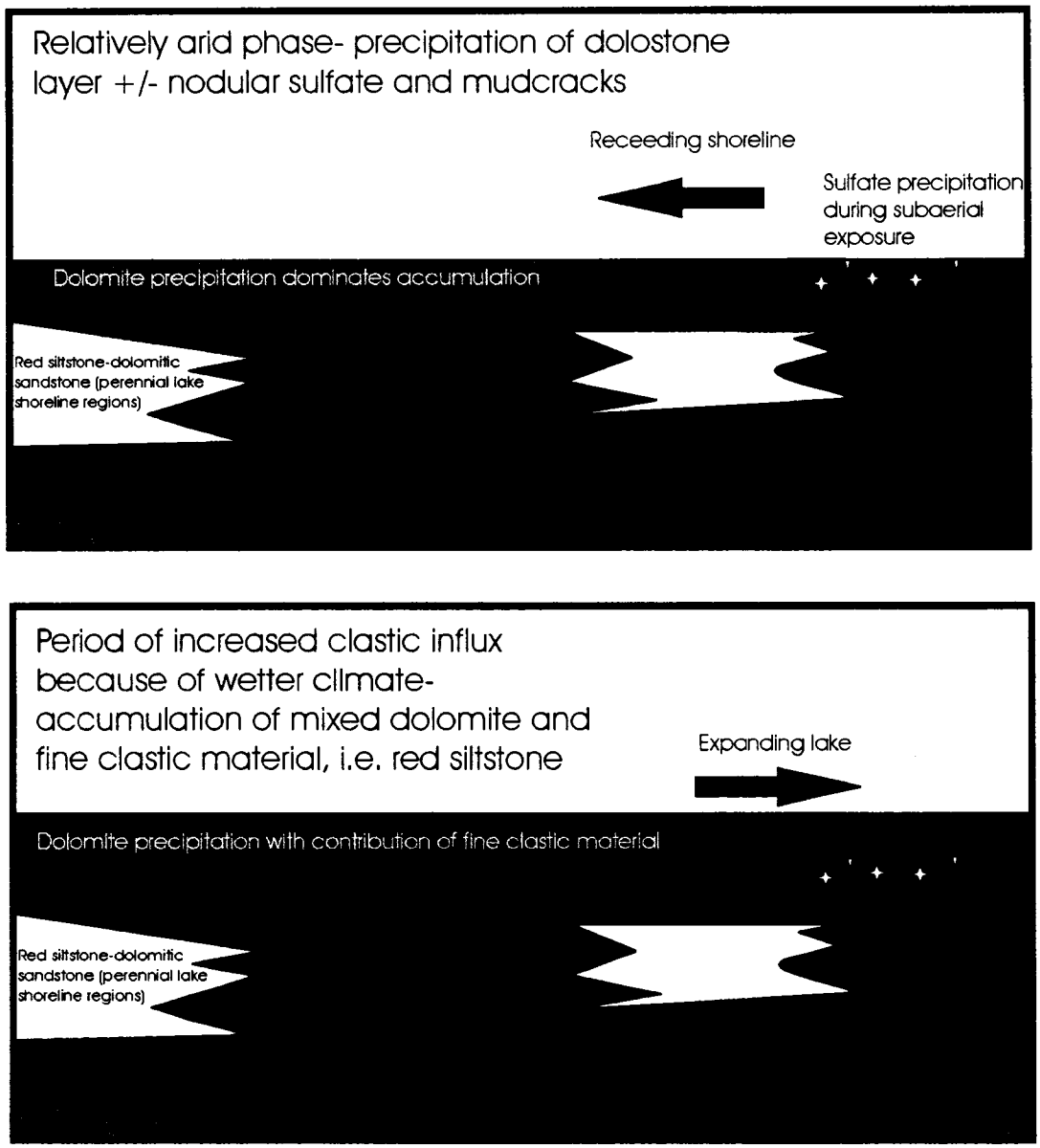

Figure 4.5. Simple climate controlled model for the perennial lake system that deposited the red siltstone-dolostone lithofacies association. The top diagram illustrates a relatively dry climatic phase with little siliciclastic sediment supply when relatively pure dolostone accumulated along with sulfate formation under subaerially exposed lake marginal areas. The bottom diagram illustrates a relatively wet climatic phase where increased siliciclastic supply lead to deposition of sediment more rich in siliciclastic material.

Rogala (2003) provided an estimate of the depositional rates in this unit based on a paleomagnetic secular variation curve for a 90 cm long section of dolomitic red siltstone from this unit. Peaks in the secular variation curve derived for a section of the Channel Island Member and estimated sedimentation rates of 0.15 mm/a and 0.5 mm/a

suggested a periodicity between 1700-5700 years (Rogala, 2003). Individual peaks were separated by decimeter scale intervals and this suggests that climatic variations preserved in decimeter scale oscillations between siltstone (wet) and dolostone (dry) climates occurred over similar time-scales.

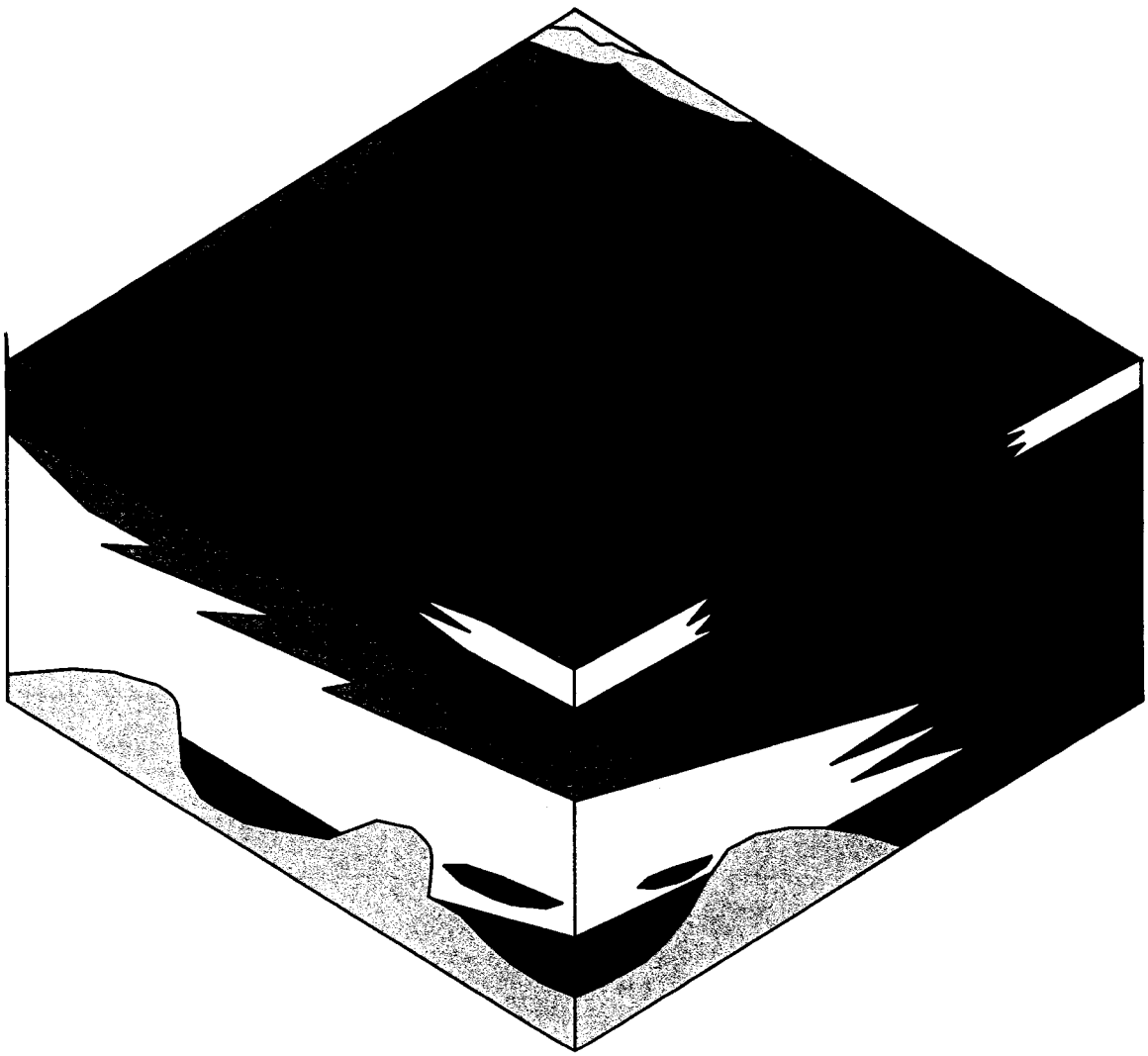

Figure 4.6. Schematic model showing the development of perennial saline lake conditions during the deposition of the mixed siliciclastic carbonate unit. Red siltstones and micritic dolostones were deposited in areas removed from clastic influx while red siltstones and dolomitic sandstones (dolomite cement and some dolomite intraclasts) were deposited at zones of clastic influx. The legend for this diagram is the same as Figure 4.4.

4.2.3 Upper clastic unit

The transition from the mixed siliciclastic carbonate unit to the upper clastic unit marks the reintroduction of coarser clastic material to the basin and the end of deposition of pure dolostone beds. Paleocurrent data is scattered (Fig. 3.6), however, they suggest a change as compared to the lower clastic unit from a southward to a northward paleoslope. Thus, the change in depositional environments may have been the result of tectonic reorganization of the basin and increase in siliciclastic sediment supply. Alternatively, the change in depositional style may be the result of a major climatic change from the relatively wet interval, represented by the underlying perennial lacustrine phase, to a dryer interval represented by ephemeral playas of the sheet sandstone lithofacies association. However, the dry playa interpretation is problematic because of the preservation of finely laminated units in a few localities and as such accumulation of most of the fine-grained clastic sediment probably occurred under water. Because of this it is difficult to support a change to more arid conditions as the main control on the change in depositional setting from the lower unit. Increased siliciclastic and water input from the south may have inhibited carbonate deposition in a lacustrine setting leading to the end of pure carbonate sedimentation intervals represented by dolostone beds. In the upper portions of this stratigraphic interval a transition from subaqeuous conditions to subaerial exposure is recorded by the change from the sheet sandstone to the black chert-carbonate lithofacies association further supporting a subaqueous origin for the sheet sandstone association. Figure 4.7 presents a generalized view of the distribution of lithofacies associations in the upper clastic unit.

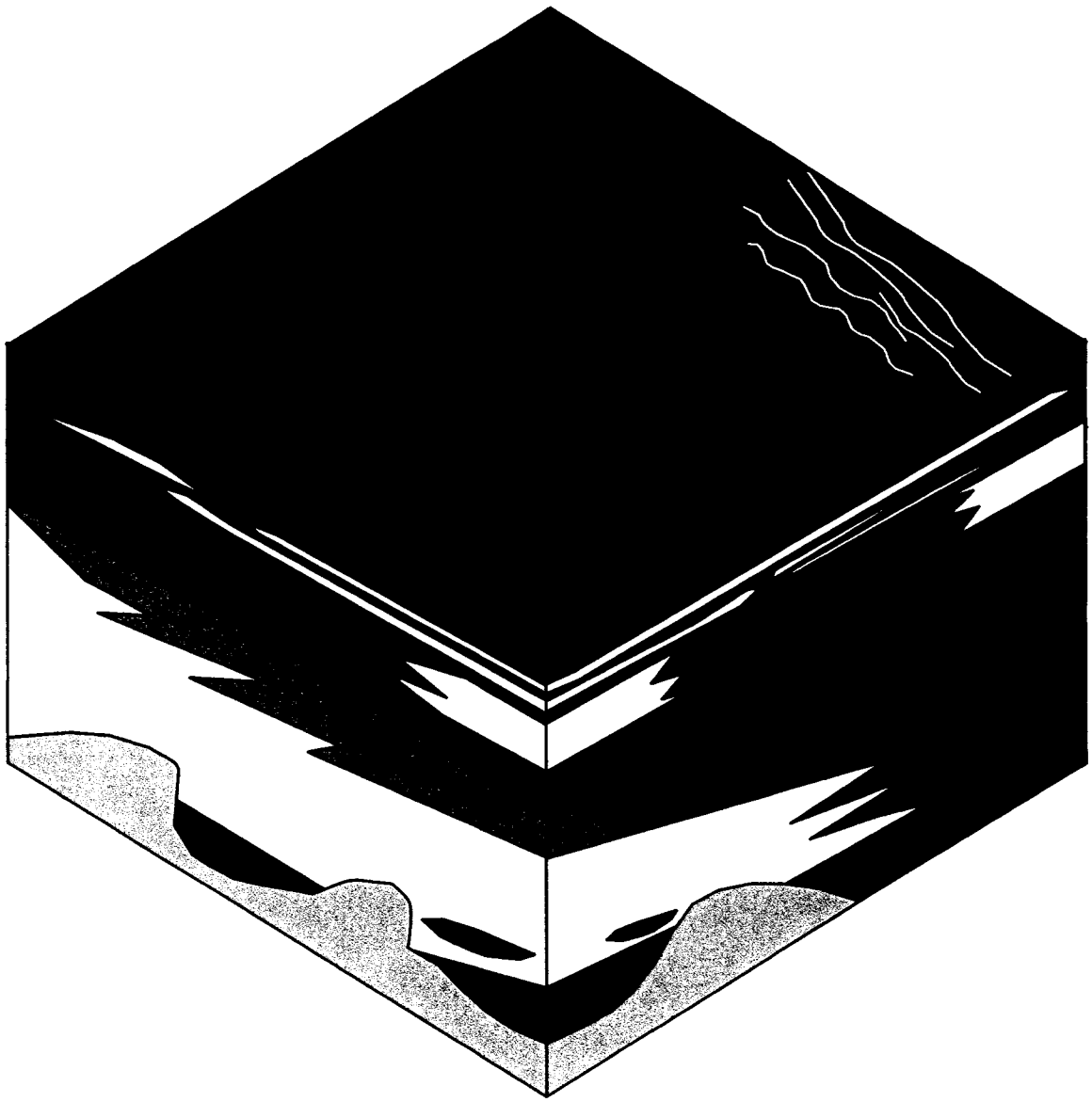

Figure 4.7. Schematic representation of lake system during the deposition of the upper clastic unit. Stromatolitic carbonates probably developed in restricted shoreline environments during the latter stages of the deposition of this unit as the lake system was shrinking prior to subaerial exposure. The legend for this diagram is the same as Figure 4.4.

4.2.4 Mixed sillciclastic-carbonate-evaporite unit

The presence of interpreted subaerial exposure features at the top of the black chert-carboante lithofacies association and the inclusion of partially lithified clasts of lithologies present in the underlying stratigraphic unit into intraformational conglomerates at the base of this unit suggests that there may have been a significant

hiatus between the deposition of the upper clastic unit and the upper mixed unit. This may have been the result of continued uplift in the southern portions of the region or a change to a drier climate. A tectonically induced period of exposure is supported by the development of debris-flow intraformational conglomerates and cannibalism of underlying units forming intrabasinal clasts. The timeframe for this apparent tectonic reorganization or its causes are unknown. However, it probably began with the introduction of sheet sandstone beds from the south. Increased tectonic activity suggested by intrusive sedimentary breccias and debris flow intraformational conglomerates may coincide with the proposed development of a half graben structure (Rogala et al. 2005). Figure 4.8 depicts the distribution of lithofacies associations related to the period of subaerial exposure that followed the deposition of the upper clastic unit.

Subaerial exposure appears to have been followed by reflooding of portions of the basin which caused resumed saline lacustrine deposition (massive dolostone lithofacies association) and associated wet (red siltstone-sulfate lithofacies association) and dry (red siltstone-fine-grained sandstone lithofacies association) mudflat deposition around the lake's margins (Fig. 4.9). Massive dolostones are interbedded with intraformational conglomerate horizons which supports continued tectonic activity during this period. The change to siliciclastic, siltstone dominated deposition that marks the lithostratigraphic contact with the Kama Hill Formation may have been the result of a climatic change to a more humid conditions with increased clastic input, which lead to an end of deposition of dolostone and sulfate lithologies.

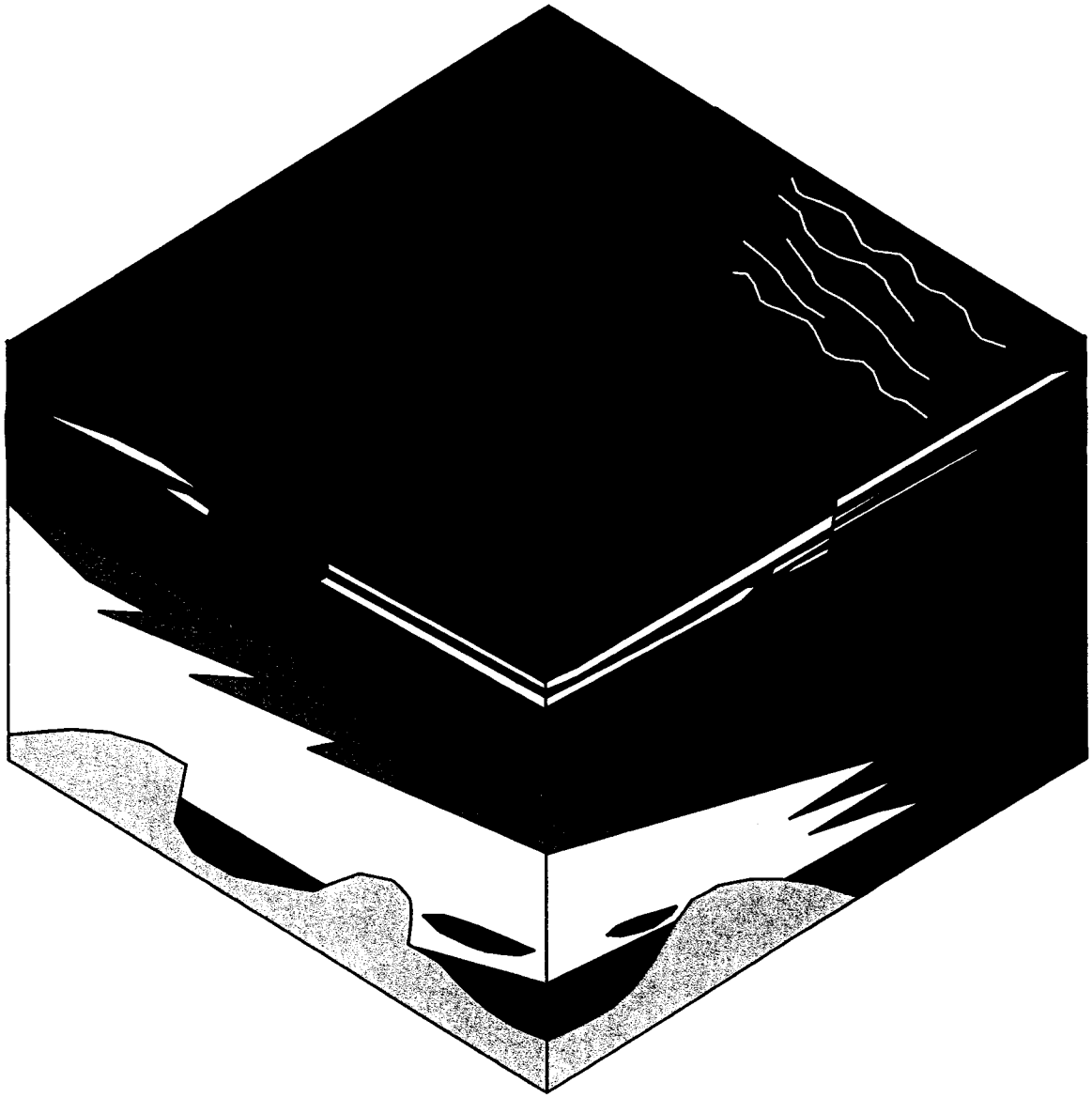

Figure 4.8. Schematic represantation of the period of subaerial exposure following the deposition of the upper clastic unit. Increased tectonic activity likely caused the intrusion of intraformational breccias, synsedimentary faulting and induced subaerial debris flows. Pedogenic processes likely created karst-like features in places (possibly evaporite dissolution breccias), terra rossa style soils and soil carbonate horizons. The legend for this diagram is the same as Figure 4.4.

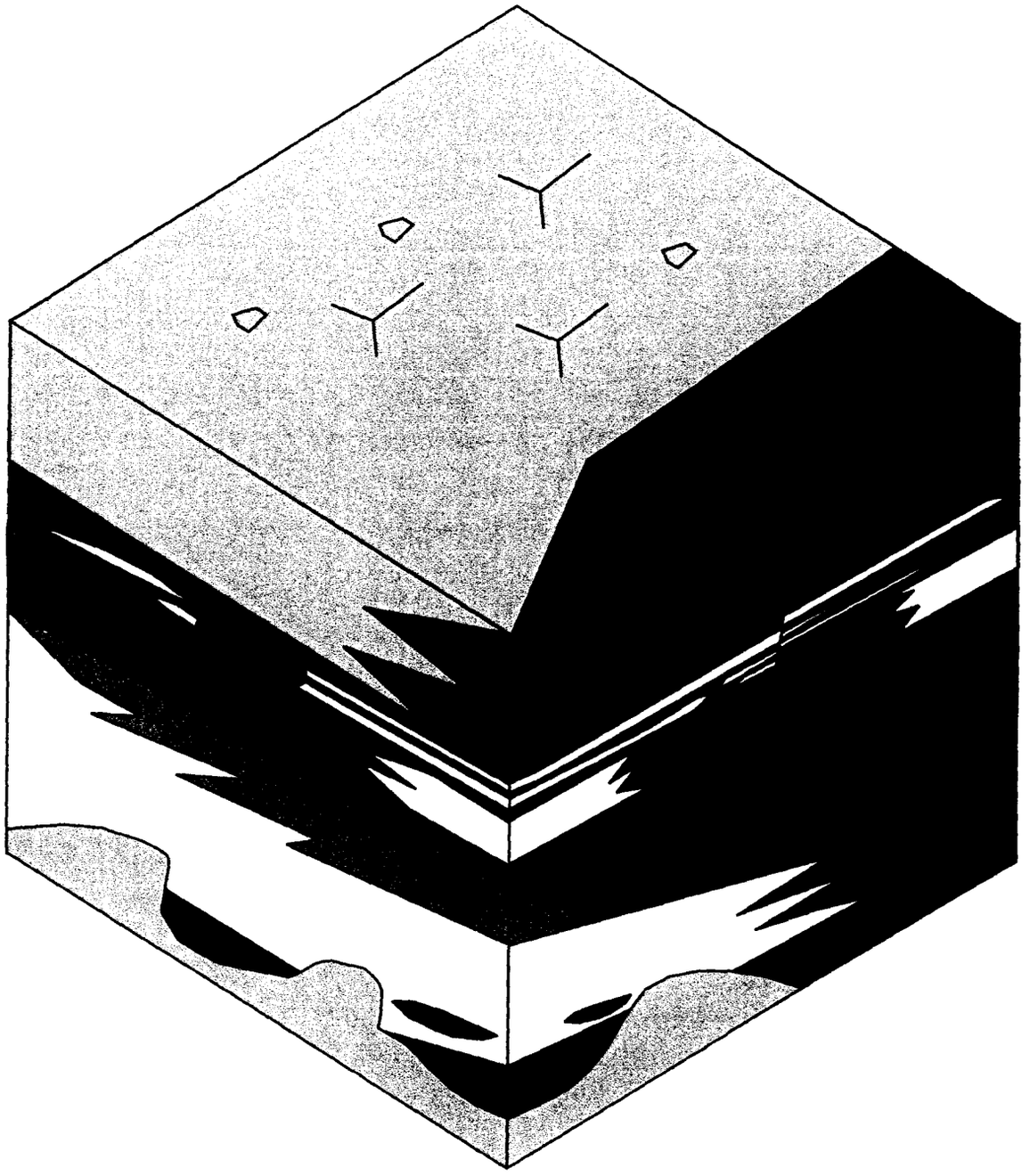

Figure 4.9. Schematic representation of the distribution of saline lake and mudflat deposits during the deposition of the upper mixed siliciclastic-carbonate evaporite unit. The legend for this diagram is the same as Figure 4.4.

Chapter 5. Geochemistry

5.1 Introduction

Stable isotope (C, O and S), radiogenic isotope (Sr), and trace element compositions, including REE's, were determined for various carbonate and sulfate lithofacies at a variety of stratigraphic levels within the Sibley Group. This chapter outlines sampling and analytical methods used, provides a brief overview of geochemical systematics, reviews relevant literature on the evolution of the Mesoproterozic oceans and atmosphere, presents raw geochemical data organized according to stratigraphic units and discusses the results. The discussion section examines indicators of diagenetic alteration and discusses the implications of geochemical data on the depositional environments and paleohydrologic conditions present during the deposition of the lower portions of the Sibley Group.

5.2 Methodology

Section 5.2 describes sampling methods and detailed analytical methods for carbon, oxygen and sulfur stable isotope analyses as well as trace element analyses. Appendices 1-6 contain complete tables of all geochemical data collected.

5.2.1 Sampling

Samples were collected from both measured drill core sections during logging and from outcrops. Polished thin sections were cut for most samples and examined via an optical microscope and/or a scanning electron microscope for petrographic characterization and to assess alteration. Powders for geochemical analysis were made

using a hand-held ceramic mortar and pestle after hand samples were crushed into mm-scale pieces and visibly unaltered and siliciclastic-free chips were picked out under a binocular microscope. Splits from these small whole rock samples were divided for analyses by the various methods detailed below.

5.2.2 Determination of carbon, oxygen and sulfur isotopic composition

Carbon, oxygen and sulfur isotopic compositions were determined at the Queens University stable isotope laboratory in Kingston Ontario. For carbonate (dolomite) samples, carbon dioxide was extracted with phosphoric acid (McCrea, 1950) and $^{12}C/^{13}C$ and $^{16}O/^{18}O$ were measured using a Gas Bench coupled to a Thermo Finnigan Delta plus XP mass spectrometer utilizing continuous flow technology. Results for both carbon and oxygen are reported in standard delta (δ) notation in per mil (‰) relative to the standard Peedee Belemnite (PDB). Sulfur was extracted and analysed using continous flow technology with a Carlo Erba NCS 2500 Elemental Analyser coupled to a Finnigan MAT 252 Mass spectrometer. Sulfur results are reported in ‰ notation relative to the Canon Diablo Troilite standard (CDT). Replicate analyses suggest a precision of 0.1 per mil for all stable isotopic analyses.

5.2.3 Determination of Sr isotopic composition

$^{87}Sr/^{86}Sr$ ratio determinations were preformed at Carleton University in Ottawa Ontario. Carbonate was separated from samples using a weak (5%) acetic acid leach method similar to that described by Bailey et al. (2000). Weak hydrochloric acid was originally used for leaching, but high Rb contents and corresponding high Sr isotopic

ratios in samples analysed by this separation method suggested significant clastic contamination.

Prior to Sr separation, 50-100 mg carbonate samples were preleached in 5% acetic acid for 1hr to remove Sr adsorbed onto clastic impurities. Samples were then leached in 5% acetic acid for 24 hrs to dissolve the carbonate fraction of the sample. Leachates were pipetted from samples and placed into clean teflon beakers and dried. Sr was then separated from this acetic acid soluble portion. Sulfate samples were leached for 1-2 days in distilled deionized water, separated by pipette into clean teflon beakers and dried. Sr was then separated from this water-soluble portion.

Sr separations were done using cation exchange chromatography. The samples were dissolved in 2.5N HCl and pipetted into a 10-ml borosilicate glass chromatography column containing 3.0 ml of Dowex AG50-X8 cation resin that was pre-cleaned in 6N HCl. Sr was eluted using 15 ml of 2.5 N HCl. Samples were loaded onto a single Ta filament with H_3PO_4 and isotopic ratios were determined using a Finnigan MAT 261 thermal ionization mass spectrometer at filament temperatures of 1480-1520°C. Isotope ratios were normalized to $^{86}Sr/^{88}Sr = 0.11940$ to correct for fractionation. The standard NIST SRM987 was run along with the samples. From Sept. 1992 - May 2003 the value of this standard as analysed at Carleton has been $^{87}Sr/^{86}Sr = 0.710251 \pm 18$, n=50.

5.2.4 Trace element geochemistry

Trace element compositions were determined by either ICP-AES at Lakehead University or ICP-MS at Ontario Geoscience Laboratories. For carbonate samples an acetic acid leach method, again similar to Bailey et al. (2000), was applied in order to

avoid contamination of carbonate geochemical signatures by clastic material. The method for the acetic acid leach was as follows:

1) 50-200 mg aliquots of powder were weighed in acid cleaned teflon beakers
2) 10ml of 5% acetic acid was added as a pre-leach and allowed to react for 1 hr to remove materials loosely bound on clastic particles
3) Pre-leach solutions were removed by pipette and discarded
4) 10ml of 5% acetic acid was again added and allowed to react for 24 hr in a covered teflon beaker
5) After 24 hr acetic acid was pipetted from the sample beakers, filtered and placed into new teflon beakers for drying
6) Dried acetic acid soluable material and teflon beakers were weighed
7) Samples were then dissolved in 5% HCl solutions for analysis by ICP-AES or ICP-MS
8) Dried teflon beakers were reweighed after sample dissolution to determine sample weights.

Several procedural blanks were run during the course of the analyses to evaluate the degree of contamination associated with acids used and impurities from the sample preparation lab and labware. In addition, several duplicate analyses were run to evaluate the reproducibility of analyses by this method. For ICP MS analyses, the river water standard SLRS-4 was also analyzed along with samples to evaluate instrumental accuracy.

Trace element geochemistry for sulfate samples was carried out by ICP-AES at Lakehead University. Sample powders were allowed to dissolved in 20-30 ml of distilled

deionized water for several days. After several days about 20-30ml of water were removed by pipette and placed into a clean teflon beaker and dried. The water soluable portions of the sample powder and teflon beaker were then weighed. After weighing, water soluble portions of the sample were dissolved in a 5% HCl solution for analysis. Empty beakers were then weighed to determine sample weights.

Replicate ICP AES analyses of two carbonate samples, CI-1a, dolomicrite from the black chert-carbonate lithofacies association and CIF-15, an Archean ankeritic dolomite from the Steep Rock Group are shown in Table 5.1. Values for Ca, Fe, Mg, Mn, Sr and Y are quite stable for each carbonate analysis and tend to deviate less than 10% from the average value in each case. Two replicate analyses of a gypsum sample, Tbg, show poor reproducibility, though this may have improved with more analyses. An ICP MS analyses of CI-1a typically showed trace element concentrations slightly lower than those determined by ICP AES. However, replicate analyses of other samples by ICP MS show good reproducibility (appendix 2).

Table 5.1. Replicate ICP-AES analyses of two carbonate samples (CI-1a and CIF-15) using the acetic acid dissolution method and a replicate analysis of one gypsum sample (Tbg) using the water dissolution method.

sample	Al ppm	Ba ppm	Ca ppm	Fe ppm	Mg ppm	Mn ppm	Na ppm	P ppm	S ppm	Si ppm	Sr ppm	Y ppm
CI-1a	41.97	431.00	137171.39	930.42	71607.18	588.58	71.48	nd	140.84	22.65	56.50	3.84
CI-1a	39.58	716.92	138808.86	940.57	77079.59	580.84	175.59	53.62	159.74	18.91	51.25	4.00
CI-1a	49.95	240.74	139093.32	834.78	82278.02	570.51	84.70	nd	58.21	16.72	47.39	4.48
CI-1a	52.92	167.04	133827.42	837.14	74771.84	538.97	70.58	0.09	53.53	22.62	47.62	3.97
CI-1a	52.27	546.24	133526.64	813.71	77830.70	556.39	171.58	22.68	161.65	7.12	43.61	4.30
CI-1a	48.74	466.16	127925.07	806.51	78923.62	551.98	180.61	6.53	185.14	8.08	41.29	4.42
CIF-15	16.39	10.12	130936.04	2294.38	78951.07	2059.11	252.13	10.59	53.49	17.57	27.63	nd
CIF-15	0.21	8.09	127461.02	2126.62	76401.22	1947.98	39.67	0.53	nd	nd	25.61	2.66
CIF-15	1.64	7.92	126899.73	2116.48	75583.56	1943.21	121.13	39.85	2.96	1.78	26.68	2.64
CIF-15	nd	6.97	130735.79	2258.97	78737.52	1958.34	44.62	nd	nd	1.86	25.38	2.69
CIF-15	15.41	9.69	128357.08	2059.32	79338.84	1918.66	45.85	nd	25.30	11.54	26.95	2.76
CIF-15	10.65	10.34	127359.69	2146.35	76763.24	1938.36	119.01	10.44	44.03	nd	27.10	2.73
Tbg1	nd	4.52	217837	nd	291.54	6.92	53.75	nd	178210	249.42	885.87	nd
Tbg2	2.90	6.13	260573	nd	342.63	3.50	170.44	nd	213359	198.92	1062.83	nd

5.3 Geochemical systematics

A synopsis of the factors controlling carbon, oxygen, sulfur and strontium isotopic systematics and rare earth element systematics is required prior to discussion of Sibley Group data. A brief discussion of each isotope system is given in the following paragraphs. In each case, a brief overview of the factors controlling the marine evolution of the respective isotopic systems and also factors controlling the compositions of each isotopic system in a non-marine depositional environment is discussed. Factors controlling the composition of REE's in chemical sedimentary rocks are also discussed. Exhaustive reviews are not possible in this thesis, however, a general overview provides a reference for interpretive discussion of the geochemistry of the Sibley Group that follows.

5.3.1 Carbon and oxygen

Fractionation between water and carbonate varies considerably with temperature for oxygen, but negligibly for carbon (e.g. Faure, 1986; Veizer, 2003). The $\delta^{13}C$ of dissolved carbon in seawater is about 1 +/- 0.5 ‰ and atmospheric CO_2 in equilibrium with dissolved carbon in the oceans has a isotopic composition of about –7 ‰ (Veizer and Mackenzie, 2005). In the rock record carbon resides in two primary reservoirs, carbonate sediments and organic material. These reservoirs are related to the carbon cycle through atmospheric CO_2 and dissolved carbon in the oceans (hydrosphere). In a simplified sense, long term variations in the carbon isotopic composition of the oceans through time, and hence marine carbonates through time, occur because of differences in the rates of burial of organic carbon versus inorganic (carbonate) carbon (e.g. Holland, 1984; Kump and Arthur, 1999; Frank et al., 2003). As organic carbon is enriched in ^{12}C,

global increases in rates of organic matter production and burial drive the oceans toward more ^{13}C enriched compositions. Figure 5.1 shows variations in marine carbonate through geologic time.

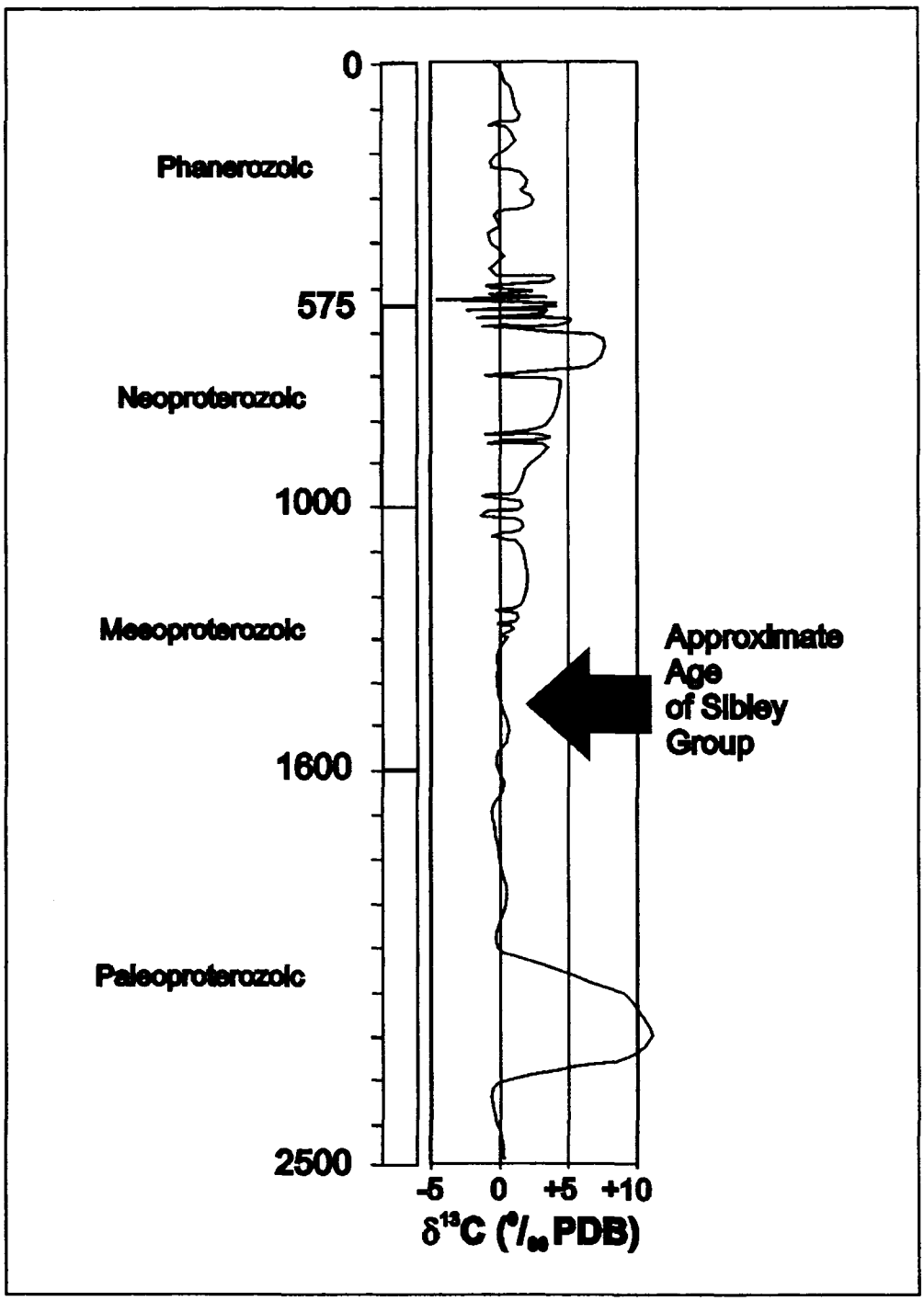

Figure 5.1. Isotopic composition of marine carbonates from the late Archean to present (modified from Brasier and Lindsay, 1998; Bartley and Kah, 2004)

The carbon isotopic composition of carbonates precipitated from lakes depends primarily on the composition of dissolved carbon in the lake water as there is little carbon isotopic fractionation during the precipitation of carbonates and little temperature affect (Emrich et al., 1970; Romanek et al., 1992; Talbot, 1990). The main controls on the $\delta^{13}C$ in most lake waters are: CO_2 added through decomposition and respiration of organic matter, dissolution of existing carbonate rocks, exchange with the atmosphere, and sequestration of ^{12}C by organisms (Valero-Garces et al., 1999). However, in saline lake settings, processes such as evaporation and residence time are often dominant in controlling the $\delta^{13}C$ composition (e.g., Valero-Garces et al., 1999; Last, 2002). Talbot (1990) reviewed paleohydrological classification of lake systems and suggested that open lake systems show relatively invariant $\delta^{13}C$ and $\delta^{18}O$ and no significant covariance between the two isotopic systems whereas closed lake systems often show statistically significant covariance. This covariance is the result of evaporitic and residence time effects that lead to coupled increases in $\delta^{13}C$ and $\delta^{18}O$ (Talbot, 1990). Primary carbonates from freshwater lakes typically have $\delta^{13}C$ compositions that are relatively light and range between –6 and –12 ‰ while saline lakes can attain heavier isotopic compositions of up to +5 ‰ (Valero-Garces et al. 1999). In some instances very high carbonate $\delta^{13}C$ enrichments (+13 ‰; Valero-Garces et al., 1999; ~+17 ‰ Melezhik et al., 1999) have been reported from evaporitic lacustrine systems. Lake carbonate can also form in equilibrium with atmospheric CO_2 and $\delta^{13}C$ for these precipitates can have typical marine values of around 0 ‰ (e.g. Valero-Garces et al., 1999).

The oxygen isotopic composition of primary lacustrine carbonates depends on the temperature and the composition of the water from which they precipitate (e.g. Chivas,

1993). $\delta^{18}O$ of lake-water is controlled by the composition of input (rainfall/runoff and groundwater) and physical processes such as evaporation within the basin (e.g. Valero-Garces et al., 2000). $\delta^{18}O$ of precipitation depends on the temperature of condensation and on the amount of water removed from the air mass from which precipitation is occurring relative to the original amount it contained (e.g., Kendall and Doctor, 2005). $\delta^{18}O$ of groundwater reflects the average composition of precipitation, but may be modified by various processes, such as evaporation or reaction with bedrock.

General reviews of the stable isotopic compositions of calcretes are found in Wright and Tucker (1991) and Alonzo-Zarza (2003). Compilations of calcrete carbon and oxygen stable isotopic compositions show that calcrete $\delta^{13}C$ values range between –12 and 4 ‰ and $\delta^{18}O$ values range between –9 and +3 ‰ (Alonzo-Zarza, 2003 and references therein). Multiple factors are important in controlling the stable isotopic composition of pedogenic carbonates and these include but are not limited to: atmospheric composition, elevation, latitude, temperature, degree of freezing, vegetation cover (type and amount), rainfall/runoff composition (also seasonal variations in rainfall composition), degree of evaporation, proximity to the ocean and contamination by existing soil and other carbonates (Wright and Tucker, 1991). $\delta^{13}C$ in pedogenic calcretes is primarily controlled by the composition of soil CO_2 (Cerling, 1991). In relatively young calcretes the composition of soil CO_2 is controlled by the relative proportions of C3, C4 or CAM plants that produce CO_2 through root respiration, microbial oxidation of organic matter and atmospheric CO_2 penetration into the soil (Cerling, 1984; Amundsen et al., 1988; Mack et al., 2000; Alonzo-Zarza, 2003). Clearly in a Mesoproterozoic setting the effects of higher plants are not factors, and as such soil

CO_2 would have been controlled by atmospheric CO_2 penetration, microbial respiration and oxidation of organic matter. $\delta^{18}O$ in calcretes is controlled primarily by rainfall/runoff composition, selective infiltration, evaporation and temperature (Talma and Netterberg, 1983; Cerling, 1984; Wright and Tucker, 1991). In a groundwater calcrete, $\delta^{13}C$ and $\delta^{18}O$ will depend primarily on the composition of dissolved carbon and oxygen in groundwater.

Calcrete stable isotopic compositions have been used in various capacities in paleoenvironmental and paleoatmospheric studies. In addition to their importance as indicators of semi-arid to arid climatic conditions, stable carbon isotopic compositions of pedogenic carbonates have been successfully used to quantitatively assess the partial pressure of CO_2 in the atmosphere through the Phanerozoic (e.g., Cerling, 1991, 1992). Cerling (1991, 1992) developed a quantitative model of the controls on pedogenic carbonate compositions and a paleobarometer for the partial pressure of CO_2 of the paleoatmosphere based on the $\delta^{13}C$ of purely pedogenic carbonates and various assumptions. In a general sense, at high atmospheric CO_2 levels relatively heavy atmospheric CO_2 can enter soil pores and pedogenic carbonates precipitated will record relatively heavy $\delta^{13}C$. Conversely, at low atmospheric CO_2 levels, relatively light CO_2 derived from plant respiration or organic matter decay dominates soil CO_2 leading to lighter carbon isotopic compositions in precipitated pedogenic carbonates. Through parts of the Phanerozoic, atmospheric CO_2 levels estimated by pedogenic carbonate $\delta^{13}C$ correlate well with those proposed through other methods, such as the stomatal index of fossil leaves (e.g., Retallack, 2001, 2002). However, applying the principles of Cerling's (1991, 1992) method is difficult with respect to Sibley Group pedogenic carbonates as

neither the $\delta^{13}C$ of atmospheric CO_2 or the $\delta^{13}C$ of soil organic matter is known. More importantly, assumptions about the proportion of CO_2 contributed by respiration and decay of organic matter that are required for the model are impossible to estimate. In relatively young well-drained soils organic related CO_2 contribution is assumed to fall within restricted limits (e.g. Cerling, 1991, 1992; Ekart et al. 1999); however, these assumptions are probably not valid in a Precambrian setting. Overestimating the proportion of CO_2 contributed by soil respiration and rotting of organic matter will lead to an underestimation of pCO_2 in the atmosphere. As the rates of soil CO_2 respiration and organic matter content may have been significantly lower in the Mesoproterozoic than in most Phanerozoic soils, the composition of a Mesoproterozoic pedogenic carbonate should have higher $\delta^{13}C$ compositions reflecting an increased influence of atmospheric CO_2.

5.3.2 Sulfur

The sulfur cycle at the surface of the Earth contains three major reservoirs: dissolved sulfate in the ocean; sulfide minerals, primarily pyrite in shales; and sulfate minerals, primarily gypsum in evaporite deposits (e.g., Bottrell and Newton, 2006). The mantle is the primary source of sulfur to the earth's surface reservoir and it is delivered to the earth's surface through volcanic degassing, hydrothermal circulation and weathering of ocean crust (Canfield, 2004). In an oxidizing atmosphere sulfur is weathered from continents as sulfate (SO_4^{2-}) and delivered to the oceans. In the oceans, sulfur-reducing bacteria can reduce sulfate to sulfide and pyrite can precipitate. If sulfate is delivered to a restricted evaporitive basin, sulfate minerals may be precipitated. Uplift eventually re-

exposes sedimentary sulfur deposits to weathering and delivery back to the oceans and this sulfur may be returned to the mantle through subduction.

The isotopic compositions of sulfate minerals precipitated from water reflect the composition of the water with very little fractionation (0 to +2.4 ‰) (e.g., Ault and Kulp, 1959; Thode et al., 1961; Thode and Monster, 1965; Nielsen, 1978). Fractionation between the sulfide and sulfate reservoirs occurs largely through the action of sulfate reducing bacteria. Sulfate reducing bacteria preferentially use ^{32}S and the reduced sulfur species generated from the process is depleted in ^{34}S. A number of factors including the type of bacteria, the type of organic substrate and the reduction rate control the actual net fractionation from this process (Harrison and Thode, 1958; Kaplan and Rittenberg, 1964; Chambers and Trudinger, 1979; Strauss 1999). Environmental effects, such as sulfate availability, are also very important and may overshadow the effects of bacterial sulfate reduction particularly in cases of low sulfate concentration (Ohmoto, 1992; Habicht and Canfield, 1996). Low sulfate availability was apparently a major factor in controlling the sulfur isotopic composition of the Archean and Proterozoic oceans (e.g., Canfield, 2004).

The compositions of both sulfide and sulfate sulfur in the oceans has varied through time. Numerous publications report curves showing the secular variation in both sulfide and sulfate sulfur isotopic compositions from the early Archean to present (e.g. Strauss, 1999; Canfield and Raiswell 1999; Veizer, 2003; Canfield, 2004). The Precambrian record of sulfate sulfur is incomplete because of poor preservation of sulfate lithologies. However, analyses of sedimentary sulfides are common and show a distinct decrease in $\delta^{34}S$ at about 2.4 Ga that is interpreted to represent a major rise in atmospheric oxygen that allowed the action of sulfur reducing bacteria to procede in a

non-sulfate limited system (Cameron, 1982; Canfield, 2004). Increased burial of ^{34}S depleted sulfides from this point in the late Archean or early Proterozoic, led to increasing $\delta^{34}S$ of the oceans. In general, the sulfur isotopic composition of the oceans through time is controlled by the mass balance effects created by differing rates of pyrite burial (i.e., increased pyrite burial leads to ^{34}S enrichement of the ocean through removal of ^{34}S depleted sulfides) and the balance between the composition of terrestrial sulfur input to the oceans and rate of pyrite burial (e.g., Claypool et al., 1980). However, other factors, such as formation of large sulfate evaporite deposits, sulfate removal as carbonate associated sulfate (CAS), burial of organic sulfur compounds, and mantle sulfur inputs have effects on the composition of seawater $\delta^{34}S$ at any given time (Bottrell and Newton, 2006).

Sulfur in lacustrine systems is generally depleted in ^{34}S relative to marine settings as most terrestrial sources of sulfur are ^{34}S depleted relative to seawater (Shanley et al., 1998; Bottrell and Newton, 2006). Thus, non-marine evaporite deposits are commonly characterised by relatively low $\delta^{34}S$ values (e.g., Lu and Meyers, 2003). Dissolved sulfate in non-marine water is primarily derived from weathering of older sulfate and/or sulfide deposits and from precipitation. Thus, the composition of dissolved sulfate in a lake reflects the composition and proportions of weathered sulfur-bearing minerals in the catchment area, atmospheric input (precipitation) and any sources of fractionation that may occur along the way (e.g., sulfate reduction, evaporation, precipitation of sulfate minerals, sulfur uptake by organisms, adsorbtion/desorbtion) (Nriagu et al., 1991). The $\delta^{34}S$ of average rivers today has a composition of +7 ‰ (Nriagu et al., 1991). In areas draining older evaporite deposits river chemistries should mimic the compositions of

seawater sulfate during deposition of the preexisting evaporite deposits and as such should display relatively high $\delta^{34}S$. In areas draining black shales with abundant biogenic pyrite, the composition of river water sulfate will be relatively light because of $\delta^{34}S$ derived from weathering of the ^{34}S depleted pyrite. According to Krouse and Mayer (2000) atmospheric sulfur compositions typically range between $-5\ ^{0}/_{00}$ and +25 ‰. Heavier values reflect marine sources whereas lighter values reflect contributions from biogenic gases (e.g., H_2S) or volcanic emissions (Kendall and Doctor, 2005).

The most important process creating fractionation of sulfur isotopes in lake systems is bacterial sulfate reduction which, if occurring in a lake system where ^{34}S depleted sulfur generated by this process can be removed from the system prior to reoxidation, would create shifts to higher $\delta^{34}S$ values in the water mass. Fractionation can also occur through closed system evaporitic precipitation of gypsum, which (though only to a small degree, 0-2.4 ‰) will preferentially include ^{34}S during crystallization, leaving residual waters depleted in ^{34}S (e.g., Lu and Meyers, 2003).

In the shallow, largely oxidizing, lacustrine depositional system represented by the Sibley Group, the primary controls on the isotopic composition of sulfate minerals precipitated were probably the isotopic composition of sulfur-bearing minerals weathering in the catchment area, the composition of precipitation, and the effects of sulfur reducing bacteria. Physical fractionation effects caused by closed system sulfate precipitation were probably insignificant as closed system precipitation of sulfates (e.g., evaporitic drying of a single closed water body) did not occur. The lack of preservation of chemically reduced lithologies in the Sibley Group, with the exception of the black chert-carbonate lithofacies association, which preserves some pyrite and organic carbon,

may exclude bacterial sulfate reduction as a major control on the sulfur isotope geochemistry of Sibley Group sulfates. However, as Faure and Mensing (2005) noted, reduced sulfur formed through bacterial sulfate reduction can be lost to the atmosphere through degassing even in oxidizing settings. Mixing of water sources of differing chemistry (i.e., lake and seawater) may also have been a control on stratigraphic variations in Sibley Group sulfate compositions.

5.3.3 Strontium

The strontium isotopic composition of the oceans has varied through time because of variations in the input balance between Sr derived from weathering of the continents and Sr derived from the mantle through hydrothermal and seawater interaction with the ocean crust (e.g., Veizer, 2003). Variations between these two fluxes are most likely strongly linked to tectonics with mantle fluxes dominating during periods of time with fast ridge spreading rates and high mid-ocean-ridge volumes. Sr delivered to the ocean through modern ocean floor hydrothermal alteration has a $^{87}Sr/^{86}Sr$ ratio of about 0.703 (e.g., Veizer, 2003) while Sr derived from continental weathering is enriched in ^{87}Sr and has an average value approximated by the modern average river water $^{87}Sr/^{86}Sr$ ratio of about 0.7110 (Wadleigh et al., 1985).

In a lacustrine system $^{87}Sr/^{86}Sr$ will depend primarily on the composition of surface and groundwater input into the basin, which is influenced by the age and Rb/Sr ratio of rocks in the catchment area and the amount of water rock interaction. Thus, lakes in areas underlain by young volcanic terranes should be characterised by low $^{87}Sr/^{86}Sr$ ratios and areas underlain by old cratonic rocks will be characterised by high, radiogenic $^{87}Sr/^{86}Sr$ ratios.

5.3.4 Rare earth elements

Shale normalized REE patterns for a variety of primary chemical sediment types have been used as a proxy for the chemistry of waters from which they have precipitated (e.g. German and Elderfield, 1990; Webb and Kamber, 1999; Picard et al., 2002). Various studies have shown the utility of REE element patterns for chemical sedimentary rocks as indicators of past geochemical conditions including: the paleoredox chemistry of seawater, the identification of distinct water mass, the identification of detrital input to coastal REE budgets, continental erosion, secular variations in ocean chemistry and diagenesis (e.g. Wright et al., 1984, 1987; Elderfield and Pagett, 1986; Grandjean et al., 1987, 1988; Schieber, 1988; Grandjean-Lecuyer et al., 1993; Felitsyn et al., 1998; Kamber and Webb, 2001; Picard et al., 2002).

La, Ce, Eu and Gd contents of marine and estuarine waters vary depending on various factors (e.g., Kamber and Webb, 2004; Shields and Webb, 2004). Ce and Eu abundance are important paleoredox indicators because, unlike other REE's, Ce and Eu can exist in both +3 and +4 oxidation states. La positive anomalies, Gd and Y anomalies, and LREE depleted or HREE enriched PAAS normalized REE patterns are characteristic of the oceans (Nothdurft et al., 2004; Shields and Webb, 2004). Superchondritic (i.e. >~28) Y/Ho ratios, between about 44 and 74, are considered to be a characteristic of seawater (Bau, 1996; Nozaki et al., 1997; Webb and Kamber, 2000) and result from differences in the rates at which the two elements complex on surfaces such as iron oxyhydroxides (e.g., Bau and Dulski, 1999) in seawater. Low Y/Ho ratios in analyses of hydrogenous marine sediments are often used as evidence for contamination by clastic impurities in samples particularly if correlated with elements more commonly associated

with clastic sediments such as Zr (e.g., Webb and Kamber, 2000). However, low Y/Ho ratios are also characteristic of non-marine waters and as such could be used as an indicator of depositional environment. Non-marine waters can have shale normalized compositions indistinguishable from seawater but, also commonly show different fractionation of REE's, particularly middle REE enrichment, which may be related to weathering of phosphate minerals that are typically enriched in MREE's relative to shale (Hannigan and Sholkovitz, 2001). In general, the REE composition of lake-water should reflect the composition of materials that are released during weathering in the catchment.

Relatively few studies were found that documented distribution coefficients between water and precipitating carbonate phases. Studies by Sholkovitz and Shen (1995) and Webb and Kamber (2000) found that the distribution coefficients across the range of REE's were constant between seawater-coral and seawater-microbialite, respectively. Although the distribution coefficient between various different water-types and various carbonate phases likely varies, the important point is that the distribution coefficients of all REE's for a particular carbonate phase are relatively constant and as such the normalized REE pattern should retain a characteristic signature of the water from which it precipitated.

5.3.5 The Mesoproterozoic marine isotopic record of carbon, oxygen, sulfur and strontium

Discriminating between a lacustrine or a marine depositional environment for Sibley Group carbonate and sulfate lithofacies requires an understanding of the constraints on Mesoproterozoic marine chemistry. The history and importance of the Mesoproterozoic evolution of the Earth has received considerable attention in recent

years (e.g., Kah et al., 2001; Anbar and Knoll, 2002; Frank et al., 2003; Arnold et al., 2004). Previously this time interval was little studied relative to the Paleoproterozoic, (e.g. Karhu, 1996) and the Neoproterozoic (e.g., Kaufmann and Knoll, 1995; Kaufmann et al., 1997; Jacobsen and Kaufmann, 1999) and various studies considered the Mesoproterozoic to represent an extended period of very stable chemical and biological conditions (Buick et al., 1995; Brasier and Lindsay, 1998). However, as outlined by Frank et al. (2003), the Mesoproterozoic was important with respect to the changing redox state of the ocean (Des Marais et al., 1992; Canfield and Teske, 1996; Canfield, 1998), the changing carbonate saturation state of the oceans (e.g., Bartley et al. 2000), the diversification eukaryotes, and the evolution of multicellualar organisms (e.g., Knoll, 1992; Butterfield, 2000).

The carbonate $\delta^{13}C$ record of the Mesoproterozoic appears to be separable into two distinct phases (Bartley and Kah, 2004; Frank et al., 2003). From the beginning of the Mesoproterozoic at 1.6 Ga to about 1.3 Ga, $\delta^{13}C$ appears to have remained close to 0 ‰. After 1.3 Ga, $\delta^{13}C$ increased to about +5 ‰ in the early Neoproterozoic (Fig 5.1) (Bartley and Kah, 2004). Early Mesoproterozoic stability in the marine $\delta^{13}C$ record has been interpreted to represent relatively constant rates of organic carbon burial throughout this period (Buick et al., 1995) possibly due to phosphorous limitation of primary productivity in the oceans (Brasier and Lindsay, 1999). Alternatively, Bartley and Kah (2004) proposed that stability in the marine $\delta^{13}C$ record resulted from high levels of dissolved inorganic carbon in the ocean, which effectively buffered against large shifts in the isotope record. The positive shift in marine $\delta^{13}C$ at about 1.3 Ga has been interpreted to represent an increase in the crustal reservoir of organic carbon related to the

diversification of eukaryotes and increased preservation of organic rich shales in anoxic deep marine deposits (Frank et al., 2003).

Recent insights into the Mesoproterozoic marine sulfur record have been gained through analysis of carbonate associated sulfate (CAS) (e.g., Kah et al., 2001; Gellaty and Lyons, 2005; Bottrell and Newton, 2006). Gellaty and Lyons (2005) analysed CAS from the 1.2 Ga Mescal Limestone, Apache Group, Arizona, USA; the 1.45–1.47 Ga Helena and Newland Formations, Belt Supergroup, Montana, USA; and the 1.65 Ga Paradise Creek Formation, McNamara Group, NW Queensland, Australia. Sulfur isotopic compositions ($\delta^{34}S$) in these units were reported to range from +9.1 ‰ to +18.9 ‰, −1.1 ‰ to +27.3 ‰, and +14.1 ‰ to +37.3 ‰, respectively. Wide ranges in $\delta^{34}S$ over relatively small stratigraphic intervals were interpreted to reflect low sulfate concentrations in the Mesoproterozoic ocean. In addition to apparent low sulfate concentrations, it has been proposed that while surface waters were likely oxidized, the remainder of the Mesoproterozoic ocean was largely anoxic and sulfide-rich (e.g. Canfield, 1998; Anbar and Knoll, 2002; Shen et al., 2003; Arnold et al., 2004; Poulton et al., 2004). $\delta^{34}S$ values in pyrites from a number of Mesoproterozoic basins (Shen, et al., 2003; Lyons et al., 2000) are quite high, and similar to inferred compositions of coeval seawater sulfate. This is consistent with low sulfate concentrations in Proterozoic seawater, and pyrite burial as the dominant sulfur removal pathway from the ocean (Canfield, 2004).

For comparison with $\delta^{34}S$ values for Sibley Group sulfate, the most chronostratigraphically equivalent data are probably the CAS analyses of the 1.45-1.47 Ga Helena and Newland Formation carbonates reported by Gellaty and Lyons (2005). As

mentioned above, these stratigraphic units show a range of sulfate $\delta^{34}S$ values of −1.1 ‰ to +27.3 ‰ (Fig. 5.2). However, CAS's associated with this section are probably not the best indicators of changes in marine sulfate compositions as the depositional environments represent a restricted, possibly non-marine setting (Winston, 1990). Data from the Paradise Creek Formation, the Mescal Limestone, the Dismal Lakes Group (~1.3 Ga) (Kah et al., 2004) the Bylot Supergroup (~1.2 Ga) (Kah et al., 2001) are better overall indicators of the composition of marine sulfate during the middle to late Mesoproterozoic. Sulfate $\delta^{34}S$ in these units, in general, ranges between +15‰ and +40‰ and Mesoproterozoic seawater sulfate probably varied within this range. Stratigraphic trends in CAS for the Bylot Supergroup and Dismal Lakes Group are shown in Figure 5.3. A generalized sulfur isotopic composition versus age curve (Fig. 5.4) adapted from Canfield (2004) shows how $\delta^{34}S$ may have varied through geologic time and suggests an average $\delta^{34}S$ composition of about +15 to +20 ‰ during most of the Mesoproterozoic.

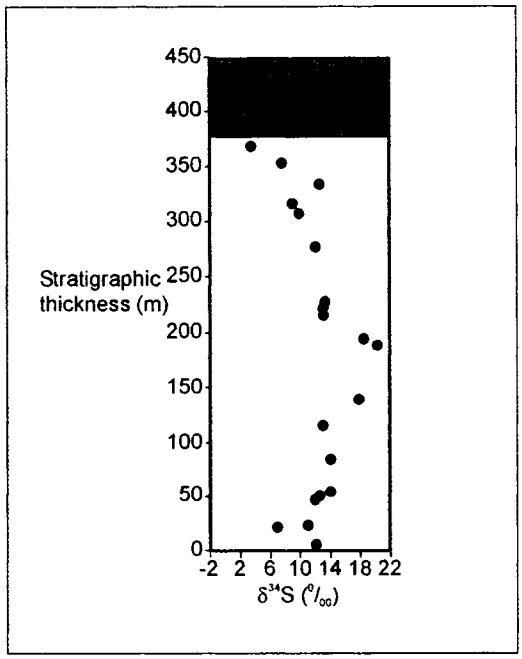

Figure 5.2. Stratigraphic variation in CAS $\delta^{34}S$ through a section of the about 1.45-1.47 Helena Formation, Belt Supergroup, Montana (Modified from Gellaty and Lyons, 2005). Maximum $\delta^{34}S$ values likely reflect the composition of seawater, whereas lower values may be reflecting the influence of non-marine water.

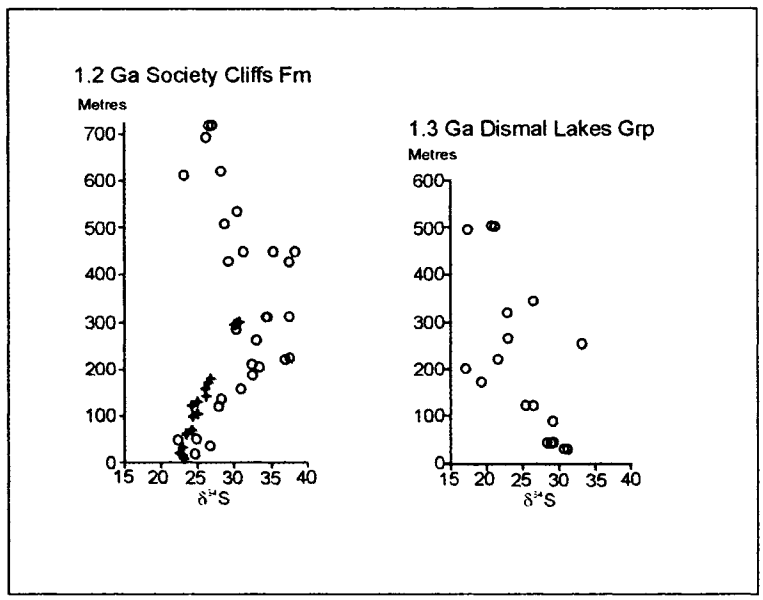

Figure 5.3. Variations in CAS (open circles) and bedded gypsum (black star shapes) $\delta^{34}S$ through the about 1.2 Ga Society Cliffs Formation and 1.3 Ga Dismal Lakes Group (Modified from Kah et al., 2004). Most marine $\delta^{34}S$ values lie between 15 and 40 ‰.

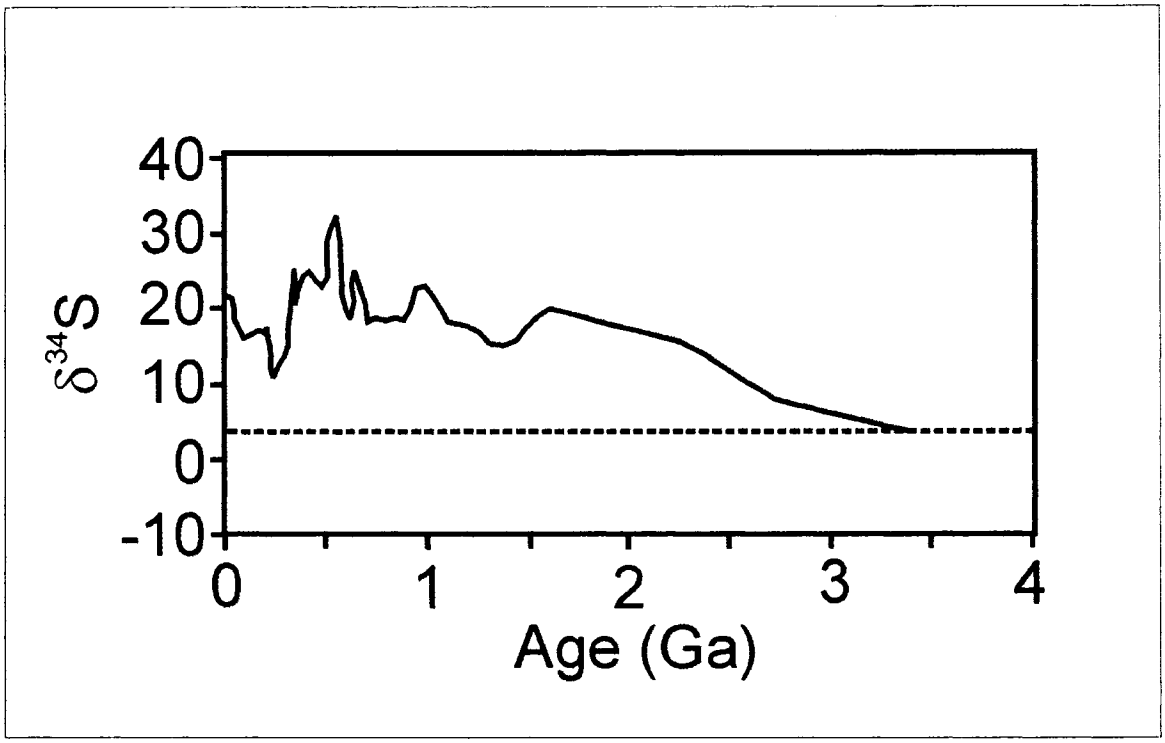

Figure 5.4. A reconstruction of marine sulfate composition through geologic time (Modified from Canfield, 2004). According to this reconstruction marine sulfate compositions during Sibley Group deposition should have ranged between about 15 and 20 ‰.

Mesoproterozoic marine strontium isotopic compositions appear to have ranged between about 0.704 and 0.705 (Fig 5.5; Shields and Veizer, 2002). Using a simple model of fluvial versus mantle fluxes controlling the marine Sr record, the relatively low $^{87}Sr/^{86}Sr$ ratio during the Mesoproterozoic suggests a dominance of mantle flux controlling the Sr isotopic composition of the ocean. For the purposes of this study the primary importance of Figure 5.5 is to provide a value of marine $^{87}Sr/^{86}Sr$ for comparison with Sibley Group data.

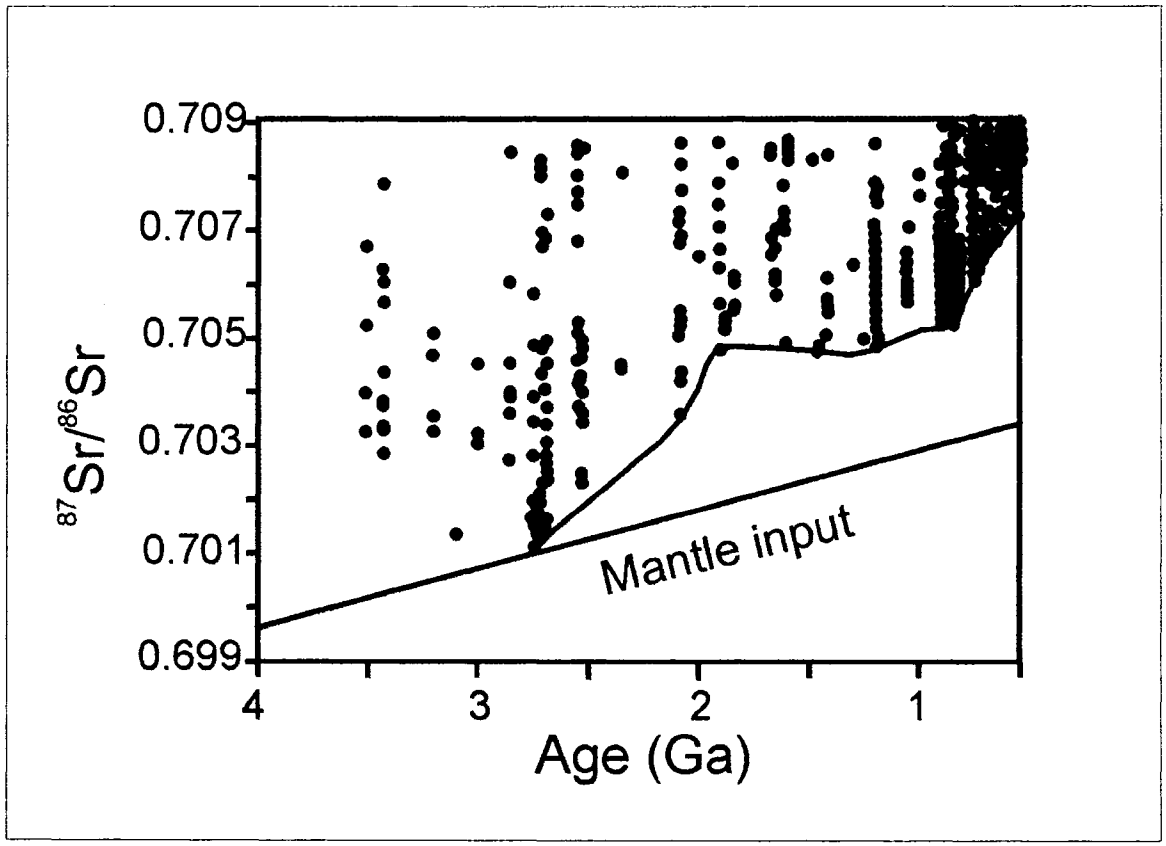

Figure 5.5. Sr isotopic composition of marine carbonates through the Precambrian. The dots represent values from various sedimentary units of the same age. The lower bounding line connects the lowest values for each unit and is interpreted to represent the best estimation of the strontium isotopic composition of the ocean at that particular time. The straight line represents the strontium isotopic evolution of the mantle (modified from Shields and Veizer, 2002 and Ray et al., 2003).

5.3.6. Geochemical indicators of diagenesis

A variety of general geochemical indicators of diagenetic alteration have been proposed to help identify unaltered carbonate compositions. These include elemental ratios such as Mn/Sr, oxygen isotopic composition and strontium isotopic composition. The use of these as diagenetic indicators in carbonate rocks is discussed below.

Low Mn/Sr ratios are often quoted as reflecting a low degree of diagenetic alteration in carbonates (e.g. Derry et al., 1992; Kaufman and Knoll, 1995; Kah et al., 1999). During diagenesis Mn and Fe are incorporated into the carbonate lattice while Sr is commonly removed causing an increase in the Mn/Sr ratio (e.g., Veizer, 1983; Derry et

al., 1992). A variety of empirically determined limits for Mn/Sr ratios in "unaltered" carbonates have been proposed and vary from Mn/Sr <10 (Kaufman and Knoll, 1995) to as low as Mn/Sr < 0.2 (Semikhatov et al., 1998). Use of such ratios for assessing diagenetic alteration is problematic as Melezhik et al. (2001) have pointed out, because Mn/Sr ratios depend not only on diagenetic alteration, but also the original carbonate composition. This is particularly important with regard to this study as the depositional environment of Sibley Group carbonates was most likely non-marine and as such the primary concentrations of Mn and Sr in carbonate mineralizing waters may have differed considerably from marine values. In particular, carbonates interpreted to be pedogenic and stromatolitic carbonates from highly saline depositional settings may have precipitated from waters that differed from typical marine chemistries (e.g. Calvo et al. 1995). Further, a single set of criteria cannot be applied in all cases as the composition of diagenetic phases depends not only on the original composition of primary carbonate phases but also the composition of diagenetic waters and the difference between them (e.g. Bartley et al., 2001). Mineralogy is also a factor in controlling Mn/Sr as the Sr content of dolomite is lower than that of calcite because of inherent differences in the structure of dolomite that excludes Sr from its lattice during crystallization. This exclusion of Sr from dolomite leads to higher Mn/Sr ratios in dolomite relative to calcite.

Oxygen isotopic compositions are also commonly used as an indicator of diagenetic alteration as they are much more susceptible to alteration than carbon isotopic compositions because of the relatively higher proportions of oxygen relative to carbon in diagenetic fluids. Carbonates effected by meteoric diagenesis usually have lower $\delta^{18}O$ relative to primary carbonate compositions as oxygen in meteoric waters is depleted in

^{18}O relative to seawater (e.g., Veizer, 2003; Frank and Lyons, 2000; Jacobsen and Kaufmann, 1999). Carbonates effected by burial diagenesis show a similar ^{18}O depleted nature because of equilibration of carbonate minerals at high temperatures (e.g., Lohmann, 1988; Kah et al., 1999). Knoll et al. (1995) proposed an empirical guideline of −10 ‰ or lower as indicating diagenetic alteration in Proterozoic carbonates.

Strontium is a trace element in carbonates and as such, carbonate Sr isotopic compositions are easily altered during meteoric and burial diagenesis. In situ addition of radiogeneic Sr by decay of Rb in clays or other siliclastic impurities may also alter the $^{87}Sr/^{86}Sr$ ratio in carbonates. In general, Sr isotopic compositions of meteoric waters will be radiogenic (i.e., ^{87}Sr enriched) relative to seawater as most meteoric waters are derived from weathering of old, Rb-rich (^{87}Sr rich) continental rocks. Hence diagenetic phases are often enriched in ^{87}Sr. However, primary carbonates precipitated from non-marine waters may also have high $^{87}Sr/^{86}Sr$ ratios.

For sulfate minerals comparatively little information about diagenetic effects on gypsum/anhydrite chemistry was found in the literature. During burial most sulfate in the Sibley Group was likely anhydrite, however, subsequent rehydration to gypsum probably occurred in many cases. Dissolution/reprecipitation, partial bacterial sulfate reduction or exchange with basinal waters can alter sulfur isotopic compositions (e.g. Claypool, 1980). During sampling areas with obvious vein-like features were avoided and for the most part, discrete nodules were sampled. These samples were considered to have acted as a closed system with respect to sulfur during burial and diagenesis.

5.4 Results

5.4.1 Samples of the Lower Clastic Unit

Five samples of carbonate, three from the calcrete lithofacies in the boulder conglomerate/sandstone/calcrete lithofacies association and two from carbonate associated with the basal Sibley Group-Archean contact south of Beardmore (Fig. 1.2) were analyzed from this stratigraphic interval. Appendix 1 contains all geochemical and isotopic data for these samples.

Carbon isotopic compositions for dolocretes in the lower clastic unit vary from –1.1 to –1.5 $^{0}/_{00}$. Oxygen isotopic compositions for samples from the West Loon locality (Fig 1.2) range from –2.4 to –3.6 $^{0}/_{00}$ whereas samples from south of Beardmore (Fig. 1.2) are considerably lower at –15.7 and –16.4 $^{0}/_{00}$. $^{87}Sr/^{86}Sr$ values for 2 dolocrete samples from West Loon are 0.70478 and 0.70428. Mn/Sr ratios for this unit are relatively high and range from about 25-50. Post Archean Australian Shale (PAAS, Table 5.2, values from Taylor and McLennan, 1985) normalized rare earth element patterns for acetic acid soluable portions of two dolocrete samples from the West Loon locality are characterized by distinct negative Ce anomalies and slight middle rare earth element enrichment (MREE) (Figs. 5.6, 5.14). Y/Ho ratios have an average value 36.6.

Table 5.2. REE composition of the standard Post Archean Australian Shale (PAAS), values are in ppm (from Taylor and McLennan, 1985).

	PAAS
La	38
Ce	80
Pr	8.9
Nd	32
Sm	5.6
Eu	1.1
Tb	0.77
Gd	4.7
Dy	4.4
Ho	1.0
Er	2.9
Tm	0.4
Yb	2.8
Lu	0.43

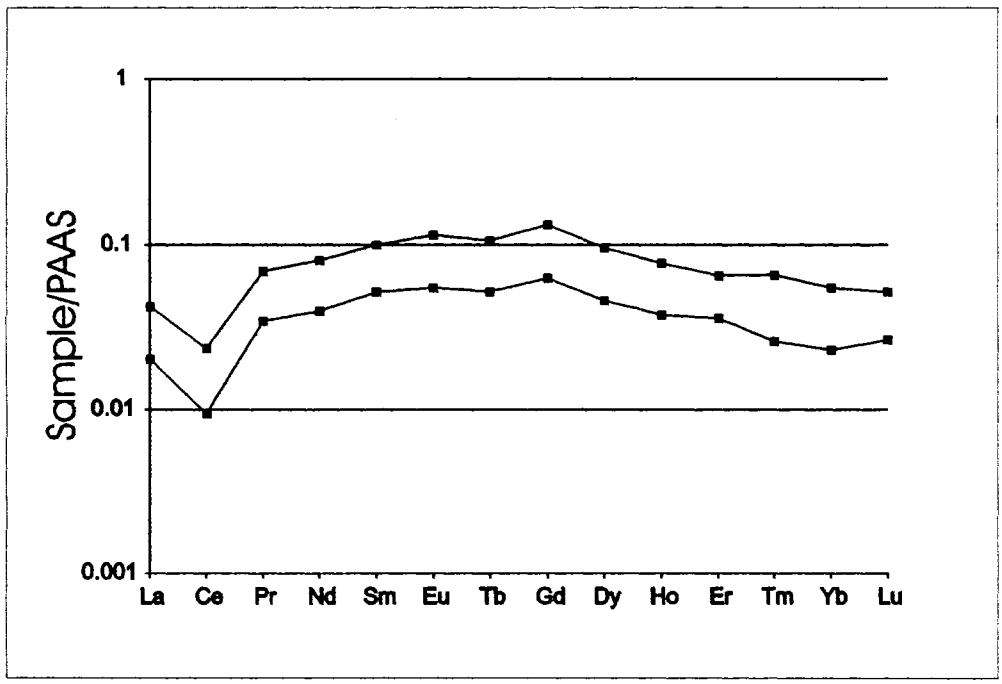

Figure 5.6. Post Archean Australian Shale normalized rare earth element compositions of two dolocrete samples from the West Loon Lake locality.

5.4.2 Samples of the mixed siliciclastic-carbonate unit

Fifty carbonate samples comprised of a mixture of dolostone and red dolomitic siltstone from the red siltstone-dolostone lithofacies association were collected from this stratigraphic unit. In addition, 10 fine-grained nodular sulfate samples from the red siltstone-dolomite lithofacies association were collected. All geochemical data for carbonate samples from this interval are shown in Appendix 2. Sulfate data is found in Appendix 6.

$\delta^{13}C$ values from this stratigraphic interval range from –3.1 ‰ to 0.8 ‰ and $\delta^{18}O$ values range from –8.4 to –4.4 ‰. $^{87}Sr/^{86}Sr$ ratios for three dolostone samples from the red siltstone-dolostone lithofacies association are 0.70646, 0.70704 and 0.70829, respectively. Mn/Sr ratios for this unit are lower than elsewhere in the Sibley Group and are generally less than 10.

Dolostone $\delta^{13}C$, and to some extent $\delta^{18}O$, appears to vary with stratigraphic height in the red siltstone-dolostone lithofacies association. Figures 5.7 and 5.8 show plots of $\delta^{13}C$ and $\delta^{18}O$ versus height for sections of the red siltstone-dolostone lithofacies association in cored drill holes NB-97-4 and NI-92-7 respectively. Figures 5.7 and 5.8 show a strong relationship between increasing stratigraphic height within the sections and increasing $\delta^{13}C$. Although more scattered, there is a similar increase in $\delta^{18}O$. $\delta^{13}C$ values increase uniformly upward through the sections from values as low as –3.1 ‰ at the base to as high as 0.8 ‰ at the top of the association in NI-92-7. Similarly, $\delta^{18}O$ is isotopically light in the basal portions of the section and becomes heavier upwards from minimum values of about –8 ‰ at the base to maximum values of about –4 ‰ at the top. This approximately 4 ‰ shift in both carbon and oxygen isotopic

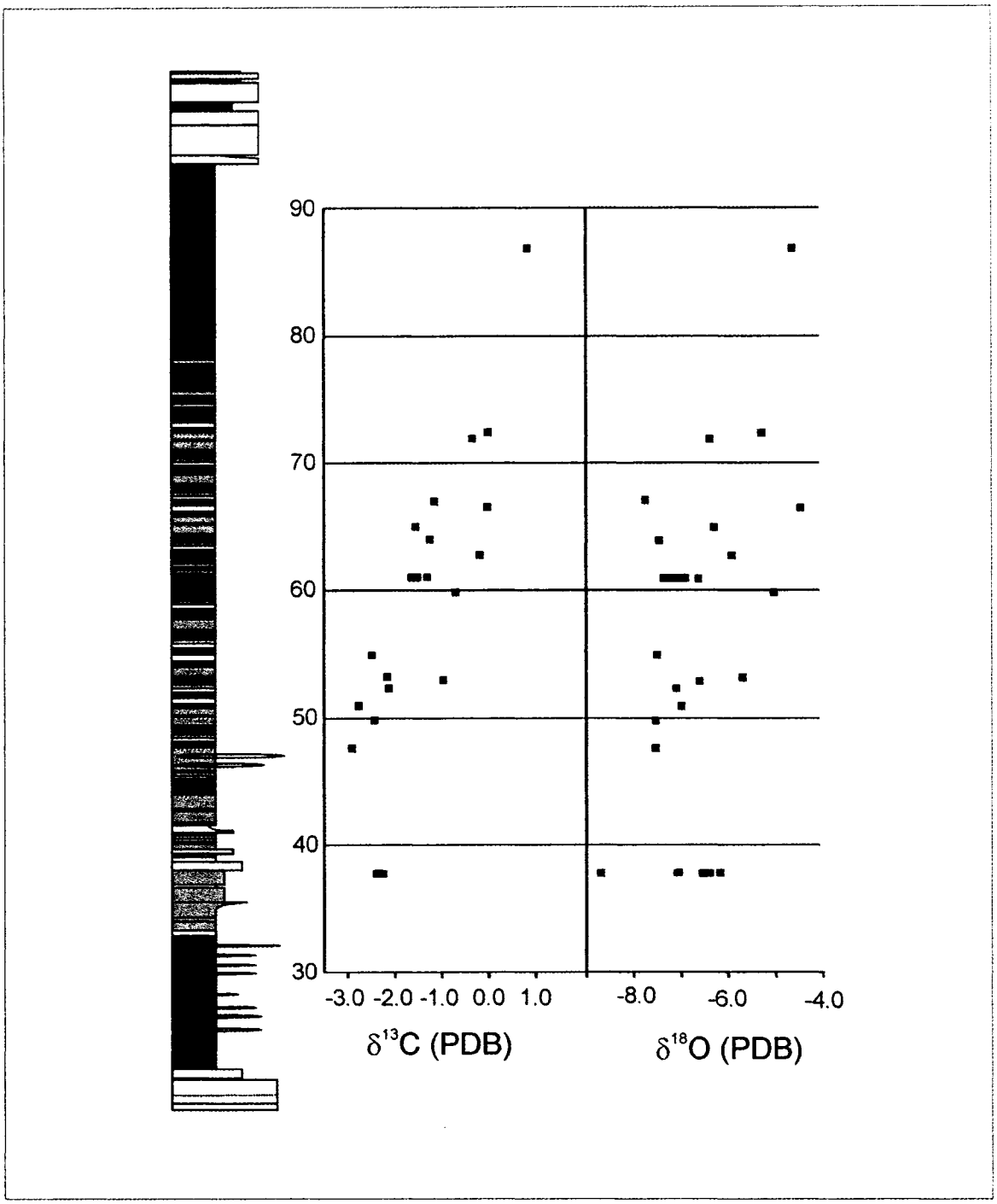

Figure 5.7. Stratigraphic variations in carbon and oxygen isotopic composition for dolostone samples from the red siltstone-dolostone lithofacies association in cored drill hole NI-92-7. Stratigraphic height is in metres above the Sibley Group-basement contact. The stratigraphic column on the left has a horizontal scale which represents grainsize and varies from mudstone to coarse-grained sandstone. Colours on the stratigraphic column represent compositional variations. White indicates siliciclastic dominated sandstone. Red indicates siliciclastic dominated siltstone. Yellow indicates dolostone. Pink indicates a more carbonate-rich siliciclastic dominated composition.

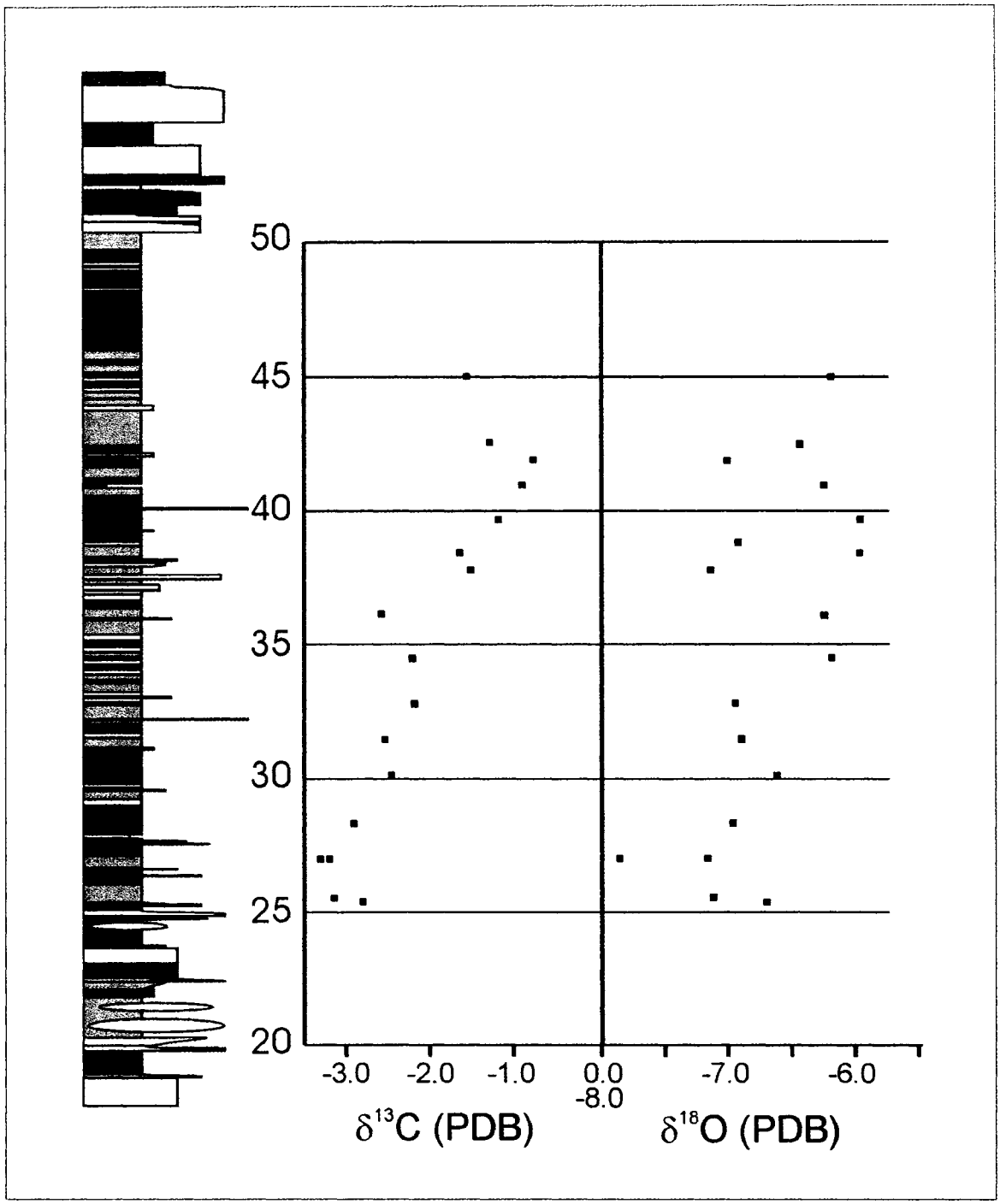

Figure 5.8. Stratigraphic variation in carbon and oxygen isotopic composition for dolostone samples from the red siltstone-dolostone lithofacies association in cored drill hole NB-97-4. Stratigraphic height is in metres above the Sibley Group-basement contact. The stratigraphic column on the left has a horizontal scale which represents grainsize and varies from mudstone to coarse-grained sandstone. Colours on the stratigraphic column represent compositional variations. White indicates siliciclastic dominated sandstone. Red indicates siliciclastic dominated siltstone. Yellow indicates dolostone. Pink indicates a more carbonate-rich siliciclastic dominated composition.

composition occurs over a stratigraphic interval of about 40-50 m. The shorter section in NB-97-4 does not reach as heavy isotope enriched compositions as the longer NI-92-7 section. If the upward shifts in isotopic composition are used as a chronostratigraphic correlation tool, this suggests that clastic influx represented by the sheet sandstone lithofacies association reached the more southerly portions of the study area prior to the more northerly NI-92-7 drill core. This is consistent with the shift in paleocurrent patterns discussed in chapter 3.

Sulfates from this stratigraphic interval have $\delta^{34}S$ values that range from 4.5 ‰ to 11.9 ‰ (Fig 5.9). Most values are between 4 ‰ and 6 ‰, but there is a shift to heavier isotopic compositions (to ca.12 $^{0}/_{00}$) upward (Fig. 5.9). $^{87}Sr/^{86}Sr$ ratios for sulfate samples are typically higher than values from carbonates and range from 0.70852 to 0.71090 and the lowest sulfate $^{87}Sr/^{86}Sr$ (0.70852) is higher than the highest value determined for carbonates from this stratigraphic interval (0.70829) (Fig. 5.10). $^{87}Sr/^{86}Sr$ for sulfates appears to increase upward through the red siltstone-dolostone lithofacies association (Fig. 5.9).

PAAS normalized REE compositions of acetic acid soluble portions of selected carbonate samples from this unit are shown in Figure 5.11. Buff coloured, unoxidized dolostone and red oxidized dolostone/red siltstone are both characterised by MREE enrichment and a lack of distinct elemental anomalies. Contrary to other carbonate lithofacies, positive La or negative Ce anomalies are generally absent (Fig. 5.14). Y/Ho ratios are similar to chondrite and range from about 22 to 29.

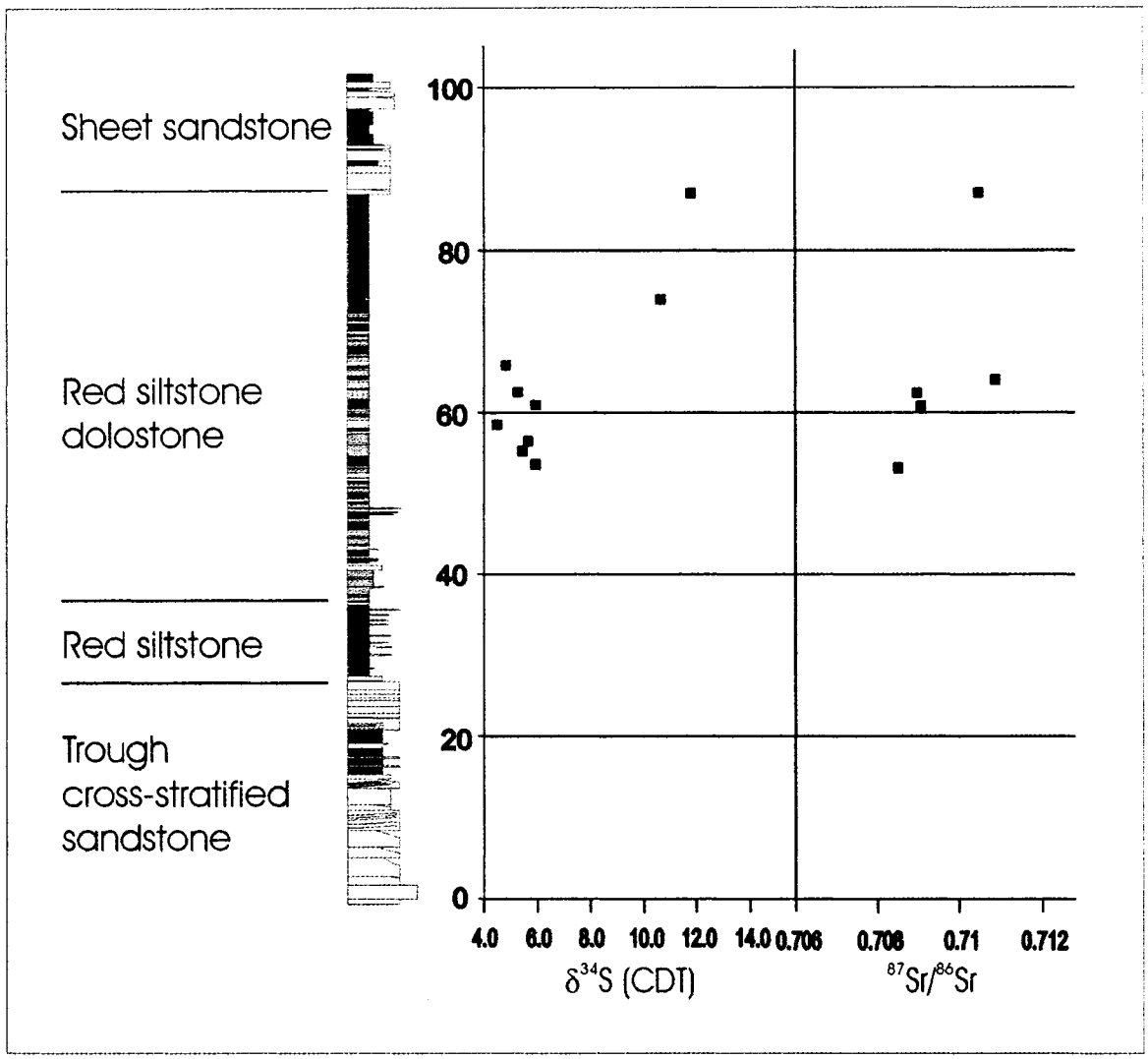

Figure 5.9. Stratigraphic variation in sulfur and strontium isotopic composition for sulfate samples from cored drill hole NI-92-7. Stratigraphic height is in metres above the Sibley Group-basement contact. The stratigraphic column on the left shows a section from Archean basement to the Sheet sandstone lithofacies association The stratigraphic column has a horizontal scale which represents grainsize and varies from mudstone to coarse-grained sandstone. Colours on the stratigraphic column represent compositional variations. White indicates siliciclastic dominated sandstone. Red indicates siliciclastic dominated siltstone. Yellow indicates dolostone. Pink indicates a more carbonate-rich siliciclastic dominated composition.

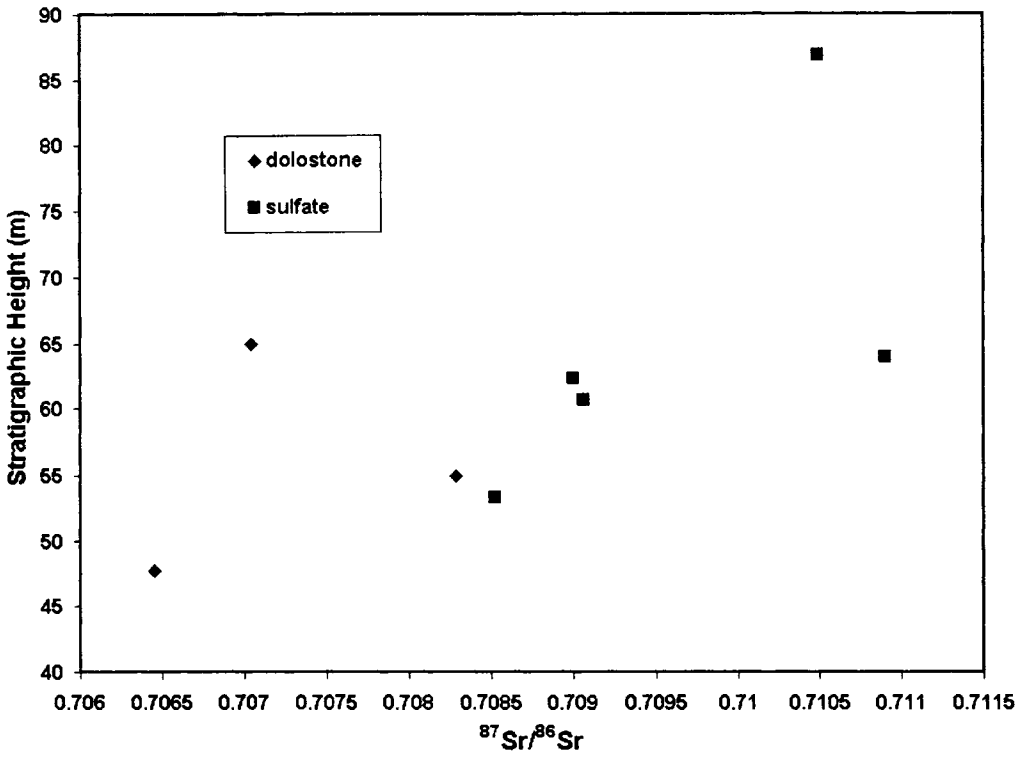

Figure 5.10. Comparison of $^{87}Sr/^{86}Sr$ ratios between dolostones and sulfate nodules from the red siltstone-dolostone lithofacies association (DDH NI-97-2). Sulfate nodules, represented by square symbols, have higher ratios than dolostones at similar stratigraphic levels.

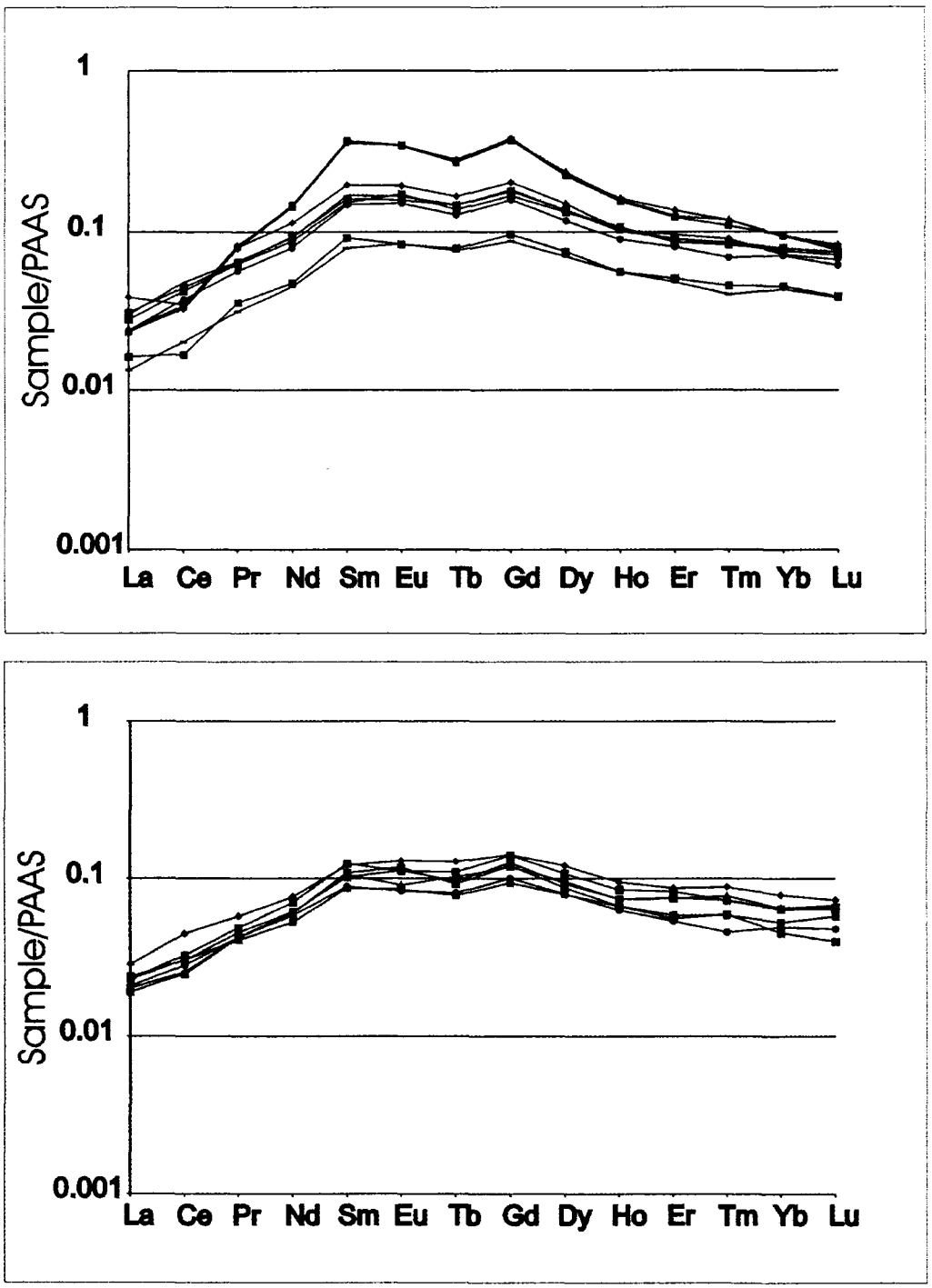

Figure 5.11. Post Archean Australian Shale normalized rare earth element diagrams for dolostone samples from the mixed carbonate siliclastic unit. The upper diagram shows buff coloured, unoxidized dolostone samples from the red siltstone-dolostone lithofacies association, the lower diagram shows red dolostone/ siltstone samples from the red siltstone-dolostone lithofacies association.

5.4.3 Samples of the upper siliciclastic unit

Six samples of micritic carbonate from the black chert-carbonate lithofacies association, three whole rock samples of pedogenic (?) carbonate from the altered top of the black-chert carbonate lithofacies association and four samples of carbonate from overlying intraformational conglomerate were analyzed from the upper siliciclastic unit. Appendix 3 contains geochemical data for this unit.

Carbonate carbon isotopic compositions from this stratigraphic unit vary from –1.5 ‰ to 1.3 ‰ and oxygen isotopic compositions range from –14.7 ‰ to –2.8 ‰. Four analyses of stromatolitic carbonate from the black chert carbonate lithofacies association yielded $^{87}Sr/^{86}Sr$ ratios of 0.71231, 0.71160, 0.70939 and 0.70815, respectively. Mn/Sr ratios in this unit are typically slightly higher than in the red siltstone-dolostone lithofacies association and range from 9 to 37. REE compositions were determined for acetic acid soluable portions of three stromatolitic carbonates from the black chert-carbonate lithofacies association and three samples from the intraformational conglomerate lithofacies association. PAAS normalized rare earth element patterns for these samples are shown in Figures 5.12 and 5.13. REE patterns for stromatolitic samples (Fig. 5.12) show a distinct negative Ce anomaly, a relatively flat light rare earth element (LREE) slope and a negative heavy rare earth element (HREE) slope. Two of the samples also show a slight positive Gd anomaly. Y/Ho ratios for these samples lie between 33 and 36. Intraformational conglomerate samples (Fig. 5.13) are similar but show a flatter HREE slope. Y/Ho for the intraformational conglomerate samples range between 28 and 37.

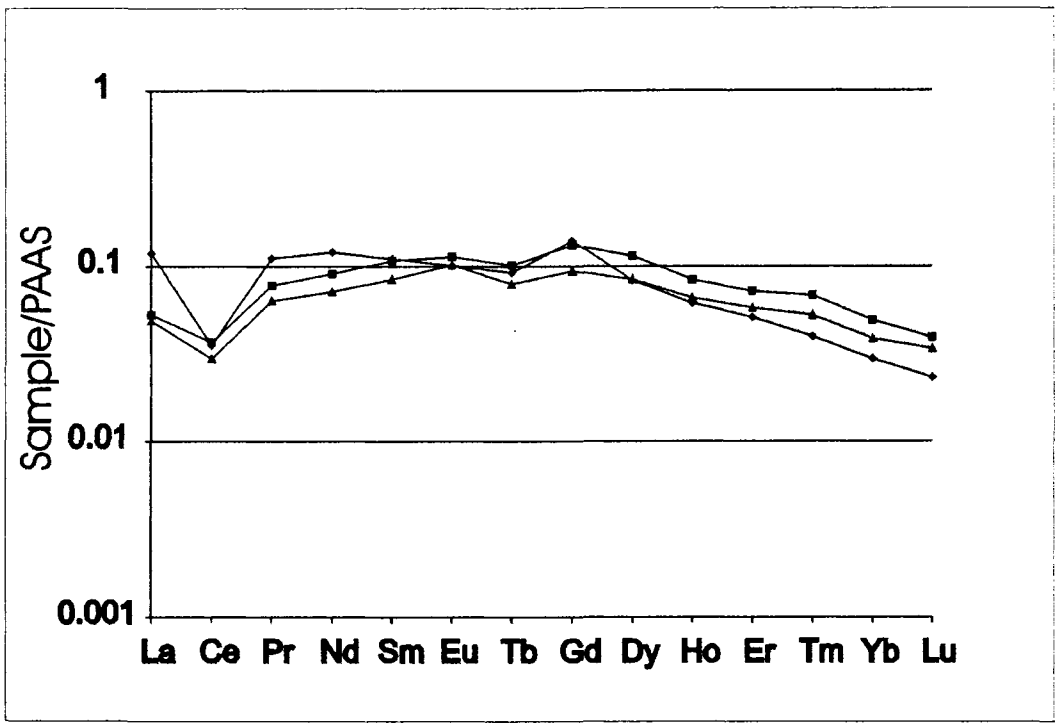

Figure 5.12. PAAS normalized rare earth element diagrams for three stromatolitic carbonate samples from the black chert-carbonate lithofacies association

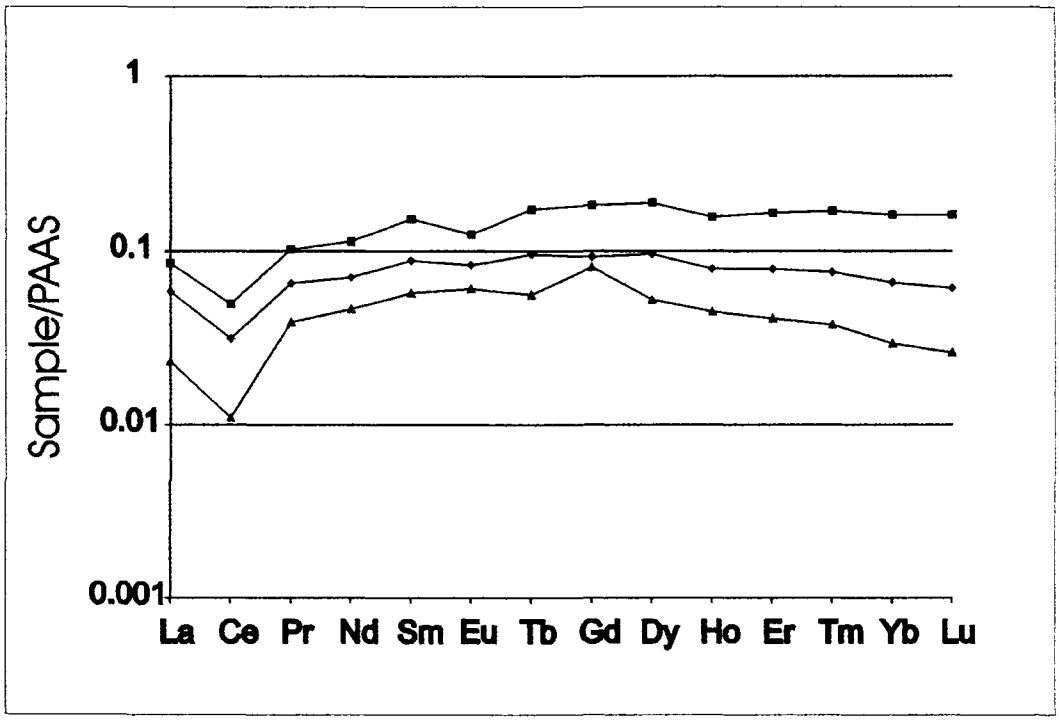

Figure 5.13. PAAS normalized rare earth element diagrams for three samples from the intraformational conglomerate lithofacies association.

5.4.4 Samples of the upper mixed carbonate-siliciclastic-sulfate unit

Two samples from the massive dolostone lithofacies association, one sample of fine-grained pervasive carbonate alteration from the red siltstone-sulfate association, one sample of a green dolocrete nodule from the red siltstone-fine grained sandstone association and seven samples of stromatolitic carbonate were collected from the upper mixed carbonate-siliciclastic-sulfate unit. In addition, 14 nodular gypsum/anhydrite samples were analysed to determine their sulphur and strontium isotopic compositions and also trace element geochemistries. Geochemical data for these samples are presented in appendix 4.

Stromatolitic carbonates from this interval have quite uniform carbon isotopic compositions and $\delta^{13}C$ varies from 1.3 to 1.5 ‰. $\delta^{18}O$ for the stromatolitic samples ranges between –6.0 and –3.5 ‰. The sample of a green dolocrete nodule has a $\delta^{13}C$ value of 0.1 ‰ and a $\delta^{18}O$ of –7.9 ‰. A whole rock sample of red shale with pervasive carbonate alteration from the red siltstone-sulfate lithofacies assoiciation has a $\delta^{13}C$ value of –0.7 ‰ and $\delta^{18}O$ of –15.1 ‰. Two massive dolostone samples have $\delta^{13}C$ values of 1.2 and –1.4 ‰ and $\delta^{18}O$ values of -5.3 and -4.5 ‰ respectively. Two analyses, one stromatolite and one massive dolostone have $^{87}Sr/^{86}Sr$ values that are relatively low at 0.70703, the dolocrete nodule, however, shows a much more radiogenic value of 0.71252. REE geochemistries of two samples from this unit are shown in Figure 5.15. The sample of a dolocrete nodule is characterised by MREE enrichment with no La or Ce anomaly. The stromatolite sample has a negative Ce anomaly, a positive La anomaly (Fig 5.14), slight MREE enrichment and a negative HREE slope. Y/Ho is about 35 for the stromatolite sample and 17 for the dolocrete sample.

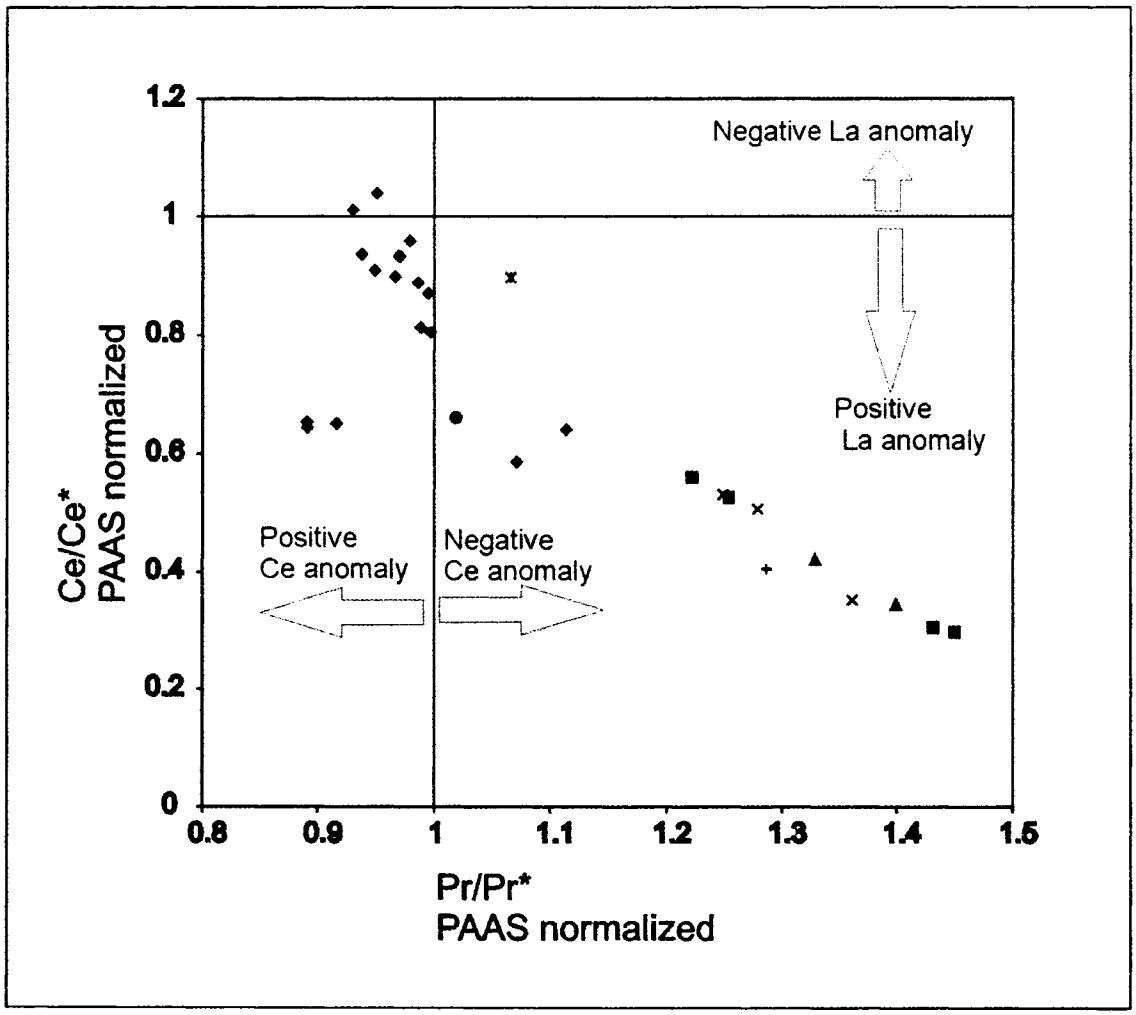

Figure 5.14. A plot of shale normalized Ce/Ce* vs Pr/Pr* designed to descriminate between Ce and La anomalies in PAAS shale normalized samples (Bau and Dulski, 1996). Samples with Ce/Ce* greater than 1 have a negative La anomaly and samples with Ce/Ce* less than 1 have a positive La anomaly. Similarly, samples with Pr/Pr* greater than 1 have a negative Ce anomaly and samples with Pr/Pr* less than 1 have a positive Ce anomaly. Triangles represent dolocrete samples from the boulder conglomerate-sandstone-dolocrete lithofacies association. Diamonds represent samples of dolostone from the red siltstone-dolostone lithofacies association. Squares are stromatolitic carbonates from the black chert-carbonate lithofacies association. "x" 's represent samples from the intraformational conglomerate unit. The single star symbol represents a sample from the weathered top of the black chert-carbonate lithofacies association. The single "+" symbol is a stromatolitic carbonate sample from the upper stratigraphic unit. The single circle symbol is pedogenic carbonate from the upper stratigraphic unit.

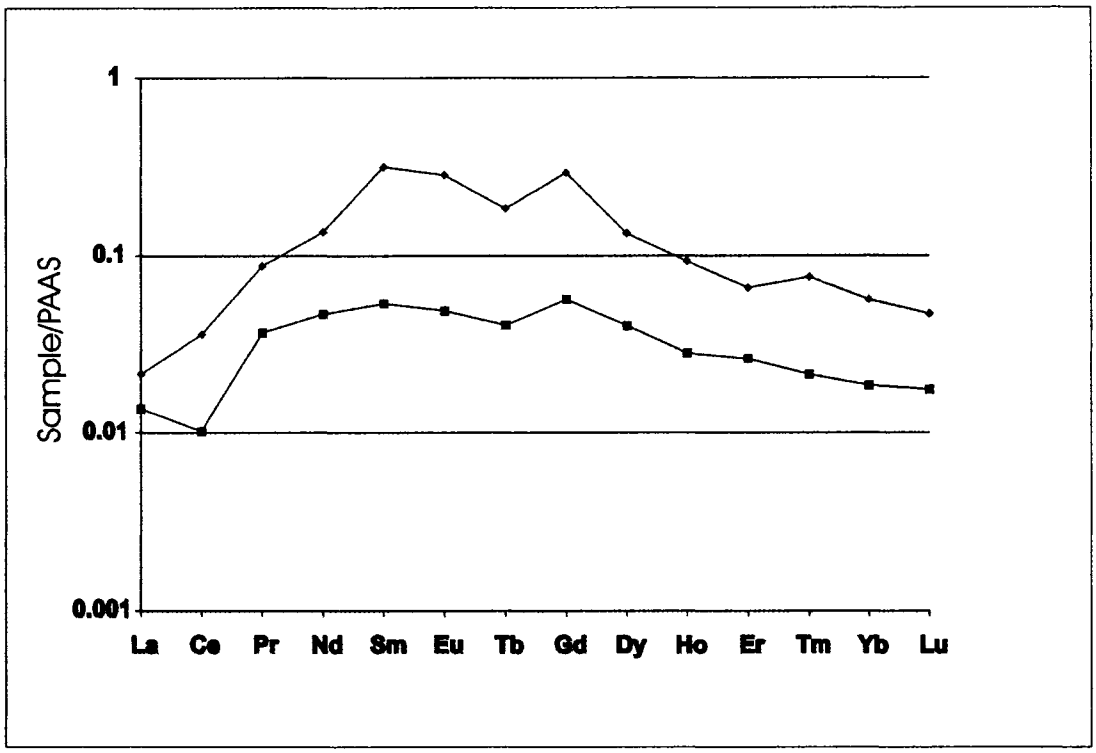

Figure 5.15. REE compositions of two samples from the upper mixed siliclastic-carbonate-evaporite unit. The upper line represents a dolocrete nodule contained within red siltstone. The lower line represents a stromatolitic carbonate sample.

Sulfates from this unit have $\delta^{34}S$ values that range from about 9 to 12 ‰. Sr isotopic compositions range from 0.70647 to 0.70884. Stratigraphic variation in both $\delta^{34}S$ and $^{87}Sr/^{86}Sr$ for samples from NI-92-7 are shown in Figure 5.16. $\delta^{34}S$ near the base of the unit in NI-92-7 is about 12 ‰, near the middle $\delta^{34}S$ is about 9 ‰ and near the top $\delta^{34}S$ is about 11 ‰. Thus, there is some small-scale variation in $\delta^{34}S$ through the section. Insufficient Sr data exists to delineate stratigraphic variations in $^{87}Sr/^{86}Sr$. However, plotting of $^{87}Sr/^{86}Sr$ versus $\delta^{34}S$ for all sulfate nodules for this unit shows a fairly good correlation between high $^{87}Sr/^{86}Sr$ and high $\delta^{34}S$ (Fig. 5.17).

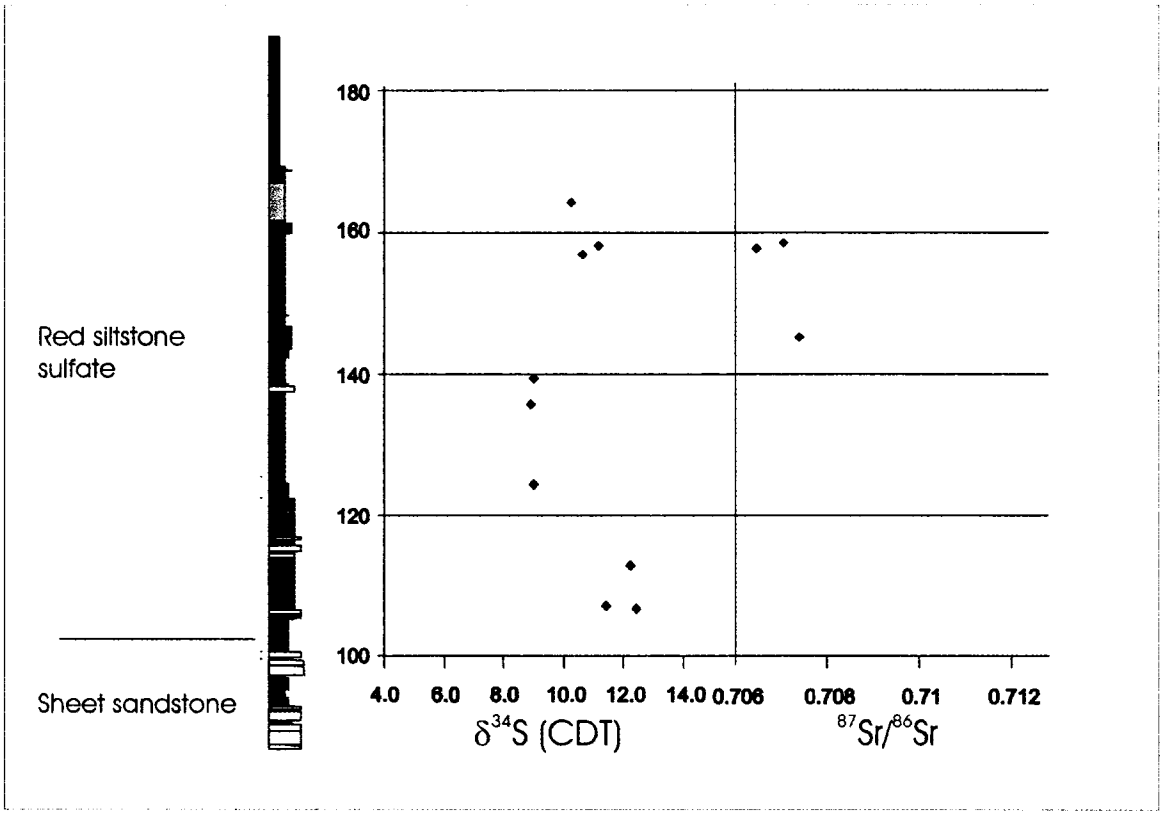

Figure 5.16. Sulfur and strontium isotopic compositions of nodular Ca-sulfates from the red siltstone sulfate lithofacies association in DDH NI-92-7. Stratigraphic height is in metres above the Sibley Group-basement contact. The stratigraphic column on the left shows a section from the Sheet sandstone lithofacies association to the base of the Kama Hill Formation. The stratigraphic column has a horizontal scale which represents grainsize and varies from mudstone to coarse-grained sandstone. Colours on the stratigraphic column represent compositional variations. White indicates siliciclastic dominated sandstone. Red and purple indicates siliciclastic dominated siltstone and mudstone. Yellow and brown units contain detrital sulfate grains. The grey unit just above 160 m is a stromatolitic carbonate with abundant sulfate nodules.

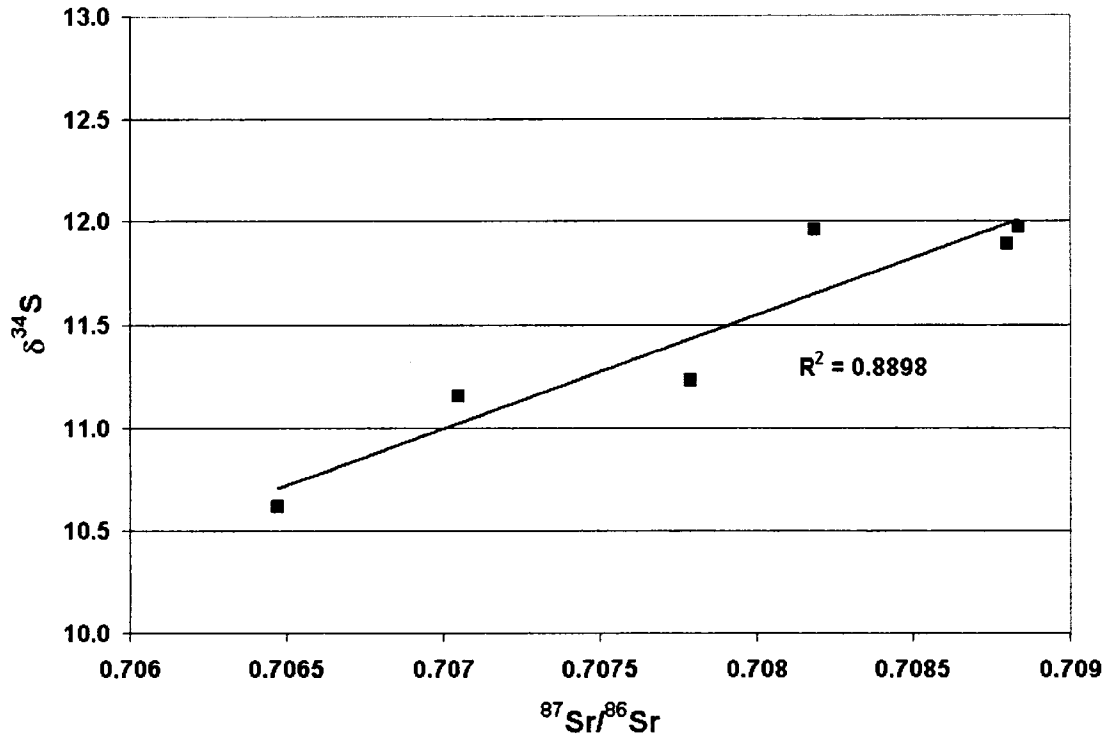

Figure 5.17. Plot of $\delta^{34}S$ versus $^{87}Sr/^{86}Sr$ for all sulfate samples from the red siltstone-sulfate lithofacies association

5.4.5 Summary of stratigraphic geochemical and isotopic variation

The following series of diagrams summarizes the geochemical data collected for this study. Figures 5.18 to 5.23 summarize stratigraphic variations in $\delta^{13}C$, $\delta^{18}O$, PAAS shale normalized REE composition, Y/Ho ratios, $^{87}Sr/^{86}Sr$ and $\delta^{34}S$, respectively. For the purposes of the interpretive discussion these are the main pieces of evidence used to discern a lake vs shallow marine depositional environment for the portions of the Sibley Group studied.

Figure 5.18 shows stratigraphic variations in $\delta^{13}C$. Dolocretes in the basal siliciclastic unit have $\delta^{13}C$ values that range from –1.0 to –1.5 ‰. $\delta^{13}C$ falls to about -3 ‰ in the lower portions of the mixed siliciclastic carbonate unit and then increases to about 1 ‰ at its top. In the upper siliciclastic unit and mixed siliciclastic-carbonate-

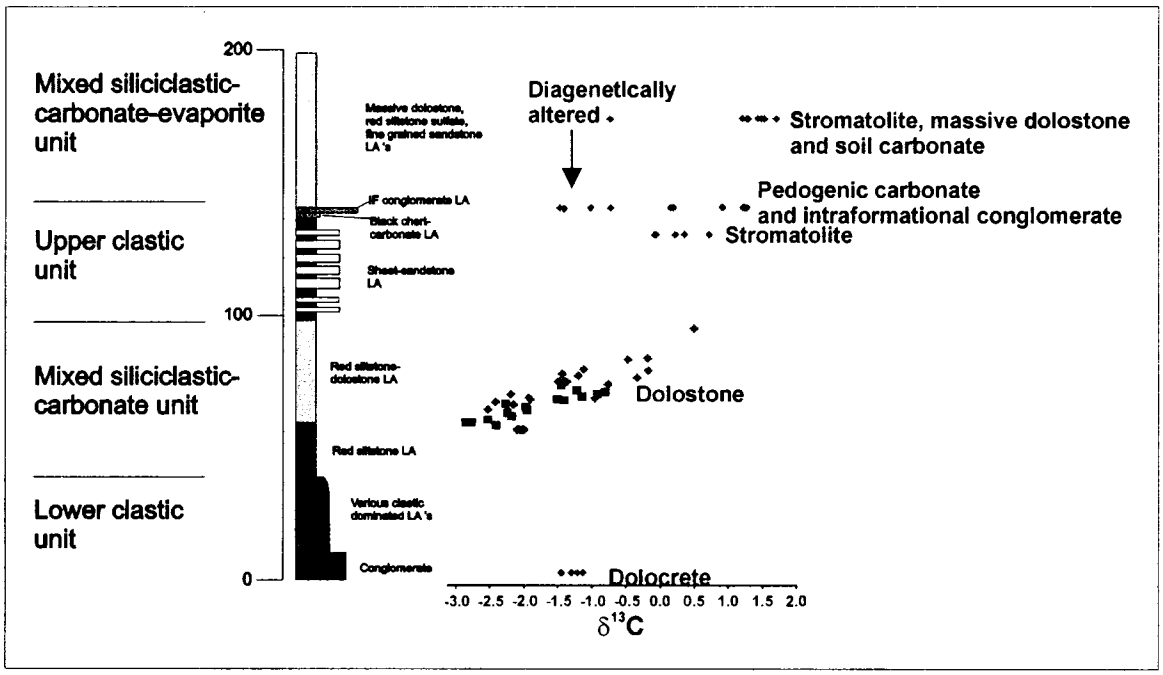

Figure 5.18. Summary of stratigraphic variations in carbonate $\delta^{13}C$. The stratigraphic column on the left shows idealized thicknesses of stratigraphic units as well as the relative positions and thicknesses of various lithofacies associations. The ranges in observed values for each sampled stratigraphic unit or lithofacies association are shown. For the red siltstone-dolostone lithofacies association the stratigraphic trends for the two sampled drill holes are shown (the blue colour is NI-92-7 and the pink is NB-97-4).

evaporite unit $\delta^{13}C$ varies with carbonate lithofacies and stromatolitic carbonates have high $\delta^{13}C$ while pedogenic carbonates have slightly lower $\delta^{13}C$. Figure 5.19 shows stratigraphic variations in $\delta^{18}O$. For the most part, variations in $\delta^{18}O$ are similar to those in $\delta^{13}C$. However, numerous $\delta^{18}O$ values are quite negative. These likely reflect alteration.

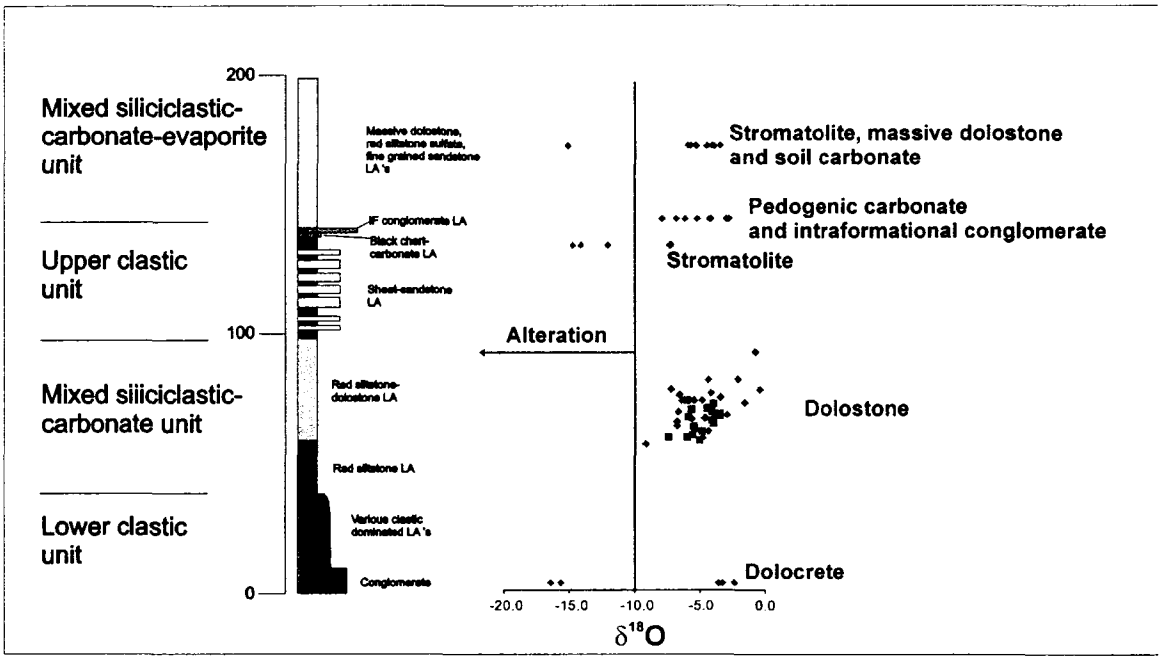

Figure 5.19. Summary of stratigraphic variations in $\delta^{18}O$. Values falling to the left of the vertical line set at $-10\ ^{0}/_{00}$ are likely reflecting diagenetic alteration. The stratigraphic column on the left shows idealized thicknesses of stratigraphic units as well as the relative positions and thicknesses of various lithofacies associations. The ranges in observed values for each sampled stratigraphic unit or lithofacies association are shown. For the red siltstone-dolostone lithofacies association the stratigraphic trends for the two sampled drill holes are shown (the blue colour is NI-92-7 and the pink is NB-97-4).

Figure 5.20 illustrates PAAS normalized REE patterns for each stratigraphic unit. Samples from both the upper and lower siliciclastic units are characterised by negative Ce anomalies. Negative Ce anomalies are distinctly absent from the majority of samples from the mixed siliciclastic-carbonate and mixed siliciclastic-carbonate-sulfate units. Also, the mixed siliciclastic-carbonate and mixed siliciclastic-carbonate-sulfate units appear to have more distinct MREE enrichments. Figure 2.1 shows variations in Y/Ho ratio between stratigraphic units. Values for all units are lower than those expected for seawater. Average Y/Ho ratios are lowest in the mixed siliciclastic carbonate unit as compared to the lower and upper clastic units.

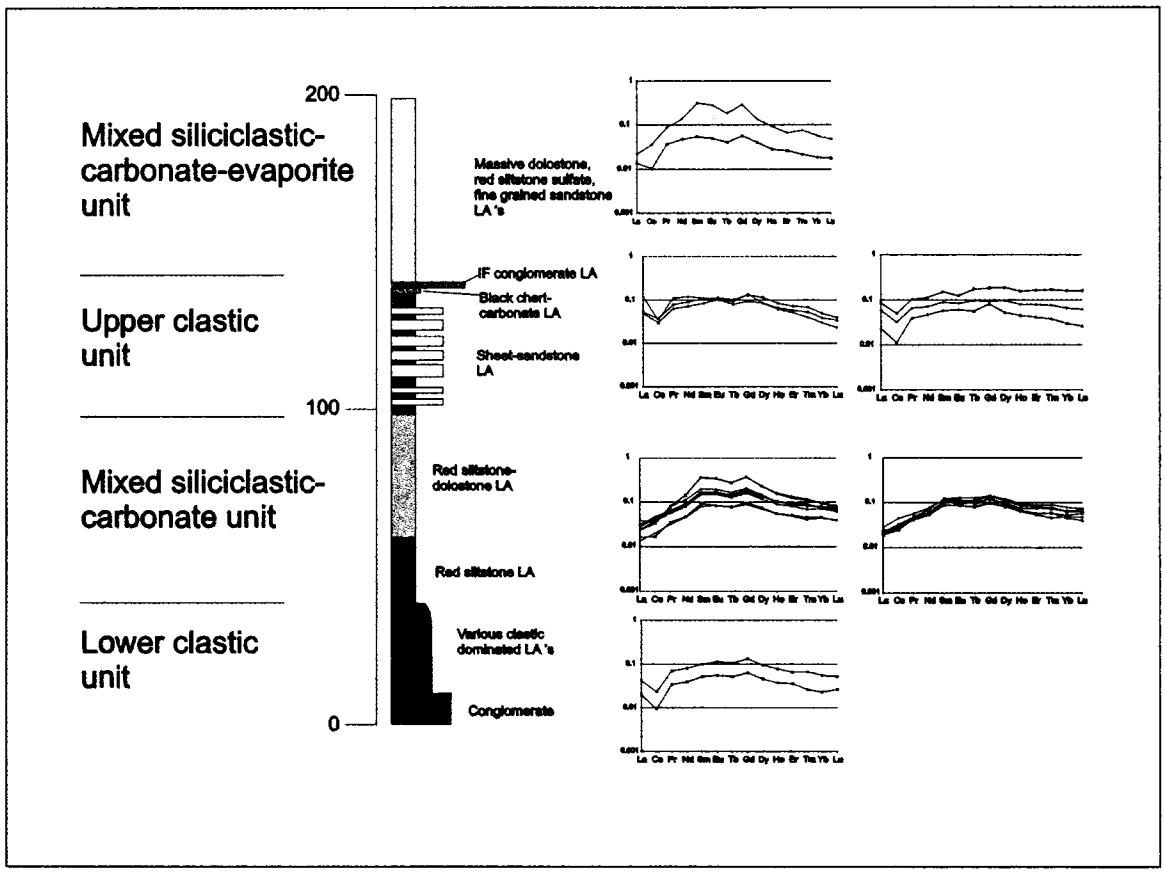

Figure 5.20 Stratigraphic and lithofacies dependent variations in REE geochemistry through the Sibley Group.

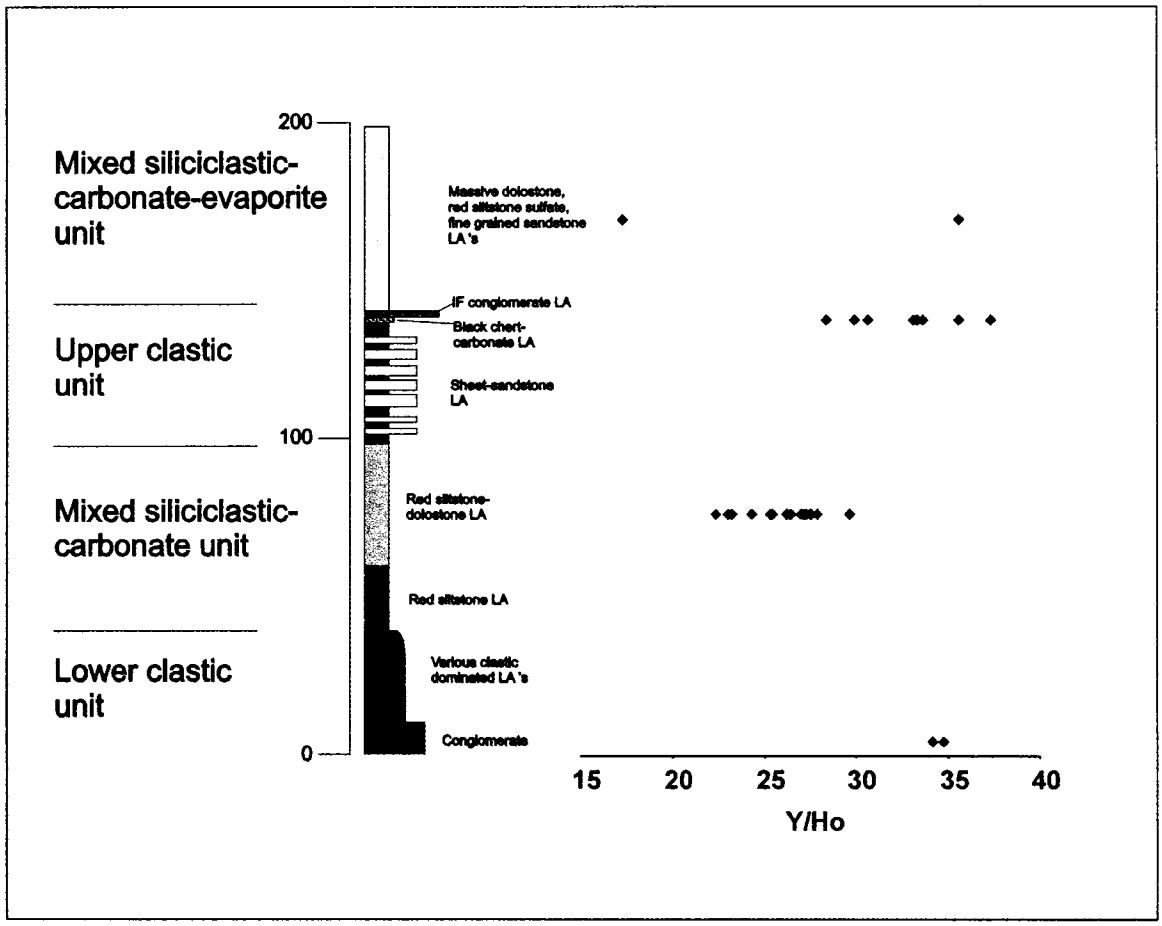

Figure 5.21. Variations in carbonate Y/Ho ratios for each stratigraphic unit. Seawater typically has Y/Ho ratios greater than about 44 (e.g. Nozaki et al. 1997; Kamber and Webb 2001) and all samples here show low Y/Ho relative to seawater.

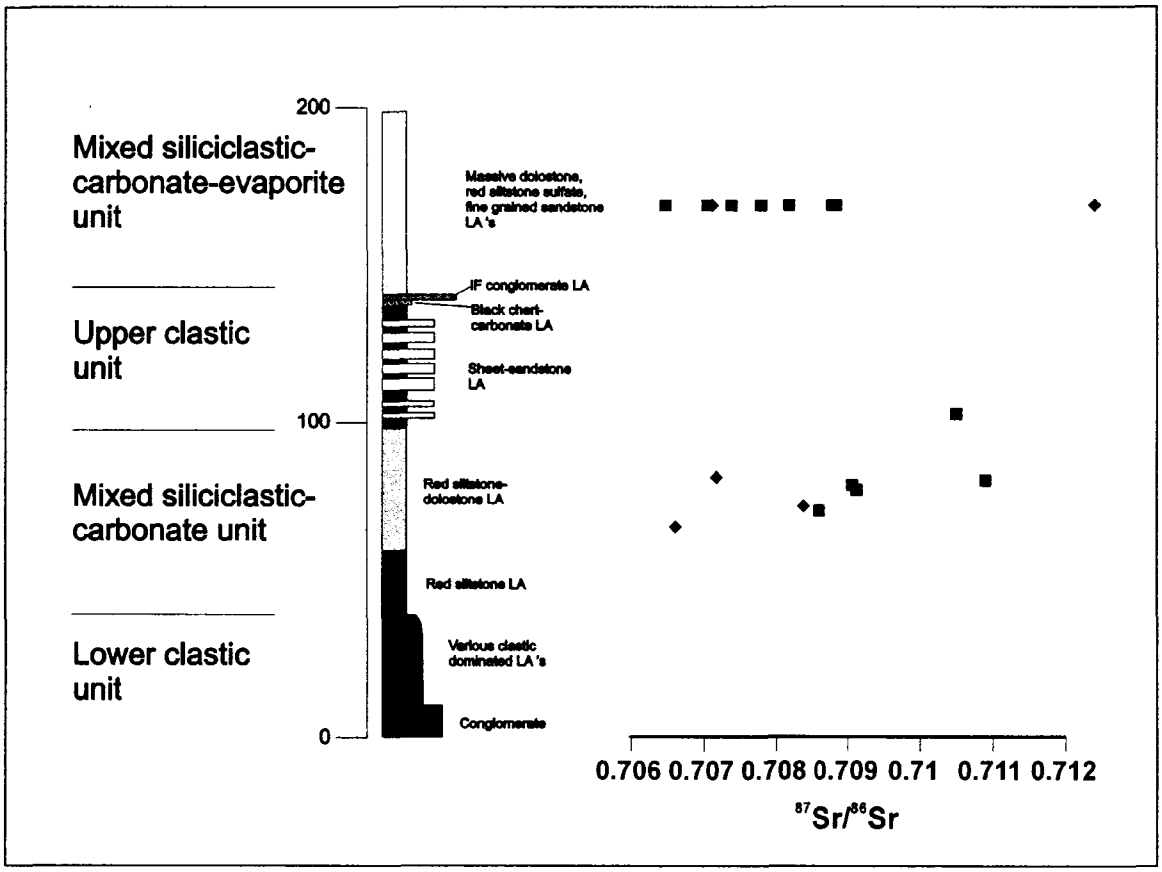

Figure 5.22. Comparison of ranges in sulfate Sr isotope ratio between red siltstone-dolostone and red siltstone-sulfate lithofacies associations. Carbonate analyses are represented by diamond shapes and sulfate analyses are represented by squares. Data for the mixed siliciclastic-carbonate-evaporite unit are from a few different drill holes so stratigraphic variation is not shown.

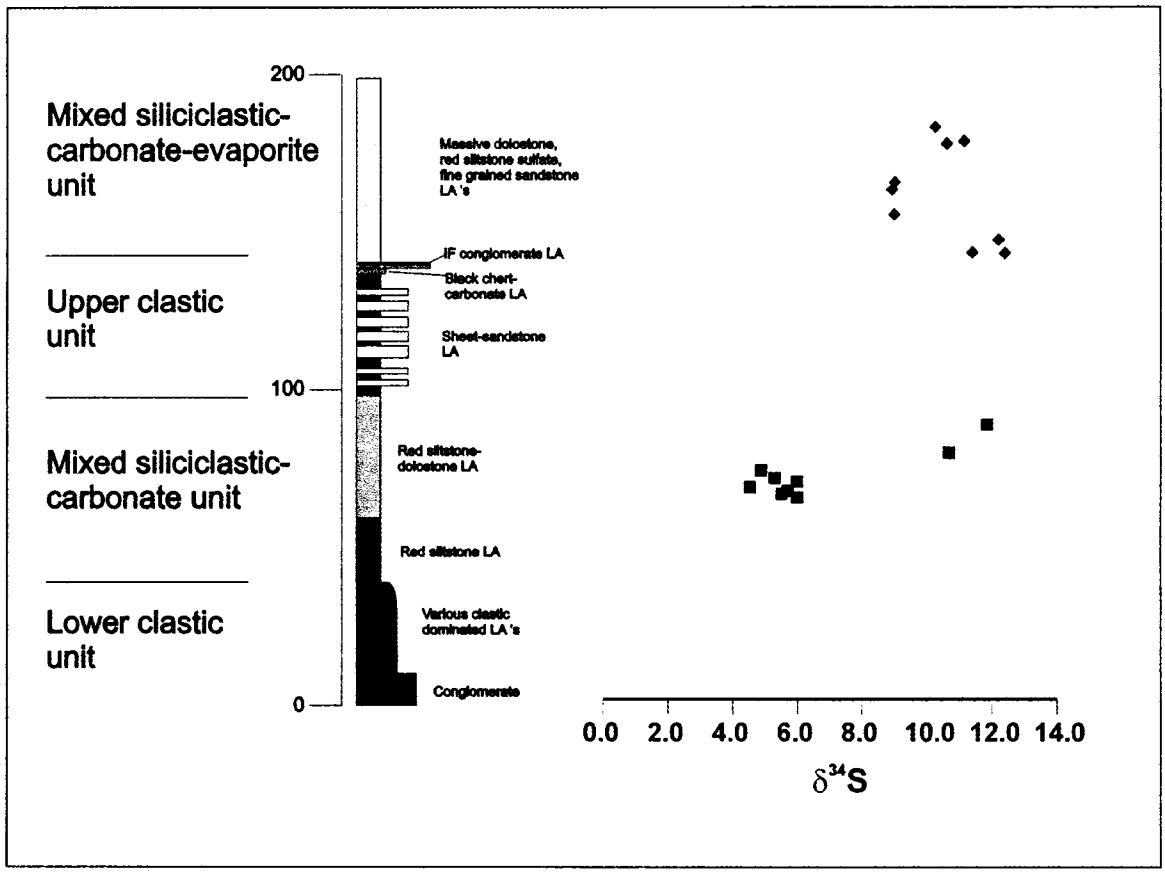

Figure 5.23. Stratigraphic variations in sulfate $\delta^{34}S$ values. Sulfate $\delta^{34}S$ values are the lowest in the lowest sampled portions of the mixed siliciclastic carbonate unit (4-6 ‰). Values at the top of the mixed siliciclastic carbonate unit and the mixed siliciclastic-carbonate-evaporite unit are higher (9-12 ‰)

Variations in Sr isotopic composition for both carbonates and sulfates is shown in Figure 5.22. Overall, there is no major difference in Sr composition between mixed siliciclastic-carbonate unit and the mixed siliciclastic-carbonate-evaporite unit as data for both units fall into the same range. However, sulfates in the mixed siliciclastic-carbonate-evaporite unit typically have lower $^{87}Sr/^{86}Sr$ ratios than the mixed siliciclastic-carbonate unit. Figure 5.23 shows stratigraphic variations in sulfur isotopic composition between stratigraphic units. A major shift towards more ^{34}S enriched compositions occurs over a short stratigraphic interval near the top of the mixed siliciclastic carbonate unit.

5.5 Discussion

5.5.1 Diagenesis and carbonate mineralogy

Previous work (Franklin et al., 1980; Cheadle, 1986b; Mailman, 1999) showed that dolomite was the dominant mineral in Sibley Group carbonates. This is supported by trace elemental data (Fig 5.24) and SEM EDS work carried out during the course of this study. Figure 5.24 plots Ca/Mg weight ratios versus carbon and oxygen isotopic compositions and shows that the majority of carbonate samples plot at Ca/Mg ratios of about 1.6 consistent with a dolomite dominated mineralogy. A few samples are calcite rich as is indicated by high Ca/Mg ratios. These samples show light $\delta^{18}O$ values relative to the rest of the samples. $\delta^{13}C$ values for the calcite-rich, low $\delta^{18}O$, samples fall within the range of values displayed by the majority of samples. Low $\delta^{18}O$ in calcitic samples supports a diagenetic origin for the O in these samples.

Petrographic examination was employed as an early step in evaluating potential post-depositional alteration of primary geochemical compositions. Figures 5.25 to 5.33 illustrate some pertrographic characteristics of typical materials sampled for analysis. For the most part petrographic features characteristic of diagenetic alteration are absent and sparry, void-filling cements and stylolites are exceedingly rare within examined samples. Samples selected for geochemical analysis are dominantly finely crystalline (Figs 5.25, 5.26, 5.27). Depositional components (or possibly early microspar cements), primarily micritic dolomite, were the primary materials sampled and there is little petrographic evidence for post-depositional alteration. However, in some cases, particularly in stromatolitic samples from the black chert-carbonate lithofacies

association and the red siltstone-sulfate lithofacies association there is some indication of post-depositional alteration.

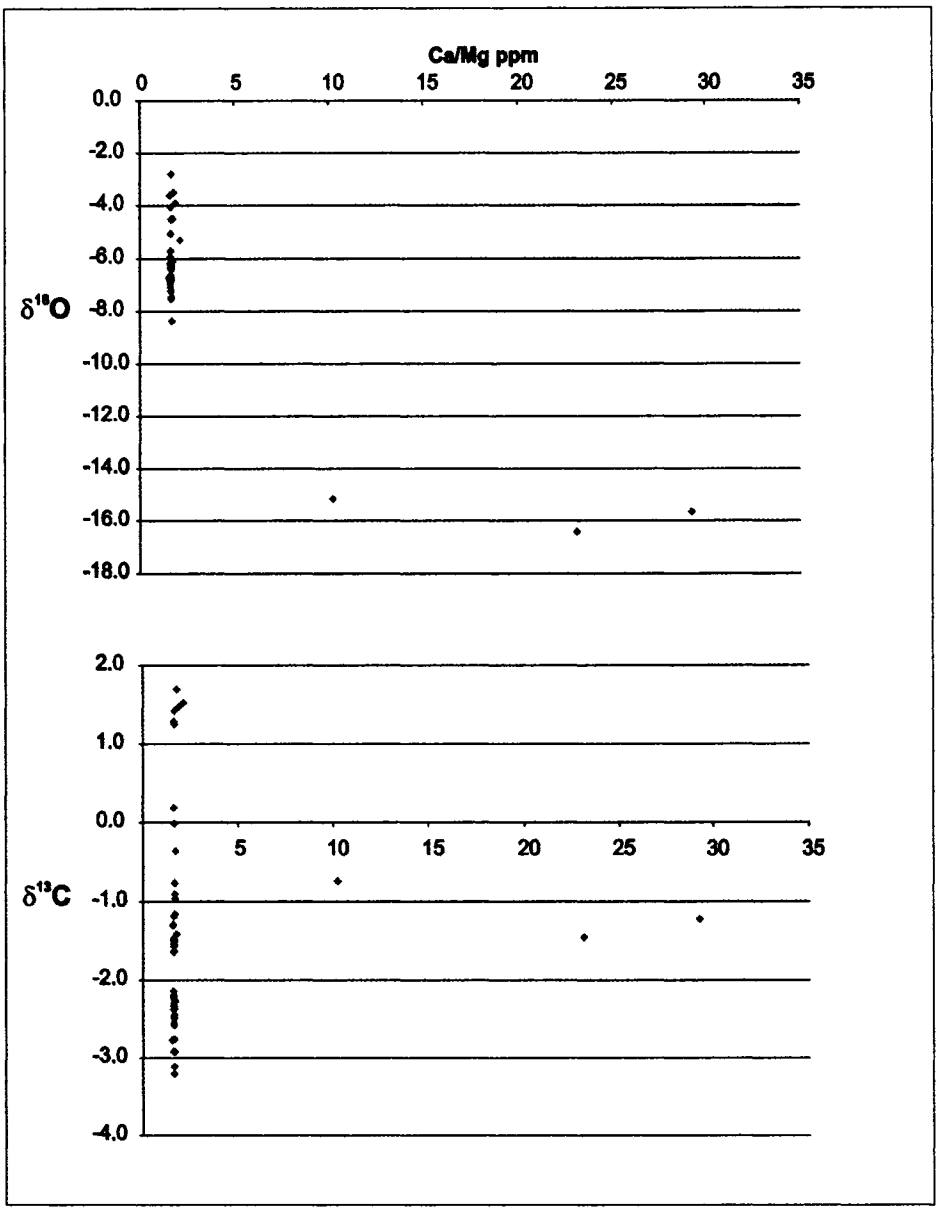

Figure 5.24. Ca/Mg weight ratios for all carbonate samples with trace element analyses versus $\delta^{18}O$ and $\delta^{13}C$. The upper diagram shows a clear relationship between high Ca/Mg ratio and light oxygen isotopic composition, whereas there is no difference in the range of carbon isotopic composition between dolomitic and calcitic samples.

At hand sample-scale materials from the black-chert carbonate lithofacies association contain veins filled with fairly coarse-grained carbonate spar. In thin section,

carbonate dominated laminae are typically micritic, but thin veins or carbonate spar and replacements of earlier sulfate nodules are common (Fig. 5.28). In addition to early silicification of organic rich laminae, there appears to have been a later pervasive silicification event. Stromatolite samples from the red siltstone-sulfate lithofacies association appear to be recrystallized based on their increased crystal-size (Fig 5.29).

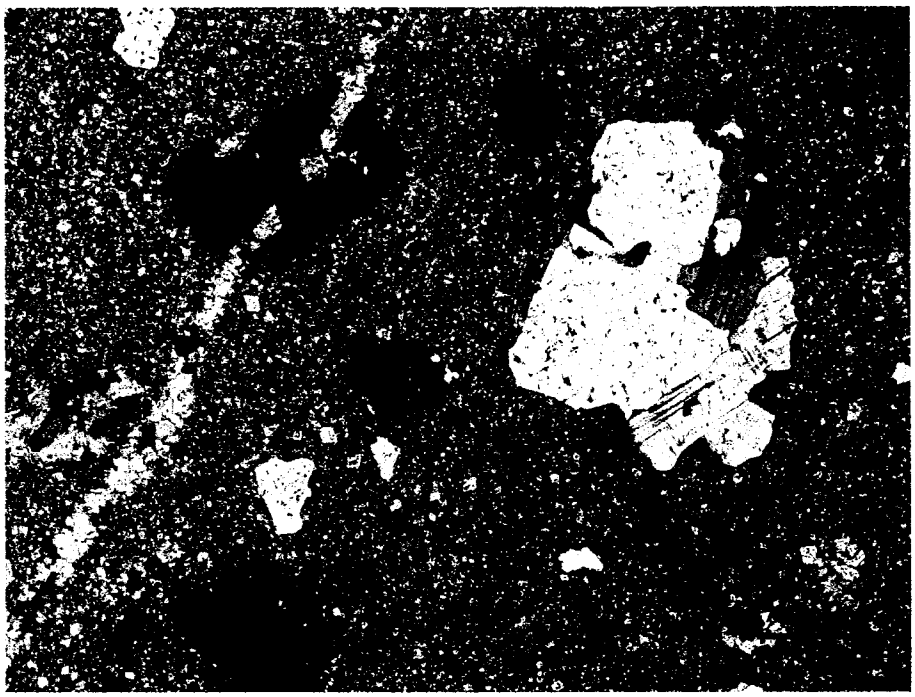

Figure 5.25. Photomicrograph (cross-polarized light) of a dolocrete sample (WL3a) showing floating clastic grains in a primarily micirtic matrix of dolomite. A minor vein of coarser dolomite spar cuts across the left side of the image. Micritic grain-size, and low Sr isotope ratios for WL labelled samples suggest little post depositional alteration.

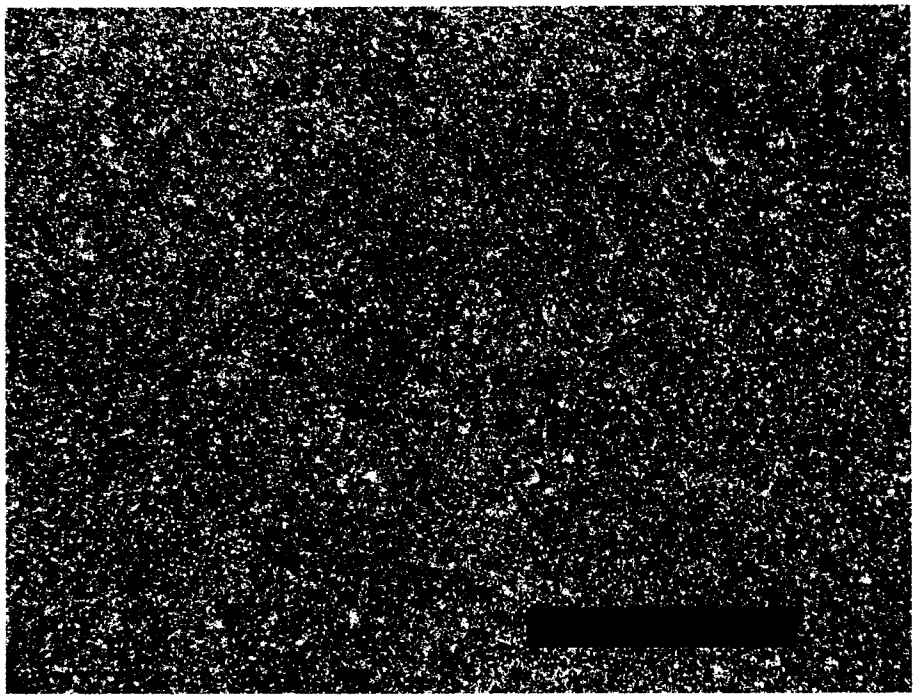

Figure 5.26. A photomicrograph showing the typical homgeneous, fine-grained dolostone lithofacies that was sampled from the red siltstone-dolostone lithofacies association (Sample 03RM31). Scale bar is 500 um. Plane-polarized light.

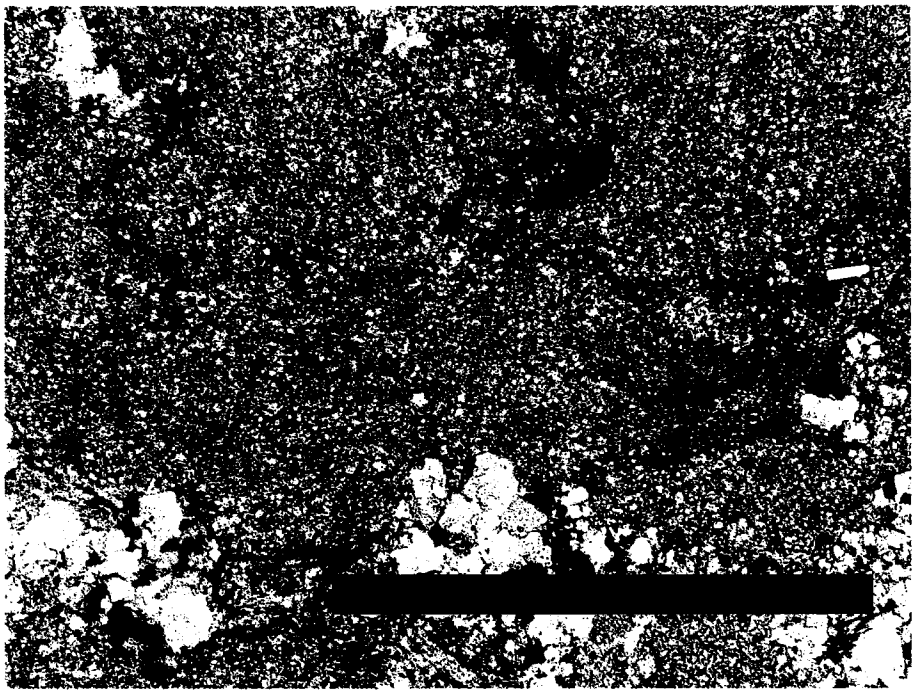

Figure 5.27. Fine-grained carbonate from a sample of the altered top of the black chert-carbonate lithofacies association with hematite-rich illuviation features and round chert nodules. Sample 03RM28. Scale bar is 2mm. Cross-polarized light.

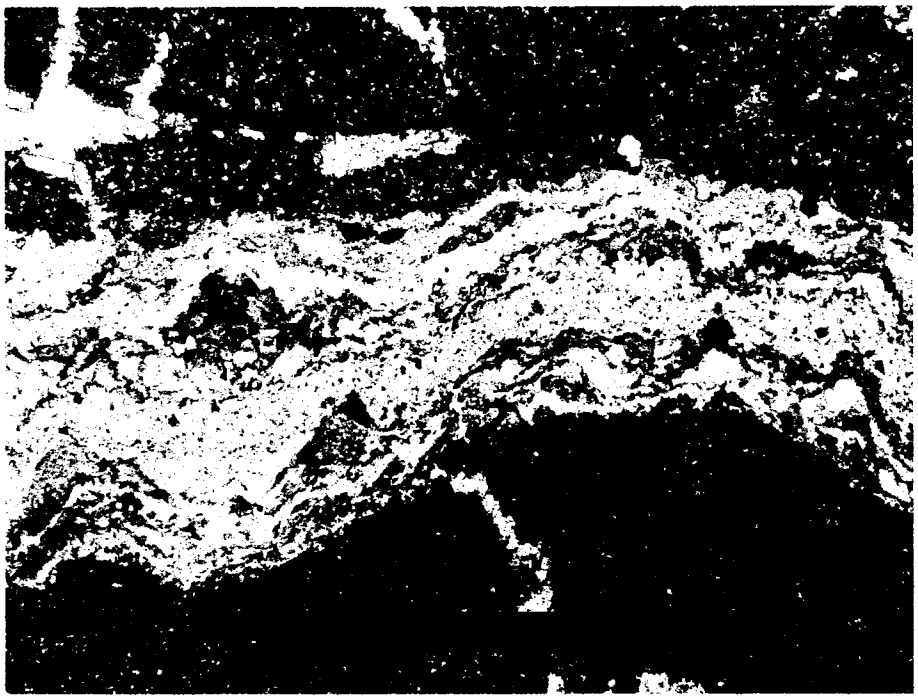

Figure 5.28. Photomicrograph showing typical lamination in stromatolites from the black chert-carbonate lithofacies assoication (cross-polarized light). The upper and lower portions of darker colour are fine-grained dolomite, they contain some zones of coarser-grained carbonate spar (e.g. top left of photomicrograph). The central portion of the photo is an organic-rich chert layer. Sample CI-1A. Scale bar is 2 mm.

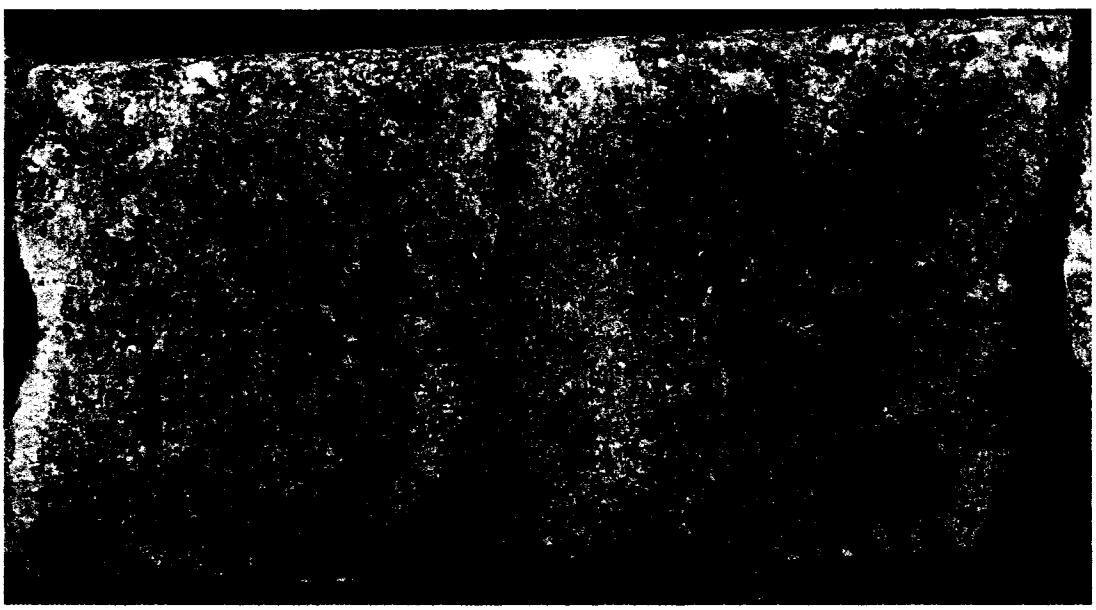

Figure 5.29. Drillcore photograph of recrystallized stromatolitic dolostone from the red siltstone-sulfate lithofacies association. Photograph shows a field of view 10cm wide.

Samples from other lithofacies associations show little evidence for post depositional alteration. Dolocrete samples from the lower clastic unit, dolostone samples from the mixed carbonate-siliciclastic horizon and some samples of carbonate from the intraformational conglomerate lithofacies association are dominated by micritic material with no evidence for diagenesis and neomorphism (Figs. 5.25, 5.26, 5.27). An exception to this are the samples of carbonate associated with the basal contact with Archean rocks south of Beardmore which appear to be recrystallized (Fig. 5.30). Thin sections were not prepared for some samples of the intraformational conglomerate lithofacies association and dolocrete from the fine-grained sandstone lithofacies association because they were too poorly indurated and for these samples only geochemical criteria were applied to evaluate diagenesis.

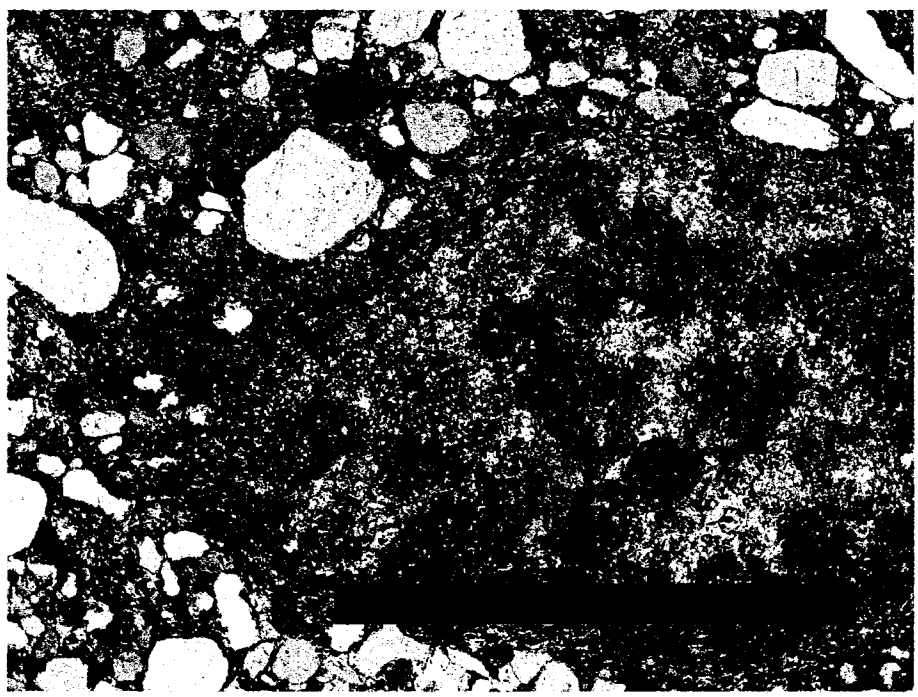

Figure 5.30. Photmicrograph of a recrystallized carbonate clast in sample BM90 (Cross-polarized light). Recrystallization and low $\delta^{18}O$ values for BM90 and 91 (section 5.3.1) suggest diagenetic alteration. Scale bar is 2 mm long.

Siliciclastic grains are common in many of the carbonate samples analysed. In most cases they are physically inseparable from carbonate; this is particularly evident in dolostone samples from the red siltstone-dolostone lithofacies association and dolocrete samples. For this reason an acetic acid leach was used for trace element analyses and Sr isotopic analyses. In addition to contamination during sample digestion, a high content of siliciclastic grains could potentially increase permeability and therefore create a preferential flow path for diagenetic fluids. Because many siliciclastic grains, particularly in the dolostones of the red siltstone-dolostone lithofacies association, occur sporadically and in matrix support, they probably would not have influence permeability of diagenetic fluids to a great degree.

Sulfate nodules within the red siltstone-dolostone lithofacies association appear to have been replaced to varying degrees by carbonate (Fig. 5.31). In some instances sulfate nodules have been replaced entirely by mosaics of coarsely-crystalline dolomite (Fig. 5.31c), while in others very little replacement has taken place (Fig. 5.31a). Sulfate nodules from the red siltstone-sulfate lithofacies association have coarse-fibrous textures suggesting dissolution and reprecipitation (Fig. 5.32). Cross-cutting veins of sulfate suggest that early forming diagenetic sulfate nodules have been remobilzed (Fig. 5.33). Samples collected for analysis are from isolated, discrete nodules, not associated with vein structures.

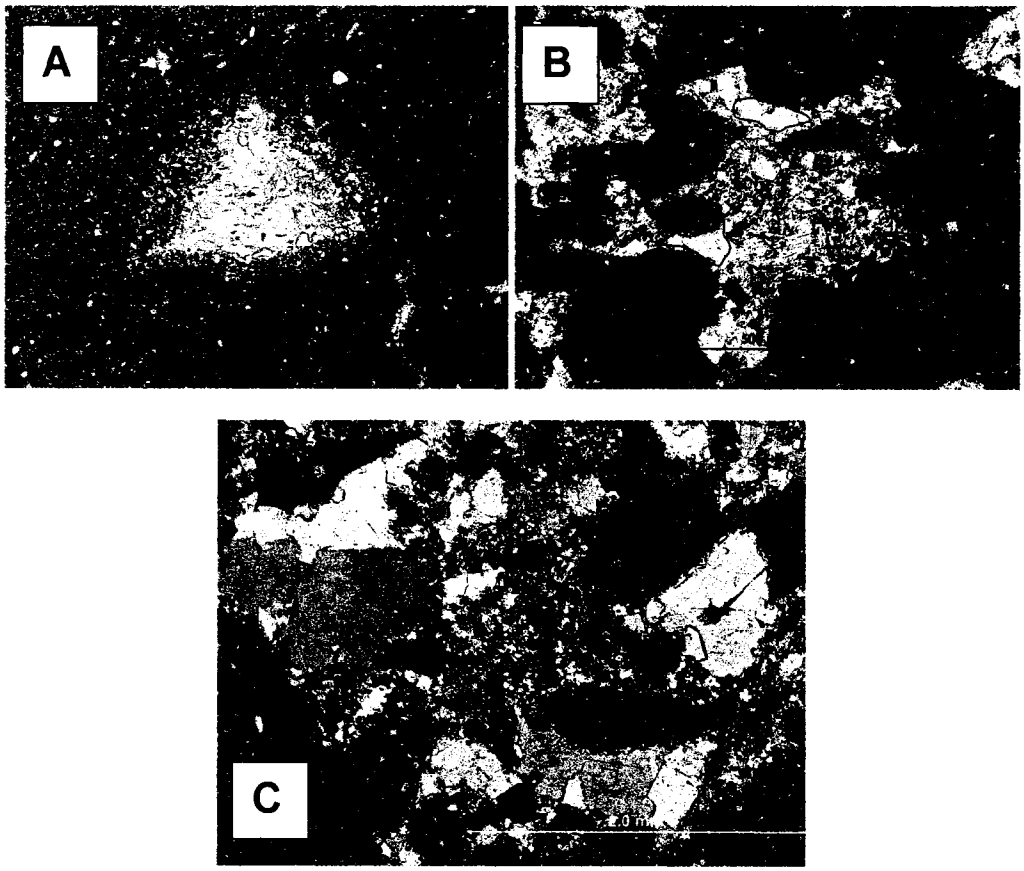

Figure 5.31. A) Early diagenetic sulfate nodule in dolostone with no carbonate replacement. B) Early diagenetic sulfate nodule in dolostone with minor carbonate replacement (red outlines some zones of carbonate) C) Early diagenetic sulfate nodules in dolostone with complete replacement by carbonate. All photomicrographs are in cross-polarized light.

Figure 5.32. Typical gypsum nodules sampled from the red siltstone sulfate lithofacies association. Dissolution and reprecipitation may have occurred, however, attempts were made to sample only discrete nodules not associated with veins.

Figure 5.33. A cross-cutting gypsum vein from the red siltstone-sulfate lithofacies association.

In addition to petrographic characterization of samples, variations in Mn/Sr, $\delta^{18}O$ and $^{87}Sr/^{86}Sr$ were used to screen samples for post depositional alteration using the general criteria outlined in section 5.3.6. Figure 5.34 is a plot of Mn/Sr ratio versus $\delta^{18}O$

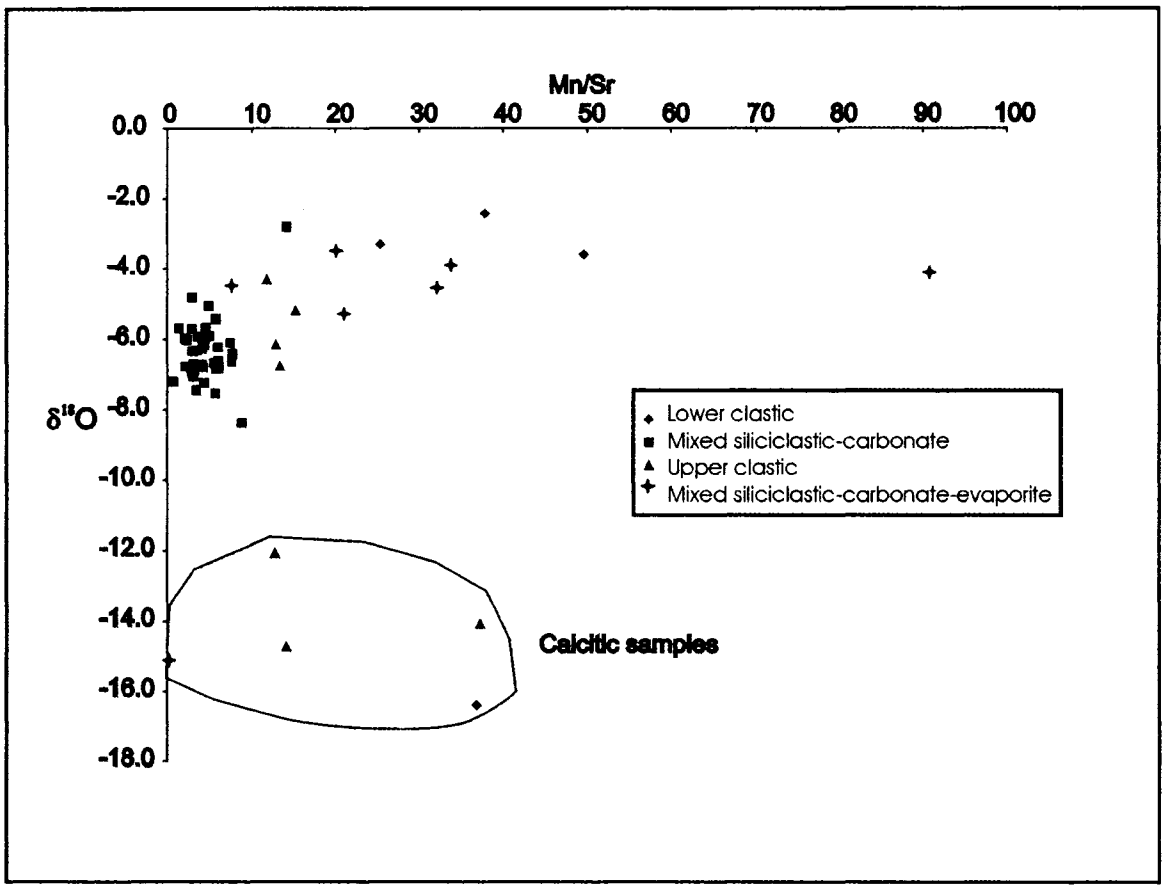

Figure 5.34. A plot of Mn/Sr versus $\delta^{18}O$ divided into the four stratigraphic units.

for carbonates from the four stratigraphic units outlined in chapter 3. Dolostone samples from the mixed siliciclastic-carbonate unit generally plot at Mn/Sr ratios of less than 10 and have $\delta^{18}O$ values that, in general, range between 4 and $8^{0}/_{00}$. Samples from other units display variably higher Mn/Sr ratios and for the most part slightly heavier $\delta^{18}O$. Some samples plot at significantly lighter $\delta^{18}O$ values and in some cases higher than average Mn/Sr ratios relative to dolomite dominated samples from the same unit. These samples appear to reflect diagenesis, and are also characterised by a calcite dominated mineralogy (Fig 5.24). High Mn/Sr ratios in dolomite dominated samples do not show a relationship with decreasing $\delta^{18}O$ as might be expected during diagenesis (Fig. 5.34).

$\delta^{18}O$ for pedogenic samples should reflect the composition of meteoric waters (e.g., Alonzo-Zarza, 2003). Because the pedogenic carbonates do not display low $\delta^{18}O$ values, low $\delta^{18}O$ carbonates probably do not reflect meteoric diagenesis. Therefore, another diagenetic process must have been involved in resetting some carbonate samples to low $\delta^{18}O$. Requilibration of carbonates at higher temperatures during burial diagenesis is possible, but not supported by the lack of features such as stylolites and the fact that resetting is not present in all samples. Another possibility is that the alteration is associated with diabase intrusions.

In the lower clastic unit, dolocrete samples WL3a, b and c do not show geochemical or petrographic evidence for extensive diagenetic alteration. Although they have relatively high Mn/Sr ratios, oxygen isotopic compositions have not been reset to low values and Sr isotopic compositions are not radiogenic. Samples BM90 and 91 are recrystallized and have light $\delta^{18}O$ values indicating alteration. In the mixed siliciclastic carbonate unit, low Mn/Sr and relatively high $\delta^{18}O$ suggest little diagenetic alteration of carbon and oxygen isotopic compositions. Samples from the black chert-carbonate lithofacies association (upper siliciclastic unit) display some evidence of diagenetic alteration both petrographically and geochemically. Petrographically, diagenetic alteration is suggested by pervasive silicification, and the presence of cross-cutting calcite veins filled with fairly coarsely-crystalline spar. Geochemically, obviously altered samples show light oxygen isotopic compositions, Mn/Sr ratios greater than 10 and high $^{87}Sr/^{86}Sr$ ratios. Figure 5.35 plots $\delta^{18}O$ vs $^{87}Sr/^{86}Sr$ and shows that samples with light $\delta^{18}O$ are also characterized by radiogenic $^{87}Sr/^{86}Sr$ suggesting that high $^{87}Sr/^{86}Sr$ samples reflect diagenesis. Carbon isotopic compositions for apparently apparently unaltered

stromatolite samples (Fig 5.36) fall between about 0 and 1 per mil, whereas obviously altered samples display trends to either light carbon isotopic composition (represented by pedogenic carbonates) or both lighter carbon and lighter oxygen compositions (interpreted to reflect later diagenesis). The observed shift towards lighter carbon isotopic composition in pedogenically altered samples may be reflecting the composition of a mixture of stromatolite material and isotopically light carbonate precipitated in equilibrium with soil CO_2. If so, the relatively low $\delta^{13}C$ supports a pedogenic origin for the alteration of the top of the black chert-carbonate unit. Samples showing shifts to both lighter carbon and oxygen isotopic composition probably reflect more extensive diagenetic alteration.

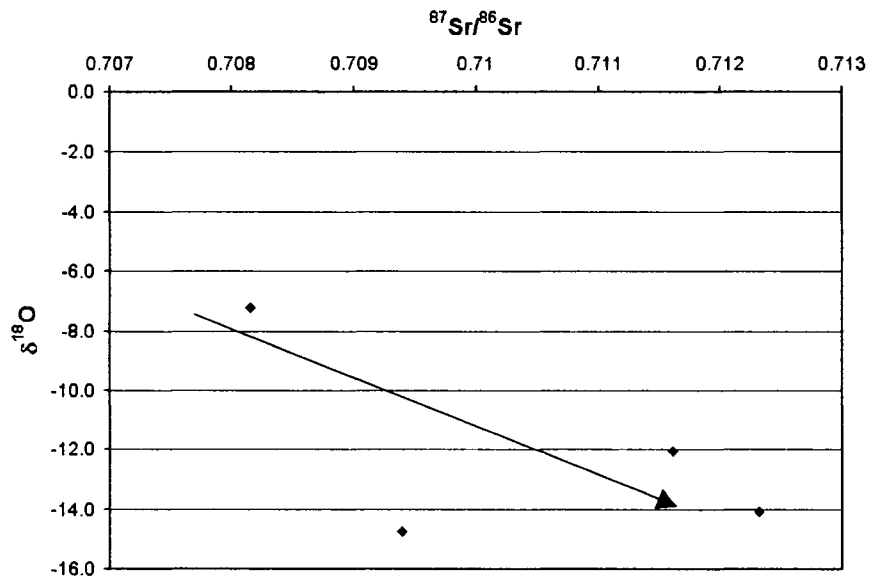

Figure 5.35. Possible diagenetic alteration towards low $\delta^{18}O$ and high $^{87}Sr/^{86}Sr$ in samples of the black chert-carbonate lithofacies association.

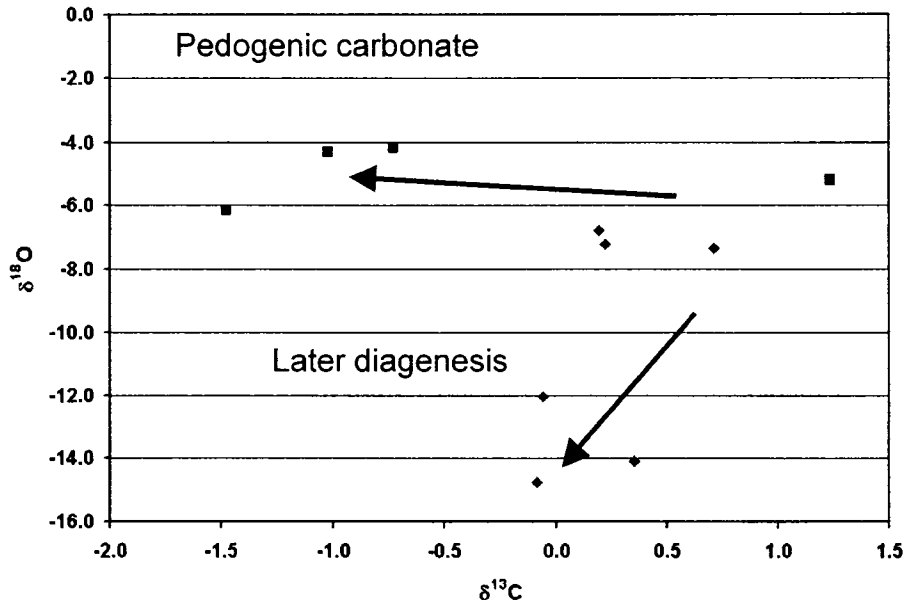

Figure 5.36. Plot of carbon vs oxygen stable isotopic compositions for samples of stromatolitic carbonate from the black chert-carbonate lithofacies association and pedogenically (?) altered samples from its top. Squares are pedogenic carbonates, diamonds are stromatolitic carbonates. Diagenetically (late) altered samples trend towards compositions enriched in lighter isotopes. Earlier diagenesis, (i.e., pedogenesis of the top of the stromatolite unit) seems to have shifted only carbon isotopic compositions to lower values.

In general, for carbonate samples, there are no apparent relationhips between high Mn/Sr and $\delta^{18}O$ or $^{87}Sr/^{86}Sr$. Altered samples appear to be characterised by light $\delta^{18}O$ values and calcite-rich mineralogies. For the most part altered samples are restricted to the black-chert carbonate lithofacies association, red siltstone sulfate lithofacies association, and the samples from the lower siliciclastic unit from the exposure south of Beardmore.

5.5.2 Geochemical constraints on the depositional environments of the Lower clastic unit

The most interesting aspect of geochemical data from dolocrete samples in the lower clastic unit is the low, marine-like $^{87}Sr/^{86}Sr$ ratio. Sr isotopic compositions are a

useful tracer of the sources of Ca in calcretes/dolocretes as Sr is geochemically similar to Ca and is found as a trace element in both carbonate and silicate Ca-bearing minerals (e.g. Stewart et al., 1998; Van der Hoven and Quade, 2002). Given the distinctly non-marine, braided fluvial/alluvial fan depositional environment of the boulder conglomerate-sandstone-dolocrete association and the Archean and Paleoproterozoic basement rocks in the region, the $^{87}Sr/^{86}Sr$ composition of dolocrete precipitating solutions should have been characterised by a more radiogenic $^{87}Sr/^{86}Sr$ ratio. This indicates that the main source of carbonate in the dolocrete lithofacies was not local silicate parent materials, but an alternative lower $^{87}Sr/^{86}Sr$ source. Various studies (e.g., Machette, 1985; Quade et al., 1995; Chiquet et al., 1999; Capo and Chadwick, 1999; Naiman et al., 2000) have shown that atmospheric inputs (precipitation and easily soluble surface dusts) and seaspray (in areas within about 100 km of oceans), with varying contributions from weathering reactions in local substrates, are a dominant source of Ca in carbonate soil formation. The low, marine-like Sr isotopic composition is consistent with largely marine derived atmospheric input as the major source of Ca cations in dolocrete units. Sr introduced from weathering of Archean basement lithologies should have added a significant radiogenic Sr contribution to soil carbonates. As such weathering of old, radiogenic bedrock sources could not have been a major source of cations in dolocretes in this stratigraphic unit. Outcrops of Gunflint Formation stromatolitic carbonates form Sibley Group basement near the sampled occurrences of dolocrete in the boulder conglomerate-sandstone-dolocrete lithofacies association and represent a possible source of non-radiogenic carbonate. The composition of Sr in carbonates from the Gunflint Formation was not determined during this study and no data

appears to be present in the literature. It is likely that unaltered carbonates from the Gunflint Formation had low $^{87}Sr/^{86}Sr$ ratios (Fig. 5.5) as they are marine in origin (e.g., Pufahl, 1996), however, subsequent diagenesis may have driven most Gunflint Formation carbonates to higher $^{87}Sr/^{86}Sr$ ratios prior to Sibley Group deposition. Analysis of Sr isotopic ratios for Gunflint Formation carbonates would need to be done in order to test the possibility of this hypothesis. The presence of weathered Archean and Paleoproterozoic clasts in the basal conglomerate units shows that there should have been a significant contribution of radiogenic Sr to groundwaters making it difficult to support a groundwater origin for the sampled dolocrete units. As such, low Sr isotopic ratios are more consistent with a pedogenic origin for the dolocretes with surface dissolution of marine deposited Gunflint Formation carbonates and marine derived atmospheric input as carbonate sources.

Preservation of unradiogenic Sr isotopic ratios suggests that samples from the West Loon dolocrete occurrence reflect unaltered values even at relatively high Mn/Sr ratios. Further, low $\delta^{18}O$ in altered samples south of Beardmore suggests that diagenetic alteration should have driven $\delta^{18}O$ to low values in West Loon samples had it occurred in them as well. These two lines of evidence suggest that both $\delta^{13}C$ and $\delta^{18}O$ reflect near primary dolocrete compositions. Carbon and oxygen stable isotopic compositions of dolocrete samples do not differ significantly from approximately coeval marine carbonate compositions, however, $\delta^{13}C$ and $\delta^{18}O$ also fall within the range of reported $\delta^{13}C$ and $\delta^{18}O$ values for calcretes compiled by Alonzo-Zarza (2003) (see section 5.3.1). Assuming a purely pedogenic orgin for carbonate, large contributions of CO_2 from oxidation of organic matter and respiration of soil microbes should have driven

dolocretes toward relatively light isotopic compositions (e.g., Quade et al., 1989a; Cerling, 1991; Wright and Tucker, 1991). Thus, the relatively heavy observed $\delta^{13}C$ (ca. -1.5 ‰) suggest that either there was little organic related CO_2 contribution to soil CO_2 or that soil pores were dominated by intrusion of atmosphere derived, relatively heavy isotope enriched CO_2. This may imply either high atmospheric CO_2 levels, or low contributions of CO_2 to the soil via organic processes.

Rare earth element patterns determined for two samples from the West Loon dolocrete show characteristics of oxygenated seawater as well as terrestrially derived water. A well-defined positive La anomaly and a well defined negative Ce anomaly supports a seawater origin, however, the lack of a positive HREE slope and relatively low Y/Ho does not support a seawater origin (e.g. Shields and Webb, 2004) (Figs. 5.6, 5.20, 5.21). Y/Ho ratios are among the highest of any of the Sibley Group samples analysed (about 34) but are still considerably lower than anticipated values for seawater (>44; e.g., Bau and Dulski, 1996; Nozaki et al., 1997; Kamber and Webb, 2002). Low concentrations of elements such as Zr and Hf in carbonate analyses suggests that this low value is not the result of contamination by clastic material. Negative Ce anomalies and low Y/Ho ratios, therefore, support precipitation from oxygenated, non-marine waters.

Overall, geochemical data from dolocretes in the lower clastic unit are useful tracers of hydrologic processes that precipitated dolocrete units and also as potential indicators of atmospheric composition. If the dolocretes are purely pedogenic (sensu Wright and Tucker, 1991; Alonzo-Zarza, 2003) Sr data suggests atmospheric, marine derived and/or surface dissolved Gunflint Formation carbonate were the major source of Ca as opposed to local silicate parent material. Also, carbon isotopic compositions would

support either low organic productivity in soils, high atmospheric CO_2 levels or both (e.g., Cerling, 1991). If the dolocretes represent groundwater dolocrete (sensu Wright and Tucker, 1991; Alonzo-Zarza, 2003) then it appears that carbonate compositions could be indicating similarities to Gunflint Formation carbonates and that the composition of shallow groundwater was controlled by dissolution of Gunflint Formation carbonate material. However, a groundwater dolocrete classification is unlikely, as there is evidence for significant weathering of silicate bedrock that would have released radiogenic Sr into the groundwater system. REE geochemistry is consistent with oxidizing non-marine water precipitating soil carbonates.

5.5.3 Mixed carbonate-siliciclastic unit

Geochemical data from the red siltstone-dolostone lithofacies association supports the non-marine depositional setting for this unit inferred from lithofacies analysis. In particular low $\delta^{34}S$ values and high $^{87}Sr/^{86}Sr$ in sulfates from this unit are more consistent with a non-marine rather than a marine depositional environment. $\delta^{34}S$ values between ~4 to 6 ‰ in the lower portions of the red siltstone-dolostone lithofacies association (Fig. 5.23) are lower than predicted values of coeval seawater (about 20 ‰, e.g., Canfield, 2004). A seawater source for sulfate is therefore unlikely. Radiogenic strontium isotope ratios also support a non-marine source for sulfates in the lower portions of this unit. Towards the top of this unit both $\delta^{34}S$ and $^{87}Sr/^{86}Sr$ increase (Figs. 5.4, 5.23). Increasing $\delta^{34}S$ may reflect an increasing contribution of isotopically heavier marine derived sulfate or it may represent a variation in the overall composition of sulfide minerals that were weathering to supply sulfate to the basin. An increased seawater contribution is not supported by the upward increase in $^{87}Sr/^{86}Sr$. As such, sulfur for the precipitation of

sulfates in this unit may have been derived largely from weathering of Archean and Paleoproterozoic sulfides in the catchment. The majority of Archean sulfides in the region likely had an average $\delta^{34}S$ value of around 0 ‰ (e.g. Strauss, 1999). Seventy-four Paleoproterozoic sulfide $\delta^{34}S$ analyses from the Gunflint and Rove Formations (Poulton et al., 2004) have an average value of about 10 ‰. It is possible that variations in the amount of sulfate derived from Archean versus Paleoproterozoic bedrock sources created the upward shift to heavier $\delta^{34}S$. Speculatively, this could be related to the observed change in paleocurrent direction from southward (northern area dominated by Archean basement with low $\delta^{34}S$) in the underlying clastic unit to northward (southern area dominated by Paleoproterozoic basement with higher $\delta^{34}S$) in the overlying sheet sandstone lithofacies association.

The observed upward change in $\delta^{34}S$ could also be related to sulfur reducing bacteria. Periods of oxygen deficiency may have been occurred in the lake system allowing for sulfate reduction to occur. Although no sedimentary pyrite is present in the mixed siliciclastic-carbonate unit, sulfate reducing bacteria may have been important in bringing about changes in sulfur isotopic composition through loss of H_2S gas produced during sulfate reduction. If sulfate reduction was a control on the observed stratigraphic trend in sulfur isotope data then H_2S gas created during bacterial sulfate reduction would have needed to escape the lake system prior to reoxidation to sulfate. This may have preferentially occurred in shallower water conditions inferred for the upper portions of this unit leading to the observed stratigraphic trend.

Further support for a non-marine depositional setting for this unit comes from the REE geochemistry of dolostone samples. The distinct, "hat-like", MREE enriched

pattern of dolostone samples on PAAS normalised REE diagrams (Figs. 5.11, 5.20) is not consistent with carbonates precipitating from seawater. Analogy with MREE enriched patterns of some major modern river systems supports a non-marine chemistry for waters precipitating the dolostones (Hannigan and Sholkovitz, 2001). In addition to a non-marine PAAS normalized shale normalized REE patterns, low Y/Ho ratios (Fig. 5.21), around that of chondrite meteorites, also supports a non-marine origin (e.g., Nozaki et al. 1997).

Phosphates commonly show a MREE enrichment relative to shale (Hannigan and Sholkovitz, 2001; Sheilds and Webb, 2004). However, MREE enrichment does not appear to be a function of partial dissolution of detrital apatite grains in samples during acetic acid leaching as there is no correlation between P content and total REE (R^2= 0.04). MREE enrichment may also be a function of partial dissolution of Fe oxyhydroxides present in samples. Studies using HCl dissolution methods (e.g., Negrel et al., 2006) suggest that MREE enriched shale normalized REE patterns are a function of the presence of MREE adsorbed on the surfaces of Fe oxyhydroxides. Again, however, there is no correlation between MREE or total REE contents and Fe or Mn contents in Sibley Group samples. Further, if REE's associated with Fe or Mn oxyhydroxides was an important control on the shale normalized REE patterns then there should be a significant difference between red dolostone samples (containing hematite) and buff coloured dolostone samples (not containing hematite). Thus, it appears that the MREE enrichment is reflecting carbonate chemistry and as such, the chemistry of the lake water mass, rather than a product of sample dissolution. Hannigan and Sholkovitz (2001) suggested that MREE enrichments in many major modern river systems results from the

weathering of phosphate minerals as a major source of REE. Gruau et al. (2004) reported similar MREE enriched patterns in shallow groundwaters under wetland domains in a small catchment study conducted in western France; more upland portions of this catchment had PAAS normalized water REE patterns similar to the patterns from dolocretes and stromatolites from this study. They suggested that the difference was a function of redox chemistry, with upland areas characterised by more oxidizing conditions, negative Ce anomalies and relatively flat REE patterns and wetland areas characterised by no Ce anomalies, slightly reducing conditions and MREE enrichment.

Sr isotopic composition varies between dolostone samples and sulfate samples from this unit (Fig. 5.10). Sulfate samples are characterized by higher $^{87}Sr/^{86}Sr$ ratios than dolostone samples. This suggests that either sulfate nodules were more susceptible to diagenetic alteration than dolostone samples, or that they were precipitated from chemically distinct water sources. There is petrographic evidence for the replacement of some sulfate nodules by relatively coarse-grained carbonate spar. This supports possible alteration of primary sulfate chemistries. However, the use of water dissolution methods should have preferentially taken sulfates into solution rather than any carbonate material that may have been included in sample powders. Further, indicators of inclusion of diagenetic carbonate phases should be indicated by increased contents of elements such as Fe or Mn but there is no correlation between increasing Mn or Fe and Sr isotopic composition. Thus, it is possible that dolostones and sulfate nodules within dolostones precipitated from geochemically distinct waters. Sulfates probably precipitated in the shallow subsurface during periods of subaerial exposure and they could either reflect lake-water chemistry or groundwater chemistry. Thus, sulfate nodules are probably

reflecting the chemistry of ground water. The water budget of the lake system, therefore, was likely dominated by river and precipitation inputs rather than by groundwater recharge. Capillary rise from more radiogenic shallow groundwaters likely occurred during periods of exposure leading to precipitation of sulfate nodules with geochemistries that differed from lake-water precipitates. This observation suggests that lake-water and groundwater did not mix over time periods shorter than the time periods between lake recharge events otherwise both dolostones and early intrasediment Ca-sulfate nodules would have been characterised by the same Sr isotopic ratios. The validity of this hypothesis is questionable as it is based on very few Sr isotope analyses.

Carbon and oxygen stable isotopic compositions for the most part do not differ significantly from proposed values for Mesoproterozoic seawater (Fig 5.1); (Bartley and Kah, 2004). Relatively light $\delta^{13}C$ values (-3 ‰) in the basal portions of the red siltstone-dolostone lithofacies association, however, could be taken as evidence for a lacustrine origin as they are somewhat lower than would be expected for seawater. The observed upward trend towards heavier isotopic composition (Figs. 5.7. 5.8) could be explained by a number of different models. If the red siltstone-dolostone lithofacies association was connected to the open Mesoproterozoic ocean, then the upwards shift could be attributable to processes that create changes in marine carbon isotopic compositions, i.e. increased organic productivity and burial of light organic carbon (e.g., Frank et al., 2003). A marine model is unlikely, as it is incompatible with other geochemical and sedimentologic data already discussed. A perennial saline lake model, as inferred from sedimentologic data, can also be used to explain observed changes in C and O isotope geochemistry. In a perennial saline lake model, the upward shift in isotopic composition

could be attributable to residence time and/or evaporation effects. The composition of lake water could have evolved over long residence times to heavy isotope enriched C and O values through evaporative loss of CO_2 from the system. CO_2 lost from the lake system would be depleted in ^{13}C and ^{18}O leading to enrichment of ^{13}C and ^{18}O in the residual water. Through repeated evaporative/recharge intervals the composition of the perennial lake water mass could have gradually become isotopically heavier. Lithofacies analysis supports increasingly evaporitic, shallower, depositional conditions upward. As such, upward changes in isotopic compositions may also be lithofacies controlled rather than recording longer term lake water evolution. Evidence for this comes from the observed changes in depositional environment from perennial saline deposits (red siltstone-dolostone lithofacies association) to ephmeral playa lake deposits (sheet sandstone lithofacies association) to restricted shoreline deposits (black chert-carbonate lithofacies association) and finally subaerial exposure though time representing a drying of the lake system. In such a model, evaporative loss of isotopically light CO_2 would have occurred more easily in hotter, shallower water settings leading to ^{13}C enrichments in more shore proximal settings. Camoin et al. (1997), Casanova and Marcell (1993) and Paz and Rosetti (in press) have all noted lithofacies dependant variations in C and O isotopic composition, particularly heavier isotopic compositions in shoreline settings or tops of shallowing upward cycles. Though evaporation is the primary physical control in both models, they are subtly different as the first model requires long residence times of carbon and oxygen in the lake to produce heavier isotopic compositions, while the second model only requires locally stronger evaporation in shallower, hotter depositional subenvironments. Large enrichments in ^{13}C found in some evaporitic lacustrine

carbonates (e.g., Valero-Garces et al., 1999) are not present, suggesting that extremely evaporitic conditions did not develop.

Increasing biologic sequestration of ^{12}C may have also controlled the stratigraphic trend towards more enriched $\delta^{13}C$ composition in a lacustrine model. However, as there is little evidence for burial of organic carbon in the red siltstone-dolostone lithofacies association, reoxidation of organic matter probably would have negated the fractionating effect of increased organic activity.

Overall, low $\delta^{34}S$ values for sulfates, generally high $^{87}Sr/^{86}Sr$ for both dolomite and sulfate, MREE enriched REE patterns and low Y/Ho ratios argue for a non-marine depositional environment for the red siltstone-dolostone lithofacies association. Observed upward increases in both $\delta^{13}C$ and $\delta^{18}O$ can also be explained using a lacustrine depositional model. Sedimentologic data, as well as isotope data, particularly $\delta^{13}C$ and $\delta^{18}O$, supports increasingly evaporitic conditions upward through the red siltstone to red siltstone-dolostone lithofacies associations. This is reflected by upward increases in $\delta^{13}C$, $\delta^{18}O$ and possibly $\delta^{34}S$ (Figs. 5.7 to 5.10). Sulfur isotope geochemistry may be reflecting increasing marine input through this stratigraphic interval or varying effects of sulfur reducing bacteria. However, a marine model is inconsistent with the majority of data and primarily oxidizing conditions probably limited sulfate reduction. As such, the upward trend towards heavier sulfur isotopic compositions is best explained by differences in the composition of sulfides that were weathering to supply sulfate to the basin.

5.5.4 Upper clastic unit

$\delta^{13}C$ values for apparently unaltered stromatolite samples from this unit are slightly more ^{13}C enriched than samples from the underlying units (Fig. 5.18). Again there is no major difference between observed $\delta^{13}C$ and seawater values (Fig. 5.1; Bartley and Kah, 2004). $\delta^{13}C$ values around 0-1 per mil are consistent with carbonate forming in equilibrium with atmospheric CO_2. Higher organic productivity and better preservation of organic carbon in the black chert lithofacies, may have been responsible for the slightly more ^{13}C-rich carbonate isotopic compositions relative to the majority samples in the underlying red siltstone-dolostone lithofacies association. Or, similar to the lithofacies dependant model for the isotopic variation in the underlying red siltstone-dolostone lithofacies association, heavier isotopic compositions could be reflecting more evaporitic conditions than those present in the underlying unit which lead to relatively greater loss of isotopically depleted CO_2 leaving residual waters,and hence precipitated carbonates, ^{13}C-enriched. The least altered $^{87}Sr/^{86}Sr$ analysis, based on the highest $\delta^{18}O$ value, is 0.70815 which is still considerably more radiogenic than proposed Mesoproterozoic seawater (Fig. 5.5; e.g., Sheilds and Veizer, 2002). These high $^{87}Sr/^{86}Sr$ ratios suggest a non-marine origin, or may reflect diagenesis. Again, like dolocretes from the lower siliciclastic unit, REE compositions for this unit have PAAS normalized patterns with some characteristics of seawater such as positive La and negative cerium anomalies. However, the seawater REE characteristics of HREE enrichment and high Y/Ho ratio are absent suggesting a non-marine depositional setting (Shields and Webb, 2004). The presence of a negative cerium anomaly is indicative of oxidizing conditions. Weathering related carbonate appear to be reflecting some contribution of isotopically

light, organic related carbon to soil CO_2, based on a slight shift towards isotopically light carbonate in pedogenic carbonate samples (Fig. 5.36; c.f., Cerling, 1991). This shift does not appear to relate to later diagenesis, as $\delta^{18}O$ is not shifted to lower values. Overall, geochemical data for stromatolitic and pedogenic carbonate from this unit support their restricted shoreline and subaerial weathering origins inferred from sedimentologic data.

5.5.5 Upper mixed siliciclastic-carbonate-evaporite unit

Sulfur isotope data for sulfates from this interval are ^{34}S enriched relative to the majority of samples from lower in the stratigraphy (Fig. 5.23) although samples from the upper red siltstone-dolostone lithofacies association have similar compositions. As the upward shift to heavier suflur isotope composition in the upper red siltstone-dolostone lithofacies association was interpreted to reflect a change in the composition of sulfides weathering to supply sulfate to the basin, a continued source of sulfate from weathering of similar sulfides derived from Paleoproterozoic rocks to the south may explain the ^{34}S compositions in this unit as well. Other possible explainations for the heavier sulfur isotope compositions are increased removal of ^{34}S depleted sulfur created during bacterial sulfate reduction or increased influence of seawater. Isotopically light H_2S produced during bacterial sulfate reduction may have been more easily lost from a largely subaerial mudflat environment compared to the perennial saline lake setting lower in the stratigraphy, however sulfate reduction itself is unlikely given the strongly oxidizing inferred depositional environment. Mixing of seawater with meteoric water is supported by a shift to less radiogenic Sr isotope ratios (Fig. 5.22) but not by other sedimentologic or geochemical data.

Carbon isotopic compositions for stromatolites and massive dolostones from this stratigraphic unit are the most ^{13}C enriched in the Sibley Group. This could be the result of increased organic activity and organic carbon preservation in this stratigraphic unit which would have removed ^{13}C depleted carbon from the water mass leaving it relatively ^{13}C enriched. However, there is no evidence for increased organic carbon burial in this unit and increased organic influence may have also created increased dissolved organic carbon in the water mass making it ^{12}C-rich instead. Alternatively, ^{13}C enriched compositions might again be reflecting the restricted, evaporitic depositional conditions represented by these lithofacies.

The single dolocrete analysis is ^{13}C depleted relative to stromatolite samples suggesting precipitation in the presence of isotopically lighter, organic related CO_2 in soil pores. The massive dolostone sample with a $\delta^{13}C$ of –1.4 ‰, is a clast from an intraformational conglomerate unit and probably represents a reworked clast of dolostone from the red siltstone-dolostone lithofacies association. This supports incorporation of clasts from lower stratigraphic units into intraformational conglomerates at higher stratigraphic levels. This also suggests a lack of large-scale alteration of isotopic compositions.

The PAAS normalized REE pattern for the stromatolite sample is similar to stromatolites from lower stratigraphic levels. Again the pattern has a positive La anomaly and a negative Ce anomaly but lacks the seawater characteristics of heavy REE enrichment and has a low Y/Ho ratio. The dolocrete nodule is enriched in MREE's and has a similar pattern to dolostones precipitating in the perennial lake system below it. The dolocrete may represent a groundwater-type dolocrete and groundwaters during the

deposition of the upper units may have had chemistries controlled by the composition of carbonates from lower units. However it is difficult to make inferences based on a single analysis. Further analyses of pedogenic carbonate from this unit are required.

5.6 Synopsis

The geochemical data presented in this chapter partially supports the depositional environments proposed in chapter 4. For the most part isotope data is consistent with a non-marine depositional setting for the portions of the Sibley Group that were studied. In particular, sulfur isotopic compositions and REE and Y geochemistry are distinctly different than would be expected for a Mesoproterozoic marine depositional setting. Sr isotopic compositions are also not consistent with seawater, though these may have been more easily shifted towards more radiogenic, non-marine compositions through meteoric diagenesis. Carbon and oxygen isotope data fall within the range of expected seawater values consistent with carbonate precipitiated in equilibrium with atmospheric carbon dioxide. Stratigraphic variations in $\delta^{13}C$ and $\delta^{18}O$ can be explained using either a marine or a non-marine depositional model. However, given evidence from other isotopic and REE data a non-marine depositional setting best fits the available data, particularly for the mixed siliciclastic-carbonate unit. In the upper mixed siliciclastic-carbonate-evaporite unit sulfur isotopic data and Sr isotopic data may reflect a mix of non-marine and marine waters. Though it is more likely that sulfur isotope data is reflecting the chemistry of sulfides that were weathering in the catchment.

Chapter 6. Conclusions

The aim of this thesis was to better understand the depositional environments of the Pass Lake and Rossport Formations of the Sibley Group, using lithofacies analysis and geochemical data. The primary conclusions of this study with respect to this objective are outlined below. First, conclusions from the lithofacies analysis are outlined, followed by those from geochemical data.

Based on the analysis of lithofacies associations and stratigraphy presented in chapters two, three and four, the following conclusions can be made:

1. The portions of the Sibley Group studied (lithostratigraphic Pass Lake and Rossport Formations) contain a variety of distinct lithofacies associations. These lithofacies associations can be divided into 4 informally defined allostratigraphic units which roughly correspond to existing lithostratigraphic subdivisions.
2. The lower clastic unit forms the base of the Sibley Group and contains the following lithofacies associations representing distinct depositional settings: boulder conglomerate-sandstone-dolocrete (proximal ephemeral braided streams), pebble to cobble conglomerate (ephemeral braided streams), trough cross-stratified sandstone (epemeral braided streams), massive cobble conglomerate (transgressive lag, reworking of braided stream deposits during lacustrine transgression), green sandstone-siltstone (wave and storm influenced fluvial dominated deltas) planar cross-stratified sandstone

(nearshore migration of large sandwaves), and thinning upward sandstone (beach and storm remobilized nearshore sandstone sheets).

3. The mixed siliciclastic-carbonate unit disconformably to conformably overlies the lower clastic unit and consists of the following lithofacies associations: red siltstone (non-saline lake), red siltstone-dolostone (perennial saline lake, distal from clastic sources) and red siltstone-dolomitic sandstone (perennial saline lake, proximal to clastic sources)
4. The upper clastic unit sharply overlies the mixed siliciclastic carbonate unit and consists of the sheet sandstone lithofacies association (ephemeral playa lake (?) or perennial lake with increased clastic supply with respect to underlying units), and the black chert-carbonate lithofacies association (shoreline). Interpreted subaerial exposure features are present at the top of the black-chert-carbonate lithofacies association and include the intraformational conglomerate lithofacies association (subaerial debris flows, intrusive and/or extrusive sedimentary breccias, terra rossa style soils, dissolution collapse breccias).
5. The mixed siliciclastic-carbonate-evaporite unit overlies the subaerial exposure surface at the top of the upper clastic unit. It consists of the massive dolostone (saline lake), the red siltstone-sulfate (wet evaporite-rich mudflats around lake margins) and the fine-grained sandstone (dry, evaporite poor mud and sand flats around lake margins) lithofacies associations.

Based on the stable isotope, Sr isotope and trace element data presented in chapter 5, the following conclusions can be made:

1. Overall, the geochemical data supports a non-marine origin for the Pass Lake and Rossport Formations.
2. Low Sr isotope ratios from dolocrete in the lower clastic unit indicates that weathering of old, radiogenic bedrock was not a major source of cations for these carbonates. It is possible that atmospheric deposition and weathering of Gunflint Formation carbonate bedrock was a major source of cations for pedogenic carbonate. Relatively ^{13}C-rich dolocrete carbon isotopic composition suggests little organic contribution to soil CO_2. REE geochemistry suggests dolocretes precipitated from oxidizing non-marine water.
3. S, Sr, REE and Y data for the mixed siliciclastic carbonate unit support a lacustrine origin for these rocks. Variations in S isotopic composition may be related to changes in the composition of sulfides weathering to supply sulfate to the system. MREE enriched PAAS normalized REE patterns for dolostone samples differ from those found in other carbonate lithofacies and this probably relates to more reducing conditions in lake waters relative to surface waters supplying the lake. Stratigraphic variations in C and O for this unit were created by evaporation and/or residence time effects.
4. Slightly enriched $\delta^{13}C$ and $\delta^{18}O$ values in the least altered samples from the upper siliciclastic unit and mixed siliciclastic-carbonate-evaporite unit reflect a generally shallower more evaporitic environment as compared to the mixed-

siliciclastic unit. Shifts toward lighter $\delta^{13}C$ in pedogenic carbonates from these units could reflect a contribution of dissolved organic carbon. Samples with relatively light $\delta^{13}C$ and $\delta^{18}O$ indicate diagenetic alteration. REE data for these units is consistent with a non-marine, oxidizing depositional setting.

References

Addison, W.D., Brumpton, G.R., Vallini, D.A., McNaughton, N.J., Davis, D.W., Kissin, S.A., Fralick, P.W. and Hammond, A.L. 2005. Discovery of distal ejecta from the 1850 Ma Sudbury impact event. Geology. 33: 193-196.

Alonzo-Zarza, A.M. 2003. Palaeoenvironmental significance of palustrine carbonates and calcretes in the geological record. Earth Science Reviews. 60: 261-298.

Alsharhan, A.S. and Kendall, C.G.St.C. 2003. Holocene coastal carbonates and evaporites of the southern Arabian Gulf and their ancient analogues. Earth-Science Reviews. 61: 191-243.

Amundson, R., Stern, L., Baisden, T. and Wray, Y. 1988. The isotopic composition of soil and soil-respired CO_2. Geoderma. 82: 83-114.

Anbar, A.D. and Knoll, A. H. 2002. Proterozoic ocean chemistry and evolution: a bioinorganic bridge? Science. 297: 1137–1142.

Andreason, M.W. 1992. Coastal siliciclastic sabkhas and related evaporitive environments of the Permian Yates Formation, North Ward-Estes Field, Ward County, Texas. The American Association of Petroleum Geologists Bulletin. 76: 1735-1759.

Angeles Garcia del Cura, M., Calvo, J.P., Ordonez, S., Jones, B.F. and Canaveras, J.C. 2001. Petrographic and geochemical evidence for the formation of primary, bacterially induced lacustrine dolomite: La Roda `white earth' (Pliocene, central Spain). Sedimentology. 48: 897-915.

Arnaud, E. 2004. Giant cross-beds in the Neoproterozoic Port Askaig Formation, Scotland: implications for snowball Earth. Sedimentary Geology. 165: 155-174.

Arnold, G. L., Anbar, A. D., Barling, J., and Lyons, T. W., 2004. Molybdenum isotope evidence for widespread anoxia in midproterozoic oceans. Science. 304: 87–90.

Ault, W.U. and Kulp, J.L. 1959. Isotopic geochemistry of sulphur. Geochimica et Cosmochimica Acta. 16: 201-235.

Baer, A.J. 1974. Grenville geology and plate tectonics. Geoscience Canada. 1: 54-60

Bailey, T.R., McArthur, J.M., Prince, H. and Thirwall, M.F. 2000. Dissolution methods for strontium isotope stratigraphy: whole rock analysis. Chemical Geology. 167: 313-319.

Blackburn, C.E., Johns, G.W., Ayer, J. and Davis, D.W. 1991. Wabigoon Subprovince. In: Geology of Ontario. Edited by Thurston, P.C., Williams, H.R., Sutcliffe, R.H. and Stott, G.M., Ontario Geological Survey Special Volume 4 (1). 303-381pp.

Bartley, J.K., Knoll, A.H., Grotzinger, J.P., Sergeev, V.N. 2000. Lithification and fabric genesis in precipitated stromatolites and associated peritidal carbonates, Mesoproterozoic Billyakh Group, Siberia. In: Grotzinger, J.P., James, N.P. (Eds.), Precambrian Carbonates, vol. 65. SEPM, Tulsa, OK, pp. 59–74.

Bartley, J.K., Kaufman, A.J., Semikhatov, M.A., Knoll, A.H., Pope, M.C., Jacobsen, S.B. 2001. Global events across the Mesoproterozoic-Neoproterozoic boundary: C and Sr isotopic evidence from Siberia. Precambrian Research. 111: 165–202.

Bartley, J.K. and Kah, L.C. 2004. Marine carbon reservoir, Corg-Ccarb coupling, and the evolution of the Proterozoic carbon cycle. Geology. 32: 129-132.

Battrum, D.D. 1975. Mineralogy and sedimentation in the Kama Hill Formation of the Sibley Group. Unpublished B.Sc thesis, Lakehead University, Thunder Bay, ON. 141pp.

Bau M. (1996) Controls on fractionation of isovalent trace elements in magmatic and aqueous systems: Evidence from Y/Ho, Zr/Hf, and lanthanide tetrad effect. Contributions to Mineralogy and Petrology. 123: 323-333.

Bau, M. and Dulski, P. 1996. REY and Nd isotope systematics of yttrium and rare-earth elements in the Penge and Kuruman iron-formations, Transvaal Supergroup, South Africa. Precambrian Research. 79: 37–55.

Bau, M. and Dulski, P. (1999) Comparing yttrium and rare earths in hydrothermal fluids from the Mid-Atlantic Ridge: Implications for Y and REE behaviour during near-vent mixing and for the Y/Ho ratio of Proterozoic seawater. Chemical Geology 155: 77-90.

Books, K.G. 1969. Magnetization of the lowermost Keweenawan lava flows in the Lake Superior area. United States Geological Survey, Professional Paper 600D. D248-D254pp.

Books, K.G. 1972. Paleomagnetism of some Lake Superior Keweenawan rocks. United States Geological Survey, Professional Paper 760. 42pp.

Borradaile, G.J. and Middleton, R.S. 2006. Proterozoic paleomagnetism in the Nipigon Embayment of northern Ontario: Pillar Lake Lava, Waweig Troctolite and Gunflint Formation tuffs. Precambrian Research. 144 (1-2): 69-91.

Blair, T.C. 1999a. Sedimentology of the debris-flow-dominated Warm Spring Canyon alluvial fan, Death Valley, California. Sedimentology. 46: 941-965.

Blair, T.C. 1999b. Sedimentary processes and facies of the waterlaid Anvil Spring Canyon alluvial fan, Death Valley, California. Sedimentology. 46: 913-940.

Bordy, E.M. and Catuneanu, O. 2001. Sedimentology of the upper Karoo fluvial strata in the Tuli Basin, South Africa. African Earth Sciences. 33-605-629.

Bottrell, S.H. and Newton, R.J. 2006. Reconstruction of changes in global sulfur cycling from marine sulfate isotopes. Earth Science Reviews. 75: 59-83.

Brasier, M.D. and Lindsay, J.F. 1998. A billion years of environmental stability and the emergence of eukaryotes: new data from northern Australia. Geology. 26: 555-558.

Brewer, R., 1964. Fabric and Mineral Analysis of Soils. Wiley, New York, 470 pp.

Bronger A, Bruhn-Lobin N (1997) Palaeopedology of Terrae rossae-Rhodoxeralfs from Quaternary calcarenites in NW Morocco. Catena. 28: 279-295.

Browne, K.M., Golubic, S. and Lee Seong-Joo. 2000. Shallow marine microbial carbonate deposits. In: Microbial sediments, edited by Riding, R. and Awramik, S.M. Springer-Verlag, Heidelberg. 233-249pp.

Buick, R., Des Marais, D., Knoll, A.H., 1995. Stable isotope compositions of carbonates from the Mesoproterozoic Bangemall Group, Australia. Chemical Geology. 123: 153-171.

Butler, B.E. 1956. Parna-An aeolian clay. Australian Journal of Science. 18: 145-151.

Butterfield, N.J., 2001. Paleobiology of the late Mesoproterozoic (ca. 1200 Ma) Hunting Formation, Somerset Island, arctic Canada. Precambrian Research. 111: 237–258.

Calvo, J.P., Jones, B.F., Bustillo, M., Fort, R., Alonzo Zarza, A.M. and Kendall, C. 1995. Sedimentology and geochemistry of carbonates from lacustrine sequences in the Madrid Basin, central Spain. Chemical Geology. 123: 173-191.

Cameron, E.M. 1983. Evidence from early Proterozoic anhydrite for sulphur isotope partitioning in Precambrian oceans. Nature. 304: 54–56.

Camoin, G., Casanova, J., Rouchy, J.M., Blanc-Valleron, M.M. and Deconinck, J.F. 1997. Environmental controls on perennial and ephemeral carbonate lakes: the Central Palaeo-Andean Basin of Bolivia during Late Cretaceous to early Tertiary times. Sedimentary Geology. 113: 1–26.

Campling, N.R. 1973. Some geological and environmental aspects of remnant pre-Gunflint and pre-Sibley weathered profiles. Unpublished B.Sc thesis, Lakehead University, Thunder Bay, ON. 43pp.

Canfield, D.E., 1998. A new model for Proterozoic ocean chemistry. Nature. 396: 450–453.

Canfield, D.E. 2004. The evolution of the earth surface sulfur reservoir. American Journal of Science. 304: 839-861.

Canfield, D. E., and Raiswell, R., 1999, The evolution of the sulfur cycle: American Journal of Science. 299: 697–723.

Canfield, D.E., Teske, A., 1996. Late Proterozoic rise in atmospheric oxygen concentration inferred from phylogenetic and sulphur-isotope studies. Nature. 382:127–132.

Capo, R.C. and Chadwick, O.A. 1999. Sources of strontium and calcium in desert soil and calcrete. Earth and Planetary Science Letters. 170: 61-72.

Card, K.D. 1990. A review of the Superior Province of the Canadian Shield, a product of Archean accretion. Precambrian Research. 48: 99-156.

Casanova, J. and Marcell, C.H., 1993. Carbon and oxygen isotopes in African lacustrine stromatolites: palaeohydrological interpretation. In: Climate Change in Continental Isotopic Record, edited by Swart, P.K., Lohmann, K.C., McKenzie, J., Savin, S. Geophysical Monograph, American Geophysical Union. 94: 123–133.

Cerling, T. E., 1984, The stable isotopic composition of modern soil carbonate and its relationship to climate. Earth and Planetary Science Letters 71: 229-240

Cerling, T. E., J. Quade, Y. Wang, and J.R. Bowman, 1989, Carbon isotopes in soils and paleosols as ecologic and paleoecologic indicators. Nature 341: 138-139.

Cerling, T. E., 1991, Carbon dioxide in the atmosphere: evidence from Cenozoic and Mesozoic paleosols. American Journal of Science 291: 377-400.

Cerling, T. E., 1992, Use of carbon isotopes in paleosols as an indicator of the $P(CO_2)$ of the paleo-atmosphere. Global Biogeochemical Cycles 6: 307-314.

Chambers, L.A. and Trudinger, P.A., 1979. Microbiological fractionation of stable sulfur isotopes: a review and critique. Geomicrobiology Journal. 1: 249–293.

Cheadle, 1981. The stratigraphy and depositional history of the Rossport Formation stratotype, Channel Island, Thunder Bay District, Ontario. Unpublished H.B.Sc thesis, Lakehead University, Thunder Bay, ON. 46pp.

Cheadle, B.A. 1986a. Alluvial-playa sedimentation in the lower Keweenawan Sibley Group, Thunder Bay district, Ontario. Canadian Journal of Earth Sciences 23: 527-542.

Cheadle, B.A. 1986b. Stratigraphy and sedimentology of the middle Proterozoic Sibley Group, Thunder Bay District, Ontario. Unpublished Ph.D thesis, University of Western Ontario, London. 434pp.

Chiquet, A., Michard, A., Nahon, D. and Hamelin, B. 1999. Atmospheric input vs in situ weathering in the genesis of calcretes: An Sr isotope study at Ga'lvez (Central Spain). Geochimica et Cosmochimica Acta. 63: 311-323.

Chivas, A.R., De Deckker, P., Cali, J.A., Chapman, A., Kiss, E. and Shelley, M.G. 1993. Coupled stable-isotope and trace-element measurements of lacustrine carbonates as paleoclimatic indicators. In: Climate change in continental isotopic records, edited by Swart, P.K., Lohmann, K.C., McKenzie, J. and Savin, S., Geophysical Monograph 78. 113-121pp.

Clauer, N. 1981. Rb-Sr and K-Ar dating of Precambrian clays and glauconies. Precambrian Research. 15: 331-352.

Claypool, G.E., Holser, W.T., Kaplan, I.R., Sakai, H. and Zak, I. 1980. The age curve of sulfur and oxygen isotopes in marine sulfates and their mutual interpretation. Chemical Geology. 28; 199-260.

Coates 1972. Geology of the Black Sturgeon River area, District of Thunder Bay. Ontario Department of Mines and Northern Affairs, Geological Report 98. 41pp.

Croke, J.C., Magee, J.M. and Price, D.M. 1998. Stratigraphy and sedimentology of the lower Neales River, West Lake Eyre, central Australia: from Paleocene to Holocene. Paleogeography, Paleoclimatology, Paleoecology. 144: 331-350.

Davis, D.W. and Sutcliffe, R.H. 1985. U-Pb ages from the Nipigon Plate and northern Lake Superior. Geological Society of America Bulletin. 96: 1572-1579.

De Deckker, P. and Last, W.M. 1989. Modern, non-marine dolomite in evaporitic playas of western Victoria, Australia. Sedimentary Geology. 64: 223-238.

Derry, L.A., Kaufman, A.J., Jacobsen, S.B., 1992. Sedimentary cycling and environmental change in the late Proterozoic: evidence from stable and radiogenic isotopes. Geochimica et Cosmochima Acta. 56: 1317–1329.

Des Marais, D.J., Strauss, H., Summons, R.E., Hayes, J.M. 1992. Carbon isotope evidence for the stepwise oxidation of the Proterozoic environment. Nature. 359: 605–609.

Ekart, D. D., Cerling, T. E. I. Montanez, and N. Tabor, 1999, A 400 million year carbon isotope record of pedogenic carbonate: Implications for atmospheric carbon dioxide. American Journal of Science. 299: 805-817.

Elderfield, H., Pagett, R., 1986. Rare Earth elements in Ichthyoliths: variations with redox conditions and depositional environment. In: Riley, J.P. (Ed.), Sciences of the Total Environment. 49: 175–197.

Elliot, T. 1974. Interdistributary bay sequences and their genesis. Sedimentology. 21: 611-622.

Emrich, K., Ehhalt, D.H. and Vogel, J.C. 1970. Carbon isotope fractionation during the precipitation of calcium carbonate. Earth and Planetary Science Letters. 8: 363-371.

Eriksson, P.G., Condie, K.C.,Tirsgaard, H., Mueller, W.U., Altermann, W., Miall, A.D., Aspler, L.B., Catuneanu, O. and Chiarenzelli. J.R. 1998. Precambrian clastic sedimentation systems. Sedimentary Geology. 120: 5-53.

Esteban, M., Klappa, C.F., 1983. Subaerial exposure environments. In: Carbonate Depositional Environments. Edited by Scholle, P.A., Bebout, D.G., Moore, C.H. American Association of Petroleum Geologists Memoir vol. 33. Tulsa. 1–96pp.

Eugster, H.P. and Kelts, K. 1983. Lacustrine chemical sediments. In: Chemical Sediments and Geomorphology. Edited by: Goudie, A.S. and Pye, K., Academy Press, London. 321-368pp.

Faure, G. 1986. Principles of isotope geology, second edition. Wiley, New York. 589pp.

Faure and Mensing 2005. Isotopes: principles and applications, third edition. Wiley, New Jersey. 897pp.

Felitsyn, S., Sturesson, U., Popov, L. and Holmer, L., 1998. Nd isotope composition and rare earth element distribution in early Paleozoic biogenic apatite from Baltoscandia: a signature of Iapetus ocean water. Geology. 26: 1083– 1086.

Frank, T.D., Kah, L.C. and Lyons, T.W. 2003. Changes in organic matter production and accumulation as a mechanism for isotopic evolution in the Mesoproterozoic ocean: Geological Magazine. 140: 373-396.

Franklin, J.M. 1978. The Sibley Group, Ontario. In: Rubidium-strontium isotopic age studies Report 2, edited by Wanless, R.K. and Loveridge, W.D., Geological Survey of Canada Paper, 77-14: 31-34pp.

Franklin, J.M. and Mitchell, R.H. 1977. Lead-zinc-barite veins of the Dorion area, Thunder Bay district, Ontario. Canadian Journal of Earth Sciences. 14: 1963-1979.

Franklin J.M., McIlwaine W.H., Poulsen K.H. and Wanless R.K. 1980. Stratigraphy and depositional setting of the Sibley Group, Thunder Bay district, Ontario, Canada. Canadian Journal of Earth Sciences. 17: 633-651.

Fralick, P.W. and Barrett, T.J. 1995. Depositional controls on iron formation associations in Canada. In: Sedimentary facies analysis, edited by Plint, A.G. International Association of Sedimentologists, Special Publication. 22: 137-156.

Fralick, P.W., Davis, D.W. and Kissin, S.A. 2002. The age of the Gunflint Formation, Ontario, Canada: single zircon U–Pb age determinations from reworked volcanic ash. Canadian Journal of Earth Sciences. 39: 1085–1091.

Gellatly, A.M., Lyons, T.W., 2005. Trace sulfate in mid-Proterozoic carbonates and the sulfur isotope record of biospheric evolution. Geochimica et Cosmochimica Acta. 69: 3813–3829.

German, C.R. and Elderfield, H., 1990. Application of the Ce anomaly as a paleoredox indicator: the ground rules. Paleoceanography. 5: 823– 833.

Giguere, J.F. 1975. Geology of St. Ignace Island and Adjacent Islands, District of Thunder Bay. Ontario Department of Mines, Geoscience Report 119. 35pp. Accompanied by Map 2285, 1 inch to 1 mile.

Gile, L.H., Peterson, F.F. and Grossman, R.B. 1966. Morphological and genetic sequences of carbonate accumulation in desert soils. Soil Science. 101: 347-360.

Grandjean, P., Cappetta, H., Michard, A., Albarede, F., 1987. The assessment of REE patterns and $^{143}Nd/^{144}Nd$ ratios in fish remains. Earth and Planetary Science Letters. 84: 181– 196.

Grandjean, P., Cappetta, H., Albare`de, F., 1988. The REE and εNd of 40– 70 Ma old fish debris from the West-African platform. Geophysical Research Letters. 15: 389– 392.

Grandjean-Lecuyer, P., Feist, R. and Albarede, F., 1993. Rare earth elements in old biogenic apatites. Geochimica et Cosmochimica Acta. 57: 2507–2514.

Grotzinger, J.P and Knoll, A.H. 1999. Stromatolites in Precambrian carbonates: evolutionary mileposts or environmental dipsticks. Annual Reviews of Earth and Planetary Science. 27: 313-358.

Gruau, G., Dia, A., Olivie-Lauquet, G., Davranche, M. and Pinay. G. 2004. Controls on the distribution of rare earth elements in shallow groundwaters. Water Research. 38: 3576–3586

Habicht, K.S. and Canfield, D.E. 1996. Sulphur isotope fractionation in modern microbial mats and the evolution of the sulphur cycle. Nature. 382: 342–343.

Hanford, C.R., Kendall, A.C., Prezbindowski, D.R., Dunham, J.B. and Logan, B.W. 1984. Salina-margin tepees, pisoliths, and aragonite cements, Lake MacLeod, Western Australia: their significance in interpreting ancient analogs. Geology. 12: 523-527.

Hanly, A.J. 2005. The uranium mineralization potential and diagenetic fluid histories of the Proterozoic Yeneena, Sibley and Sioux basins. Unpublished Ph.D thesis, Queens University, Kingston Ontario. 295pp.

Hannigan, R.E. and Sholkovitz, E.R. 2001. The development of middle rare earth element enrichments in freshwater: weathering of phosphate minerals. Chemical Geology. 175: 495-508.

Hardie, L.A. 1968. The origin of recent non-marine evaporite deposits of Saline Valley, Inyo County, California. Geochimica et Cosmochimca Acta. 32: 1279-1301.

Hardie, L.A., Smoot, J.P. and Eugster, H.P. 1978. Saline lakes and their deposits: a sedimentological approach. In: Modern and ancient lake sediments, edited by Matter, A. and Tucker, M.E. International Association of Sedimentologists, Special Publication 2. 7-41pp.

Harrison A.G. and Thode, H.G. 1958. Mechanism of the bacterial reduction of sulphate from isotope fractionation studies. Transactions of the Faraday Society. 54: 84–92.

Hart, T.R. 2005. Project unit 05-002. Lake Nipigon Synthesis. Ontario Geological Survey, Summary of Field Work and Other Activities 2005, Open File Report 6172, p.12-1 to 12-6.

Heaman, L.M. and Easton, R.M. 2005. Proterozoic history of the Lake Nipigon area, Ontario: Constraints from U-Pb zircon and baddeleyite dating. Part 1 Proceedings and Abstracts, 51st Annual Meeting, Institute on Lake Superior Geology, Nipigon Ontario. 51: 23-24.

Heaman, L.M. and Easton, R.M. 2006. Preliminary U-Pb geochronology results from the Lake Nipigon Region Geoscience Initiative; Ontario Geological Survey, Miscellaneous Release—Data 191, 1 CD-ROM.

Hofmann, H.J. 1969. Stromatolites from the Proterozoic Animikie and Sibley Groups, Ontario. Geological Survey of Canada, Paper 68-69. 77 p.

Hofmann, H.J. 1973. Stromatolites: characteristics and utility. Earth Science Reviews. 9: 339-373.

Holland, H.D. 1984. The chemical evolution of the atmosphere and oceans. Wiley, New York.

Hollings, P., Fralick, P.W. and Kissin, S.K. 2004. Geochemistry and geodynamic implications of the Mesoproterozoic English Bay granite–rhyolite complex, northwestern Ontario. Canadian Journal of Earth Science. 41: 1329-1338.

Hollings, P., Fralick, P. and Cousens, B., 2006. Geochemistry and sedimentology of the Osler Group: Evaluating rifting in the Proterozoic. Canadian Journal of Earth Sciences. Submitted.

Jacobsen, S.B. and Kaufman, A.J., 1999. The Sr, C and O isotopic evolution of Neoproterozoic seawater. Chemical Geology. 161: 37-57.

Kah, L.C., Sherman, A.G., Narbonne, G.M., Knoll, A.H., Kaufman, A.J., 1999. $\delta^{13}C$ isotope stratigraphy of the Mesoproterozoic Bylot Supergroup, northern Baffin Island: implications for regional lithostratigraphic correlations. Canadian Journal of Earth Sciences. 36: 313–332.

Kah, L.C., Lyons, T.W. and Chelsey, J.T. 2001. Geochemistry of a 1.2 Ga carbonate-evaporite succession, northern Baffin and Bylot Islands: implications for Mesoproterozoic marine evolution. Precambrian Research. 111: 203-234.

Karhu, J. A. and Holland, H. D. 1996. Carbon isotopes and the rise in atmospheric oxygen. Geology. 24: 867–870.

Kaplan I.R. and Rittenberg, S.C. 1964. Microbiological fractionation of sulphur isotopes. Journal of General Microbiology. 34: 195–212.

Kaufman, A.J. and Knoll, A.H. 1995. Neoproterozoic variations in the C-isotopic composition of seawater: stratigraphic and biogeochemical implications. Precambrian Research. 73: 27-49.

Kaufman, A.J., Knoll, A.H. and Narbonne, G.M. 1997. Isotopes, ice ages,and terminal Proterozoic earth history. Proceedings National Academy of Science. 95: 6600-6605.

Kendall, C. and Doctor, D.H. 2005. Stable isotope applications in hydrologic studies. In: Surface and ground water, weathering and soils (edited by Drever, J.J.), volume 5, Treatise on Geochemistry, edited by Holland, H.D. and Turekian, K.K., Elsevier-Pergamon, Oxford. 319-364pp.

Knoll, A.H., 1992. Biological and biogeochemical preludes to the Ediacaran radiation. In: Lipps, J.H., Signor, P.W. (Eds.), Origin and Early Evolution of the Metazoa. Plenum Press, New York, pp. 53–84.

Koncurek, G. and Fielder, G. 1982. Adhesion structures. Journal of Sedimentary Petrology. 52: 1229-1241.

Kump, L.R. and Arthur, M.A. 1999. Interpreting carbon-isotope excursions: carbonates and organic matter. Chemical Geology. 161:181-198.

Last, W.M. 1990. Lacustrine Dolomite: An Overview of Modern, Holocene, and Pleistocene Occurrences. Earth Sciences Reviews. 27: 221-263.

Last, W.M. 2002. Geolimnology of salt lakes. Geosciences Journal. 6: 347-369.
Lohmann, K.C. and Walkerm J.C.G. 1989. The $\delta^{18}O$ record of Phanerozoic abiotic marine calcite cements. Geophysical Research Letters. 16: 319-322.

Lu, F.H. and Meyers, W.J. 2003. Sr, S and O_{SO_4} isotopes and the depositional environments of the upper Miocene Evaporites, Spain. Journal of Sedimentary Research. 73: 444-450.

MacDonald, C.A. 2004. Precambrian Geology of the South Armstrong-Gull Bay Area, Nipigon Embayment, Norhtwestern Ontario. Ontario Geological Survey, Open File Report 6136. 42pp.

Machette, M.N. 1985. Calcic soils of southwestern United States. In: Soil and Quaternary Geology of the Southwestern United States. Edited by Weide, D.L., Special Paper, Geological Society of America. 203: 1-21pp.

Mack, G.H., Cole, D.R. and Trevino, L. 2000. The distribution and discrimination of shallow authigenic carbonate in the Pliocene-Pleistocene Palomas Basin, southern Rio Grande rift. Geological Society of America Bulletin. 112: 643-656.

Mailman, M.1999. Laminated dolomite and shale in the Rossport Formation of Northwestern Ontario: a paleoclimatic study. Unpublished H.B.Sc thesis, Lakehead University, Thunder Bay, ON. 46pp.

Maric, M. 2006. Sedimentology and Sequence Stratigraphy of the Paleoproterozoic Rove and Virginia Formations, Southwest Superior Province. Unpublished MSc thesis, Lakehead University, Thunder Bay ON.

Mazzulo, J., Malicise, A. and Siegel, J. 1991. Facies and depositional environments of the Shattuck Sandstone on the northwest shelf of the Permian Basin. Journal of Sedimentary Petrology. 61: 940-958.

McCormick, D.S. and Grotzinger, J.P. 1993. Distinction of marine from alluvial facies in the Paleoproterozoic (1.9 Ga) Burnside Formation, Kilohigok basin, NWT; Canada. Journal of Sedimentary Petrology. 63: 398-419

McGowen, J.H. and Groat, C.G. 1971. Van Horne Sandstone, West Texas: an Alluvial Fan Model for Mineral Exploration. Bureau of economic geology., Report of Investigations, vol. 72. Austin. 57pp.

Mckenzie, D. 1978. Some remarks on the development of sedimentary basins. Earth and Planetary Science Letters. 40: 25-32.

McIlwaine, W.H. 1971a. McTavish Township (west part of north half), District of Thunder Bay, Ontario Department of Mines and Northern Affairs, Preliminary Geological Map, P721.

McIlwaine, W.H. 1971b. McTavish Township (east part of north half), District of Thunder Bay, Ontario Department of Mines and Northern Affairs, Preliminary Geological Map, P721.

McIlwaine, W.H. 1975. McTavish Township (south half), District of Thunder Bay, Ontario Department of Mines and Northern Affairs, Preliminary Geological Map, P990.

McTanish, G.H. 1989. Quaternary aeolian dust processes and sediments in the Australian region. Quaternary Science Reviews. 8: 235-253.

Marriott, S.B. and Wright, V.P. 2004. Mudrock deposition in an ancient dryland system: Moor Cliffs Formation, Lower Old Red Sandstone, southwest Wales, UK. Geological Journal. 39: 277-298.

Medaris, L.G. Jr., Singer, B.S., Dott, R.H. Jr, Naymark, A., Johnson, C.M. and Schott, R.C. 2003. Late Paleoproterozoic climate, tectonics, and metamorphism in the southern Lake Superior region and proto-North America: evidence from Baraboo interval quartzites. Journal of Geology. 111: 243-257.

Melezhik, V.A., Fallick, A.E., Medvedeev, P.V. and Makarikhin, V.V. 1999. Extreme $^{13}C_{carb}$ enrichment in ca. 2.0 Ga magnesite-stromatolite-dolomite-red beds association in a global context: a case for the world-wide signal enhanced by a local environment. Earth Science Reviews. 48: 71-120.

Melezhik, V.A., Gorokhov, I.M., Kuznetsov, A.B. and Fallick, A.E. 2001. Chemostratigraphy of Neoproterozoic carbonates: implications for "blind dating". Terra Nova. 13: 1-11.

Metsaranta, R.T. and Fralick, P.W. 2004. Lake Nipigon Region Geoscience Initiative. Stratigraphy of the Sibley Group and its Relationship to Sedimentary Units of the Basal Osler Group and the Nipigon Sills. Summary of Fieldwork and Other Activities 2004, Ontario Geological Survey, Open File Report 6145. p50-1 to 50-5.

Miall, A.D. 1996. The geology of fluvial deposits: sedimentary facies, basin anlysis, and petroleum geology. Springer-Verlag. Berlin. 551pp.

Mohr, P. 1982. Musings on continental rifts. In: Continental and oceanic rifts, edited by Palmason, G. American Geophysical Union, Geodynamics Series. 8: 293-309.

Muller, G., Irion, G. and Forstner, U. 1972. Formation and diagenesis of inorganic Ca-Mg carbonates in the lacustrine environment. Naturwissenschaften. 59: 158-164.

Naiman, Z., Quade, J. and Patchett, J.P. 2000. Isotopic evidence for eolian recycling of pedogenic carbonate and variations in carbonate dust sources throughout the southwest United States. Geochimica et Cosmochimica Acta. 64: 3099-3109.

Negrel, P., Casanova, J. and Brulhet, J. 2006. REE and Nd isotope stratigraphy of a Late Jurassic carbonate platform, eastern Paris Basin, France. Journal of Sedimentary Research. 76:

Nemec, W. and Steel, R.J. 1984. Alluvial and coastal conglomerates: Their significant features and some comments on gravelly mass-flow deposits. In: Sedimentology of Gravels and Conglomerates, edited b Koster, E.H. and Steel, R.J. Canadian Society of Petroleum Geologists Memoir 10. 1-31pp.

Nielsen, H., 1978. Sulphur isotopes. In: Handbook of Geochemistry, edited by Wedepohl, K.H., Springer-Verlag, Berlin Heidelberg, New York. 16-B-1–16-B-40pp.

Nozaki Y., Zhang J., and Amakawa, H. 1997. The fractionation between Y and Ho in the marine environment. Earth and Planetary Science Letters. 148: 329–340.

Nothdurft, L.D., Webb, G.E. and Kamber, B.S. 2004. Rare earth element geochemistry of Late Devonian reefal carbonates, Canning Basin, Western Australia: confirmation of a seawater REE proxy in ancient limestones. Geochimica et Cosmochimica Acta. 68: 263-283.

Nriagu, J.O., Rees, C.E., Mekhtiyeva, V.L., Lein, A.Yu, Fritz, P., Drimmie, R.D., Pankina, R.G., Robinson, R.W. and Krouse, H.R. 1991. Hydrosphere. In: Stable Isotopes: Natural and anthropogenic sulphur in the environment, Scope 43, edited by Krouse, H.R. and Grineko, V.A., John Wiley and Sons. Chichester. 177-265pp.

Ohmoto, H., 1992. Biogeochemistry of sulphur and the mechanisms of sulphide–sulphate mineralization in Archaean oceans. In: Early OrganicEvolution, edited by Schidlowski, M., Golubic,S., Kimberley, M.M., McKirdy, D.M. and Trudinger, P.D., Springer-Verlag, Berlin, Heidelberg, New York. 378–397pp.

Ojakangas, R., Morey, G.B. and Southwick, D.L. 2001. Paleoproterozoic basin development and sedimentation in the Lake Superior region, North America. Sedimentary Geology. 141-142: 319-341.

Olsen, H. 1987. Ancient ephemeral stream deposits: a local terminal fan model from the Bunter Sandstone Formation (L. Triassic) in the Tronder-3, -4 and –5 wells, Denmark. In: Desert Sediments Ancient and Modern, edited by Frostick, L.E. and Reid, I. Special Publication geological Society of London, 35. 69-86pp.

Paz, J.D.S. and Rosetti, D.F. 2006 (in press). Paleohydrology of an Upper Aptian lacustrine system from northeastern Brazil: Integration of facies and isotopic geochemistry. Palaeogeography, Palaeoclimatology, Palaeoecology. xx: xxx–xxx.

Picard, S., Lecuyer, C., Barrat, J.-A., Garcia, J.-P., Dromart, G. and Sheppard, S.M.F., 2002. Rare earth element contents of Jurassic fish and reptile teeth and their potential relation to seawater composition (Anglo-Paris Basin, France and England). Chemical Geology. 186: 1 – 16.

Pufahl, P.K. 1996. Stratigraphic architecture of a Paleoproterozoic iron formation depositional system: the Gunflint, Mesabi and Cuyuna iron ranges. Unpublished MSc thesis, Lakehead University, Thunder Bay ON. 152 pp.

Pufahl, P.K. and Fralick, P.W., 2004. Depositional controls on Paleoproterozoic iron formation accumulation, Gogebic Range, Lake Superior Region, USA. Sedimentology. 51: 791-808.

Pulham, A.J. 1989. Controls on internal structure and architecture of sandstone bodies within Upper Carboniferous fluvial-dominated deltas, County Clare, western Ireland. In: Deltas: sites and traps for fossil fuels, edited by, Whateley, M.K.G. and Pickering, K.T. Special Publication Geological Society of London, 41. 179-203pp.

Quade, J., Cerling, T. E. and Bowman, J. R. 1989. Systematic variations in the carbon and oxygen isotopic composition of pedogenic carbonate along elevation transects in the southern Great Basin, USA. Geological Society of America Bulletin. 101: 464-475.

Quade J., Chivas A. R., and McCulloch M. T. 1995. Strontium and carbon isotope tracers and the origins of soil carbonate in South Australia and Victoria. Palaeogeography, Palaeoclimatology, Palaeoecology. 113: 103–117.

Rainbird, R.H. 1992. Anatomy of a large-scale braid-plain quartzarenite from the Neoproterozoic Shaler Group, Victoria Island, Northwest Territories, Canada. Canadian Jounal of Earth Sciences. 29: 2537-2550.

Ray, J.S., Veizer, J. and Davis, W.J. 2003. C, O, Sr and Pb isotope systematics of carbonate sequences of the Vindhyan Supergroup, India: age, diagenesis, correlations and implications for global events. Precambrian Research. 121: 103-140.

Reading, H.G. and Collinson, J.D. 1996. Clastic coasts. In: Sedimentary Environments: processses, facies and stratigraphy, edited by Reading, H.G. 3rd edition. Blackwell Science. Oxford. 154-231pp.

Reinhardt, L and, Ricken, W. 2000. The stratigraphic and geochemical record of Playa Cycles: monitoring a Pangaean monsoon-like system (Triassic, Middle Keuper, S. Germany). Palaeogeography, Palaeoclimatology, Palaeoecology 161: 205–227

Retallack, G.J. 2001. A 300 million year record of atmospheric CO_2 from fossil plant cuticles. Nature. 411: 287-290.

Retallack, G.J. 2002. Carbon dioxide and climate over the past 300 Myr. Philosophical Transactions of the Royal Society of London. A360: 659-674.

Riding, R.R. 2000. Microbial carbonates: the geological record of calcified bacterial-algal mats and biofilms. Sedimentology. 47:179-214.

Rivers, T., and Corrigan, D. 2000. Convergent margin on southeastern Laurentia during the Mesoproterozoic; tectonic implications. Canadian Journal of Earth Sciences. 37: 359–383.

Robertson, W.A. 1973. Pole position from thermally cleaned Sibley group sediments and its relevance to Proterozoic magnetic stratigraphy. Canadian Journal of Earth Sciences. 10: 180-193.

Rogala, B. 2000. A metamorphosed evaporite sequence from the Sibley Basin. Unpublished H.B.Sc thesis, Lakehead University, Thunder Bay, ON. 38pp.

Rogala, B. 2003. The Sibley Group: a lithostratigraphic, geochemical, and paleomagnetic study. Unpublished MSc thesis, Lakehead University, Thunder Bay ON. 254 pp.

Rogala, B., Fralick, P.W. and Metsaranta, R.T. 2005. Stratigraphy and sedimentology of the Mesoproterozoic Sibley Group and related igneous intrusions, northwestern Ontario: Lake Nipigon Region Geoscience Initiative; Ontario Geological Survey, Open File Report 6174. 128p.

Rogala, B., Fralick, P.W., Heaman, L. and Metsaranta, R.T. 2006. Lithostratigraphy and chemostratigraphy of the Mesoproterozoic Sibley Group, Northwestern Ontario, Canada. Submitted to Canadian Journal of Earth Sciences.

Romanek, C.S., Grossman, E.L. and Morse, J.W. 1992. Carbon isotope fractionation in synthetic aragonite and calcite: effects of temparature and precipitation rate. Geochimica et Cosmochimica Acta. 56: 419-430.

Rosen, M.R. 1994. The importance of groundwater in playas: a review of playa classifications and the sedimentology and hydrology of playas. In: Paleoclimate and basin evolution of playa systems, edited by Rosen, M.R. Geological Society of America Special Paper 289. Boulder, Colorado. 1-18pp.

Royer, D.L. 1999. Depth to pedogenic carbonate horizon as a paleoprecipitation indicator? Geology. 27: 1123-1126.

Rust, B.R. 1978. Depositional models for braided alluvium. In: Fluvial Sedimentology, edited by Miall, A.D. Canadian Society of Petroleum Geologists Memoir. 5: 605-625.

Salvany, J.M., Munoz, A. and Perez, A. 1994. Non-marine evaporitic sedimentation and associated diagenetic processes of the southwestern margin of the Ebro Basin (Lower Miocene), Spain. Journal of Sedimentary Research. 64: 190-203.

Schieber J. 1988. Redistribution of rare-earth elements during diagenesis of carbonate rocks from the mid-Proterozoic Newland Formation, Montana, U.S.A. Chemical Geology. 69:111–126.

Semikhatov, M.A., Gorokhov, I.M., Kuznetsov, A.B. et al., 1998. The strontium isotopic composition in early Late Riphean seawater: Limestones of the Lakhanda Group, the Uchur-Maya region, Siberia. Transactions (Doklady) Russian Academy of Science, Earth Science Section. 360: 488-492.

Shanley, J. B., Pendall, E, Kendall, C., Stevens, L.R., Michel, R.L., Phillips, P.J., Forester, R.M., Naftz, D.L., Liu, B., Stern, L., Wolfe, B., Chamberlain, C.P., Leavitt, S.W., Heaton, T.H.E., Mayer, B., Cecil, L.D., Lyons, W.B., Katz, B.G., Betancourt, J.L., McKnight, D.M., Blum, J.D., Edwards, T.W.D., House, H.R., Ito, E., Aravena, R.O., Whelan, J.F. 1998. Isotopes as indicators of environmental change. In: Isotope Tracers in Catchment Hydrology. Edited by In Kendall, C. and McDonnell, J.J. Elsevier Science, New York. 761–816pp.

Shields, G.Aa and Webb, G.E. 2004. Has the REE composition of seawater changed over geological time? Chemical Geology. 204: 103-107.

Shen, Y., Knoll, A. H. and Walter, M. R. 2003. Evidence for low sulphate and anoxia in a mid-Proterozoic marine basin. Nature. 423: 632–635.

Shields, G., Veizer, J., 2002. Precambrian marine carbonate isotope database: version 1.1. Geochemistry, Geophysics, Geosystems. 3: U1–U12.

Sholkovitz, E. and Shen, G.T. 1995. The incorporation of rare earth elements in modern coral. Geochimica et cosmochimica acta. 59: 2749-2756.

Spotl, C. and Wright, V.P. 1992. Groundwater dolocretes from the Upper Triassic of the Paris Basin, France: a case study of an arid, continental diagenetic facies. Sedimentology. 39: 1119-1136.

Stear, W.M. 1985. Comparison of bedform distribution and dynamics of modern and ancient sandy ephemeral flood deposits in the southwestern Karoo region, South Africa. Sedimentary Geology. 45: 209-230.

Steel, R.J. and Thompson, D.B. 1983. Structures and textures in Triassic braided stream conglomerates ("Bunter" Pebble Beds) in the Sherwood Sandstone Group, North Stratffordshire, England. Sedimentology. 30: 341-367.

Stewart B. W., Capo R. C., and Chadwick O. A. (1998) Quantitative strontium isotope models for weathering, pedogenesis and biogeochemical cycling. In Biogeochemistry of isotopes in soil environments: Theory and application, edited by: Nordt, L.C., Kelly, E.F., Boutton, T.W. and Chadwick, O.A.. Geoderma 82: 173–195..

Strauss, H., 1999. Geological evolution from isotope proxy signals-sulphur. Chemical Geology. 161: 89–101.

Sumner, D.Y. and Grotzinger, J.P. 2004. Implications for Neoarchaean ocean chemistry from primary carbonate mineralogy of the Campbellrand-Malmani Platform, South Africa. Sedimentology. 51: 1273-1299.

Svendsen, J., Stollhofen, H., Krapf, C.B.E., and Stanistreet, I.G. 2003. Mass and hyperconcentrated flow deposits record dune damming and catastrophic breakthrough of ephemeral rivers, Skeleton Coast Erg, Namibia. Sedimentary Geology. 160: 7-31.

Talbot, M.R. 1990. A review of the paleohydrological interpretation of carbon and oxygen isotopic ratios in primary lacustrine carbonates. Chemical Geology. 80: 261-279.

Talbot, M.R., Holm, K. and Williams, M.A.J. 1994. Sedimentation in low-gradient desert margin systems: a comparison of the Late Triassic of northwest Somerset (England) and the late Quaternary of east-central Australia. In: Paleoclimate and basin evolution of playa systems, edited by Rosen, M.R., Geological Society of America Special Paper 289. Boulder, Colorado. 97-177pp.

Taylor, S.R. and McLennan, S.M. 1985. The Continental Crust; Its composition and evolution; an examination of the geochemical record preserved in sedimentary rocks. Blackwell, Oxford. 312pp.

Talma, A.S. and Netterberg, F. 1983. Stable isotopic abundances in calcretes. In: Residual deposits: surface related weathering processes and materials, edited by Wilson, R.C.L., Geological Society London, Special Publication volume 11. Blackwell, Oxford. 221-233pp.

Thode, H.G., Monster, J., 1965. Sulfur isotope geochemistry of petroleum, evaporites and ancient seas. Memoir-American Association of Petroleum Geologists. 4: 367–377.

Thode, H.G., Monster, J., Dunford, H.B., 1961. Sulphur isotope geochemistry. Geochimica et Cosmochimica Acta. 25: 159–174.

Ulicny, D. 2001. Depositional systems and sequence stratigraphy of coarse-grained deltas in a shallow-marine, strike-slip setting: the Bohemian Cretaceous Basin, Czech Republic. Sedimentology. 48: 599-628.

Valero-Garces, B.L., Delgado-Huertas, A., Ratto, N and Navas, A. 1999. Large ^{13}C enrichment in primary carbonates from Andean Altiplano lakes, northwest Argentina. Earth and Planetary Science Letters. 171: 253-266.

Valero-Garces, B.L., Delgado-Huertas, A., Ratto, N, Navas, A. and Edwards, L. 2000. Paleohydrology of Andean saline lakes from sedimentological and isotopic records, northewestern Argentina. Journal of Paleolimnology. 24: 343-359.

Valero-Garcés, B.L., Arenas, C. and Delgado-Huertas, A. 2001. Depositional environments of Quaternary lacustrine travertines and stromatolites from high-altitude Andean lakes, northwestern Argentina. Canadian Journal of Earth Sciences. 38: 1263-1283.

Van der Hoven S. J. and Quade J. 2002. Tracing spatial and temporal variations in the

sources of calcium in pedogenic carbonates in a semiarid environment. Geoderma. 108: 259-276.

Van Schmus, W.R., Green, J.C., and Halls, H.C. 1982. Geochronology of Keweenawan rocks of the Lake Superior region: a summary. In: Geology and tectonics of the Lake Superior basin, edited by Wold, R.J. and Hinze, W.J. Geological Society of America, Memoir 156. 165-171pp.

Veizer, J. 1983. Chemical diagenesis of carbonates: theory and application of trace element techniques. In: Stable Isotopes in Sedimentary Geology. Edited by Arthur, M.A., Anderson, T.F., Kaplan, I.R., Veizer, J. and Land, L.S., Society of Economic Paleontologists and Mineralogists Short Course 10. Tulsa. 3-100pp.

Veizer, J. 2003. Isotopic evolution of seawater on geological time scales: sedimentological perspective. In: Geochemistry of Sediments and Sedimentary Rocks: Evolutionary Considerations to Mineral Deposit-Forming Environments, edited by Lentz, D., Geological Association of Canada, Geotext 4. 53-66pp.

Veizer, J. and Mackenzie, F.T. 2005. Evolution of sedimentary rocks. In: Sediments, diagenesis, and sedimentary rocks (edited by Mackenzie, F.T.), volume 7, Treatise on Geochemistry, edited by Holland, H.D. and Turekian, K.K. Elsevier-Pergamon, Oxford. 369-402pp.

Wadleigh, M.A., Veizer, J. and Brooks, C. 1985. Strontium and its isotopes in Canadian rivers: fluxes and global implications. Geochimica et Cosmochimica Acta. 49: 1727-1736.

White, A.H. and Youngs, B.C. 1980. Cambrian alkali playa-lacustrine sequence in the northeastern Office Basin, South Australia. Journal of Sedimentary Petrology. 50: 1279-1286.

Williams, H.R. 1991. Quetico Subprovince. In: Geology of Ontario. Edited by Thurston, P.C., Williams, H.R., Sutcliffe, R.H. and Stott, G.M., Ontario Geological Survey Special Volume 4 (1). 303-381pp.

Winston, D. 1990. Evidence for intracratonic, fluvial and lacustrine settings of Middle to Late Proterozoic Basins of Western U.S.A. In: Mid-Proterozoic Laurentia-Baltica. Edited by: Gower, C.F., Rivers, T. and Ryan, A.B., Geological Association of Canada, Special Paper 38. 535-564pp.

Wright, J., Seymour, R.S., Shaw, H.F., 1984. REE and Nd isotopes in conodont apatite: variations with geological age and depositional environment. In: Conodont Biofacies and Provincialism. Edited by, Clarck, D.L., Special Paper Geological Society of America vol. 196. 325–340pp.

Wright, J., Schrader, H., Holser, W.T., 1987. Paleoredox variations in ancient oceans recorded by rare earth elements in fossil apatite. Geochimica et Cosmochima Acta. 51: 631–644.

Wright, V.P and Tucker, M.E. 1991. Calcretes: an introduction. In: Calcretes, edited by Wright, V.P. and Tucker, M.E. IAS Reprint Series, vol. 2. Blackwell, Oxford. 1-22pp.

Wright, V.P., 1990. A micromorphological classification of fossil and recent calcic and petrocalcic microstructures. In: Soil Micromorphology: A Basic and Applied Science. Edited by Douglas, Developments in Soil Science, vol. 19. Elsevier, Amsterdam. 401– 407pp.

Appendix 1. Geochemical data for lower clastic unit carbonate samples							
Sample	**Method**	**Detection Limit**	**WL3a**	**WL3b**	**WL3c**	**BM90**	**BM91**
Stratigraphic unit			Lower Clastic	Lower Clastic	Lower Clastic	Lower Clastic	Lower Clastic
Lithofacies association			Boulder conglomerate-sandstone-dolocrete	Boulder conglomerate-sandstone-dolocrete	Boulder conglomerate-sandstone-dolocrete	Boulder conglomerate-sandstone-dolocrete	Boulder conglomerate-sandstone-dolocrete
Drill Hole			n/a	n/a	n/a	n/a	n/a
Outcrop Locality			West Loon	West Loon	West Loon	South of Beardmore	South of Beardmore
Easting (m)			368006	368006	368006	?	?
Northing (m)			5387586	5387586	5387586	?	?
Description			dolocrete horizon, pink carbonate matrix material, silicified?	silicified dolocrete matirx	massive pink silicified dolocrete	carb nodule, soil (?)	discontinuous soil (?) carbonate layer
$\delta^{13}C$ (PDB)			-1.1	-1.2	-1.3	-1.2	-1.5
$\delta^{18}O$ (SMOW)			28.4	27.5	27.2	14.8	14.0
$\delta^{18}O$ (PDB)			-2.4	-3.3	-3.6	-15.7	-16.4
$^{87}Sr/^{86}Sr$			0.704782	0.704284			
2σ			0.00002	0.000012			
Al (ppm)	ICP-AES	0.06			47.98	756.77	313.96
Ba	ICP-AES	0.006			27.457	25.521	10.239
Ca	ICP-AES	0.01			122265.33	454804.17	200854.26
Fe	ICP-AES	0.02			461.51	1553.12	784.31
K	ICP-AES	0.25			17.5	N.D.	N.D.
Mg	ICP-AES	0.01			77384.05	15539.06	8688.70
Mn	ICP-AES	0.003			1680.606	917.708	411.968
Na	ICP-AES	0.01			85.78	3445.31	2437.10
P	ICP-AES	0.1			28.4	1118.7	872.3
S	ICP-AES	0.1			74.1	4393.1	1256.7
Si	ICP-AES	0.025			21.76	891.67	378.72
Sr	ICP-AES	0.005			33.864	N.D.	11.170
Y	ICP-AES	0.03			4.41	10.42	4.26
Al (ppm)	ICP-MS	0.5	38.0	79.3			
Ca	ICP-MS	1000	47,600	82,800			
Fe	ICP-MS	0.3	141	301			
Mn	ICP-MS	0.4	579	750			
Mg	ICP-MS	250	>20000	>20000			
Cs	ICP-MS	0.001	0.00990	0.0193			
Hf	ICP-MS	0.05	N.D.	N.D.			
Rb	ICP-MS	0.02	N.D.	N.D.			
Sr	ICP-MS	0.00	15.3	29.5			
Ta	ICP-MS	0.10%	N.D.	N.D.			
Nb	ICP-MS	0.01	N.D.	N.D.			
Th	ICP-MS	0.02	0.0332	0.0574			
U	ICP-MS	2	0.0599	0.130			
Y	ICP-MS	0.025	1.37	2.84			
Zr	ICP-MS	0.2	0.0609	0.0881			
La	ICP-MS	0.02	0.772	1.61			
Ce	ICP-MS	0.01	0.756	1.88			
Pr	ICP-MS	0.0035	0.306	0.614			
Nd	ICP-MS	0.002	1.27	2.57			
Sm	ICP-MS	0.005	0.290	0.558			
Eu	ICP-MS	0.005	0.0604	0.126			
Gd	ICP-MS	0.005	0.295	0.622			
Tb	ICP-MS	0.015	0.0401	0.0817			
Dy	ICP-MS	0.0015	0.202	0.420			
Ho	ICP-MS	0.004	0.0376	0.0772			
Er	ICP-MS	0.0015	0.104	0.188			
Tm	ICP-MS	0.005	0.0104	0.0262			
Yb	ICP-MS	0.002	0.0644	0.154			
Lu	ICP-MS	0.0035	0.0114	0.0223			
Li (ppm)	ICP-MS	0.1	0.355	0.716			
Be	ICP-MS	0.04	0.103	0.116			
Sc	ICP-MS	0.3	N.D.	0.436			
V	ICP-MS	0.4	N.D.	N.D.			
Mo	ICP-MS	0.02	0.256	0.0485			
Ba	ICP-MS	0.0015	6.37	3.42			

Appendix 1. Geochemical data for lower clastic unit carbonate samples							
Sample	Method	Detection Limit	WL3a	WL3b	WL3c	BM90	BM91
Tl	ICP-MS	0.0035	N.D.	0.00297			
Pb	ICP-MS	0.15	1.18	1.18			
Ti	ICP-MS	0.005	0.693	1.11			
Cr	ICP-MS	0.03	0.391	0.340			
Co	ICP-MS	0.5	1.09	1.97			
Ni	ICP-MS	0.005	4.18	5.24			
Cu	ICP-MS	0.35	3.68	10.7			
Zn	ICP-MS	10	36.4	40.8			
Ag	ICP-MS	0.015	N.D.	N.D.			
Cd	ICP-MS	0.0015	0.142	0.221			
Sn	ICP-MS	0.15	0.0401	0.0574			
Sb	ICP-MS	0.005	0.0233	0.0208			
W	ICP-MS	0.01	N.D.	0.0119			
Au	ICP-MS	0.005	N.D.	N.D.			
Ga	ICP-MS	0.015	0.0629	0.121			
* blank cells = not analyzed; N.D. = not detected							

Appendix 2. Geochemical data for the mixed siliciclastic-carbonate unit.

Sample			RC1	RC2	RC3	RC4	RC5	RC5	RC6	RC7	03RM78-1	03RM78-2	03RM78-3
stratigraphic unit			mixed siliciclastic carbonate	mixed siliciclastic carbonate	mixed siliciclastic carbonate	mixed siliciclastic carbonate	mixed siliciclastic carbonate	mixed siliciclastic carbonate	mixed siliciclastic carbonate	mixed siliciclastic carbonate	mixed siliciclastic carbonate	mixed siliciclastic carbonate	mixed siliciclastic carbonate
lithofacies association													
Drill Hole			NI-92-7	NI-92-7	NI-92-7	NI-92-7	NI-92-7		NI-92-7	NI-92-7	NI-92-7	NI-92-7	NI-92-7
Stratigraphic Height (above basement) (m)			53.27	59.85	66.54	62.79					61	61	61
Easting (m)			353850	353850	353850	353850	353850		353850	353850	353850	353850	353850
Northing (m)			5443000	5443000	5443000	5443000	5443000		5443000	5443000	5443000	5443000	5443000
Description			red dolomitic mudstone	red dolomitic mudstone	red dolomitic mudstone	red dolomitic mudstone	red dolomitic mudstone		red dolomitic mudstone	red dolomitic mudstone	micritic dolostone	micritic dolostone	micritic dolostone
$\delta^{13}C$ (PDB)			-2.2	-0.7	0.0	-0.2					-1.63	-1.48	-1.48
$\delta^{18}O$ (SMOW)			25.3	25.9	26.5	25.1					23.92	23.88	24.37
$\delta^{18}O$ (PDB)			-5.4	-4.8	-4.3	-5.7					-6.8	-6.8	-6.4
$^{87}Sr/^{86}Sr$													
2σ													
	Method	Detection Limit											
Al (ppm)	ICP-AES	0.05									594.87	340.96	205.79
Ba	ICP-AES	0.005									215.044	95.351	65.430
Ca	ICP-AES	0.01									145317	127396	99987
Fe	ICP-AES	0.02									447.61	289.74	255.27
K	ICP-AES	0.25									1683.009	221.156	226.261
Mg	ICP-AES	0.01									88701	79241	60087
Mn	ICP-AES	0.003									136.283	84.846	65.282
Na	ICP-AES	0.01									753.10	120.15	188.28
P	ICP-AES	0.1									59.3	65.0	55.0
S	ICP-AES	0.1									597.5	137.9	71.4
Si	ICP-AES	0.025									1351.50	189.47	137.02
Sr	ICP-AES	0.005									63.186	29.988	22.033
V	ICP-AES	0.03									3.01	4.90	N.D.
Al (ppm)	ICP-MS	0.5	183.0	117.2	103.6	230.1	157.9	*110.1*	134.3	123.6			186
Fe	ICP-MS	2	35.6	44.0	32.3	36.2	33.6	*19.2*	34.4	127.4			131
Mn	ICP-MS	0.4	37.6	27.4	73.6	39.0	39.7	*31.0*	26.9	27.9			53.1
Mg	ICP-MS	250	46,751	35,027	31,942	32,368	33,207	*24,190*	30,121	33,252			>20000
Ca	ICP-MS	1000	79,500	59,260	54,380	54,180	54,430	*41,180*	50,690	56,770			72,600
Cs	ICP-MS	0.0015	0.0098	0.0491	0.0130	0.0125	0.0520	*0.0234*	0.0220	0.0239			0.0229
Hf	ICP-MS	0.005	N.D.	N.D.	0.006	0.006	N.D.	*N.D.*	N.D.	0.005			0.00634
Rb	ICP-MS	0.35	N.D.	0.5	N.D.	N.D.	0.4	*N.D.*	N.D.	N.D.			N.D.
Sr	ICP-MS	10.00	18	14	12	13	13	*11*	13	31			17.3
Ta	ICP-MS	0.002	0.0041	N.D.	N.D.	0.0029	0.0039	*N.D.*	N.D.	0.0060			N.D.
Nb	ICP-MS	0.004	0.005	0.005	0.006	N.D.	N.D.	*N.D.*	N.D.	N.D.			N.D.
Th	ICP-MS	0.005	0.196	0.145	0.154	0.167	0.131	*0.088*	0.128	0.139			0.328
U	ICP-MS	0.0035	0.248	0.093	0.076	0.078	0.057	*0.080*	0.051	0.083			0.102
Y	ICP-MS	0.015	2.666	1.786	2.203	2.341	1.879	*1.479*	1.705	2.043			2.86
Zr	ICP-MS	0.02	0.045	0.037	0.059	0.036	0.042	*0.033*	0.053	0.038			0.0702
La	ICP-MS	0.005	1.082	0.867	0.760	0.869	0.721	*0.583*	0.786	0.907			1.15
Ce	ICP-MS	0.001	3.5873	2.4424	2.0365	2.6121	1.9733	*1.5923*	2.2523	2.4200			3.86
Pr	ICP-MS	0.0015	0.5138	0.3634	0.3793	0.4351	0.3766	*0.2862*	0.3796	0.4062			0.580
Nd	ICP-MS	0.02	2.451	1.692	1.945	2.251	1.928	*1.529*	1.866	1.968			2.94
Sm	ICP-MS	0.01	0.680	0.487	0.591	0.697	0.612	*0.464*	0.498	0.573			0.948
Eu	ICP-MS	0.0035	0.143	0.094	0.100	0.123	0.130	*0.098*	0.092	0.124			0.184
Gd	ICP-MS	0.005	0.670	0.442	0.558	0.663	0.570	*0.437*	0.473	0.594			0.863
Tb	ICP-MS	0.002	0.0988	0.0602	0.0790	0.0850	0.0711	*0.0599*	0.0625	0.0743			0.113
Dy	ICP-MS	0.005	0.533	0.348	0.423	0.475	0.385	*0.330*	0.352	0.410			0.597
Ho	ICP-MS	0.015	0.095	0.067	0.074	0.085	0.067	*0.053*	0.063	0.074			0.101
Er	ICP-MS	0.005	0.253	0.170	0.217	0.241	0.162	*0.138*	0.156	0.219			0.262
Tm	ICP-MS	0.0015	0.0354	0.0234	0.0310	0.0290	0.0237	*0.0169*	0.0183	0.0292			0.0337
Yb	ICP-MS	0.004	0.220	0.148	0.182	0.179	0.127	*0.111*	0.138	0.180			0.220
Lu	ICP-MS	0.0015	0.0314	0.0248	0.0292	0.0276	0.0172	*0.0141*	0.0206	0.0282			0.0322
Total REE			10.3937	7.2292	7.4050	8.7718	7.1639	5.7124	7.1573	8.0069			11.8839
Li (ppm)	ICP-MS	0.1	2.33	1.60	0.97	2.18	1.69	*1.39*	1.74	1.27			1.61
Be	ICP-MS	0.04	0.06	0.05	N.D.	0.07	N.D.	*0.04*	0.07	0.07			0.0580
Sc	ICP-MS	0.3	1.12	0.63	0.70	1.15	0.86	*0.68*	0.67	0.85			1.17
V	ICP-MS	0.15	0.32	0.20	N.D.	0.24	0.23	*N.D.*	N.D.	0.20			1.66
Mo	ICP-MS	0.025	0.070	0.050	0.068	0.070	N.D.	*N.D.*	N.D.	0.036			0.278
Ba	ICP-MS	0.15	13.19	24.39	25.06	32.17	67.08	*45.61*	29.46	18.29			48.9
Tl	ICP-MS	0.001	0.0021	0.0020	0.0031	0.0012	0.0022	*0.0015*	N.D.	N.D.			0.00195
Pb	ICP-MS	0.01	0.575	0.309	0.646	0.587	0.255	*0.167*	0.251	0.597			0.984
Ti	ICP-MS	0.005	0.642	1.936	0.800	0.754	1.800	*0.810*	1.011	1.347			1.91
Cr	ICP-MS	0.02	0.779	0.333	0.506	0.658	0.746	*0.349*	0.362	0.498			0.899
Co	ICP-MS	0.03	0.206	0.226	0.175	0.185	0.215	*0.138*	0.161	0.173			0.232
Ni	ICP-MS	0.4	1.5	1.4	1.8	2.0	2.0	*0.7*	1.1	1.4			2.25
Cu	ICP-MS	0.3	1.28	0.94	4.93	0.91	0.71	*0.50*	0.55	0.74			2.83
Zn	ICP-MS	0.5	5.2	11.1	9.1	12.1	11.0	*4.1*	8.6	11.8			8.32
Ag	ICP-MS	0.15	N.D.	N.D.	N.D.	N.D.	N.D.	N.D.	N.D.	N.D.			N.D.
Cd	ICP-MS	0.01	0.027	0.031	0.034	0.036	0.024	*0.014*	0.025	0.036			N.D.
Sn	ICP-MS	0.02	0.054	0.031	0.043	0.056	N.D.	*N.D.*	N.D.	N.D.			N.D.
Sb	ICP-MS	0.015	N.D.	N.D.	N.D.	N.D.	N.D.	*N.D.*	N.D.	0.015			N.D.
W	ICP-MS	0.0035	0.017	0.007	0.013	0.010	0.012	*N.D.*	0.007	0.007			0.00634
Au	ICP-MS	0.05	N.D.	N.D.	N.D.	N.D.	N.D.	*N.D.*	N.D.	N.D.			N.D.
Ga	ICP-MS	0.005	0.036	0.068	0.048	0.053	0.055	*0.034*	0.047	0.048			0.0620

* blank cells = not analyzed; N.D. = not detected

Appendix 2. Geoche															
Sample	03RM178-4	03RM178-5	03RM178-6	03RM178-7	03RM130-1	03RM130-2	03RM130-3	03RM130-4	*03RM130-4*	*03RM130-4*	03RM132	03RM133	03RM134	03RM135
stratigraphic unit	mixed siliciclastic carbonate	mixed siliciclastic carbonate	mixed siliciclastic carbonate	mixed siliciclastic carbonate	mixed siliciclastic carbonate	mixed siliciclastic carbonate	mixed siliciclastic carbonate	mixed siliciclastic carbonate	mixed siliciclastic carbonate	mixed siliciclastic carbonate	mixed siliciclastic carbonate	mixed siliciclastic carbonate	mixed siliciclastic carbonate	mixed siliciclastic carbonate
lithofacies association														
Drill Hole	NI-92-7	NI-92-7	NI-92-7	NI-92-7	NI-92-7	NI-92-7	NI-92-7	NI-92-7			NI-92-7	NI-92-7	NI-92-7	NI-92-7
Stratigraphic Height (above basement) (m)	61	61	61	61	37.76	37.76	37.76	37.76			49.82	52.39	71.97	86.93
Easting (m)	353850	353850	353850	353850	353850	353850	353850	353850			353850	353850	353850	353850
Northing (m)	5443000	5443000	5443000	5443000	5443000	5443000	5443000	5443000			5443000	5443000	5443000	5443000
Description	micritic dolostone	micritic dolostone	micritic dolostone	micritic dolostone	micritic dolostone	micritic dolostone	micritic dolostone	micritic dolostone	micritic dolostone	micritic dolostone	micritic dolostone	micritic dolostone	micritic dolostone	micritic dolostone
$\delta^{13}C$ (PDB)	-1.60	-1.63	-1.47	-1.53	-2.37	-2.36	-2.26	-2.27			-2.44	-2.14	-0.36	0.8
$\delta^{18}O$ (SMOW)	24.08	23.82	23.63	23.74	24.82	24.62	23.92	22.28			23.45	23.90	24.62	26.4
$\delta^{18}O$ (PDB)	-6.6	-6.9	-7.1	-7.0	-5.9	-6.1	-6.8	-8.4			-7.2	-6.8	-6.1	-4.4
$^{87}Sr/^{86}Sr$														
2σ														
Al (ppm)		70.12	81.38	419.23	566.49	395.73		221.63			157.39	241.67	319.85	
Ba		36.510	36.803	83.602	108.245	461.663		460.848			75.802	69.729	54.230	
Ca		128555	126112	126357	129529	139817		137470			137017	134959	157789	
Fe		226.46	200.70	291.01	333.11	347.69		327.68			302.79	283.19	349.35	
K		45.668	56.990	208.221	524.691	615.935		479.068			333.9	293.3	461.5	
Mg		79311	78169	78656	80944	84408		81452			83352	83353	91516	
Mn		84.134	84.706	91.381	162.081	213.395		568.567			123.570	109.972	400.976	
Na		90.82	82.03	128.73	112.43	414.09		301.11			319.32	259.47	424.62	
P		59.7	50.4	58.9	22.5	96.3		39.9			80.5	71.5	68.2	
S		260.1	368.7	195.0	79.6	246.7		286.4			140.7	142.7	5344.1	
Si		40.82	54.70	263.20	576.28	220.09		100.76			98.26	169.30	187.85	
Sr		26.757	27.327	31.028	32.451	49.423		63.978			28.452	25.855	53.796	
V		4.73	4.90	5.28	4.10	N.D.		8.69			4.67	4.49	5.64	
Al (ppm)								105	*105*	*101*	98.8	141	155	53.3
Fe								97.4	*99.1*	*99.3*	101	99.1	105	163
Mn								334	*333*	*324*	76.7	78.5	187	159
Mg								>20000	*>20000*	*>20000*	>20000	>20000	>20000	19,700
Ca								75.800	*73.900*	*63.000*	72,200	81.700	65.700	31,400
Cs								0.0319	*0.0278*	*0.0301*	0.0259	0.0285	0.0365	0.00773
Hf								0.0106	*0.0100*	*0.0110*	0.00829	0.0100	0.00700	N.D.
Rb								0.391	*0.380*	*0.351*	0.356	0.397	0.408	N.D.
Sr								41.4	*41.6*	*41.6*	18.9	18.9	29.7	14.7
Ta								N.D.	*N.D.*	*N.D.*	N.D.	N.D.	N.D.	N.D.
Nb								0.00435	*0.0115*	*0.00766*	0.0122	0.00800	0.00800	N.D.
Th								0.205	*0.204*	*0.214*	0.300	0.316	0.266	0.119
U								0.0309	*0.0306*	*0.0306*	0.0800	0.0700	0.0695	0.0372
Y								4.83	*4.88*	*4.83*	2.80	2.96	2.57	1.64
Zr								0.0536	*0.0522*	*0.0535*	0.0585	0.0630	0.0725	0.0304
La								0.892	*0.886*	*0.913*	1.07	1.18	0.907	0.619
Ce								2.63	*2.72*	*2.75*	3.40	3.58	3.01	1.34
Pr								0.699	*0.718*	*0.726*	0.560	0.574	0.505	0.320
Nd								4.59	*4.71*	*4.60*	2.79	2.97	2.54	1.53
Sm								2.00	*2.05*	*2.05*	0.856	0.900	0.829	0.512
Eu								0.378	*0.380*	*0.375*	0.189	0.174	0.166	0.0918
Gd								1.79	*1.74*	*1.73*	0.790	0.845	0.746	0.452
Tb								0.216	*0.212*	*0.208*	0.106	0.113	0.0980	0.0604
Dy								1.00	*0.990*	*1.04*	0.583	0.602	0.515	0.331
Ho								0.162	*0.155*	*0.159*	0.107	0.104	0.0895	0.0560
Er								0.395	*0.358*	*0.364*	0.249	0.261	0.233	0.148
Tm								0.0473	*0.0435*	*0.0474*	0.0332	0.0340	0.0275	0.0184
Yb								0.262	*0.267*	*0.264*	0.213	0.221	0.198	0.128
Lu								0.0357	*0.0344*	*0.0330*	0.0307	0.0320	0.0265	0.0169
Total REE								15.0970	15.2639	15.2594	10.9769	11.5900	9.8905	5.6235
Li (ppm)								0.863	*0.823*	*0.667*	1.24	1.37	1.14	0.501
Be								N.D.	*0.0440*	*0.0502*	N.D.	0.0535	N.D.	N.D.
Sc								0.696	*0.664*	*0.520*	0.846	1.07	0.880	0.571
V								2.42	*2.52*	*2.51*	1.80	1.45	2.26	0.305
Mo								0.306	*0.271*	*0.240*	0.0854	0.0620	0.335	0.0353
Ba								357	*355*	*360*	62.6	57.1	54.6	58.8
Tl								0.00193	*0.00191*	*0.00287*	0.00146	0.00250	0.00250	N.D.
Pb								1.23	*1.22*	*1.27*	0.575	0.604	0.869	0.902
Ti								2.45	*2.04*	*2.23*	2.72	2.59	2.46	0.610
Cr								0.709	*0.666*	*0.894*	1.03	1.18	0.938	0.391
Co								0.713	*0.712*	*0.725*	0.395	0.387	0.347	0.292
Ni								3.79	*3.82*	*4.44*	1.62	1.86	2.57	1.77
Cu								2.68	*2.75*	*2.75*	0.966	3.25	3.79	2.63
Zn								19.0	*19.5*	*17.3*	1.50	3.52	8.97	8.79
Ag								N.D.	*N.D.*	*N.D.*	N.D.	N.D.	N.D.	N.D.
Cd								0.0271	*0.0144*	*0.0153*	N.D.	0.0200	0.0155	0.0111
Sn								0.0246	*0.0230*	*N.D.*	0.0278	N.D.	0.0235	0.0357
Sb								0.0193	*0.0177*	*0.0167*	N.D.	N.D.	N.D.	N.D.
W								0.0261	*0.0335*	*0.0124*	0.0239	0.0155	0.0210	0.0140
Au								N.D.	*N.D.*	*N.D.*	N.D.	N.D.	N.D.	N.D.
Ga								0.0739	*0.0818*	*0.0885*	0.0585	0.0640	0.0880	0.0343
* blank cells = not ana														

Appendix 2. Geoche															
Sample	03RM144	03RM130-5	03RM130-6	03RM130-7	04RM130	04RM131	04RM132	04RM133	04RM134	04RM2	04RM4	NB-97-4-0	NB-97-4-1	NB-97-4-2
stratigraphic unit	mixed siliciclastic carbonate	mixed siliciclastic carbonate	mixed siliciclastic carbonate	mixed siliciclastic carbonate	mixed siliciclastic carbonate	mixed siliciclastic carbonate	mixed siliciclastic carbonate	mixed siliciclastic carbonate	mixed siliciclastic carbonate	mixed siliciclastic carbonate	mixed siliciclastic carbonate	mixed siliciclastic carbonate	mixed siliciclastic carbonate	mixed siliciclastic carbonate
lithofacies association														
Drill Hole	NI-92-7	NI-92-7	NI-92-7	NI-92-7	NI-92-7	NI-92-7	NI-92-7	NI-92-7	NI-92-7	NI-92-7	NI-92-7	NB-97-4	NB-97-4	NB-97-4
Stratigraphic Height (above basement) (m)	64	37.76	37.76	37.76	51	67	55	65	53	47.69	72.45	25.53	25.4	27.02
Easting (m)	353850	353850	353850	353850	353850	353850	353850	353850	353850	353850	353850	425430	425430	425430
Northing (m)	5443000	5443000	5443000	5443000	5443000	5443000	5443000	5443000	5443000	5443000	5443000	5410540	5410540	5410540
Description	micritic dolostone	micritic dolostone	micritic dolostone	micritic dolostone	micritic dolostone	micritic dolostone	micritic dolostone	micritic dolostone	micritic dolostone	micritic dolostone	micritic dolostone	micritic dolostone	micritic dolostone	micritic dolostone
$\delta^{13}C$ (PDB)	-1.26	-2.33	-2.29	-2.24	-2.8	-1.2	-2.5	-1.6	-1.0	-2.9	0.0	-3.1	-2.8	-3.2
$\delta^{18}O$ (SMOW)	23.54	24.49	23.91	24.45	24.0	23.2	23.5	24.7	24.4	23.4	25.7	23.9	24.3	23.1
$\delta^{18}O$ (PDB)	-7.2	-6.2	-6.8	-6.3	-6.7	-7.5	-7.2	-6.0	-6.3	-7.2	-5.1	-6.8	-6.4	-7.5
$^{87}Sr/^{86}Sr$						0.708288	0.70704			0.706455				
2σ						0.000016	0.000021			0.000014				
Al (ppm)		133.74	112.65	391.02	187.91	277.22	133.11	149.28	119.78	80.94	70.84	30.66	73.36	68.23
Ba		162.481	136.265	208.638	18.349	362.556	71.754	141.124	13.750	7.862	37.511	4.805	3.512	10.160
Ca		135887	128183	129009	124325	141741	95336	133891	135891	140294	136062	115129	133429	131818
Fe		291.06	248.55	262.14	195.89	345.67	210.13	261.07	281.12	259.81	182.62	229.14	261.09	233.56
K		266.9	163.7	294.6	138.3	126.4	106.3	97.3	81.9	35.3	52.7	691.6	38.2	N.D.
Mg		83457	78459	78915	81370	84444	58188	81448	81409	84949	83025	70548	80926	80777
Mn		214.715	191.432	150.839	79.770	161.556	66.930	70.693	105.216	103.459	303.207	128.345	171.683	139.532
Na		228.04	101.86	86.38	74.74	97.33	53.55	94.12	77.37	51.70	84.98	522.99	132.50	179.93
P		44.8	25.7	19.6	54.4	122.4	52.6	65.9	64.5	39.1	48.5	96.0	66.2	92.8
S		96.5	49.3	64.7	8.7	79.6	135.1	36.4	25.0	90.1	539.7	6.9	12.0	N.D.
Si		91.68	138.30	431.49	113.01	133.44	91.54	99.14	85.39	41.38	44.43	34.25	96.27	80.79
Sr		35.901	31.324	36.426	26.142	47.111	98.553	31.320	29.526	23.396	61.561	21.229	22.241	24.507
V		5.16	4.49	4.20	4.76	6.00	4.21	4.86	5.78	3.90	3.46	2.80	3.29	3.26
Al (ppm)										59.4	36.1			
Fe										63.6	34.5			
Mn										87.1	159			
Mg										>20000	>20000			
Ca										84,000	48,400			
Cs										0.0158	0.00758			
Hf										0.00887	N.D.			
Rb										N.D.	N.D.			
Sr										17.8	12.5			
Ta										N.D.	N.D.			
Nb										0.00493	0.00404			
Th										0.237	0.146			
U										0.0581	0.0273			
Y										3.11	1.49			
Zr										0.0665	0.0268			
La										1.48	0.507			
Ce										2.78	1.62			
Pr										0.708	0.282			
Nd										3.64	1.45			
Sm										1.10	0.442			
Eu										0.214	0.0924			
Gd										0.963	0.409			
Tb										0.128	0.0586			
Dy										0.659	0.308			
Ho										0.103	0.0556			
Er										0.279	0.141			
Tm										0.0360	0.0162			
Yb										0.202	0.122			
Lu										0.0286	0.0167			
Total REE										12.3206	5.5205			
Li (ppm)										1.12	0.592			
Be										N.D.	0.0465			
Sc										0.910	0.319			
V										1.23	0.345			
Mo										0.0764	0.0566			
Ba										8.27	8.21			
Tl										0.00148	0.00202			
Pb										1.67	1.24			
Tl										1.42	0.771			
Cr										0.738	0.406			
Co										0.395	0.225			
Ni										3.86	2.37			
Cu										2.26	0.913			
Zn										13.2	9.09			
Ag										N.D.	N.D.			
Cd										0.0192	N.D.			
Sn										0.0483	N.D.			
Sb										N.D.	N.D.			
W										0.0133	0.00960			
Au										N.D.	N.D.			
Ga										0.0453	0.0364			
* blank cells = not an														

Appendix 2. Geoche															
Sample	NB-97-4-2	NB-97-4-3	NB-97-4-4	NB-97-4-5	NB-97-4-6	NB-97-4-7	NB-97-4-8	NB-97-4-9	NB-97-4-10	NB-97-4-11	NB-97-4-12	NB-97-4-13	NB-97-4-14	NB-97-4-15
stratigraphic unit	mixed siliciclastic carbonate	mixed siliciclastic carbonate	mixed siliciclastic carbonate	mixed siliciclastic carbonate	mixed siliciclastic carbonate	mixed siliciclastic carbonate	mixed siliciclastic carbonate	mixed siliciclastic carbonate	mixed siliciclastic carbonate	mixed siliciclastic carbonate	mixed siliciclastic carbonate	mixed siliciclastic carbonate	mixed siliciclastic carbonate	mixed siliciclastic carbonate
lithofacies association														
Drill Hole	NB-97-4	NB-97-4	NB-97-4	NB-97-4	NB-97-4	NB-97-4	NB-97-4	NB-97-4	NB-97-4	NB-97-4	NB-97-4	NB-97-4	NB-97-4	NB-97-4
Stratigraphic Height (above basement) (m)	27.02	30.16	31.48	32.78	34.5	36.12	37.8	38.45	39.68	40.98	41.92	42.57	45.01	28.34
Easting (m)	425430	425430	425430	425430	425430	425430	425430	425430	425430	425430	425430	425430	425430	425430
Northing (m)	5410540	5410540	5410540	5410540	5410540	5410540	5410540	5410540	5410540	5410540	5410540	5410540	5410540	5410540
Description	micritic dolostone	micritic dolostone	micritic dolostone	micritic dolostone	micritic dolostone	micritic dolostone	micritic dolostone	micritic dolostone	micritic dolostone	micritic dolostone	micritic dolostone	micritic dolostone	micritic dolostone	micritic dolostone
$\delta^{13}C$ (PDB)	-3.3	-2.5	-2.5	-2.2	-2.2	-2.6	-1.5	-1.6	-1.2	-0.9	-0.8	-1.3	-1.6	-2.9
$\delta^{18}O$ (SMOW)	23.8	24.4	24.1	24.1	24.8	24.8	23.9	25.0	25.0	24.8	24.0	24.6	24.8	24.0
$\delta^{18}O$ (PDB)	-6.9	-6.3	-6.6	-6.6	-5.9	-6.0	-6.8	-5.7	-5.7	-6.0	-6.7	-6.2	-5.9	-6.7
$^{87}Sr/^{86}Sr$														
2σ														
Al (ppm)		104.10	72.95	75.25	24.57	82.60	56.54	46.46	63.56	33.28	54.35	17.38	133.50	56.42
Ba		131.530	2.856	15.688	3.400	31.154	12.181	34.280	320.063	218.647	148.586	24.603	22.211	8.175
Ca		133054	130567	128357	132956	136239	131199	133377	132578	132899	135463	129466	126291	121898
Fe		257.26	221.81	266.69	168.54	229.72	198.70	208.15	218.08	225.46	206.70	198.77	237.30	255.68
K		38.1	24.9	30.8	59.0	92.2	84.8	82.4	106.7	57.7	129.7	N.D.	N.D.	N.D.
Mg		82134	79949	79988	83253	83752	80606	82804	81619	80160	81643	81557	78447	76581
Mn		111.901	141.537	187.438	105.266	112.780	139.717	81.257	90.709	93.133	161.257	94.682	79.368	112.919
Na		266.69	197.30	207.63	61.06	25.24	104.87	59.33	104.25	120.40	146.70	114.38	298.76	347.92
P		128.4	86.2	97.9	38.7	53.9	54.8	43.4	63.6	53.1	39.1	69.5	135.2	76.8
S		18.2	N.D.	N.D.	56.0	N.D.	2.8	9.6	121.2	47.5	N.D.	81.8	211.1	161.6
Si		108.50	78.61	66.25	17.50	50.15	37.85	44.07	43.65	14.24	28.06	9.67	77.82	33.84
Sr		36.631	23.364	24.500	23.165	27.382	24.023	28.256	66.016	44.812	39.162	21.319	22.312	20.351
V		4.33	4.36	4.81	4.42	5.20	6.12	4.51	5.10	5.21	4.92	3.95	4.03	3.43
Al (ppm)														
Fe														
Mn														
Mg														
Ca														
Cs														
Hf														
Rb														
Sr														
Ta														
Nb														
Th														
U														
Y														
Zr														
La														
Ce														
Pr														
Nd														
Sm														
Eu														
Gd														
Tb														
Dy														
Ho														
Er														
Tm														
Yb														
Lu														
Total REE														
Li (ppm)														
Be														
Sc														
V														
Mo														
Ba														
Tl														
Pb														
Ti														
Cr														
Co														
Ni														
Cu														
Zn														
Ag														
Cd														
Sn														
Sb														
W														
Au														
Ga														
* blank cells = not an														

Appendix 3. Geochemical data for carbonate samples from the upper siliciclastic unit

Sample			BO2-4a	*BO2-4a*	BO2-4b	BO2-4c	CI1b	CI1a	04RM77
Stratigraphic unit			Upper siliciclastic	Upper siliciclastic	Upper siliciclastic	Upper siliciclastic	Upper siliciclastic	Upper siliciclastic	Upper siliciclastic
lithofacies association									
Drill Hole			n/a		n/a	n/a	n/a	n/a	n/a
Outcrop Locality			Channel Island	Channel Island	Channel Island	Channel Island	Channel Island	Channel Island	Red Rock Railway
Easting (m)			462992		462992	462992	462992	462992	407703
Northing (m)			5406020		5406020	5406020	5406020	5406020	5423237
Description			stromatolite, massive white layer		stromatolite, massive white layer	fine dark krinkly laminae	stromatolite	stromatolite	stromatolitic chert/limstone
$\delta^{13}C$ (PDB)			-0.1		-0.1	0.4	0.71	0.22	0.2
$\delta^{18}O$ (SMOW)			15.7		18.5	16.4	23.37	23.47	23.9
$\delta^{18}O$ (PDB)			-14.7		-12.1	-14.1	-7.3	-7.2	-6.8
$^{87}Sr/^{86}Sr$			0.709386		0.711604	0.712309		0.708152	
2σ			0.000016		0.000025	0.000023		0.000013	
	Method	Detection Limit							
Al (ppm)	ICP-AES	0.06							105.76
Ba	ICP-AES	0.006							185.312
Ca	ICP-AES	0.01							124741.32
Fe	ICP-AES	0.02							309.00
K	ICP-AES	0.25							N.D.
Mg	ICP-AES	0.01							77503.13
Mn	ICP-AES	0.003							336.800
Na	ICP-AES	0.01							247.32
P	ICP-AES	0.1							61.7
S	ICP-AES	0.1							203.4
Si	ICP-AES	0.025							46.15
Sr	ICP-AES	0.005							26.541
Y	ICP-AES	0.03							4.76
Al (ppm)	ICP-MS	0.5	24.0	*21.1*			51.7	45.5	
Fe	ICP-MS	0.3	83.0	*84.1*			160	427	
Mn	ICP-MS	0.4	499	*475*			420	386	
Mg	ICP-MS	250	>20000	*>20000*			>20000	>20000	
Ca	ICP-MS	1000	96,400	*72,600*			113,000	77,600	
Cs	ICP-MS	0.001	0.00198	*0.00396*			0.00300	0.00297	
Hf	ICP-MS	0.05	N.D.	*N.D.*			N.D.	N.D.	
Rb	ICP-MS	0.02	N.D.	*N.D.*			N.D.	N.D.	
Sr	ICP-MS	0.004	37.2	*36.8*			27.5	32.6	
Ta	ICP-MS	0.10%	N.D.	*N.D.*			N.D.	N.D.	
Nb	ICP-MS	0.01	N.D.	*N.D.*			0.00550	N.D.	
Th	ICP-MS	0.02	0.0144	*0.0134*			0.0230	0.0144	
U	ICP-MS	2	0.0802	*0.0807*			0.169	0.273	
Y	ICP-MS	0.025	2.33	*2.36*			2.17	2.63	
Zr	ICP-MS	0.15	N.D.	*N.D.*			0.0230	N.D.	
La	ICP-MS	0.02	4.35	*4.52*			1.85	2.01	
Ce	ICP-MS	0.01	2.70	*2.82*			2.36	2.93	
Pr	ICP-MS	0.0035	0.992	*0.991*			0.564	0.692	
Nd	ICP-MS	0.002	3.84	*3.85*			2.29	2.90	
Sm	ICP-MS	0.005	0.651	*0.619*			0.471	0.602	
Eu	ICP-MS	0.005	0.112	*0.111*			0.112	0.125	
Gd	ICP-MS	0.005	0.623	*0.657*			0.440	0.620	
Tb	ICP-MS	0.015	0.0703	*0.0708*			0.0610	0.0782	
Dy	ICP-MS	0.0015	0.383	*0.365*			0.370	0.505	
Ho	ICP-MS	0.004	0.0624	*0.0614*			0.0660	0.0837	
Er	ICP-MS	0.0015	0.150	*0.148*			0.167	0.208	
Tm	ICP-MS	0.005	0.0168	*0.0158*			0.0210	0.0272	
Yb	ICP-MS	0.002	0.0807	*0.0822*			0.108	0.138	
Lu	ICP-MS	0.0035	0.0114	*0.00990*			0.0145	0.0168	
Li (ppm)	ICP-MS	0.1	0.192	*0.122*			0.227	0.122	
Be	ICP-MS	0.04	0.0634	*0.0525*			N.D.	N.D.	
Sc	ICP-MS	0.3	0.433	*N.D.*			0.482	0.564	
V	ICP-MS	0.4	2.00	*1.73*			6.55	4.91	
Mo	ICP-MS	0.02	0.0465	*0.0332*			0.0790	0.111	
Ba	ICP-MS	0.0015	290	*295*			523	433	
Tl	ICP-MS	0.0035	N.D.	*N.D.*			0.00150	0.00149	
Pb	ICP-MS	0.15	0.837	*0.938*			0.925	0.825	
Ti	ICP-MS	0.005	2.52	*4.18*			0.925	0.549	
Cr	ICP-MS	0.03	0.266	*0.276*			0.315	0.623	
Co	ICP-MS	0.5	0.450	*0.447*			0.555	0.503	
Ni	ICP-MS	0.005	1.09	*1.68*			1.73	1.55	
Cu	ICP-MS	0.35	1.18	*1.32*			4.71	4.83	
Zn	ICP-MS	10	5.84	*4.83*			11.3	2.99	
Ag	ICP-MS	0.015	N.D.	*N.D.*			N.D.	N.D.	
Cd	ICP-MS	0.0015	0.0312	*0.0267*			0.0225	0.0223	
Sn	ICP-MS	0.15	0.0861	*0.101*			0.0530	0.0327	
Sb	ICP-MS	0.005	0.0213	*0.0203*			N.D.	N.D.	
W	ICP-MS	0.01	0.0183	*0.0104*			0.0175	0.0144	
Au	ICP-MS	0.005	N.D.	*N.D.*			N.D.	N.D.	
Ga	ICP-MS	0.015	0.0812	*0.0673*			0.0605	0.0733	

* blank cells = not analyzed; N.D. = not detected

Appendix 3. Geochei								
Sample	**04RM26 carb**	**04RM28a carb breccia**	***04RM28a***	**04RM28b carb breccia**	**03RM28 stromatolite**	**04-59 carb**	**04-60 silicified carb**	**04-61 carb**
Stratigraphic unit	Upper siliciclastic	Upper siliciclastic	Upper siliciclastic	Upper siliciclastic	Upper siliciclastic	Upper siliciclastic	Upper siliciclastic	Upper siliciclastic
lithofacies association								
Drill Hole	n/a	n/a		n/a	n/a	n/a	n/a	n/a
Outcrop Locality	Pass Lake	Pass Lake	Pass Lake	Pass Lake	Kama Hill	Channel Island	Channel Island	Channel Island
Easting (m)	372820	372820		372820	425488	462992	462992	462992
Northing (m)	5377714	5377714		5377714	5428453	5406020	5406020	5406020
Description	carb nodule overlying carb breccia Pass Lake Rd	clast in carb breccia, Pass Lake Rd, light green cloudy carb at edge		clast in carb breccia, Pass Lake Rd, massive dark green carb in centre	weathered horizon developed on stromatolitic unit at Kama Hill	altered light green carbonate from top of weathered carbonate unit	silicified carb nodule in weathered top of carb unit	mass flow carb rich matrix
$\delta^{13}C$ (PDB)	0.9	1.2		1.3	-1.5	-0.7	1.2	-1.0
$\delta^{18}O$ (SMOW)	28.1	27.9		28.0	24.6	26.6	25.6	26.5
$\delta^{18}O$ (PDB)	-2.8	-3.0		-2.8	-6.2	-4.2	-5.2	-4.3
$^{87}Sr/^{86}Sr$								
2σ								
Al (ppm)				160.69				
Ba				167.835				
Ca				129422.18				
Fe				264.70				
K				187.4				
Mg				78083.07				
Mn				383.001				
Na				265.29				
P				123.3				
S				128.4				
Si				142.68				
Sr				39.725				
Y				10.90				
Al (ppm)	105	114	*36.0*		78.0			
Fe	37,500	45,000	*57,900*		48,800			
Mn	87.5	63.0	*149*		100			
Mg	176	184	*664*		213			
Ca	>20000	>20000	*>20000*		>20000			
Cs	0.0995	0.0470	*0.00829*		0.00900			
Hf	0.00746	0.00950	*N.D.*		0.0100			
Rb	N.D.	N.D.	*N.D.*		N.D.			
Sr	12.4	14.4	*17.8*		21.5			
Ta	N.D.	N.D.	*N.D.*		N.D.			
Nb	0.00498	N.D.	*N.D.*		0.00600			
Th	0.202	0.231	*0.0341*		0.0995			
U	0.0502	0.0400	*0.0668*		0.0370			
Y	2.09	4.11	*1.62*		4.52			
Zr	0.109	0.0765	*0.0488*		0.0350			
La	2.23	3.24	*0.885*		1.81			
Ce	2.52	3.99	*0.882*		4.50			
Pr	0.583	0.911	*0.349*		0.691			
Nd	2.27	3.65	*1.49*		2.86			
Sm	0.495	0.859	*0.323*		0.834			
Eu	0.0915	0.137	*0.0668*		0.136			
Gd	0.436	0.863	*0.381*		0.854			
Tb	0.0736	0.134	*0.0434*		0.151			
Dy	0.422	0.832	*0.232*		0.909			
Ho	0.0791	0.157	*0.0449*		0.174			
Er	0.229	0.481	*0.119*		0.479			
Tm	0.0303	0.0680	*0.0151*		0.0665			
Yb	0.185	0.452	*0.0824*		0.467			
Lu	0.0264	0.0695	*0.0112*		0.0695			
Li (ppm)	0.587	0.576	*0.453*		0.235			
Be	0.0527	0.0695	*0.0766*		N.D.			
Sc	0.801	1.16	*0.361*		1.17			
V	0.623	0.349	*N.D.*		0.471			
Mo	0.0418	0.0405	*0.120*		0.0395			
Ba	63.8	65.1	*6.92*		210			
Tl	0.00149	0.00150	*N.D.*		N.D.			
Pb	0.890	0.845	*1.14*		1.30			
Ti	1.20	1.17	*0.621*		0.385			
Cr	0.509	0.446	*0.410*		0.474			
Co	0.373	0.444	*1.26*		0.294			
Ni	0.755	0.972	*1.54*		2.75			
Cu	1.68	3.49	*3.09*		4.69			
Zn	5.81	7.37	*25.0*		20.7			
Ag	N.D.	N.D.	*N.D.*		N.D.			
Cd	0.0159	0.0265	*0.160*		0.0290			
Sn	N.D.	N.D.	*0.0395*		0.0255			
Sb	N.D.	N.D.	*0.0180*		0.0225			
W	0.0144	0.0140	*0.0112*		0.0300			
Au	N.D.	N.D.	*N.D.*		N.D.			
Ga	0.0567	0.0650	*0.0659*		0.0645			
* blank cells = not analyzec								

Appendix 4 Geochemical data for carbonate samples from the mixed siliciclastic-carbonate-evaporite unit

Sample			04RM40	BRO1-3	03RM37 dolo mudstone	TH1	TH2	GF7-L	GF7-W	04RM10	04RM15a	04RM15b
Stratigraphic unit			mixed siliciclastic-carbonate-evaporite	mixed siliciclastic-carbonate-evaporite	mixed siliciclastic-carbonate-evaporite	mixed siliciclastic-carbonate-evaporite	mixed siliciclastic-carbonate-evaporite	mixed siliciclastic-carbonate-evaporite	mixed siliciclastic-carbonate-evaporite	mixed siliciclastic-carbonate-evaporite	mixed siliciclastic-carbonate-evaporite	mixed siliciclastic-carbonate-evaporite
lithofacies association			massive dolostone/ intraformational conglomerate	red siltstone-sulfate	massive dolostone	red siltstone-sulfate	red siltstone-sulfate	red siltstone-sulfate	red siltstone-sulfate	red siltstone-sulfate	red siltstone-sulfate	red siltstone-sulfate
Drill Hole			n/a	NI-92-7	n/a	n/a	n/a	n/a	n/a	NI-92-7	HE-02-02	HE02-02
Stratigraphic height above basement			n/a	n/a	n/a	n/a	n/a	n/a	n/a	165.5	78 (above base of hole)	78 (above base of hole)
Outcrop Locality			red rock railway	n/a	Kama Hill	boulder, NW of Dorion	boulder, NW of Dorion	Hwy 11-17, near Dorion	Hwy 11-17, near Dorion	n/a	n/a	n/a
Easting (m)			407703	353850	425488	363774	363774	384322	384322	353850	393007	393007
Northing (m)			5423237	5443000	5428453	5425172	5425172	5401639	5401639	5443000	5449701	5449701
Description			dolo siltstone/mudstone clast a few m above Middlebrun Bay Member	disseminated carbonate associated with sulphates	massive fine-grained dolo. overlies stromatolite unit at Kama Hill	recrystallized stromatolite boulder	recrystallized stromatolite boulder	finely laminated pink carbonate	weathered top of finely laminated pink carbonate	recrystallized, stromatolitic with abundant diagenetic gypsum	finely laminated pink carbonate from stromatolitic horizon in core	clast of massive white carb in breccia above 15a
$\delta^{13}C$ (PDB)			-1.4	-0.7	1.2	1.3	1.3	1.3	1.4	1.5	1.7	1.5
$\delta^{18}O$ (SMOW)			26.3	15.3	25.4	24.8	25.0	26.7	26.3	25.5	27.3	26.9
$\delta^{18}O$ (PDB)			-4.5	-15.1	-5.3	-6.0	-5.7	-4.1	-4.5	-5.3	-3.5	-3.9
$^{87}Sr/^{86}Sr$			0.707028			0.707031						
2σ			0.000013			0.000023						
	Method	Detection Limit										
Al (ppm)	ICP-AES	0.04	193.95	1037.09				2.21	39.07	N.D.	100.06	83.28
Ba	ICP-AES	0.006	43.627	28.074				9.735	402.932	1.384	3.779	2.486
Ca	ICP-AES	0.01	135189.02	130742.62				131026.40	129657.95	150235.12	127831.04	139814.58
Fe	ICP-AES	0.02	308.16	120.90				324.63	340.71	437.02	751.48	849.04
K	ICP-AES	0.25	60.2	N.D.				N.D.	N.D.	N.D.	102.2	N.D.
Mg	ICP-AES	0.01	76724.98	12798.98				80517.33	78320.83	70719.29	71860.55	74565.82
Mn	ICP-AES	0.002	279.057	356.967				1371.165	1061.282	950.952	785.189	1046.497
Na	ICP-AES	0.01	369.00	N.D.				68.29	67.54	87.11	173.53	252.37
P	ICP-AES	0.1	133.7	1027.0				4.7	N.D.	N.D	15.0	68.2
S	ICP-AES	0.1	176.3	83794.8				N.D.	94.1	28060.9	85.6	14.6
Sr	ICP-AES	0.025	73.85	681.15				14.23	73.66	N.D.	90.67	98.70
Sr	ICP-AES	0.005	37.459	1302.459				15.044	33.002	45.329	39.069	30.960
Y	ICP-AES	0.03	9.59	8.20				4.65	7.50	0.52	4.49	4.52
Al (ppm)	ICPMS	0.5				41.8						
Ca	ICPMS	1000				335						
Fe	ICPMS	0.3				750						
Mn	ICPMS	0.4				>20000						
Mg	ICPMS	250				105,000						
Ca	ICPMS	0.001				0.120						
Hf	ICPMS	0.05				N.D.						
Rb	ICPMS	0.02				N.D.						
Sr	ICPMS	0.00				19.1						
Ta	ICPMS	0.10%				N.D.						
Nb	ICPMS	0.01				N.D.						
Th	ICPMS	0.02				0.0367						
U	ICPMS	2				0.0141						
Y	ICPMS	0.025				1.11						
Zr	ICPMS	0.2				0.0402						
La	ICPMS	0.02				0.519						
Ce	ICPMS	0.01				0.818						
Pr	ICPMS	0.0035				0.327						
Nd	ICPMS	0.002				1.50						
Sm	ICPMS	0.005				0.300						
Eu	ICPMS	0.005				0.0538						
Gd	ICPMS	0.005				0.266						
Tb	ICPMS	0.015				0.0312						
Dy	ICPMS	0.0015				0.177						
Ho	ICPMS	0.004				0.0281						
Er	ICPMS	0.0015				0.0759						
Tm	ICPMS	0.005				0.00854						
Yb	ICPMS	0.002				0.0518						
Lu	ICPMS	0.0035				0.00754						
Li (ppm)	ICPMS	0.1				0.333						
Be	ICPMS	0.04				N.D.						
Sc	ICPMS	0.3				0.491						
V	ICPMS	0.4				0.208						
Mo	ICPMS	0.02				N.D.						
Ba	ICPMS	0.0015				3.60						
Tl	ICPMS	0.0035				0.00151						
Pb	ICPMS	0.15				0.783						
Tl	ICPMS	0.005				1.95						
Cr	ICPMS	0.03				1.92						
Co	ICPMS	0.5				0.956						
Ni	ICPMS	0.005				2.16						
Cu	ICPMS	0.35				1.18						
Zn	ICPMS	10				9.56						
Ag	ICPMS	0.015				N.D.						
Cd	ICPMS	0.0015				0.0462						
Sn	ICPMS	0.15				0.0623						
Sb	ICPMS	0.005				N.D.						
W	ICPMS	0.01				0.00754						
Au	ICPMS	0.005				N.D.						
Ga	ICPMS	0.015				0.0754						

* blank cells = not analyzed; N.D. = not detected

Appendix 5. Geochemical data for all sulfate samples.											
Sample			**03RM27**	**03RM28**	**03RM29**	**BR0136**	**BR0138**	**BR0144**	**BR0146**	**04RM5**	**04RM8**
stratigraphic unit			mixed siliciclastic-carbonate-evaporite	mixed siliciclastic-carbonate-evaporite	mixed siliciclastic-carbonate-evaporite	mixed siliciclastic-carbonate-evaporite	mixed siliciclastic-carbonate-evaporite	mixed siliciclastic-carbonate-evaporite	mixed siliciclastic-carbonate-evaporite	mixed siliciclastic-carbonate-evaporite	mixed siliciclastic-carbonate-evaporite
lithofacies association			red siltstone-sulfate	red siltstone-sulfate	red siltstone-sulfate	red siltstone-sulfate	red siltstone-sulfate	red siltstone-sulfate	red siltstone-sulfate	red siltstone-sulfate	red siltstone-sulfate
Drill Hole			NI-92-7	NI-92-7	NI-92-7	NI-92-7	NI-92-7	NI-92-7	NI-92-7	NI-92-7	NI-92-7
Stratigraphic Height (above basement) (m)			157.45	158.6	145.2	107.6	125	136.48	140	107.27	113.32
Easting (m)			353850	353850	353850	353850	353850	353850	353850	353850	353850
Northing (m)			5443000	5443000	5443000	5443000	5443000	5443000	5443000	5443000	5443000
Description			gyp/anh nodule	gyp/anh nodule	gyp/anh nodule	gyp/anh nodule	gyp/anh nodule	gyp/anh nodule	gyp/anh nodule	sulphate cement	gyp/anh nodule
$^{87}Sr/^{86}Sr$			0.70647	0.707047	0.707383						
2σ			0.000037	0.000012	0.000013						
Approximate %S			18	18		22	15	20	16	25	33
$\delta^{34}S$ (CDT)			10.6	11.2		11.4	9.0	8.9	9.0	12.4	12.2
	Method	**Detection Limit**									
Al (ppm)	ICP-AES	0.06	N.D.	N.D.		28.77	N.D.	11.84	N.D.	N.D.	N.D.
Ba	ICP-AES	0.006	20.301	7.451		5.802	4.366	3.596	N.D.	2326.429	N.D.
Ca	ICP-AES	0.01	273239.01	80151.71		289816.05	226325.35	256974.56	229057.53	2474302.86	230382.51
Fe	ICP-AES	0.02	7.18	N.D.		67.28	N.D.	37.63	17.42	N.D.	N.D.
K	ICP-AES	0.25	N.D.	71.8		175.1	N.D.	N.D.	N.D.	N.D.	N.D.
Mg	ICP-AES	0.01	107.37	55.25		263.95	49.86	426.67	3153.88	3725.00	124.79
Mn	ICP-AES	0.003	0.712	0.033		21.975	0.563	8.947	33.596	10.000	N.D.
Na	ICP-AES	0.01	83.70	98.93		295.68	360.99	229.91	194.33	3487.86	337.63
P	ICP-AES	0.1	44.6	23.6		N.D.	N.D.	N.D.	73.5	477.1	39.8
S	ICP-AES	0.1	232934.8	67271.7		220985.7	184110.4	209507.4	187287.6	2070656.2	192842.7
Si	ICP-AES	0.025	23.67	12.63		43.46	113.80	53.33	42.47	491.43	10.79
Sr	ICP-AES	0.005	1253.699	429.605		712.222	641.549	1459.912	1295.281	19242.857	2093.023
Y	ICP-AES	0.03	N.D.	N.D.		N.D.	N.D.	N.D.	N.D.	N.D.	N.D.

Appendix 5. Geochemical data for all sulfate samples.											
Sample			M-14	03RM61	03RM62	03RM63	03RM64	CFG3	CFG4	CFG5	CFG6
stratigraphic unit			mixed siliciclastic-carbonate-evaporite	mixed siliciclastic-carbonate-evaporite	mixed siliciclastic-carbonate-evaporite	mixed siliciclastic-carbonate-evaporite	mixed siliciclastic-carbonate-evaporite	mixed siliciclastic-carbonate	mixed siliciclastic-carbonate	mixed siliciclastic-carbonate	mixed siliciclastic-carbonate
lithofacies association			red siltstone-sulfate	red siltstone-sulfate	red siltstone-sulfate	red siltstone-sulfate	red siltstone-sulfate	red siltstone-dolostone	red siltstone-dolostone	red siltstone-dolostone	red siltstone-dolostone
Drill Hole			NI-92-7	D00-02	D00-02	D00-02	D00-02	NI-92-7	NI-92-7	NI-92-7	NI-92-7
Stratigraphic Height (above basement) (m)			165	n/a	n/a	n/a	n/a	62.32	56.53	58.18	65.86
Easting (m)			353850	357206	357206	357206	357206	353850	353850	353850	353850
Northing (m)			5443000	5440995	5440995	5440995	5440995	5443000	5443000	5443000	5443000
Description			gyp/anh nodule	gyp/anh nodule	gyp/anh nodule	gyp/anh nodule	gyp/anh nodule	gyp/anh nodule	gyp/anh nodule	gyp/anh nodule	gyp/anh nodule
$^{87}Sr/^{86}Sr$				0.708836	0.708186	0.707788	0.708799	0.708999			
2σ				0.000015	0.000013	0.000018	0.000015	0.000005			
Approximate %S			24	19	20	19	16	18	26	15	24
$\delta^{34}S$ (CDT)			10.3	12.0	12.0	11.2	11.9	5.3	5.7	4.5	4.9
	Method	Detection Limit									
Al (ppm)	ICP-AES	0.06	11.38	N.D.	N.D.	N.D.	N.D.	N.D.	14.09	61.64	24.67
Ba	ICP-AES	0.006	0.331	8.357	2.440	3.348	5.413	11.818	353.960	38.630	6.000
Ca	ICP-AES	0.01	250774.59	263201.71	234329.08	230140.17	236367.71	262793.51	265706.04	252687.67	245454.67
Fe	ICP-AES	0.02	46.30	1.00	N.D.	N.D.	20.12	16.49	111.28	9.04	4.13
K	ICP-AES	0.25	N.D.	N.D.	91.6908213	N.D.	N.D.	213.0	811.5	N.D.	N.D.
Mg	ICP-AES	0.01	1348.95	320.79	28.48	45.17	12.20	1481.56	2094.77	2951.23	1582.13
Mn	ICP-AES	0.003	14.586	8.429	N.D.	N.D.	N.D.	3.896	8.591	4.384	6.667
Na	ICP-AES	0.01	49.83	256.21	179.78	165.35	9.14	221.95	584.30	44.66	344.40
P	ICP-AES	0.1	N.D.	123.4	41.1	71.0	70.8	N.D.	N.D.	N.D.	N.D.
S	ICP-AES	0.1	200771.7	219722.8	199181.6	195222.6	199208.5	212309.6	209393.8	194132.6	198904.5
Si	ICP-AES	0.025	32.04	70.00	16.62	36.00	13.70	39.48	63.89	203.29	97.07
Sr	ICP-AES	0.005	799.448	926.286	278.164	185.565	574.067	220.909	439.060	381.096	1094.267
Y	ICP-AES	0.03	N.D.	N.D.	N.D.	N.D.	N.D.	N.D.	N.D.	N.D.	N.D.

Appendix 5. Geochemical data for all sulfate samples.								
Sample			03RM35g	03RM26	04RM32	CFG1	CFG2	03RM44g
stratigraphic unit			mixed siliciclastic-carbonate	mixed siliciclastic-carbonate	mixed siliciclastic-carbonate	mixed siliciclastic-carbonate	mixed siliciclastic-carbonate	mixed siliciclastic-carbonate
lithofacies association			red siltstone-dolostone	red siltstone-dolostone	red siltstone-dolostone	red siltstone-dolostone	red siltstone-dolostone	red siltstone-dolostone
Drill Hole			NI-92-7	NI-92-7	NI-92-7	NI-92-7	NI-92-7	NI-92-7
Stratigraphic Height (above basement) (m)			86.93	74.04	55	53.36	60.72	64
Easting (m)			353850	353850	353850	353850	353850	353850
Northing (m)			5443000	5443000	5443000	5443000	5443000	5443000
Description			gyp/anh nodule	gyp/anh nodule	gyp/anh nodule	gyp/anh nodule	gyp/anh nodule	cyclic gypsum
$^{87}Sr/^{86}Sr$			0.710492			0.708522	0.709063	0.710899
2σ			0.000008			0.000011	0.000008	0.000018
Approximate %S			13	46	21	22	23	
$\delta^{34}S$ (CDT)			11.9	10.7	5.5	6.0	6.0	
	Method	Detection Limit						
Al (ppm)	ICP-AES	0.06	25.18	7.36	3.88	16.58	N.D.	
Ba	ICP-AES	0.006	788.684	27.917	45.426	14.188	58.387	
Ca	ICP-AES	0.01	442764.04	376876.39	280637.21	253386.32	204878.97	
Fe	ICP-AES	0.02	82.37	158.47	N.D.	15.21	19.23	
K	ICP-AES	0.25	N.D.	N.D.	N.D.	454.7	N.D.	
Mg	ICP-AES	0.01	2106.14	4770.83	1849.61	1740.17	3116.06	
Mn	ICP-AES	0.003	49.298	31.944	4.651	6.496	40.903	
Na	ICP-AES	0.01	325.00	318.19	127.91	814.19	217.23	
P	ICP-AES	0.1	14.0	N.D.	N.D.	N.D.	46.2	
S	ICP-AES	0.1	320560.0	271608.9	226013.0	203313.5	168059.3	
Si	ICP-AES	0.025	108.77	45.00	65.74	107.69	102.45	
Sr	ICP-AES	0.005	1091.316	1322.917	623.411	541.026	363.613	
Y	ICP-AES	0.03	N.D.	N.D.	N.D.	N.D.	N.D.	